Source, transport and deposition of sediments of the Sunda Subduction Zone from Bangladesh, Burma and the Andaman Islands: Implications on the history of early evolution of the Himalaya.

A thesis presented in fulfilment of the requirements for the degree of Doctor of Philosophy by

Ruth Allen
BSc (Birmingham) 2004

Department of Environmental Science
Lancaster University

ProQuest LLC.
789 East Eisenhower Parkway
P.O. Box 1346
Ann Arbor, MI 48106 – 1346

Declaration of Contribution

This work has not been submitted for the award of a higher degree elsewhere, and where chapters have been published (or submitted for publication) this is identified at the beginning of each chapter.

The work of this dissertation is primarily my own. As lead author on the papers documented in chapter 3, 4 and 5, I have written the papers myself with supervision from Y. Najman, A. Carter and E. Willett. I have synthesised and interpreted all of the data within the thesis myself. A detailed breakdown of my own contribution to data collection is presented in Chapter 2, as well as the contribution of co-authors. Below is a summary of this contribution made by each co-author listed in chapters 3, 4 and 5.

R. Allen – first author on all papers and thesis. Sole writer with supervision from Y. Najman, A. Carter and E. Willett. Synthesis and interpretation of *all* data collected. Conducted fieldwork and data collection for ^{40}Ar-^{39}Ar dating, Sm-Nd bulk rock analysis, U-Pb dating and seismic interpretation.

Y. Najman – First supervisor and collection of Burma field samples (due to student travel restrictions)

A. Carter – Second supervisor and thermochronology lab manager (UCL). Conducted the fission track analysis (data used and interpreted by R. Allen)

E. Willett – Third supervisor at Cairn Energy Plc. (CASE partners). Supervised seismic interpretation

E. Garzanti – Lab manager and supervision pertaining to heavy mineral and petrographic study (Milan University)

G. Vezzoli/S. Ando – Technicians at Milan University. Conducted the petrography and heavy mineral study (data used and interpreted by R. Allen)

E. Bickle – Lab manager for Sm-Nd analysis (Cambridge University)

D. Barfod – Argon isotope lab manager (SUERC, East Kilbride)

J. Wijbrans – Argon isotope lab manager (Vrije University, Amsterdam)

H. Chapman – Technician in the Sm-Nd lab (Cambridge University)

P. Bandopadhyay – field guide, S. Andaman (Geological Survey of India)

G. L. Foster – conducted the pilot samples for single grain apatite Sm-Nd (Bristol University, Chapter 3 only)

G. Oliver – Lab manager (St Andrews University). Conducted XRD illite crystallinity (data used and interpreted by R. Allen)

R. Parrish – completed one U-Pb analysis on a sample from Burma (Chapter 4 only. NIGL BGS Keyworth. Data used and interpreted by R. Allen)

Supervisor(s) confirmation of contribution:

I confirm that the contribution of Ruth Allen and co-authors is as described above

Dr Y. Najman (First supervisor)

Dr A. Carter (Second supervisor)

Mr E. Willett (Supervisor at Cairn Energy Plc. CASE sponsors)

Abstract

Studying the erosion record of a mountain belt is useful for understanding processes of mountain building, such as crustal deformation and the coupling of tectonics and erosion. It is also important for understanding its potential affect on regional and global climate and changes to marine geochemistry. With respect to the Himalaya, erosion has been suggested as a primary cause of global cooling and changes to ocean geochemistry in the Cenozoic. Often the erosion record preserved in a mountain's sedimentary repositories are the only way of gaining information of these processes in the absence of a hinterland record, which may have been overprinted by metamorphism or eroded from the mountain belt itself over time.

Little is known of the early erosive history of the Himalaya. In the foreland basin a widespread unconformity separates pre-collisional sedimentary rocks from Himalayan-derived sedimentary rocks. Furthermore, the record of collision and erosion preserved in the suture zone does not relate to erosion of the southern flank and the potential record stored in offshore fans such as the Indus and Bengal is on the whole poorly constrained due to current drill depth restrictions. However, it has been proposed that an early record of Himalayan erosion may be preserved in sedimentary deposits found in the Andaman Islands and the Indo-Burman Ranges/Chittagong Hill Tracts as offscraped material from the proto Bengal Fan.

My key aim is to determine the provenance of the Tertiary sedimentary (accretionary prism) rocks that run along the India-Asia (Sunda) subduction zone from Bangladesh and Burma (Myanmar) to the Andaman Islands. To achieve this a unique multi-proxy approach is used.

Three main conclusions can be drawn. Firstly, that the Palaeogene sedimentary rocks of both South Andaman and the Indo-Burman Ranges (Burma) show

appreciable magmatic arc derivation with additional orogenic input. Although a subordinate continental source to these regions is observable from the data it is most likely that this source is the Burman continental margin and not the Himalaya. However, I do not altogether rule out the possibility of minor Himalayan contribution. Unambiguous evidence of Himalayan derivation is not found in the region until ~ 38 Ma in the Bengal Basin. In younger Palaeogene to Neogene sedimentary rocks of the Andaman Islands (30-20 Ma) a provenance change to dominantly recycled orogen with minor arc sources is seen. This is most easily explained by derivation from Burman continental margin sources and not from the Himalaya.

Secondly, the Neogene rocks west of the Kaladan Fault, preserve evidence for Himalayan derivation which is unambiguous. The rocks in the westernmost Indo-Burman Ranges and the Chittagong Hill Tracts/Hatia Trough are isotopically and petrographically distinct from their Palaeogene counterparts, but similar to coeval rocks of known Himalayan derivation in the orogen's foreland basin.

Thirdly, seismic mapping of the Neogene sedimentary rocks have given new insight to palaeodrainage of the Brahmaputra. New seismic data suggests that it was not the uplift of the Shillong Plateau at ~3.5 Ma that caused the deflection of the Brahmaputra around the northern flank of the massif, but instead the encroachment of the leading edge of the growing Chittagong Hill Tracts onto the already uplifted plateau that closed the northeast drainage route to the Brahmaputra, forcing it to divert its course.

Our data is consistent with the hypothesis that erosion of the Himalaya could have caused an increase in global ocean $^{87}Sr/^{86}Sr$ ratios since ~40 Ma (Richter *et al.* 1992). However, it does not appear to be consistent with the theory that onset of substantial erosion from the Himalaya at ~55 Ma caused global cooling, due to the lack of any

substantial evidence as yet, of erosion since collision. The results of this thesis support models of crustal deformation, which require a delay in erosion or do not require erosion at all in early stages of convergence.

Time and tide wait for no man

For Dad

~ 1955 – 2006 ~

Acknowledgements

First and foremost my thanks go to my supervisors. Thanks to Yani Najman for choosing me for the project and guiding me through it for 3 years. Thanks for your support in the more trying of times and for being patient all the way through. I had a lot of fun working with you. Thanks also to Andy Carter for your supervision and accepting the endless debate over whether to run more samples, and to Ed Willett for making my time at Cairn Energy interesting and enjoyable.

Thank you to all of the collaborators who made this project possible by giving their time, labs and support: Special thanks to Eduardo Garzanti, Mike Bickle, Dan Barfod and Jan Wijbrans.

Thanks to the technician crew at the labs in Milan, East Kilbride and Cambridge, and to the fieldwork guys and the folk at Cairn Energy.

Especially important to me are the friends I have made since being at Lancaster. Thanks for being a good laugh and reliably going for coffee every day (usually more than once, often back to back!). In particular the last few months of writing up in the new office with the 'Sauna Girls' has been really fun and made the whole process far less stressful than I thought it would be: thanks to Alex, Jane and Jo.

Thanks to Mum for always being proud of me even when I know I am a fraud and Gazz for being the kind of tonic only a younger brother can be.

Finally, thanks to Matt. Coming here led me to you and since then life has been brilliant and exciting. Thanks for always supporting me during my constantly changing, mad cap schemes and ideas (PhD included). You really understand me and I can't wait to see what happens next.

Table of Contents

Chapter 6

Appendix 4 Seismic data – CD

Appendix 5 Abstracts and co-authored publications

List of Figures

Chapter 1

Chapter 3

Chapter 4

Chapter 5

List of Tables

Chapter 3

Chapter 4

Chapter 5

List of Papers

New Constraints on the sedimentation and uplift history of the Andaman Accretionary Prism, South Andaman Island (Chapter 3) **59-106**

R. Allen[1], A. Carter[2], Y. Najman[1], P.C. Bandopadhyay[3], H. J. Chapman[4], M. J. Bickle[4], E. Garzanti[5], G. Vezzoli[5], S. Andò[5], G. L. Foster[6], C. Gerring[7]

[1]Department of Environmental Science, Lancaster University LA1 4YQ, United Kingdom
[2]Research School of Earth Sciences, Birkbeck and University College London, Gower St., London, WC1E 6BT, United Kingdom
[3]Geological Survey of India, Geodata Division, Salt Lake, Kolkata, 91, India
[4]Department of Earth Sciences, Cambridge University, Downing St. Cambridge CB2 3EQ, UK.
[5]Dipartimento di Scienze Geologiche e Geotecnologie, Universita Milano-Bicocca, Piazza della Scienza 4, 20126 Milano, Italy,
[6]Department of Earth Sciences, Bristol University, Queens Rd, Bristol BS8 1RJ, United Kingdom
[7]Department of Earth Sciences, The Open University. Walton Hall, Milton Keynes, MK7 6AA, United Kingdom

Geological Society of America Bulletin, Special Publication, 436 (2007), *Published*

Provenance of the Tertiary sedimentary rocks of the Indo-Burman Ranges, Burma (Myanmar): Burman arc or Himalayan derived? (Chapter 4) **107-135**

R. Allen[1], Y. Najman[1], A. Carter[2], D. Barfod[3], M. J. Bickle[4] and H. J. Chapman[4], E. Garzanti[5], G. Vezzoli[5], S. Andò[5], R. Parrish[6]

[1]Department of Environmental Science, Lancaster University LA1 4YQ, United Kingdom
[2]Research School of Earth Sciences, Birkbeck and University College London, Gower St., London, WC1E 6BT, United Kingdom
[3]Argon Isotope Laboratory, SUERC, East Kilbride, Scotland
[4]Department of Earth Sciences, Cambridge University, Downing St. Cambridge CB2 3EQ, UK.
[5]Dipartimento di Scienze Geologiche e Geotecnologie, Universita Milano-Bicocca, Piazza della Scienza 4, 20126 Milano, Italy.
[6]NIGL, BGS Keyworth, Nottingham NG12 9GG, UK *and* Dept of Geology, Leicester University, UK.

Journal of the Geological Society, London, *Accepted for publication*

New seismic, biostratigraphic and isotopic constraints to the geological evolution and sedimentary provenance of the SE Bengal Basin, Bangladesh. (Chapter 5) **136-185**

R. Allen[1], Y.Najman[1], E. A. F. Willett[2]*, A. Carter[3], D. Barfod[4], E. Garzanti[5], J. Wijbrans[6], M. J. Bickle[7], G. Vezzoli[5], S. Ando[5], G. Oliver[8], M.J. Uddin[9]

[1]Dept. of Environmental Science, Lancaster University, LA1 4YQ, UK
[2]Cairn Energy Plc, *currently Bowleven, 1 North St Andrew Lane, Edinburgh, EH2 1HX
[3]Research School of Earth Sciences, Birkbeck and University College London, Gower Street, London, WC1E 6BT, UK
[4] NERC Argon Isotope Laboratory, SUERC, East Kilbride, Scotland
[5]Dipartimento di Scienze Geologiche e Geotechnologie, Universita Milano-Bicocca, Piazza della Scienza 4, 20126, Milano, Italy.
[6] Dept Isotope Geology, Vrije Universiteit, De Boelelaan 1085, 1081 Amsterdam, Netherlands
[7]Department of Earth Sciences, Cambridge University, Downing Street, Cambridge, CB2 3EQ, UK
[8] School of Geog. and Geosciences, Irvince Building, University if St Andrews, Fife, Scotland
[9]Tullow Bangladesh Ltd, House no.17, Road no.9, Baridhara R/A, Dhaka-1212, Bangladesh

Basin Research, *Submitted*

Chapter 1: Introduction

1.1 Aims, objectives and structure of the thesis

1.1.1 Rationale and Aims of the thesis

The Himalaya is a type-example of mountain building processes as a result of continental-continental collision of the Indian and Asian plates. The region preserves a wide variety of observable features directly as a result of orogenesis, including extensive metamorphism, widespread deformation, the main suture zone representing final closure of the Tethys Ocean and major sedimentary repositories south of both the east and west Himalaya, including the widespread Peripheral Foreland basin, the Indus, Katawaz and Bengal Remnant Ocean Basins, the suture zone molasse basin and the Indus and Bengal Fan (Figure 1.1 and Section 1.2.2)

Studying the erosion record is important for constraining models of crustal deformation (Section 1.3) that differ in the timing and extent of erosion, and for understanding the feedback and coupling between tectonics and erosion. The erosion record preserved in sedimentary repositories of the Himalaya is also important for studying the evolution of the mountain belt over time in the absence of data from the hinterland, which is often lost by later metamorphic overprinting or erosion. Furthermore, the onset and extent of erosion has a valuable role to play in understanding changes in marine chemistry in the Tertiary and large-scale climate changes since widespread uplift of the Himalaya (Section 1.3).

Little is known of the early erosive history of the Himalaya. In the foreland basin, a widespread unconformity throughout the majority of the Oligocene separates pre-collisional Palaeocene-early Eocene sedimentary rocks from Himalayan derived Oligo-Miocene sedimentary rocks (e.g., Najman, 2006) (Section 1.2.3). It is debated whether the suture zone of India and Asia records early input from the Himalaya as far

back as ~50 Ma (Clift *et al.,* 2001a; Wu *et al.,* 2007) and elsewhere the earliest unequivocal record of Himalayan erosion appears at ~38 Ma in the Bengal Basin (Najman *et al.,* in press). Largely, Palaeogene fan sediments are also not yet accessible in the deep sea fans south of the Himalaya. However, the Indus Fan may preserve a record of deposition since the middle Eocene based on studied samples from the Murray Ridge (Clift *et al.,* 2001b)

However, it has been proposed (Curray et al., 1979, 2005) that an early record of Himalayan erosion may be preserved in sedimentary deposits found in the Andaman Islands and the Indo-Burman Ranges (Figure 1.1). Modelling of Southeast Asia prior and during collision shows the key strategic position of such areas during collision (Tapponnier *et al.,* 1982; Lee and Lawver, 1995; Hall, 2002; Replumaz and Tapponier, 2003). The Andaman Islands, Indo-Burman Ranges (and its western continuation as the Chittagong Hill Tracts, Bangladesh), are thought to preserve accretionary prism deposits sourced from the offscraped Bengal Fan (e.g., Curray et al., 1979, 2005; Bender, 1983) and as such may show derivation from the nascent Himalaya, however their provenance has been disputed (e.g., Mitchell, 1993; Pal et al., 2003) (Section 1.1.2).

My aim is to determine the provenance of the Tertiary sedimentary rocks from the Andaman Islands and the Indo-Burman Ranges and where a Himalayan provenance is identified, I look to use it to better understand Himalayan evolution in the Palaeogene and Neogene.

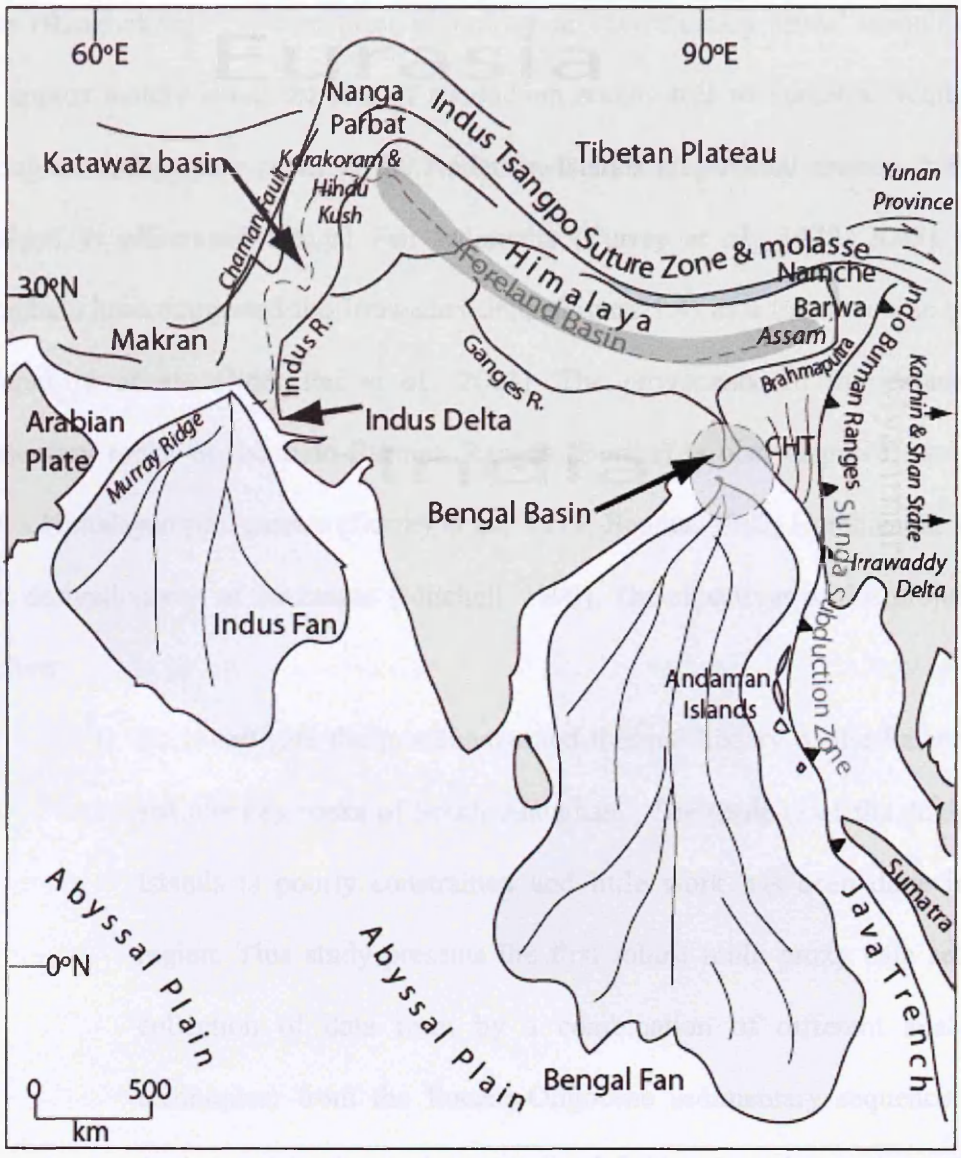

Figure 1.1 shows the salient features of the Himalaya and surrounding region including the areas of study (CHT= Chittagong Hill Tracts, Indo-Burman Ranges and the Andaman Islands), major sedimentary respositories, compressional features in the east and west and major drainage routes. The relative locations of the India-Asia subduction zone and suture zone is also shown.

1.1.2 Objectives of the thesis

The purpose of this project was to address some of the gaps in knowledge from regions, which have been suggested, might preserve a record of early Himalayan erosion not found elsewhere (e.g., Curray, 1979; Curray, 1994). Three such areas are the Andaman Islands, The Indo-Burman Ranges (Burma) and the Chittagong Hill

Tracts (Bangladesh). Together these units form an 'accretionary prism' complex that runs approximately along the line of subduction southwards to Sumatra. Whilst the Palaeogene sedimentary rocks of the Andaman Islands may record erosion from the Himalaya as offscraped Bengal Fan sediments (Curray *et al.,* 1979, 2005), other researchers have suggested the Irrawaddy delta (Figure 1.4) as a major source region (Karunakara *et al.,* 1968; Pal *et al.,* 2003). The provenance of the Palaeogene sedimentary rocks of the Indo-Burman Ranges (Burma) is also disputed, and may show a Himalayan provenance (Curray *et al.,* 1979; Bender, 1983; Hutchinson, 1989) or arc derivation east of the ranges (Mitchell, 1993). The objectives of this project are therefore:

1. To investigate the provenance and thermal history of the Palaeogene sedimentary rocks of South Andaman. The geology of the Andaman Islands is poorly constrained and little work has been done in the region. This study presents the first robust multi-proxy data set (i.e. collection of data from by a combination of different analytical techniques) from the Eocene-Oligocene sedimentary sequence. The Andaman Islands are the most distal field area in this project relative to the Himalaya.
2. To investigate the provenance and evolution of the Palaeogene and Neogene Indo-Burman Ranges (Burma)/Chittagong Hill Tracts (Bangladesh), respectively. We aim to determine its provenance and, where a Himalayan record is identified refine its stratigraphy so that it can be used as a record of Himalayan evolution.

To achieve the above objectives a variety of primary techniques were used, including Sm-Nd isotopic fingerprinting on bulk sediment and single grain apatite,

^{40}Ar-^{39}Ar dating on detrital white mica, detrital zircon U-Pb dating and detrital zircon and apatite and fission track dating. A petrographic and heavy mineral study was conducted on all samples. These techniques have been chosen because different geological units of the Himalaya have been found to show distinct isotopic and petrographic characteristics, which help to differentiate between each unit and provide a provenance signature for which to compare samples from Bangladesh, Burma and the Andaman Islands. Furthermore, it should be possible to distinguish a Himalayan signature from an Indian cratonic and Burman continental margin signature, which will also be considered. Biostratigraphy has been analysed on samples with suitable fossil content to provide better age constraint for the rocks in this study, and illite crystallinity is used to test for metamorphic resetting of minerals. 2D seismic data has been extensively used for objective 2 courtesy of partnership with Cairn Energy Plc. Chapter 2 describes in more detail why the techniques used in this study were chosen, and how and why they are useful for this project in particular.

1.1.3 Structure of the thesis

The thesis is divided into six chapters plus associated appendices. The chapters are as follows,

Chapter 1 (Introduction) provides the background to the thesis. Discussion of Himalayan geology and the study of orogenesis provide a context for deciphering provenance of the sediments and sedimentary rocks from the study areas, and their relevance within a wider context. This is followed by an introduction to the regional tectonics of the study areas and an introduction on all the field areas that are expanded on in later chapters (papers).

Chapter 2 is an overview of the analytical techniques chosen for this project, and how they fulfil the identified aims and objectives. Detailed methodology is presented in Appendices 1-3. A full statement of participation for each method used is provided.

Chapter 3 is a published paper by Allen *et al.,* titled *'New Constraints on the sedimentation and uplift history of the Andaman-Nicobar accretionary prism, South Andaman Island'* and published by the **Geological Society of America**, Special Paper 436, 11 (2008) pp1-34

The paper presents data from the South Andaman field area (discussed in Section 1.4) and aims to resolve the disputed provenance of the Palaeogene sedimentary rocks of South Andaman (Karunakaran *et al.,* 1968; Curray *et al.,* 1979, 2005; Pal *et al.,* 2003), to assess whether the nascent Himalaya to the north of the region was a source at that time, evidence of which would provide some of the earliest eroded sediments from the eastern Himalaya that are otherwise 'missing' elsewhere in repositories such as the foreland basin and Bengal Fan. New constraints to the age of the rocks and the thermal history of the region are also presented.

Chapter 4 is a paper *In Press* with the **Journal of the Geological Society**, London, by Allen *et al.,* entitled *'Provenance of the Tertiary sedimentary rocks of the Indo-Burman Ranges, Burma (Myanmar): Burman arc or Himalayan-derived?'*

The purpose of this study was to resolve the disputed provenance of the sedimentary rocks of the Indo-Burman Ranges, which may preserve a record of Himalayan erosion (Curray *et al.,* 1979; Bender, 1983; Hutchinson, 1989). However, a

Burman magmatic arc source has also been suggested for the Palaeogene rocks of the Indo-Burman ranges (Mitchell, 1993). The paper presents data from the western Indo-Burman Ranges study area (discussed in Section 1.4) The accretionary prism or forearc deposits of the Indo-Burman Ranges in western Myanmar extend along the India-Eurasian subduction zone (Sunda arc) and are divided into a westward portion of Neogene sedimentary rocks, and an eastward Cretaceous-Palaeogene belt.

Chapter 5 is a paper submitted to **Basin Research** by Allen *et al.,* entitled '*New seismic, biostratigraphic and isotopic constraints to the geological evolution and sedimentary provenance of the SE Bengal Basin, Bangladesh'.*

The Chittagong Hill Tracts preserves Neogene sediments and sedimentary rocks formed in an accretionary prism setting. The sedimentary rocks preserve a record of Himalayan erosion since the Miocene, however the timing of deposition and deformation is disputed (Sikder and Alam, 2003; Mandal *et al.,* 2006). Constraining basin evolution is a primary objective of this study. The stratigraphy of the Chittagong Hill Tracts is refined using a seismic stratigraphic framework that is calibrated by well penetrations and biostratigraphic data obtained by partnership with Cairn Energy Plc. This has made the stratigraphy useable as an accurate sedimentary record of Himalayan evolution. A new geology map for the region is presented. Seismic mapping of the palaeoshelf over time has allowed for a consideration of source direction for the sedimentary rocks of the Bengal Basin. We provide new constraint to the exhumation history of the Chittagong Hill Tracts based on seismic and thermochronological data. Of note are the conclusions drawn on the geological evolution of the region from western Myanmar to Bangladesh since substantial clastic input to the Bengal Basin began in the Miocene.

Chapter 6 addresses the initial aims of the project and aims to give the reader an over-arching discussion of all 3 papers and the conclusions within each, in relation to the title of the thesis: Do the sedimentary rocks of the Sunda subduction zone preserve a record of early Himalayan erosion? A review of the main findings of the thesis is presented as well as a discussion on further directions of study, and any questions that remain on completion of the project.

Following Chapter 6, the appendices section contains methodology and data for the laboratory techniques used (petrography and heavy mineral analysis, ^{40}Ar-^{39}Ar analysis, Sm-Nd isotope fingerprinting, zircon fission track, zircon U-Pb analysis, U-Th-He, illite crystallinity and biostratigraphy) as well as inventory of samples, and an archive of seismic material not contained within the papers but used elsewhere in the thesis or for presentations during the duration of the PhD. Finally, a list of conference abstracts/proceedings and papers including those by the author and in preparation by the author is included (Najman *et al., in press*; Curray and Allen, *in review.*)

1.2 The Himalaya

The collision between India and Asia has resulted in one of the physically longest active orogens on the planet becoming nature's laboratory for understanding mountain building processes in older collisional orogenic belts. Behind the hinterland of the Himalaya is the Tibetan Plateau – partly internally drained, of low relief and the highest elevated surface on Earth. The largest rivers that drain the Himalaya from the west and east are the Indus River and Ganges River and the Brahmaputra/Jamuna respectively. The major sedimentary repositories for eroded material from the south flank of the Himalaya include the peripheral foreland basin, remnant ocean basins

such as the Bengal Basin and Katawaz Basin and deep sea fans such as the Indus Fan and the Bengal Fan, the largest submarine fan in the world. The Himalaya and surrounding sedimentary repositories represent a complicated tectonic region with numerous salient features summarised in Figure 1.1 and discussed below. Section 1.2.1 and 1.2.2 will discuss further the features of the Himalaya relevant to this study.

1.2.1 The Geology of the Himalaya

Tectonic History

The Himalaya, running ~2500 km from the Nanga Parbat western syntaxis to the eastern Namche Barwa syntaxis (Figure 1.1), was formed due to the continental collision of the north-journeying Indian plate and relatively stable Eurasia in the Tertiary after the closure of the Tethys Ocean which lay between the two continents. Island arcs are caught up in the line of collision between the two continents now represented by the Indus-Yarlung suture zone (see Figure 1.1) that extends for ~3000 km from southern Pakistan to southern Burma. The eastern and western edges of the Himalaya are mainly transpressional boundaries characterised by accretionary prisms and strike slip faults. In the east the orographic bend diffuses into a series of north-northeast trending ranges in Assam (India), Kachin and Shan (Myanmar) and Yunan Province (China). The Chittagong Hill Tracts (SE Bengal Basin, Bangladesh) accretionary prism is one such transpressional feature in the east and the focus of this project, along with the Indo-Burman Ranges of western Myanmar and the Andaman Islands further south. Equivalent transpressional features in the west include the Makran wedge and the Chaman Fault, and mountain ranges such as the Karakoram and Hindu Kush.

The collision of India and Eurasia has been an ongoing process since the Tertiary, but the exact timing of collision of India and Eurasia is much disputed and controversial. Concepts such as 'hard' and 'soft' collision (Lee and Lawver, 1995), a "Greater India" (e.g., Argand, 1924; Besse and Courtillot, 1988; Klootwijk *et al.,* 1992; Zhou and Murphy, 2005; Ali and Aitchinson, 2006) and issues of diachroneity of collision (Searle *et al.,* 1997; Rowley, 1998) from west to east are made more complicated by the sheer size of the mountain belt. Data are offered from disciplines as varied as biostratigraphy and structural geology, with faunal assemblages and subduction-related magmatism each contributing data to constrain deposition and deformation.

Rapid decline of spreading rates on the SW Indian Ridge (Patriat and Achache, 1984) with a coeval slowdown in India's northward migration (Klootwijk *et al.,* 1992; Acton, 1999) constrained early estimates of collision to between 55-57 Ma. The cessation of marine facies in the Tethyan Himalaya provided evidence for hard collision at ~ 52 Ma (Rowley, 1996) and the development of flexure-related unconformities in the suture zone and Tethyan Himalaya (Garzanti *et al.,* 1987; Searle *et al.,* 1997) as well as pressure-temperature-time paths of eclogites in the same region gave further evidence of initial collision in the subduction regime at around 55 Ma, followed by a collisional regime at ~47 Ma (De Sigoyer *et al.,* 2000). Most researchers consider the timing of collision to be between 55-50 Ma, although some cite evidence for collision as early as 70 Ma (Yin and Harrison, 2000; Ding *et al.,* 2005) or as late as the Oligocene ~ 34-24 Ma (Aitchison *et al.,* 2007).

Subduction of India beneath Asia continues at present with India subducting obliquely beneath Asia. In the region of the Andaman Islands continental collision has not occurred.

Metamorphism in the Himalaya

Prior to the collision of India and Eurasia deformation occurred in the Transhimalaya and suture zone. This is manifested in south to southwest-directed fold-thrust structures recording a history of crustal shortening (England and Searle, 1986). Collision in the Eocene marked the onset of a widespread and continuous Barrovian metamorphic event in the Himalaya resulting in a full suite of metamorphic facies similar to those in Scotland as described by Barrow (1893). Two major stages within the Himalaya are described by Hodges (2000) as the EoHimalayan phase of burial and heating and the NeoHimalayan phase of crustal melting and emplacement of leucrogranites. Generally speaking however, the two major phases of Barrovian metamorphism can be constrained to ~30-25 Ma and a later phase from ~23-12 Ma (Hodges *et al.,* 1996; Searle 1996, 1997; Godin *et al.,* 1999; Foster *et al.,* 2000). Young metamorphism and rapid exhumation at around 10 Ma is also evident in both the east and west syntaxes (Searle *et al.,* 2006)

Geological Units

The Himalaya itself is a structure of southward propagating thrust sheets formed as a result of crustal thickening initiated post-collision in the Eocene (Ratschbacher *et al.,* 1994; Searle *et al.,* 1997). The best maps of the geology are based on areas of good exposure, which is variable across the whole range and within different units. For example in the Greater Himalaya, exposure in places is 100% particularly around the central Himalaya; however, exposure of foreland rock sequences and structures are best in the western Himalaya, and get poorer moving eastward and as a result less is known about the geology of the eastern Himalaya.

Figure 1.2 shows the main Himalayan units. From north to south the geology is as follows.

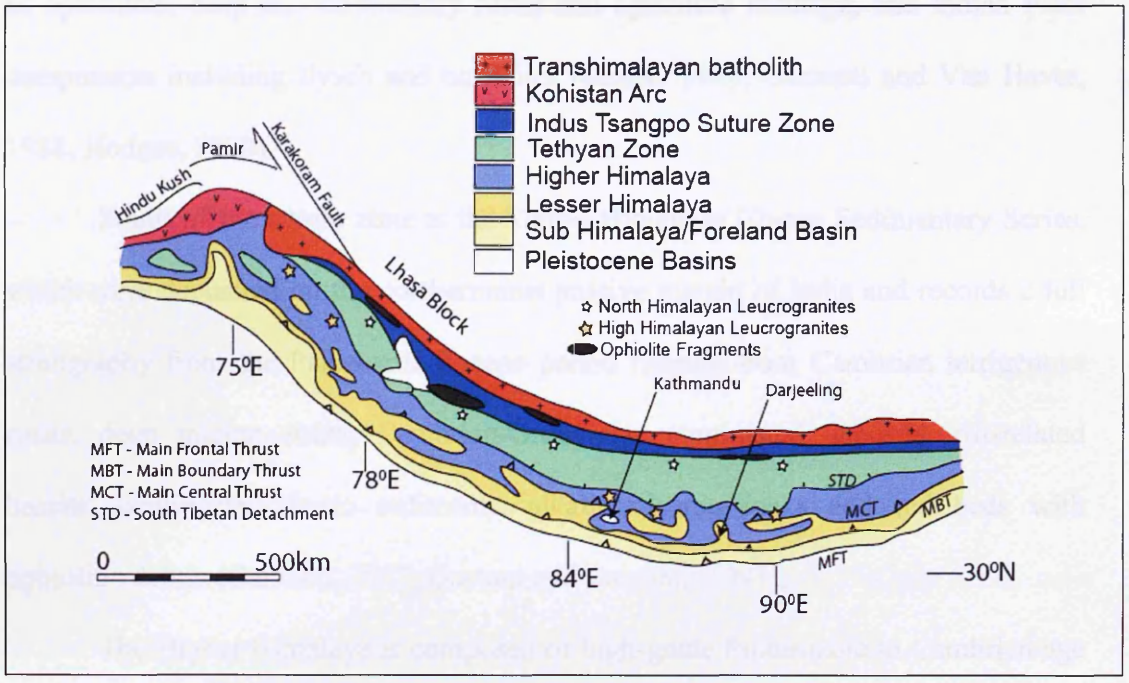

Figure 1.2 The geotectonic units of the Himalaya (adapted from Searle *et al.*, 2003) and main fault systems which separate the units.

In the north, metamorphic and sedimentary terrains such as the Lhasa Block represent Asian crust. Moving southward, the Transhimalaya represent the Andean-type continental arc of the Asian active margin (Searle *et al.*, 1991), which marks the point where Tethyan oceanic lithosphere were subducting, and as such contains volcanic and plutonic elements of this arc, metamorphosed country rock and Cretaceous-Tertiary forearc basin sediments.

The limit of Asian crust is then marked by the Indus-Yarlung Suture Zone, which separates the Asian crustal material from the northern extent of the Indian crust. The suture zone can be traced diachronously for approximately 3000 km from

Afghanistan to Burma. The suture zone itself is chiefly composed of Transhimalaya sedimentary rocks and volcaniclastic strata, Neotethyan ocean floor components such as ophiolites, deep-sea sedimentary rocks and ophiolitic melange, and Indian Plate components including flysch and turbidites (Searle, 1983; Garzanti and Van Haver, 1988; Hodges, 2000).

South of the suture zone is the Tethys Himalaya/Tibetan Sedimentary Series, which were deposited on the northernmost passive margin of India and records a full stratigraphy from the Palaeozoic-Eocene period ranging from Cambrian terrigenous rocks, deep marine strata, Cambrian-Ordovician continental deposits, rift-related basalts, continental clastic sediments, alkali volcanic rocks and red beds with ophiolitic debris (Garzanti, 1987; Gaetani and Garzanti, 1991).

The Higher Himalaya is composed of high-grade Proterozoic to Cambrian age metasedimentary and meta-igneous rocks with attendant leucrogranites (Parrish and Hodges, 1996; Searle *et al.,* 1999a). The base of the sequence is largely composed of clastic metasedimentary rocks. Biotite-muscovite gneiss is prevalent. Above this calc-alkaline gneiss is the dominant rock type. Stratigraphically overlying this is augen orthogneiss (Le Fort, 1994). However, across the range the stratigraphy of the greater Himalaya will vary locally.

South of the Greater Himalaya lie the predominantly metasedimentary low-grade (greenschist facies) to unmetamorphosed Indian crustal Lesser Himalaya that preserves a stratigraphy approximately 8-10 km thick and comprises of clastic metasedimentary units, including quartzites, phyllites and schists and high-grade crystalline nappes (Gansser, 1964; Colchen *et al.,* 1986) and Palaeogene foreland basin sedimentary rocks (Sakai, 1989). Age constraint in the Lesser Himalaya sequence is poor due to a paucity of fossils and as such much controversy remains on

the relationship between this sequence and the Tibetan Sedimentary Series, as well as the ages of its constituent parts.

Furthest south are the Subhimalaya, dominated by the Foreland Basin. This foreland basin, which will be discussed in greater detail, contains sedimentary sequences, which thicken from south to north to excesses of 10 km near the contact with the Lesser Himalaya. Sedimentary rocks of Palaeogene and Neogene age are predominantly eroded from the rising Himalaya (Burbank *et al.,* 1996).

1.2.2 The Sediment Repositories

The peripheral foreland basin

A peripheral foreland basin is formed in a collisional mountain belt in response to flexural loading of the lithosphere by the adjacent thrust belt (Beaumont, 1981). The Himalayan foreland basin stretches east west across the entire length of the Himalaya (Figure 1.1), receiving sediment predominantly from the southern margin of the orogen. The majority of the foreland basin rocks are located in the Sub Himalaya (Figure 1.2), however significant outcrop is also found in the Nepalese Lesser Himalaya. The peripheral foreland basin can be broadly split into Palaeocene-Eocene marine strata and Oligo-Miocene alluvial strata, largely comprised of the uniform Neogene Siwalik Group. The two divisions are separated by a basin–wide unconformity, leaving the Oligocene (~ 34–24 Ma) unrepresented in the stratigraphy throughout the foreland (Najman, 2006). The Palaeogene and Neogene foreland basin sedimentary rocks from Pakistan, India and Nepal record erosion of the southern flanks of the Himalaya by transverse (formation cross-cutting) river transport and as such their Himalayan provenance is on the whole, well documented (Critelli and Garzanti, 1994; Critelli and Ingersoll, 1994; DeCelles *et al.,* 1998a,b, 2004; Najman *et*

al., 1997, 2001, 2002a, 2003, 2004, 2005; Najman and Garzanti, 2000; Robinson *et al.,* 2001; Szulc *et al.,* 2006; White *et al.,* 2001, 2002). They therefore provide provenance characteristics that are useful for comparison with rocks from this study, when assessing Himalayan contribution. The coeval rocks used for comparison are:

- The Bhainskati Formation (~49–43 Ma), Nepal (Sakai, 1983)
- The Oligo-Miocene (~20–16 Ma) Dumre Formation, Nepal (DeCelles *et al.,*2001; Najman *et al.,*2005; T. P. Ojha unpublished data cited in DeCelles *et al.,*2001)
- The Neogene (~16–4 Ma) Siwalik, Nepal (e.g., Gautam and Fujiwara, 2000; Quade *et al.,*1995; DeCelles *et al.,*1998b)
- The Subathu (~53–45 Ma) and Dagshai Formations (<30 Ma), India (Mathur, 1978; Batra, 1989 and Najman *et al.,* 1997)

The provenance characteristics of these formations are well documented with associated references in Chapter 3, 4 and 5.

The Suture Zone

The Indus-Yarlung Suture Zone (Figure 1.1) is the main suture zone that represents the contact between India and Eurasia. It runs the length of the Himalaya and records the transition from pre-collisional marine sediments to syn-collision and post collisional continental input. The major rock sequences are Transhimalayan forearc sequences, Neotethyan ocean floor components and Indian plate components. Stratigraphy in the suture zone is variably age constrained and suffers from a collection of local names. In northwest India (the most intensively studied region of the suture zone) the Chogdo Formation is the first continental sedimentary unit above

a completely marine succession and dated at 54.9 Ma (O. Green cited in e.g., Clift *et al.,* 2001). The stratigraphy between the Palaeocene Chogdo Formation and the early Miocene Uppermost Nimu Formation (equivalent Gangrinboche Conglomerate in south Tibet) is well documented by e.g., Sinclair and Jaffey (2001) and Clift *et al.* (2000, 2001, 2002a).

The remnant ocean basins

Remnant ocean basins develop in mountain belts as a result of diachronous development of the main fold-thrust belt in an orogen (Ingersoll *et al.,* 1995). Major rivers transport eroded material axially relative to the basin axis. In this sense, western Himalayan sediment was transported by the Indus River to the Katawaz remnant basin and the Makran (Figure 1.1). The Katawaz basin consists of Eocene-Oligocene deltaic and submarine fan turbidites, overlain by Lower Miocene shallow marine sedimentary rocks (Qayyum *et al.,* 1996) and the Makran preserves Oligocene deep sea turbidites and the Miocene to Recent Makran Group accretionary complex (Critelli *et al.,* 1990).

In the eastern Himalaya, the Ganges and Brahmaputra Rivers deposit sediments to the remnant ocean Bengal Basin (Figure 1.1). The Bengal Basin (e.g., Johnson and Nur Alam, 1991; Reimann, 1993; Uddin and Lundberg, 1998, 2004; Gani and Alam, 2003, 2004) is of relevance to this study, particularly with regard to objective 2. It is thought that the Bengal Basin/Floodplain system of Bangladesh traps 70% of sediment flux from the eroding eastern Himalayan orogeny, with the remainder in the Brahmaputra itself and the deep sea fan (Galy and France-Lanord, 2001) Section 1.4.3 and Chapter 5 provide a detailed background to the geology and evolution of the Bengal Basin.

The deep sea fans

Eroded material from the east and west Himalaya ultimately finds its sink in the deep sea Indus Fan and Bengal Fan respectively (Figure 1.1). This detrital record may therefore provide valuable information needed to reconstruct the uplift and erosion history of the Hinterland. The thickness of sediment, and former technological constraints in both has so far precluded deep drilling to the absolute base of either, with the Indus drilled to an approximate depth that has been dated as Upper Oligocene (Whitmarsh *et al.,* 1974), and the Bengal Fan drilled base dated to ~17 Ma (Curray and Moore, 1971). As a result of this, the date of initiation of both fans remains elusive and much debated. Best estimates suggest that Bengal Fan deposition may have been initiated as early as Palaeocene to Mid Eocene pre-45 Ma based on the presence of a lower fan hiatus which appears to separate pre-fan from fan sediments (Cochran, 1990; Curray and Moore, 1971, Curray *et al.,* 2003). However, the initiation of sedimentation was likely diachronous, starting in the Early Eocene in the northern Bay of Bengal and during the Oligocene in distal portions of the fan (Curray, 1994). Furthermore, the Bengal Fan has had more than one submarine canyon feeding the fan over time (Curray *et al.,* 2003), and as such the locus of deposition has shifted with time, leading to the abandonment of parts of the fan (such as the southeastern sub-Nicobar fan portion). The current feeder canyon is the Swatch of No Ground lying on the Bangladesh continental shelf (Figure 1.3). The onset of the Indus Fan is also difficult to constrain but may have been as early as the middle Eocene based on suture zone sediments present on the Murray Ridge (Figure 1.1), which indicates deposition must have occurred by this time, enabling the Indus River to feed sediment into the Indus Basin and out to the Indus Fan (Clift *et al.*, 2001b).

The eastern Bengal Fan is one of the largest sedimentary repositories in the world, at 3000 km in length it is considerably larger than the Indus and despite the fact it is currently showing slower accumulation rates than the Indus, it has a volume of ~ 12.5 x 10^6 km^3 (Curray *et al.,* 2003). The Bengal Fan is presently subducting beneath Asia at its eastern margins, and it has long been suggested that the offscraped material has led to the development of an accretionary prism complex that is today represented by the sedimentary rocks of Bangladesh, western Burma and the Andaman Islands.

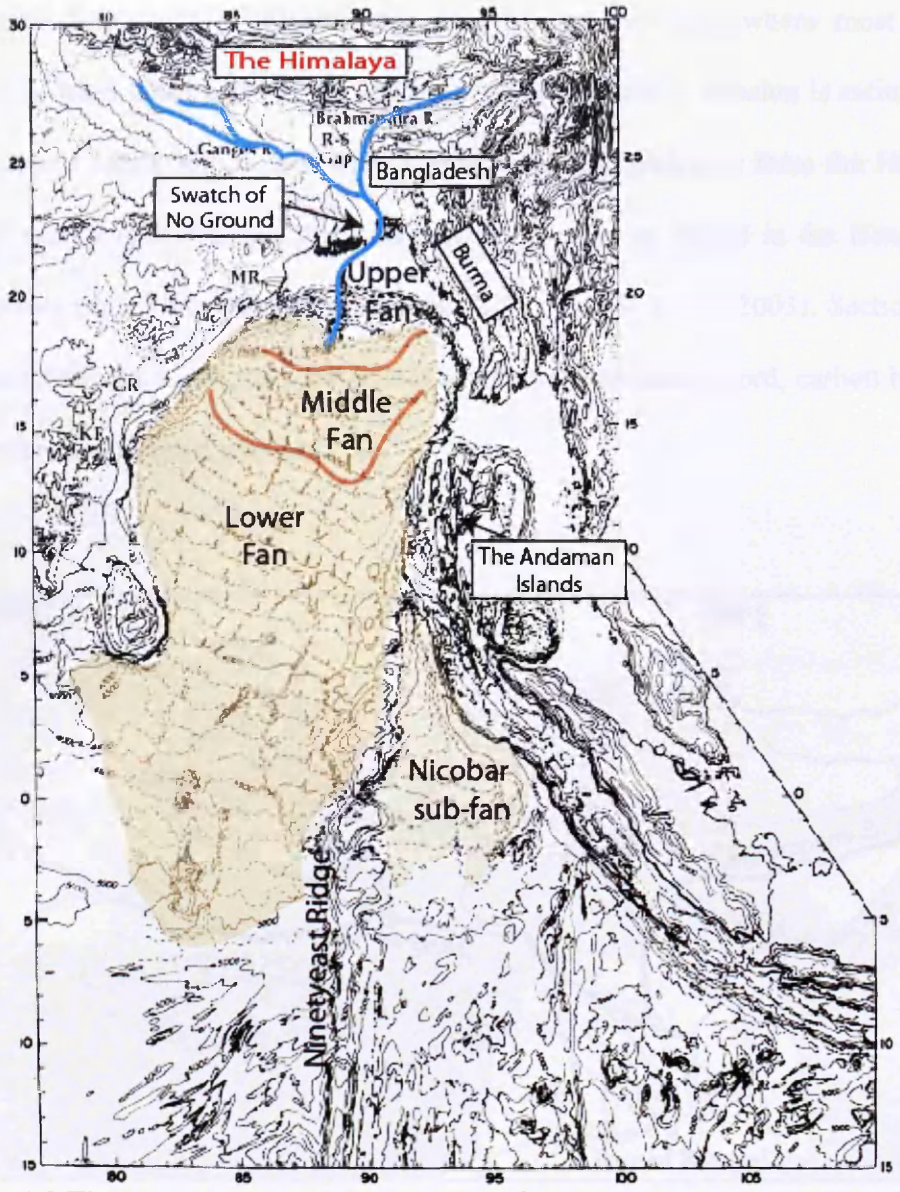

Figure 1.3 The Bengal Fan and Nicobar sub-fan. The present day feeder canyon 'Swatch of No Ground' is highlighted and the upper, Middle and Lower Bengal Fan (Adapted from Curray *et al.*, 1982)

Major drainage systems

Many rivers cross the Himalaya and remove and redistribute eroded material from across the region; however the Brahmaputra and Ganges River are the major drainage system for material eroded from the eastern Himalaya, and both exit through the Bengal Basin, Bangladesh (Figure 1.4). Himalayan rivers, especially the Brahmaputra, are characterized by very high topographic gradients on the south

Himalayan flank, which collect monsoonal precipitation and where most of the physical erosion takes place (Galy and France-Lanord, 2001). Erosion is estimated to be between 1 and 2 billion tons of sediments exported each year from the Himalaya through the Ganges-Brahmaputra system and this ends up buried in the Bengal Fan sedimentary unit (Galy and France-Lanord, 2001; Curray *et al.,* 2003). Section 1.3.1 explains in greater depth the relationship between the erosion record, carbon budgets, and climate and ocean chemistry.

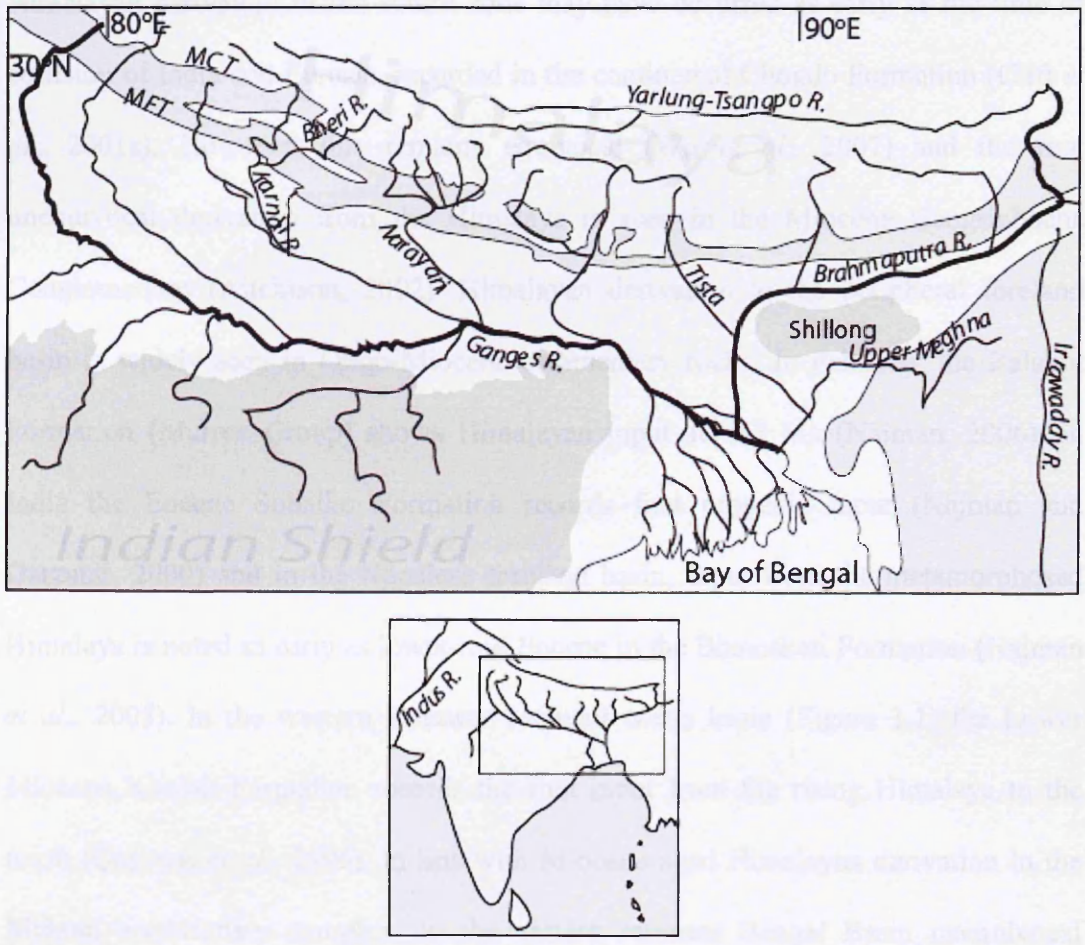

Figure 1.4 Major drainage of the eastern Himalaya

Other suggested but disputed sedimentary repositories of eastern Himalayan erosion include the Indo-Burman Ranges (Burma) and the Andaman Islands. Both lie along the Sunda subduction zone that runs from Myanmar to Sumatra (Figure 1.1). These are the regions that have been studied for this thesis.

1.2.3 Initiation of Himalayan Erosion in the Sedimentary Repositories

The point at which erosion of the Himalaya is first recorded in the sedimentary repositories has been studied variably across the mountain belt, and is much debated. Himalayan derivation in the suture zone may have occurred as early as the time of collision of India and Eurasia, recorded in the continental Chogdo Formation (Clift *et al.,* 2001a). However, this remains equivocal (Wu *et al.,* 2007) and the first unequivocal derivation from the Himalaya is seen in the Miocene Gangrinboche Conglomerates (Aitchison, 2002). Himalayan derivation to the peripheral foreland basin is widely seen in Oligo-Miocene sedimentary rocks. In Pakistan, the Balakot Formation (Murree Group) shows Himalayan input at ~37 Ma (Najman, 2006). In India the Eocene Subathu Formation records first orogenic input (Najman and Garzanti, 2000) and in the Nepalese foreland basin, input from the metamorphosed Himalaya is noted as early as lower-mid Eocene in the Bhainskati Formation (Najman *et al.,* 2005). In the western Katawaz remnant ocean basin (Figure 1.1) the Lower Miocene Khojak Formation records the first input from the rising Himalaya to the north (Qayyum *et al.,* 1996), in line with Miocene aged Himalayan derivation in the Makran accretionary complex. In the eastern remnant Bengal Basin unequivocal Himalayan derivation has recently been found in the Oligocene Barail Formation at ~38 Ma (Najman *et al.,* in press, co-authored paper). In the Bengal Fan, the onset of Himalayan erosion is recorded unequivocally by ~18 Ma (e.g., Copeland and

Harrison, 1990) but drilling restrictions at present preclude finding an earlier unambiguous record of Himalayan erosion in the Bengal Fan itself. However, it has been suggested that the Andaman Islands, Indo-Burman Ranges (Burma) and Chittagong Hill Tracts (Bangladesh) preserve sediments of the early Bengal Fan as an accretionary complex, and as such these regions may preserve a record of Himalayan erosion, discussed earlier in Section 1.1.2 and in later chapters. The onset of Himalayan derivation in the Indus Fan is also difficult to constrain but may have been as early as mid-Eocene pre-45 Ma to Oligocene (Clift *et al.,* 2001b; Daley and Alam, 2002).

1.3 Erosion and Orogenesis

The term orogenesis pertains to the process of mountain formation, especially by folding and faulting of the Earth's crust and by plastic folding, metamorphism, and the intrusion of magmas in the lower parts of the lithosphere. The processes that control mountain building are becoming increasingly understood largely as a result of improvements in quantitative modelling of lithospheric deformation, as well as a more thorough understanding of the mechanical behaviours of crustal materials (Harris, 2007). Within this context it is now possible to assess the role of surface erosion and its coupling with crustal deformation. Studying the process and products of erosion in a mountain belt is critical to our understanding of mountain building and mountain destruction over time (e.g., models of crustal deformation) and the consequences of the mountain 'life-cycle' on, e.g., the regional geology, climate, palaeodrainage, seawater chemistry. Erosion can both degrade the mountain system but may also be one process involved in mountain building, e.g., tectonic erosion causing bouyanct driven uplift.

1.3.1 The importance of the erosion record: A Summary

Throughout the evolution of any given mountain belt, its history is marked by a series of processes and events that have led to the mountain belt seen in the present day. However, information on its early evolution history is often lost in the mountain belt itself due to erosion literally removing the record, or by metamorphic overprinting during the phase of mountain building. It is for this reason that the sedimentary record of material eroded from a mountain belt is vital for understanding the early development of a mountain belt such as the Himalaya.

By conventional reason a mountain range that exceeds a critical height should erode and collapse within a few million years as a result of gravitational spreading of its crustal root (Burov *et al.,* 2007). However, this is not the case in nature and mountains persist over geologically significant timescales in the order of tens of millions of years (Burov *et al.,* 2007). A need to explain this paradox has led to the reassessment of the conventional thought that tectonics results in topography, which leads to erosion and denudation. It is now recognised that the relationship between tectonics and erosion is far more dynamic - where tectonics may force erosion and/or erosion may force tectonics, and where erosion can exceed tectonic exhumation in the process of unloading and cooling of a rock within an orogenic setting (Burbank, 2002; Wobus *et al.*, 2003; Thiede *et al.*, 2005). Specifically, high erosion rates may reinforce the effect of erosion processes on the unloading and isostatic rebound that partially control the tectonic evolution of the orogen as a whole (Avouac and Burov, 1996).

However, many variables complicate the study of the erosion record including the quantity and nature of erosion as well as complex arguable concepts such as isostatic rebound and lateral ductile flow in the Earth's crust, and as such a variety of

models have been developed which differ in the processes at work, and the extent to which erosion coupled with tectonics plays a role.

In the Himalaya, a continuing understanding of the volume and process of erosion from the mountain belt is not just important for constraining models of crustal deformation and evolution (Section 1.3.2) but is also important for understanding the role of orogenesis in changes to seawater chemistry (Richter *et al.,* 1992) and observed climate perturbations (Raymo and Ruddiman, 1992) since collision initiated at ~55-50 Ma (Garzanti *et al.,* 1987; Klootwijk *et al.,* 1992; Searle *et al.,* 1997) discussed in Section 1.3.3-1.3.5.

1.3.2 The Importance of the erosion record for models of crustal evolution

Our understanding of the creation and subduction of oceanic lithosphere has advanced rapidly over the past few decades but the processes that control mountain building within the continents remain highly contentious, in particular the role of erosion in influencing the distribution of crustal deformation is widely debated (e.g., Zeitler *et al.,* 2001). However, recent developments in quantitative modelling of lithospheric deformation, coupled with an improved understanding of the mechanical behaviour of crustal materials, have provided a context within which the interactions between surface erosion and deep crustal deformation can now be explored (Harris, 2007). The importance of erosion in each major model of crustal deformation varies from being a key process to explain the exhumation of the Higher Himalaya (Channel Flow, e.g., Beaumont *et al.*, 2001, and Cold Dense Root Model, e.g., Chemenda *et al.*, 2000), to being a process that exists in response to topography but is not required to explain crustal deformation patterns seen in the Himalaya since collision (e.g., lateral extrusion model, e.g., Tapponnier *et al.*, 1982). Models of crustal deformation

therefore vary in the timing and extent of required erosion and studying the erosion record can therefore provide valuable input parameters for models, which vary in the required onset and extent of erosion. It is important to know when erosion in the Himalaya started in order to test the applicability of the models to the Himalayan system. A brief discussion follows on the main models of crustal deformation that have been applied to the study of Himalayan orogenesis. The relative importance of erosion in each model is also discussed.

The Lateral Extrusion Model

The concept of crustal deformation in the Himalaya by the lateral extrusion of continental crust can be achieved by motions of coherent blocks separated by long and narrow fault zones (Figure 1.5a), along which deformation remains localized at any given time (Replumaz and Tapponier, 2003; Tapponier *et al.,* 1982; Pelzer and Saucier, 1996).

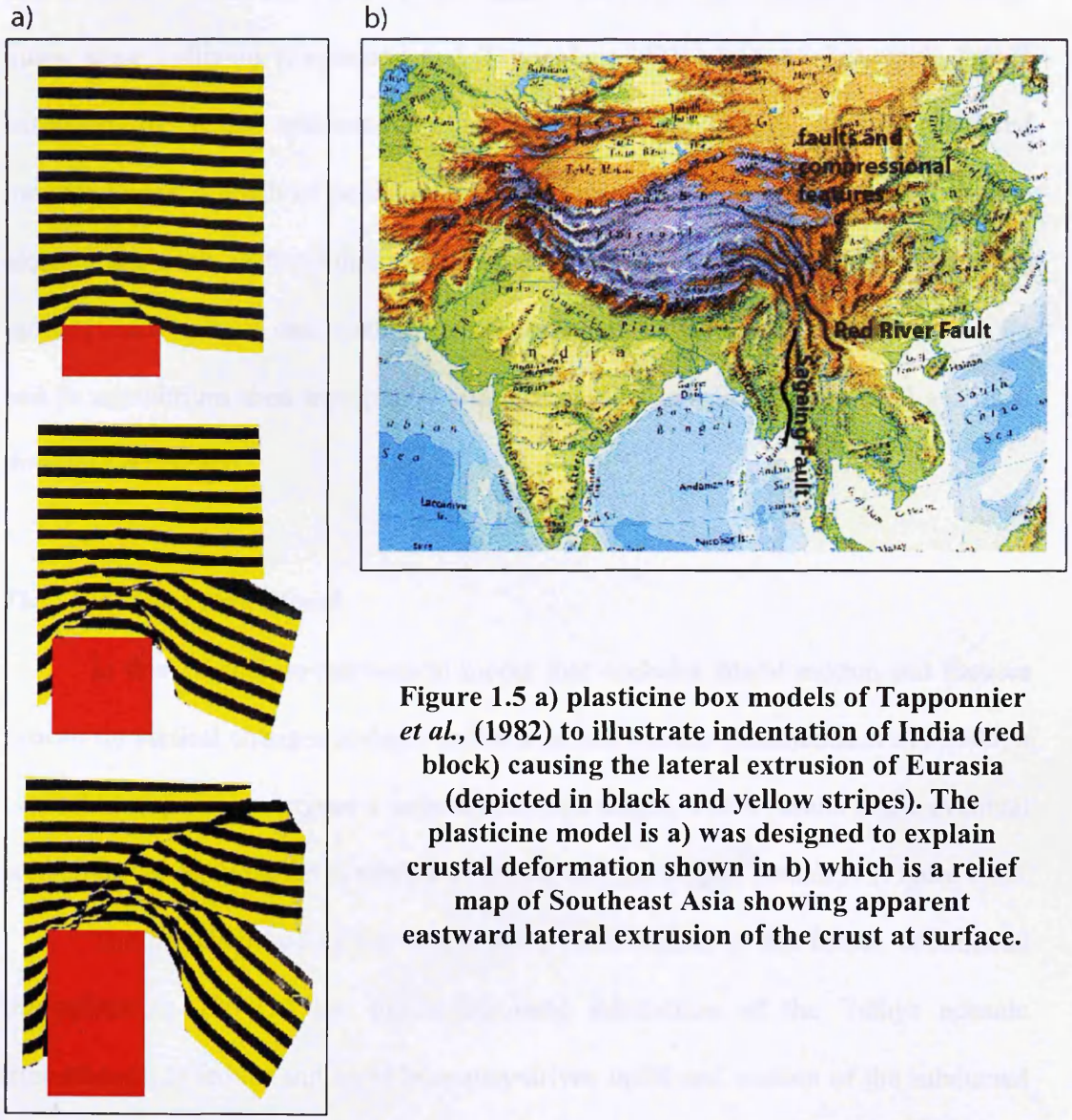

Figure 1.5 a) plasticine box models of Tapponnier *et al.,* (1982) to illustrate indentation of India (red block) causing the lateral extrusion of Eurasia (depicted in black and yellow stripes). The plasticine model is a) was designed to explain crustal deformation shown in b) which is a relief map of Southeast Asia showing apparent eastward lateral extrusion of the crust at surface.

Finite block motion data has grown in recent years and it has now been possible to retro-deform much of the area affected by collision of India and Asia, by using a block model governed by plate tectonics. Moving back in time since collision at ~ 50 Ma it is possible to test the behaviour of the lithospheric blocks in order to reach a plausible model of crustal deformation. Initial results suggest that on average lateral extrusion along rigid lithospheric blocks has accounted for ~30% of the convergence of India and Asia, but this figure varied between 3% and 60% at different times since collision (Replumaz and Tapponier, 2003). In a model where lateral extrusion of mass accommodates convergence, topography is not required immediately as a result of collision, and therefore may be absent. If lateral extrusion along faults such as the sinistral Red River Fault and Sagaing Fault (Figure 1.5b) (among many others) can 'soak up' early stages of convergence to keep a mountain belt in equilibrium then topography and erosion need not be invoked until a critical threshold is reached.

The Cold Dense Root Model

In this 2D thermo-mechanical model that excludes lateral motion and focuses instead on vertical changes at depth in the crust and mantle (Chemenda *et al.,* 2000) a layered lithosphere undergoes a series of tectonic stages, which results in the eventual erosion driven exhumation to surface of the Crystalline Higher Himalaya (Figure 1.6).

The principal successive stages are (1) subduction of the Indian continental lithosphere to 200-250 km depth following subduction of the Tethys oceanic lithosphere; (2) failure and rapid buoyancy-driven uplift and erosion of the subducted continental crust from ~ 100 km depth to depth that varies along the mountain belt (20-30 km on average) with attendant erosion (3) break-off of the Indian subducted

lithospheric mantle with the attached oceanic lithosphere; (4) subduction/underplating of the Indian lithosphere under Asia over a few to several hundred kilometers; (5) delamination, roll-back, and break-off of the Indian lithospheric mantle; (6) failure of the Indian crust in front of the mountain belt (formation of the main central thrust) and underthrusting of the next portion of Indian lithosphere beneath Tibet for a few hundred kilometers. Underplating results in crustal thickening below the Himalayas, which results in the formation of high, intensively eroded relief. Erosional unloading at the end of stage (6) then triggered both the exhumation of the Crystalline Himalayas and the formation of the South Tibetan normal fault system, after a long process of prior deformation (Chemenda *et al.,* 2001).

In this model erosion is activated as buoyancy-driven uplift is created by the failure of the continental root, at between 40-25 Ma. Erosion then continues more intensively with increasing uplift until it drives the exhumation of the Higher Himalaya.

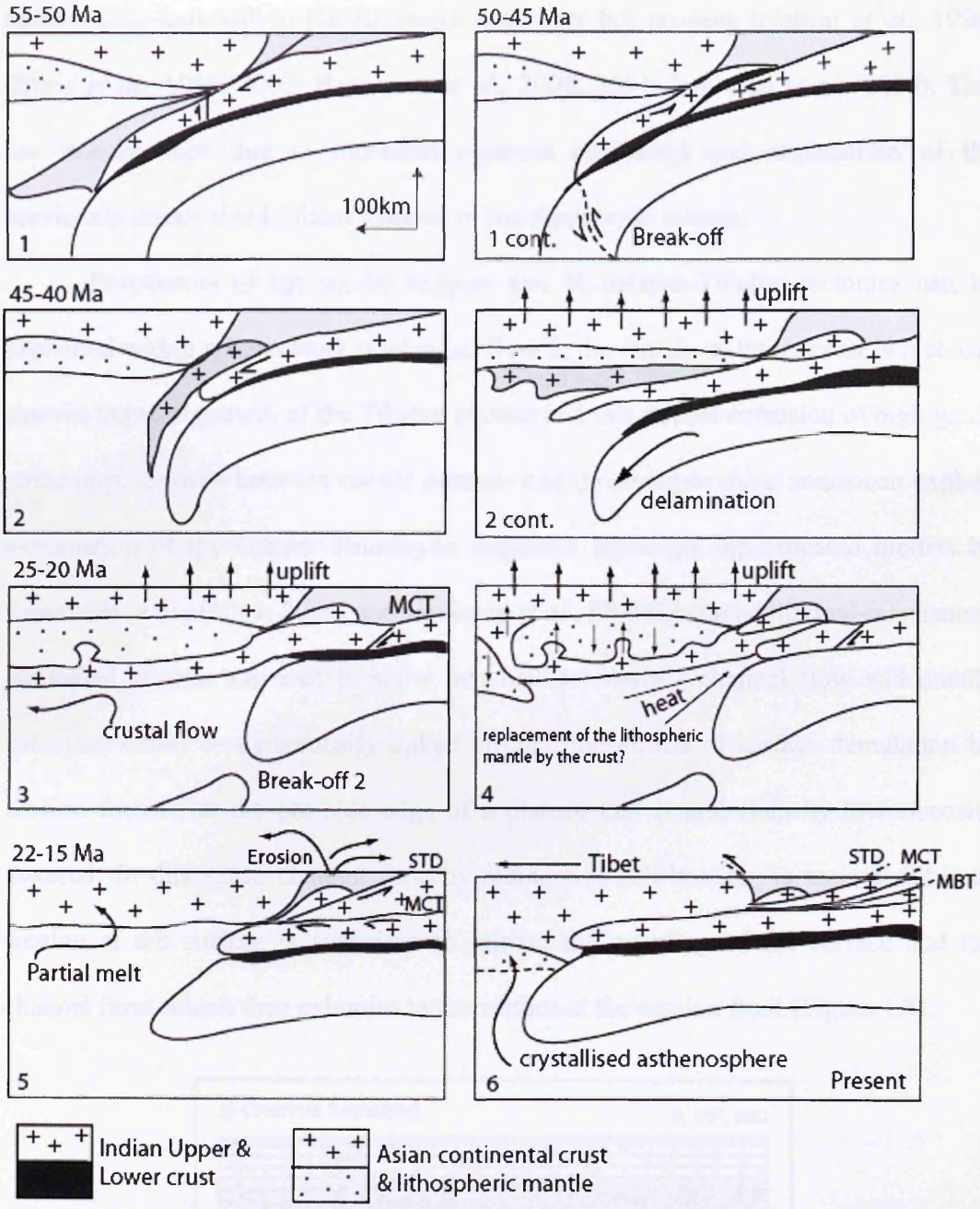

Figure 1.6 Cold dense root model (Chemenda *et al.*,2000)

The Channel Flow Model

Although crustal deformation by flow of the Earth's crust along channels has been previously suggested (Bird, 1991; Burov and Diament, 1995) it is only relatively recently that channel flow models have risen in popularity to explain crustal

deformation style within the Himalaya and other hot orogens (Nelson *et al.*, 1996; Grujic *et al.*, 1996, 2002; Beaumont *et al.*, 2001, 2004; Jamieson *et al.*, 2004). This has mainly been due to increased rigorous modelling and explanation of the previously unexplained salient features of the Himalayan system.

Proponents of the model suggest that Himalayan-Tibetan tectonics can be explained within a framework of channel flow in the middle to lower crust, which can explain outward growth of the Tibetan plateau and that ductile extrusion of high-grade metamorphic rocks between coeval normal- and thrust sense shear zones can explain exhumation of the Greater Himalayan sequence. In recent sophisticated models by Beaumont *et al.*, (2001, 2004) and Jamieson *et al.*, (2006) coupled thermal-mechanical numerical models are used to show that two processes - channel flow and ductile extrusion - may be dynamically linked through the effects of surface denudation by erosion focused at the pro-side edge of a plateau that is underlain by low-viscosity material. In this sense channel flow by radioactive self-heating, is maintained until erosion at the surface is sufficient to initiate the coupling of the surface and the channel flow, which then exhumes to the surface at the erosion front (Figure 1.7).

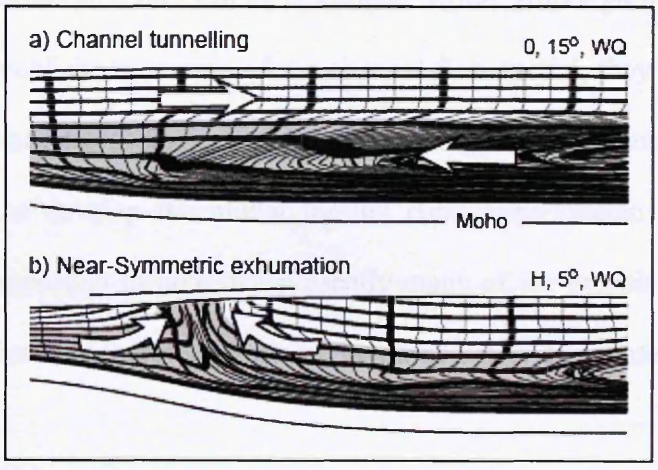

Figure 1.7 Crustal flow and the coupling of the channel at the erosion front at surface (Beaumont *et al.*, 2001)

This model allows for moderate erosion while topography grows sufficiently to maintain crustal flow by 'melt weakening' caused and maintained by approximately 10^{19} Pascals of overburden pressure, which reduces viscosity within mid-crustal levels. If intense erosion is initiated too early in the model, flow is unable to be maintained, and if erosion is too low may result in abandonment of the extrusion zone. In the most up-to-date model orogenic erosion is initiated at ~30 Ma in-keeping with observable geological features and remains at a high rate until 15 Ma, when it then gradually declines (Jamieson *et al.,* 2004, 2006). Whilst many support erosional advection processes that create the southward propagation of the mid crustal flow (e.g., Searle and Szulc, 2005) others still dispute it and the model remains controversial (Harrison, 2004). For example, Robinson *et al.,* (2006) finds the geometry and kinematic history of the thrust belt in western Nepal to be incompatible with recent models for southward ductile extrusion of Greater Himalayan rocks in a mid-crustal channel. Instead it is suggested that the thrust belt in western Nepal behaved like a typical forward propagating thrust system, involving unmetamorphosed, brittlely deformed rocks in its frontal part and ductile deformed, higher-grade metamorphic rocks in its hinterland region. Although their results do not support current published versions of the channel flow model, they maintain that the data provide additional geological and geochronological constraints that may assist future attempts to develop the model for the Himalayan-Tibetan orogenic system. However, it is important to note that presently many of the models are valid aunder different conditions and therefore none can be immediately discounted but instead rely on more data.

Testing the hypothesis that erosion coupled with climate can exert fundamental control on orogen-scale tectonics requires the development of reliable techniques for

quantifying tectonic and geomorphological processes on a range of scales (Ruhl and Hodges, 2005). Detrital mineral dating techniques are one such way of illuminating erosion-tectonic mechanisms and are the chosen method for this thesis.

1.3.3 Erosion and marine geochemistry

The Himalaya is an important source of strontium to the world oceans. Both the Ganges and Brahmaputra, which drain the Himalaya are characterized by high strontium concentrations and $^{87}Sr/^{86}Sr$ ratios. It has been suggested that since uplift of the Himalaya, erosion has increased significantly enough to cause the rise in the global marine $^{87}Sr/^{86}Sr$ values since ~40 Ma (Richter *et al.,* 1992). Testing this hypothesis, and differentiating the Himalayan erosional flux from a global silicate weathering flux (Galy *et al.,* 1999), requires detailed information on the onset of Himalayan erosion and the extent to which it occurred throughout the Tertiary. Constraining the time of earliest erosion of the Himalaya is key to determining whether uplift of the Himalaya *could* be responsible for changes to global ocean geochemistry since ~40 Ma.

1.3.4 Erosion and the global carbon budget

Continental erosion controls atmospheric carbon dioxide levels through silicate weathering, riverine transport and subsequent burial of organic carbon in oceanic sediments (Hayes *et al.,* 1999). Himalayan erosion generates the largest known flux of sediments to the global oceans, with 1-2 billion tonnes of sediments exported each year from the Ganges-Brahmaputra river system, which is ultimately buried in the Bengal Fan (Curray *et al.,* 2003). A record of Himalayan erosion is, therefore, vital for quantifying the effect of this huge sediment flux to the oceans on the global carbon

budget. Without an accurate record of when erosion in the Himalaya was initiated and where all of the erosional products are stored today, it is difficult to fully quantify satisfactorily the impact of the uplift of the Himalaya on the global carbon budget taking into account all the sedimentary repositories. The Bengal Fan alone in the last 15 million years is thought to have buried ~15% of the global carbon burial flux (France-Lanord and Derry, 1997). Recent work suggests the amount of organic carbon deposited in the Bengal Basin represents 10-20% of the total terrestrial organic carbon burial in oceanic sediments (Galy *et al.,* 2007). The Himalayan erosion record is, therefore, a key proxy for investigating the role of major orogens on the global carbon cycle, and this will in turn have a major role to play in quantifying the effect of erosion on climate both globally and regionally (Section 1.3.5).

1.3.5 Erosion and Climate

The coupling between erosion and climate is complex, with weathering suggested as a cause for climatic changes, and the increase in erosion as a result of climate change. It has been suggested that the uplift of the Himalaya, which has increased erosion, has caused Cenozoic global cooling as a result of the drawdown of carbon dioxide by chemical weathering of silicates (Raymo and Ruddiman, 1992). Moreover, the uplift of the Himalaya, in particular the Tibetan Plateau, is thought to have intensified the strong Asian monsoon, which was fully 'switched on' by 15 Ma (e.g., Prell and Kutzbach, 1992; Clift *et al.,* 2002; Kitoh, 2004; Harris 2006 and references therein). Erosion then continues by positive feedback as a result of increased monsoonal precipitation, and reinforces the drawdown of carbon dioxide which has an effect on global carbon budgets (Section 1.3.4) and thus on the overall global climate. Dupont-Nivet *et al.,* (2007) attribute the uplift of the Himalaya and

subsequent increases in erosion to the intensification of monsoons and increased regional erosion since ~34 Ma, leading ultimately to global cooling by the instigation of atmospheric climate perturbations and carbon dioxide lowering associated with rock weathering.

Fully understanding the effect of erosion on climate and climate on erosion requires a thorough understanding of the erosion record and climatology. Constraining the initiation of erosion in the Himalaya will add further constraint to models that aim to link tectonic processes (such as tectonic rock uplift) with erosion and climate perturbations such as the Asian Monsoon, and global cooling. The feedback between erosion and climate, and therefore the importance of the erosion record, is discussed further in Chapter 6.

1.4 Overview of the study areas

With the importance of the erosion record in mind, a brief introduction to the study areas that may preserve an early record of Himalayan erosion follows. A detailed review of the stratigraphy, overall geology and tectonic setting for each field area is included within Chapters 3, 4 and 5 for the Andaman Islands, western Burma (Myanmar) and The Chittagong Hill Tracts (Bangladesh) respectively. Detailed sample locations are listed in the appendices 2-1 and 3-1. The following section is a generalised tectonic and geological overview of each region in order to place their location within a regional framework.

1.4.1 The Andaman Islands

The Andaman Islands and other southerly islands such as the Nicobar, form the subaerial parts of the forearc ridge in the Indonesian island-arc system. The

Andaman-Java trench lies to the west of the forearc ridge and the Quaternary Narcondium and Barren Island volcanoes rise from a submarine ridge to the east. The Andaman Islands are separated from the continental mass of Burma (Myanmar) peninsula by the Andaman back arc marginal sea (Curray, 2005 and references therein) (Figure 1.8)

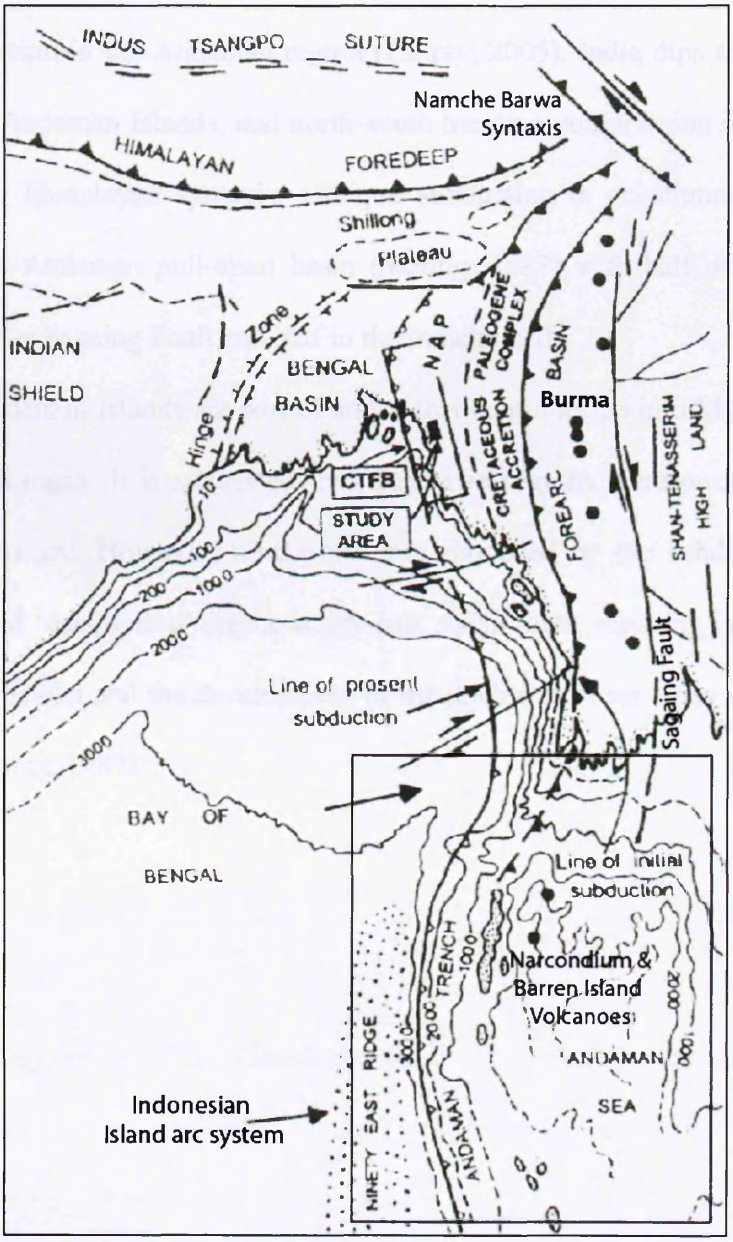

Figure 1.8 Regional map of the Andaman Sea region and Andaman Trench adapted from Curray, 2005. Salient features shown are the line of subduction, major faults, study areas of the Chittagong Hill Tracts, Cretaceous-Palaeogene Indo-Burman Ranges and the Andaman Islands, relative to the surrounding region of the Himalaya and Bay of Bengal.

The Andaman arc-trench system has been described as the result of active subduction of the eastern margin of the Indian plate below the Eurasian plate along the Andaman-Java trench from the Cretaceous to present (Curray and Moore, 1974). The northern motion of India with respect to Southeast Asia is accommodated along three trenches in the east: Java, Sumatra and Andaman. The curvature of these trenches shows progressive oblique subduction - normal subduction in the Java region to hyper oblique subduction in the Andaman region (Curray, 2005). India dips to at least 250 km below the Andaman Islands, and north-south trending compression is observed in relation to the Himalayan syntaxis. Oblique subduction is accommodated by the opening of the Andaman pull-apart basin (Maung, 1987) with half of the opening transmitted to the Sagaing Fault and half to the trench itself.

The Andaman Islands are part of an arc that continues up into Myanmar as the Indo-Burman Ranges. It is suggested that these two regions were once part of one long continuous arc. However, northward drag produced by the subducting Indian plate has caused 'decoupling' on the south–east Asian plate, resulting in the creation of the Burma platelet and the development of the double arc seen today and shown in Figure 1.9 (Maung, 1987).

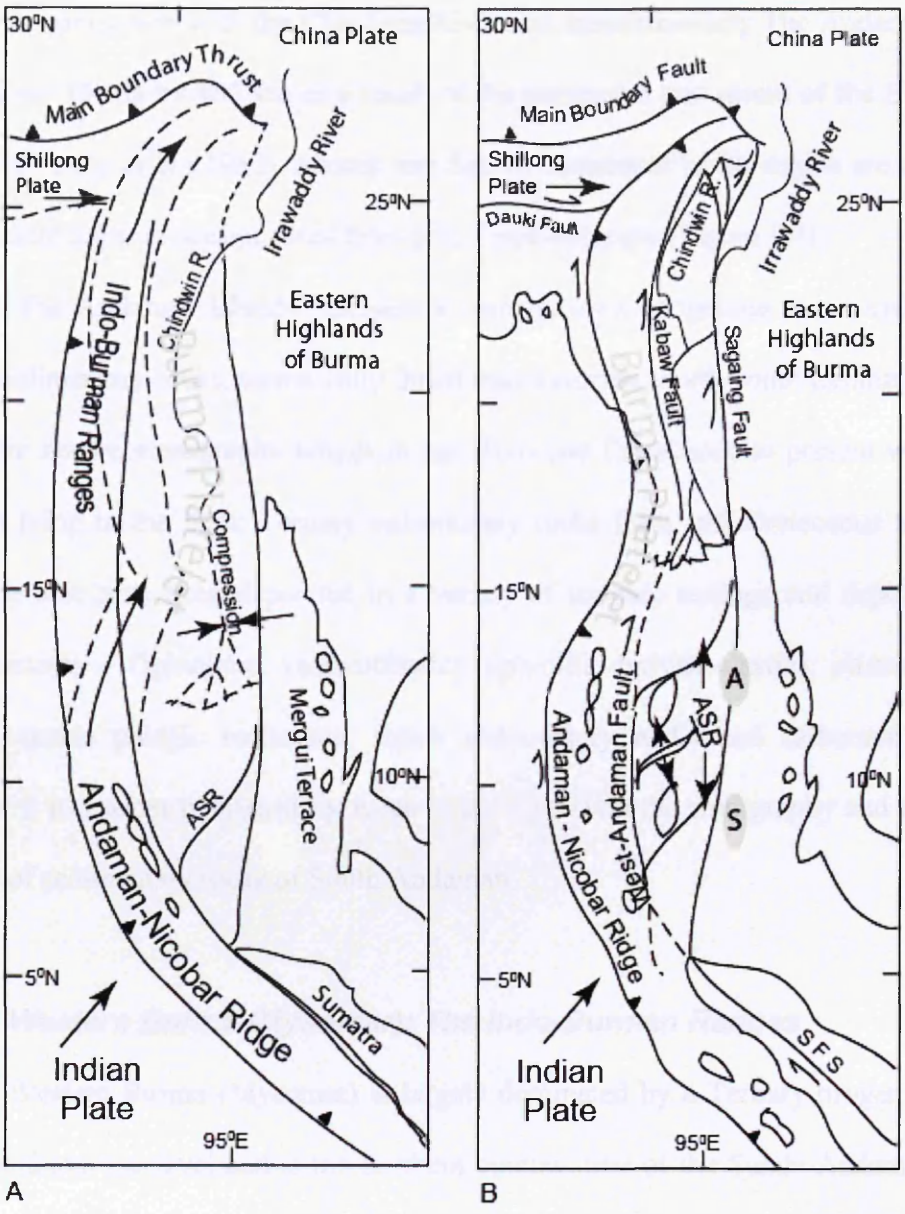

Figure 1.9 Decoupling of the Southeast Asian Plate (From Maung, 1987) ASB = Andaman Spreading Basin, A = Alcock Seamount, S = Sewell Seamount

The eastern extent of the Burma platelet sheared off of the leading edge of the south–east Asian plate is represented by the Sagaing Fault. Drag has caused the Indo-Burman Ranges and the Andaman ridge section to decouple along several major faults including the Sagaing Fault and the Kabaw Fault, which accommodate the resultant movement. Northward translation caused ~ 400 km offset of the Irrawaddy River from

its earlier connection with the Chindwin River and simultaneously The Andaman Sea opened at ~13 Ma by 460 km as a result of the northward movement of the Burmese platelet (Curray *et al.,* 1982). Alcock and Sewell seamounts in the region are thought to represent uplifted oceanic crust from post – mid-Miocene (Figure 1.9).

The Andaman Islands represent a complex mix of igneous and accretionary prism sedimentary rocks, tectonically thrust into a narrow, north-south trending linear belt. The known stratigraphy ranges in age from late Cretaceous to present with our interest lying in the thick Tertiary sedimentary rocks from late Cretaceous to Mio-Pliocene that have been deposited in a variety of tectonic settings and depositional environments – Ophiolites, volcaniclastics, ophiolite derived clastics, olistostromal units, oceanic pelagic sediments, flysch sedimentary rocks and carbonate rocks. Chapter 3 is a paper published by Allen *et al.,* (2007) on the stratigraphy and thermal history of sedimentary rocks of South Andaman.

1.4.2 Western Burma (Myanmar): The Indo-Burman Ranges

Western Burma (Myanmar) is largely dominated by a Tertiary orogen that is entirely above sea level and is the northern continuation of the Sunda-Andaman arc, which is represented by the Andaman and Nicobar Islands in the south, and further northwards by the eastern syntaxis of the Himalaya. The tectonic evolution of western Myanmar or the Indo-Burman region is, therefore, interpreted as a result of the oblique convergence between the Indian plate and the Asian plate including the Burma platelet (Curray *et al.,* 1979). As discussed above, the development of western Myanmar is intimately related to that of the Andaman Islands. However, this Cretaceous to Palaeogene system is thought to be better exposed in the Myanmar region as opposed to the Andaman Islands where much of the sediment is offshore or

buried beneath a thick cover of younger sedimentary rocks (Mitchell, 1993). The majority of western Myanmar and the Naga Hills of Assam (India) are situated on the Burma platelet. Western Myanmar can be split in to 4 general regions (Figure 1.10). Briefly, these are defined by Mitchell (1993) as the *magmatic arc*, the *eastern trough*, the *western trough* and the *Indo-Burman Ranges*, broadly consisting of an eastern and a western belt (Figure 1.10). The Indo-Burman Ranges trend north-south and comprise the Arakan Yoma (south), Chinn Hills and Naga Hills (north), eventually joining the Mishmi thrust belts of the eastern Himalayan syntaxis (Brunnschweiler, 1966; Ni *et al.,* 1989).

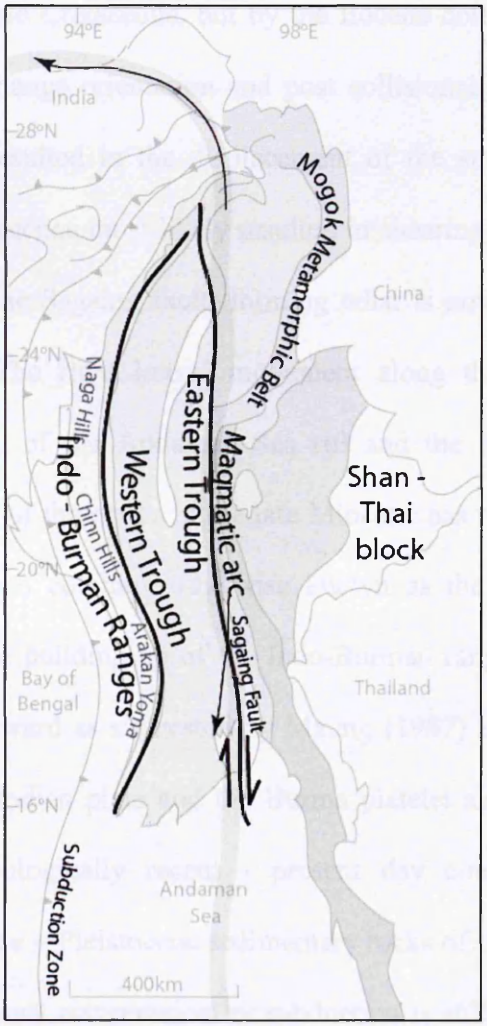

Figure 1.10 Generalised tectonic divisions of Burma (Myanmar)

Previous interpretation of the Cretaceous and Cenozoic system of western Myanmar, has generally favoured the idea that the Indo-Burman ranges are accretionary prism sediments scraped off the underthrusting Indian plate during semi-continuous eastward subduction below the Asian plate. Seismicity beneath the Indo-Burman ranges indicates an eastward dipping Benioff zone. Ni et al., (1989) suggest that the lack of seismicity within the plates indicates that the Indo-Burman ranges must either be accreted onto and moving with the Indian plate, due to the "bulldozing" of sediments onto the plate by the Burma platelet or that subduction continues aseismically. Northward to northeastward subduction of oceanic lithosphere beneath Tibet occurred in the late Cretaceous, but by the Eocene collision of the Indian and Asian plate began to change orientation and post collisional crustal shortening then began in Assam and resulted in the displacement of the suture zone. In the early Miocene oblique convergence most likely resulted in shearing off the leading edge of the Asian plate along the Sagaing fault, forming what is now known as the Burma platelet (Figure 1.9). The right lateral movement along the fault simultaneously resulted in the opening of the Andaman Sea rift and the Irrawaddy River offset. Continued convergence of the plates in the late Miocene has resulted in the accretion of the sedimentary prism complex otherwise known as the Indo-Burman Ranges. Following the continued building up of the Indo-Burman ranges, the Burma platelet has been dragged northward as suggested by Maung (1987) leaving the modern day boundary between the Indian plate and the Burma platelet as the Sagaing fault that still accommodates geologically recent - present day convergence. North-south trending folds in Pliocene – Pleistocene sedimentary rocks of the Indo-Burman ranges demonstrates that east-west compression by subduction is still active (Le Dain *et al.*, 1984). Controversy about the geological history of the region remains including

whether the Indo-Burman Ranges are an accretionary prism from Indian subduction, or deposits of the Asian plate margin (Mitchell, 1993). The alternative theories are revisited in Chapter 4.

1.4.3 The Chittagong Hill Tracts (and Hatia Trough), Bangladesh

The sediment repository preserved in the Bengal Basin of Bangladesh is predominantly a large delta complex with a present coverage of approximately 144,000 km^2 onshore and 63,000 km^2 offshore. It preserves a Tertiary sequence of sediments with a thickness of up to ~16-20 km (Curray and Moore, 1971; Gani and Alam, 1999; Uddin and Lundberg, 2004) sourced principally by the Himalaya to the distal north. The Bengal Basin can be broadly split into two geotectonic provinces, (1) the Indian platform or stable shelf in the northwest and (2) the deeper basin, including the Hatia Trough in the southeast and Sylhet Trough (Surma subbasin) in the northeast (Uddin and Lundberg, 1998; Alam *et al.*, 2003). This deeper basin passes east into the Chittagong Hill Tracts of the accretionary prism in southeast Bangladesh (Figure 1.11).

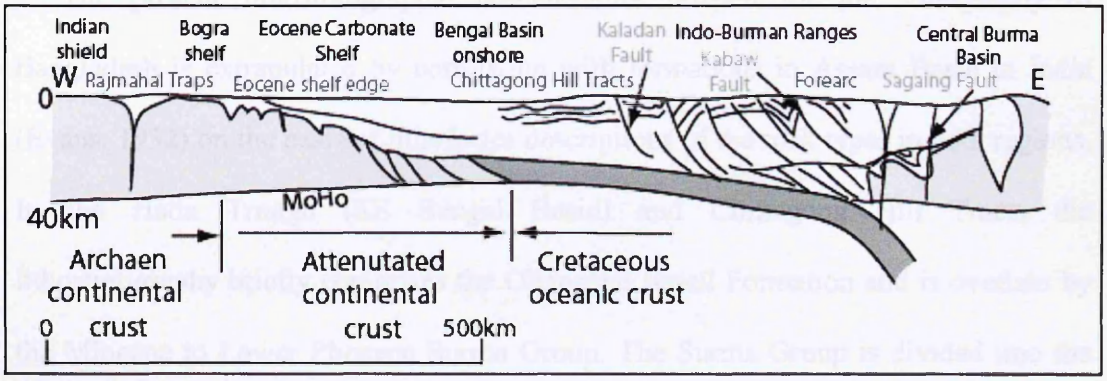

Figure 1.11 Cross section of the Bay of Bengal from India to Burma (Alam *et al.*, 2003)

Sedimentary rocks of the Bengal Basin may preserve a record of erosion beyond the dated base of ~17 Ma currently inaccessible in the Bengal Fan (Curray, 1994; Galy *et al.,* 1996). The Chittagong Hill Tracts (also called the Chittagong-Tripura Fold Belt or Eastern Fold Belt) extends into the Hatia trough and consists of sediments deposited in to the Bengal Basin and subsequently incorporated into the accretionary prism as material progressively offscraped from the Bengal Fan during subduction.

The Chittagong Hill Tracts is a belt of en-echelon northwest-southeast trending folds in Burma and Bangladesh, and northeast-southwest furthest north where they stop abruptly against the faulted block of the Shillong Plateau (Figure 1.12 overleaf), which represents uplifted cratonic Indian basement separated from the Indo-Burman Ranges by the Kaladan fault (Sikder and Alam, 2003). Compressive east-west tectonics (Gani *et al.,* 1999) in the Chittagong Hill Tracts have given rise to a structure comprising mainly east-dipping, high angle thrust faults that build into thrust sheets. The region may have developed on a folded detachment or decollement at depth as a result of initial buckling and subsequent fault propagation (Sikder and Alam, 2003), which may have given rise to the region's distinctive folds.

The present lithostratigraphic nomenclature utilised for the stratigraphy of Bangladesh is extrapolated by correlation with formations in Assam Basin in India (Evans, 1932) on the basis of lithofacies descriptions of the rock types in both regions. In the Hatia Trough (SE Bengal Basin) and Chittagong Hill Tracts the lithostratigraphy briefly comprises the Oligocene Barail Formation and is overlain by the Miocene to Lower Pliocene Surma Group. The Surma Group is divided into the Bhuban and Boka Bil Formations and overlain by the Pliocene Tipam Formation and the Plio-Pleistocene Dupi Tila Formation (Uddin and Lundberg, 1998a, Gani and Alam, 1999).

However, as pointed out by previous workers (Gani and Alam. 1999; Alam *et al.*, 2003) the lithostratigraphic nomenclature is inadequate. An extensive discussion of this region is presented in Chapter 4 including a new classification and seismic framework to improve definition of the lithostratigraphy.

Figure 1.12 LANSAT image of the Chittagong Hill Tracts, Bangladesh

Chapter 2: Methods Rationale

2.1 Introduction

This chapter is a training record of the work undertaken in this project, and includes a rationale for using each chosen method/technique as well as a detailed breakdown of the work undertaken by the author. The declaration of authorship and a breakdown of contributions from each co-author are provided at the beginning of the thesis.

An introduction to the theoretical background of the methods is presented, whilst the full, project-specific, procedural methodological detail is presented in the appendices associated with chapters 3, 4 and 5, and discussed briefly within each chapter or paper.

2.2 Rationale

The analytical techniques employed in this project were undertaken for the purposes of determining the provenance of the sedimentary rocks under study. Some techniques were also employed in order to determine the post-depositional thermal / exhumation history of the rock. The definition of clear and precise objectives before starting any analyses allows for the appropriate choice of techniques. This is particularly important with detrital thermochronology, where the effective 'closure temperature' of any thermochronological system will determine what type of geological process can be addressed by its study. Choice of technique may also be dependant on the mineralogy of the samples and may rule out the use of certain techniques, e.g., a lack of potassium rich minerals for ^{40}Ar-^{39}Ar dating.

2.2.1 Thermochronometers for provenance analysis

Traditionally, provenance analysis has been heavily dependent on the petrography and dense mineral study of sands and sandstones. In this sense, quantitative information on the contributing source region lithologies for sandstones of mixed provenance based on constituent minerals and lithics has been used as a 'first step' of provenance identification. The occurrence of specific metamorphic index minerals is useful for providing initial information on metamorphic grade in the source region, whilst the proportion of ultrastable minerals can provide information on the amount of recycling. Increasingly however, isotopic methods are being used in regions where source terranes vary considerably. The Himalaya is a type example of a mountain belt with considerable variation in source terrain, geology and metamorphism, both spatially and temporally. Much work has already been done on using isotopic data to characterize the different lithotectonic units of the Himalaya and the surrounding drainage basins (e. g. Critelli and Ingersoll, 1994; Parrish and Hodges, 1996; DeCelles *et al.,* 1998, 2001; Najman, 2000; Robinson *et al.,* 2001; Clift *et al.,* 2001; White *et al.,* 2001; Najman *et al.,* 2003; Garzanti *et al.,* 2004, 2007; Najman, 2006; Bernet *et al.,* 2006; Szulc *et al.,* 2006) making them ideal for comparison with sediments stored in the sedimentary repositories of the Himalaya (such as the Bengal basin), and establishing provenance within the sedimentary basins, or identifying Himalayan provenance where multiple sources are suggested.

2.2.2 Overview of the theoretical background to the main thermochronometers chosen

A mineral's isotopic age reflects the time it cooled through its closure temperature. The closure temperature is the temperature below which a mineral will retain its age record of crystallization or metamorphism. If the mineral subsequently

exceeds this temperature the age information will be erased and the mineral age 'reset' either fully or partially. This can happen with increasing burial depth in a sedimentary basin.

Thermochronometers such as fission track and U-Pb on zircon are medium and high temperature systems respectively, which relate to their respective closure temperatures. The suitability of zircon for analysis is based on their chemical stability and mechanically durability in erosional and depositional environments and furthermore, their closure temperature for both systems is high, and they therefore retain uranium well for analysis.

Fission track analysis

Fission track analysis gives information on the low-temperature thermal histories of rocks, below ~120°C for tracks in apatite (Green *et al.,* 1995), and below ~310°C (Tagami *et al.,* 1998) for zircon. Fission tracks are essentially damage features caused by charged nuclear particles undergoing spontaneous nuclear fission, primarily of ^{238}U. Zircon fission track annealing takes place between 200-310°C (Partial Annealing Zone). Above this temperature fission tracks will fully anneal (self-repair). Between 200-310°C (for heating durations > 10^6 yrs) track shortening occurs and this leads to a reduction in countable track density causing a decrease in apparent age. Below ~ 200°C there is no discernable shortening. The Partial Annealing zone for apatite is ~60-120°C.

Natural spontaneous fission tracks are observed by optical microscopy following enlargement by chemical etching. The density of spontaneous tracks is a function of time and uranium content. The latter is derived by neutron activation with a mica external detector placed against the sample during neutron irradiation. After

irradiation the mica detector is etched with hydrofluoric acid to expose induced fission tracks. A sample age is therefore the ratio of sample spontaneous track density (daughter product) against mica induced track density (parent).

Many types of sediment are derived from the erosion of pre-existing rocks. Detrital apatite and zircon are common chemically-stable uranium bearing minerals that become concentrated in most clastic sediments. Providing these sediments have not been buried sufficiently deep to cause heating and resetting of fission tracks (i.e. >100°C for apatite and > 250°C for zircon), the zircon FT ages recorded in these detrital minerals may reflect the 'thermal history' of their original source rock, (However, much of this history can be effectively 'erased' by subsequent annealing of fission tracks with sufficient temperature and pressure conditions). It is suggested that the thermal history of a zircon may therefore represent the parent rock's exhumation history driven by erosion. In apatite fission track analysis, the apatite is usually reset and its age in a detrital sample usually reflects post-depositional burial/exhumation history.

U-Pb isotopic dating

U-Pb dating is based on the decay chain of uranium to lead. ^{238}U decays to ^{206}Pb and ^{235}U decays to ^{207}Pb. Zircon is a mineral that strongly incorporates uranium but not lead, so that the majority of ^{206}Pb and ^{207}Pb should be radiogenically produced in situ. Minerals that have remained closed systems for uranium and lead give concordant values and when both decay–systems are plotted together they define a curve termed the Concordia. However, early dating on U-rich minerals revealed that in some cases samples yield discordant $^{206}Pb/^{238}U$ and $^{207}Pb/^{235}U$ ages. This was attributed to lead loss by diffusion, and exacerbated by damage to the crystal lattice by alpha particles

emitted in long decay schemes such as this. Many discordant ages were found to fit on a linear pattern on the Concordia plot and so were termed Discordia. The upper intersection of the Discordia with the Concordia corresponds to the time of formation of the mineral and the lower intersection may have age significance if supported by geological evidence, e.g., a thermal event resulting in lead loss. Significant age data may come from concordant and discordant data as long as the discordant data are consistent with the concordant. For some ages it is necessary to correct for common Pb i.e. any composition Pb from a rock or mineral that contains a large amount of stable-isotope Pb and a small amount of the radioactive progenitors of Pb. and measured by analysis of ^{204}Pb (the exact procedure is described in the relevant chapters). In the case of U-Pb dating of detrital minerals it is important to note that minerals cannot be treated and interpreted in exactly the same way as more traditional studies of minerals in, e.g., igneous rocks. Unlike minerals in igneous rocks, detrital minerals are unlikely to have homogenous cooling histories. It is *expected* that the cooling history of the minerals will differ from each other and, hence, a variety of U-Pb ages will be produced, making the interpretation of Concordia and Discordia more complex.

U-Pb dating of detrital zircon is a popular approach to obtaining crystallisation age of the zircon crystal (or overgrowth). Zircon, durable and resistant to weathering, is used commonly because it has a very high closure temperature for Pb diffusion of ~750°C (Carter and Bristow, 2000), which is higher than most metamorphic temperatures except for granulite settings. Consequently, nearly all U-Pb detrital zircon ages reflect zircon growth, making it potentially an ideal method for determining the age structure of lithologies that comprise a sediment source terrain such as orogenic belts. However, due to a high resistance to resetting there is an

increased probability of preserving very old U-Pb ages, which may not exclusively represent the immediate source terrain. Instead, they may derive from older sources as a consequence of a polycyclic history (Carter and Bristow, 2000). Furthermore, because the U-Pb system is able to effectively 'see through' later thermal events affecting a source region, then on its own the technique does not fully account for hinterland evolution. Used on their own, U-Pb ages of detrital minerals can be matched with potential source regions in order to determine the provenance of the basin fill. However, the strength of this method for provenance analysis is in its combination with other techniques such as zircon fission track analysis, which is better placed to constrain, for example, thermal events after initial zircon formation.

$^{40}Ar/^{39}Ar$ isotopic dating

The $^{40}Ar/^{39}Ar$ method of dating is developed from the earlier K-Ar dating technique, which involved absolute determination of the amounts of parent ^{40}K and daughter ^{40}Ar (that is the radiogenic component designated $^{40}Ar^*$). Potassium rich minerals are used for $^{40}Ar/^{39}Ar$ dating. White mica typically contains high concentrations of potassium accounting for 8-10% of total content by weight. Muscovite is retentive of radiogenic argon below ~400°C (McDougall and Harrison, 1999), above which point the argon is gradually lost and the age obtained becomes geologically meaningless for provenance study.

For $^{40}Ar/^{39}Ar$ analysis the sample to be dated is irradiated with fast neutrons in a reactor in order to convert a small amount of the principal isotope of potassium, ^{39}K, into ^{39}Ar. ^{39}Ar has a half life of 269 years and is therefore considered virtually stable for analysis (an almost negligible correction to the measured ^{39}Ar). The sample is then fused in a high vacuum and the resultant evolved gas is cleaned from any

contaminating gases and analysed on a mass spectrometer to obtain the $^{40}Ar^*/^{39}Ar_K$ ratio. Because the ^{39}Ar produced is proportional to the ^{39}K of the sample, and there is a fixed ratio of ^{39}K to ^{40}K then a measure of ^{39}Ar in the sample yields a measure of the ^{40}K. Therefore the $^{40}Ar^*/^{39}Ar$ ratio is proportional to the $^{40}Ar^*/^{40}K$ ratio and hence the ratio can be used to calculate the age of the sample. $^{40}Ar/^{39}Ar$ analysis may be conducted by total fusion (total sample is fused and gas content measured in a single step) of the mineral or by step heating (which involves progressive outgassing). Step heating is useful for the identification of anomalous subsections in a mineral, or to interpret samples with inherited argon, whereas total fusion is typically used in samples with reliable or recoverable gas diffusion information. Total fusion was used in this study as testing revealed that sediments in the Bengal Basin do not typically show a stepped profile and instead show one main age plateau indicative of a closed system since formation, making step heating unnecessary. Due to the high retention temperature of white mica $^{40}Ar/^{39}Ar$ dating is ideally suited to studying hinterland metamorphism, cooling and exhumation in order to characterise provenance.

Other thermochronometers have lower temperature systematics, e.g., apatite fission track analysis and apatite (U-Th)/He. Temperatures corresponding to the approximate partial annealing zone of, e.g., apatite (~60-110°C) are typically encountered in sedimentary basins with a typical geothermal gradient at a few kilometres of depth. For this reason, apatite is ideally suited for the study of post-burial thermal histories of the basin sediment. (U-Th)/He is the lowest temperature chronometer used in this study and based on the production of He by alpha decay of Uranium and Thorium (and Samarium). The closure temperature or 'partial retention zone' for apatite is 40-75°C (e.g., Farley, 2000). As such, although the technique is in

its relative infancy, it is ideally suited for studying near surface processes and geomorphology.

High temperature systems are useful for constraining deeper, longer-term processes in the source region. Low temperature systems are less useful due to the mineral's susceptibility to being 'reset'. The strength of low temperature systems lies in tracking short-term variations in denudation and thermal histories of basin sediments. These processes are not identifiable using high temperature systems (Van Der Beek *et al.*, 2006).

2.2.3 Choosing the right analysis for purpose and objectives

As a consequence of the differences between low and high temperature thermochronometers, their applications are varied and dependent on the systematics of the given isotope being studied. For this reason, each analytical technique can potentially tell the researcher something different, leading to a more complete, reliable and robust data set on a given set of samples. The different techniques are therefore highly complimentary if combined well and can provide a variety of data for multiple objectives. For example, the similar closure temperatures for zircon fission track analysis and ^{40}Ar-^{39}Ar mica dating make them ideally suited together to verify the data produced from the other. Both typically record the metamorphic cooling temperature in the source region. Apatite helium analysis is also compatible with apatite fission track analysis as the system is sensitive to closure at ~60°C – the temperature at which the fission track analysis begins to lose sensitivity to changes in cooling rate. Alternatively, where the mineralogy of a sample prevents the use of one method, the other may be used for the same information. Another example of the complimentary nature of such techniques is the combination of apatite and zircon

fission track analysis, where the former typically gives information on the source region and the later provides a picture of post depositional thermal histories.

Rare earth elements are also widely used in detrital studies to determine source terrane provenance because they are relatively insoluble and resistant to fractionation by sedimentary sorting or grain size variations. For example, Sm/Nd isotope fingerprinting. $^{143}Nd/^{144}Nd$ ratios are normalised and expressed in epsilon units as derivation from a chondritic uniform reservoir (CHUR). For clastic sedimentary rocks, ε_{Nd} will represent the weighted average of the time when the sediment sources were extracted from the mantle. When melt is extracted from the mantle it has a lower Sm/Nd ratio than its parent and therefore evolves over time to have a lower ε_{Nd} than CHUR. The residual has a higher ratio than CHUR evolving to higher ε_{Nd} over time. This technique is applicable to bulk sediment and single grain analysis, with the strength lying in the application of the two methods together. The bulk sediment analysis will provide an average value when sources are mixed, but single grain analysis should provide the individual isotope signature per mineral. Combined, it will then be possible to assess the relative importance of each identified source to the bulk sediment.

The techniques for this project were chosen in order to achieve the best, most reliable and robust data in order to achieve the research objectives. The primary objective of the thesis is to characterise the provenance of the sediments of Bangladesh, Burma and the Andaman Islands, and to establish whether they show any record of Himalayan erosion. To do this, medium-high temperature methods were chosen to gain information on the possible source regions of the Himalaya, the Indian Craton and the Burman margin. ^{40}Ar-^{39}Ar mica ages are good for provenance in the

Himalaya, Indian Craton and Burma where geological units can be characterised by different mica populations. The same is true for U-Pb dating of detrital zircons, which has also been used widely throughout Asia to define provenance based on characteristic U-Pb age populations. Zircon fission track dating was used both as a verification method combined with the ^{40}Ar-^{39}Ar data, and used in the absence of mica in Palaeogene samples. In addition, isotope fingerprinting using Sm/Nd isotopes was chosen to explore palaeodrainage (as different rivers have different Sm/Nd isotopic signatures) and to assess the contributions of continental and mafic sources to the samples. This was deemed important in the field areas studied which potentially record derivation from mixed continental and mafic sources.

Other techniques were also chosen in order to fulfil secondary objectives. In order to define the thermal history of sediments of the Andaman Islands, apatite fission track analysis and (U-Th)/He were used.

Whilst detrital mineral age data is ideal for providing provenance information, other techniques are better suited to obtaining absolute ages of the host sediment. Establishing the age of a rock or sediment is vital for constraining the stratigraphy and relationship of rock units with overlying and underlying units. Biostratigraphy is a reliable method of accurately dating a rock where fossils are present, and as such biostratigraphy was used where possible in this study to add further constraint to the studied geology. This was especially important for samples from the Chittagong Hill Tracts and Hatia Trough; where it was necessary to age constrain the geology in order to create a new sequence stratigraphic framework for the region using 2D seismic interpretation. This method was only used in Bangladesh, as no seismic data were available for Burma or the Andaman Islands.

To be sure that the ages obtained from fission track analysis and ^{40}Ar-^{39}Ar dating represent cooling in the source region and not post-depositional metamorphic cooling, X-Ray Diffraction (XRD) Illite Crystallinity was used to ascertain post depositional temperatures and metamorphic grade that the sediment has been subjected to. Mudstone is ideal for this analysis due to its clay content and the consequent abundance of illite relative to detrital mica (that interferes with measured illite peaks and contaminates the sample). The 2μm clay fraction is separated and analysed in an attempt to measure the diagenetic rather than detrital component, and thus obtain an indication of the temperatures to which the rock has been subjected after deposition. XRD is used to assess the purity of the mudstone sample and the illite study yields information about the nature and origin of clay minerals in the mudstone to be dated. The 'illite crystallinity index' (Kubler, 1967), is defined as the width of the (001) XRD peak at half its height (Hb) A well crystallised illite, characteristic of a relatively high temperature history, has sharp peaks and therefore a low index, whereas low temperature illites have irregular peaks with large indices. The thickness of illite is therefore dependant on and indicative of metamorphic grade. Deeper burial and higher grade forms thicker crystals and thicker crystals cause the illite XRD peak widths to become narrower (Scherrer's equation). Using a quartz standard with the Hb value gives an Hbrel value (relative full width at half maximum) and represents the Hb value relative to the quartz standard. The resultant values are used to make the index of illite crystallinity and can be used to define the typical boundaries of different metamorphic zones, to which other illite crystals can be compared.

2.3 Fieldwork and sample preparation

Samples used in this study were collected over four field seasons, in addition to core data collected prior to the start of this project. At the beginning of year one samples were collected on two trips, from the Andaman Islands and from the Chittagong Hill Tracts, Bangladesh (Chittagong/Rangamati Region and the southernmost onshore anticlines). Cairn Energy Plc. and Y. Najman conducted a second sampling trip to the Chittagong Hill Tracts and fieldwork in the Indo-Burman Ranges, Burma, respectively. On both occasions the political status of both regions at the time put a restriction on my attendance.

On return of the rocks to the UK, sample preparation was done primarily by the author, including the crushing and grinding of rocks and subsequent heavy mineral and mica separation. Heavy mineral separation was conducted at University College London and the zircons and apatites used for Sm/Nd, U-Pb and fission track analysis. Micas where picked from each sample at Lancaster University, Vrije University (Amsterdam), and SUERC Argon Isotope Lab (East Kilbride), and used for detrital mica ^{40}Ar-^{39}Ar analysis. Below is a comprehensive guide to the contribution of the author to the techniques used.

2.4 Techniques

A total of 10 techniques were used for this project. These can be divided into 'Primary techniques' (6) and 'Secondary techniques' (4). A primary technique is one that was central to the project and from which a large amount of data was generated. Secondary techniques are those that may only have been used to gain a small amount of data or have been used on a small number of samples for the purpose of a 'pilot study' (see

Chapter 3). Below is a statement of contribution to each method by the author (R. Allen). The full methodologies are detailed in the appendices for each chapter.

2.4.1 Primary techniques

^{40}Ar-^{39}Ar dating on detrital white mica

Sandstones were prepared in their entirety by the author. After initial crushing and grinding, mica was collected from each sample. This was done at Lancaster University, Vrije Universty and SUERC Argon Isotope Lab (East Kilbride). The micas were irradiated (Petten, Netherlands), and on arrival to their respective labs were unpacked in the radioactive lab by the author and loaded into samples holders, ready for analysis. Two mass spectrometers were used to analyse the samples. Initially, at Vrije University under the guidance of J. Wijbrans (MAP 215-250 mass spectrometer) and later extensively at SUERC Argon Isotope Lab with P. Alexandre and D. Barfod (GVi Argus faraday multi-collector). Approximately 3 months were spent preparing the samples and running the ^{40}Ar-^{39}Ar analyses. Extensive problem solving was a key part of the ^{40}Ar-^{39}Ar analyses due to the unforeseen problems that occurred with the mass spectrometer at various times during the project. Issues that needed to be resolved *in situ* included;

- Unacceptable high blank values of ^{40}Ar relative to the typical sample output.
- Low levels of ^{40}Ar from some samples

Much time was spent learning how to identify the route of a problem, and how to solve it. This involved navigating around the problem of appropriate grain size for ^{40}Ar-^{39}Ar analyses. The best grains should be approximately 250-1000μm. Smaller than this and the grains are difficult to manipulate and furthermore, small and young aged grains may not contain sufficient radiogenic argon for ^{40}Ar-^{39}Ar analyses.

All data were regressed, processed and interpreted by the author using ArArCALC (Koppers, 2002), and in-house methods corroborated with ArArCALC.

U-Pb dating on detrital zircons

Zircons were separated for analysis by the author (using heavy liquids) but mounted onto slides and polished by A. Carter (UCL). The specific zircons used were then chosen by the author after initial guidance on the best minerals to look for, for the purpose of laser ablation. The samples were analysed by the author on an LA-ICP-MS (Agilent 750 quadrupole and New Wave 213 laser ablation system). Training was also received on tuning the ICP-MS every morning before a new run of analyses. Data were analysed (GLITTER), processed and interpreted by the author. Two weeks were spent running the analyses with additional time for sample preparation (approx. 10 days).

Sm/Nd bulk rock isotope fingerprinting

Samples were prepared for Sm/Nd bulk rock thermal-ionisation mass spectrometry (TIMS) analysis at Cambridge University with guidance and tuition from M. Bickle and H. Chapman, respectively. This included leaching, cation exchange columns I and II and reverse phase columns. Isotope ratios were analysed on the T40 Sector 54 VG Mass Spectrometer using a triple filament assembly. All samples were prepared, loaded and analysed by the author over a period of approximately 1 month. The data were then converted by the author to a format suitable for the study (Epsilon Nd (t=0) and interpreted.

Seismic interpretation and mapping

An extensive set of 2D seismic reflection data was interpreted and mapped by the author at Cairn Energy Plc (Edinburgh, Scotland). Data were acquired prior to the project and most of which had not been interpreted before (Chittagong Hill Tracts). Other data were re-interpreted by the author (parts of the Hatia Trough). Guidance was provided by E. Willett culminating in independent seismic interpretation by the author by the end of a 3-year period. Geoframe 4.3 was later used by the author to reproduce scaled maps and figures suitable for publication.

Fission track analysis on detrital zircons and apatites

Samples were chosen and the zircons and apatites separated using heavy liquids for analysis by the author (~10 days). Further preparation (such as mounting and etching) and the analyses were subsequently run by A. Carter (UCL). The author later interpreted the data obtained, as with other techniques mentioned above.

Petrography and Heavy Mineral analysis

Samples were chosen by the author and sent away for thin sectioning at the Open University. The thin sections were then sent to Milan University where a petrographic and heavy mineral study was made by E. Garzanti. The resultant data were returned to the author for interpretation.

2.4.2 Secondary techniques

Sm/Nd single grain analysis on apatite

Using apatite previously separated by the author, G. Foster (Bristol University) conducted the Sm/Nd analysis on the single mineral grains. A small number of

samples from the Andaman Island were analysed using an LA-ICPMS, and the author interpreted the data.

Apatite Helium dating

Helium dating was conducted by A. Carter (UCL) on a small dataset of 3 samples from the Andaman Islands. These data were collected during a trial of a newly constructed quadrupole mass spectrometer at UCL whilst the author was present. The data obtained was discussed with A. Carter and added to Chapter 3 accordingly.

Biostratigraphy

Mudstones were selected by the author from a wide number of samples and sent away for analysis. However, Andaman samples were found to be barren and were therefore not included in the study any further. In the case of data obtained prior to the start of this project i.e. reports commissioned by Cairn Energy Plc, were newly interpreted for the field areas within this study and were used by the author to calibrate a new sequence stratigraphic framework for the Chittagong Hill Tracts, Bangladesh (Chapter 5).

XRD Illite Crystallinity

The author for use in Chapter 5 interpreted data from an XRD Illite Crystallinity study of core samples collected prior to the start of this project.

Chapter 3: New Constraints on the sedimentation and uplift history of the Andaman-Nicobar accretionary prism, South Andaman Island

Published in the Geological Society of America, Special Paper 436, 2007.
Please note American spelling throughout chapter for publication

3.1 Abstract

The Andaman Islands are part of the Andaman-Nicobar Ridge; an accretionary complex that forms part of the outer-arc ridge of the Sunda subduction zone. The Tertiary rocks exposed on the Andaman Islands preserve a record of the tectonic evolution of the surrounding region, including the evolution and closure of the Tethys Ocean. Some of the Paleogene sediments on Andaman may represent an offscraped part of the early Bengal Fan. Through field and petrographic observations, and use of a number of isotopic tracers new age and provenance constraints are placed on the key Palaeogene formations exposed on South Andaman. Paucity of biostratigraphic data poorly define sediment depositional ages. Constraints on timing of deposition obtained by dating detrital minerals for the Mithakhari Group indicate sedimentation after 60 Ma, possibly younger than 40 Ma. Better constraint is obtained for the Andaman Flysch Formation, which was deposited between 30 and 20 Ma based on Ar-Ar ages of youngest detrital muscovites at ~30 Ma and thermal history modelling of apatite fission-track and U-Th/He data. The latter record sediment burial and inversion (uplift) at ~ 20 Ma. In terms of sediment sources the Mithakhari Group shows a predominantly arc-derived composition, with a very subordinate contribution from the continental margin to the east of the arc. The Oligocene Andaman Flysch at Corbyn's Cove is dominated by recycled orogenic sources, but also contains subordinate arc-derived input. It is likely that the sources of the Andaman Flysch included rocks from Myanmar affected by India-Asia collision. Any contribution of

material from the nascent Himalayas must have been minor. Nd isotope data discount any major input from cratonic Greater India sources.

Keywords: Andaman, accretionary wedge, arc, subduction, thermochronology, provenance, uplift

3.2 Introduction

The Andaman-Nicobar Islands are part of an accretionary complex that forms the outer arc ridge of the northern Sunda subduction zone (Figure 3.1). The Andaman Islands are in the southeastern portion of the Bay of Bengal and comprise part of a 3000–5000 km chain that runs from the Myanmar Arakan-Yoma down to Sumatra and Java in the south. The Indian plate is subducting northwards below the Eurasian plate and obliquely below the Sino-Burman plate along the Burman-Andaman-Javan Trench.

The structure of Andaman Islands comprises an accretionary prism formed by an imbricate stack of east-dipping fault slices and folds that young to the west (Figure 3.2) linked to a westward-shifting subduction zone (e.g., Roy, 1992; Pal *et al.* 2003). The geology of an accretionary wedge is complex, reflecting its dynamic environments involving subduction, folding and thrusting. Depositional ages and environments can change rapidly over relatively short distances, and uplift leads to recycling of sediment from the eroding wedge. Throughout subduction, new material introduced at the bottom of the accretionary wedge is accreted, uplifted or subducted. Some of the accreted material may be uplifted and brought to the sea floor. Slope basins may develop behind folds in the accreted sedimentary rocks and trap sediment in a deep-water environment. Simultaneously shallow-water sediments, such as reefs can form on the prism top and be eroded and transported down the slope.

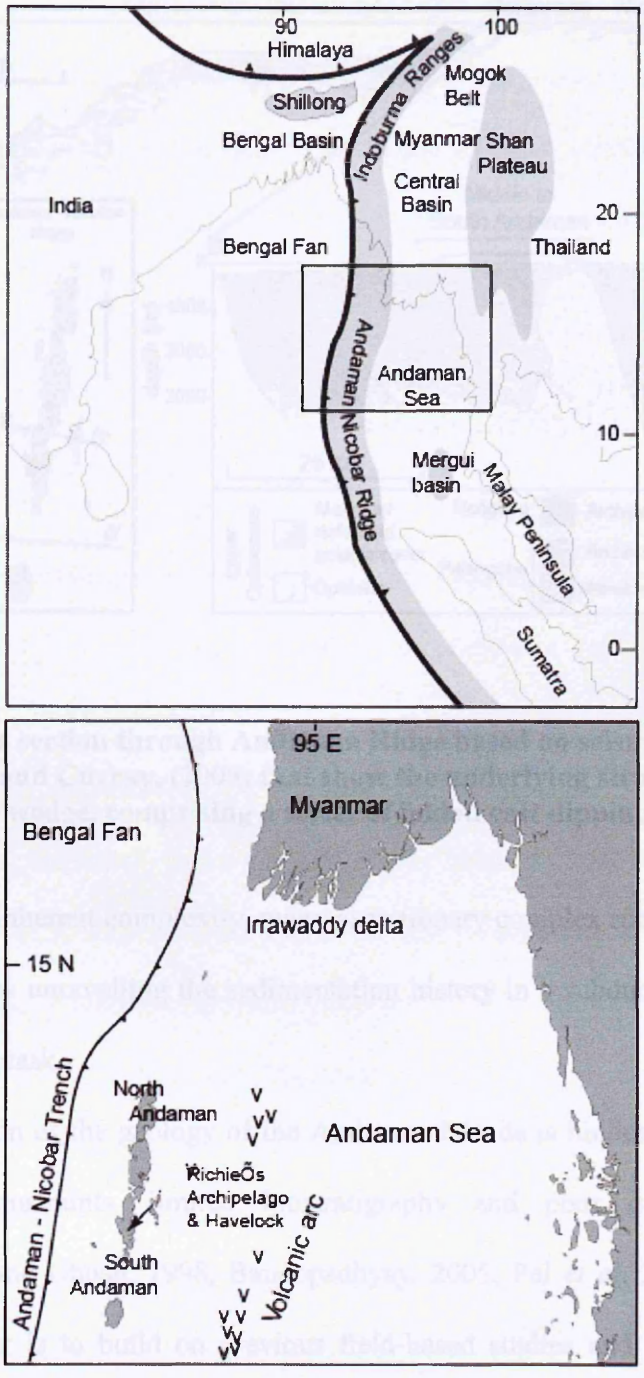

Figure 3.1 General location map of Andaman Islands and location of potential source regions. Lower figure corresponds to boxed area in top figure.

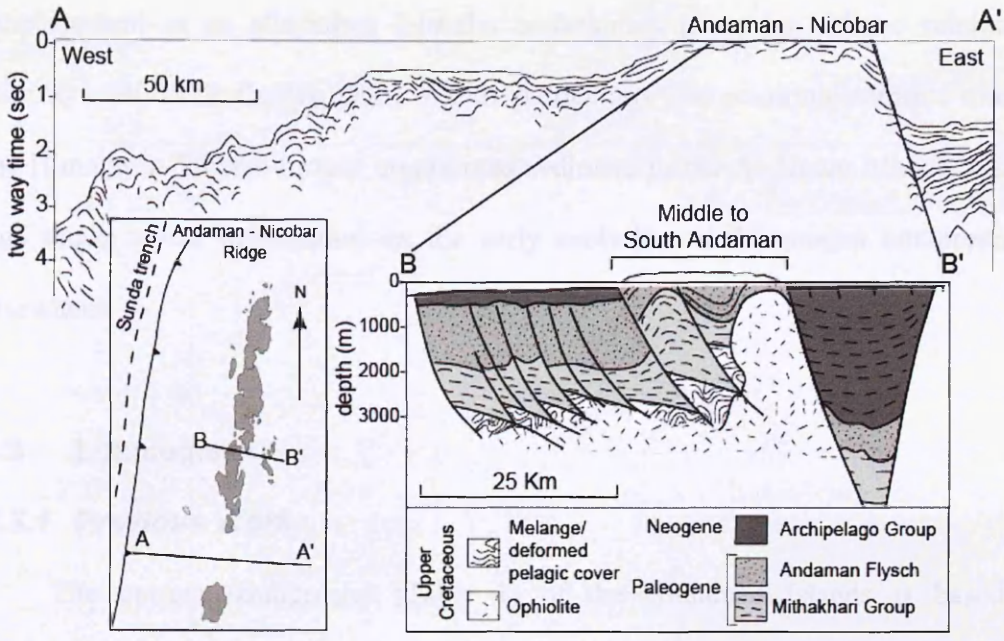

Figure 3.2 Cross section through Andaman Ridge based on seismic sections from Roy (1992) and Curray, (2005) that show the underlying structure of the accretionary wedge, comprising a series of folded east dipping thrust slices

Given this inherent complexity, many accretionary complex rocks are referred to as "mélange" thus unravelling the sedimentation history in a subduction-accretionary setting is a major task.

Interpretation of the geology of the Andaman Islands is hindered by the lack of isotopic age constraints, limited biostratigraphy and poor outcrop exposure (Bandopadhyay and Ghosh, 1998, Bandopadhyay, 2005; Pal *et al.* 2003, 2005). The aim of this paper is to build on previous field-based studies and apply petrologic, isotopic and thermochronometric techniques to better understand the provenance, sediment deposition and uplift history.

The origin of the Andaman Flysch has been debated for over 20 years. It has been variously proposed that the Andaman Flysch has been derived from the Irrawaddy (Karunakaran *et al.* 1968; Pal *et al.* 2003) or, alternatively, from Bengal Fan material shed from the nascent Himalaya sourced either directly or by

emplacement as an allochthon into the accretionary prism by oblique subduction (Curray *et al*, 1979; Curray 2005). We are particularly interested to determine whether the Himalayan-Tibetan orogen contributed sediment to the Andaman Islands because this might reveal information on the early evolution of the orogen not preserved elsewhere.

3.3 Lithologies

3.3.1 Previous Work

The current stratigraphy (Table 1) of the Andaman Islands is based on lithological mapping and can be traced back to the pioneering work of Oldham (1885) who first divided the Andaman geology into an older Port Blair Series and a younger Archipelago Series separated by volcanic rocks and serpentinites later recognised as an ophiolite. Over the last 50 years the stratigraphy has been modified and formation names changed, but it was not until the 1960s that paleontological constraints were used to place the Paleogene-Neogene lithostratigraphic units within a temporal framework (Guha and Mohan, 1965; Karunakaran *et al.* 1964, 1968). The stratigraphy now comprises four units, which in ascending order are Cretaceous sedimentary rocks and ophiolite, Eocene Baratang/ Mithakhari Group, Eocene to upper Oligocene Port Blair/Andaman Flysch Group and lower to upper Miocene Archipelago Group. In the mid-1970's the Indian state Oil and Natural Gas Commission (ONGC) carried out a detailed seismic reflection study across the Islands, calibrated against offshore boreholes drilled to the east and west of the Andaman Islands (Figure 3.2) that helped place the exposed geology within the context of the accretionary setting. Below we briefly describe the main rock units exposed on the Andaman Islands and report key observations from previous field and petrographic studies.

Approximate depositional age range	Group	Formation	Lithology
Miocene to Pliocene	**Archipelago Group**		Cross-stratified and graded sandstones, silty mudstones and limestones marls, and chalky limestones
Oligocene-Late Eocene ??	**Andaman Flysch Group** *(formerly Port Blair Group)*		Bouma sequences, sandstone-shale and mudstones
Early to Middle Eocene ??	**Mithakhari Group** *(formerly Baratang and Port Meadow Groups)*	Namunagarh Grit	Pebbly and coarse to fine grained volcaniclastic sandstones and grits
		Hope Town conglomerate	Interstratified massive and graded polymict conglomerates, massive cross-stratified and graded sandstones, shales and thin coals
		Lipa Black Shale	Pyritiferous black shale
Late Cretaceous to Palaeocene ??	**Ophiolite Group**		Pillow lava, basalt, gabbro, pyroxinite, harzburgite, serpentinite, andesite, diorite, plagiogranite, rhyolite, serpentinized harzburgite, pyroxinite and pelagic sediments radiolarian chert and hematitic mudstones

Table 1. Simplified stratigraphy of the Andaman Islands

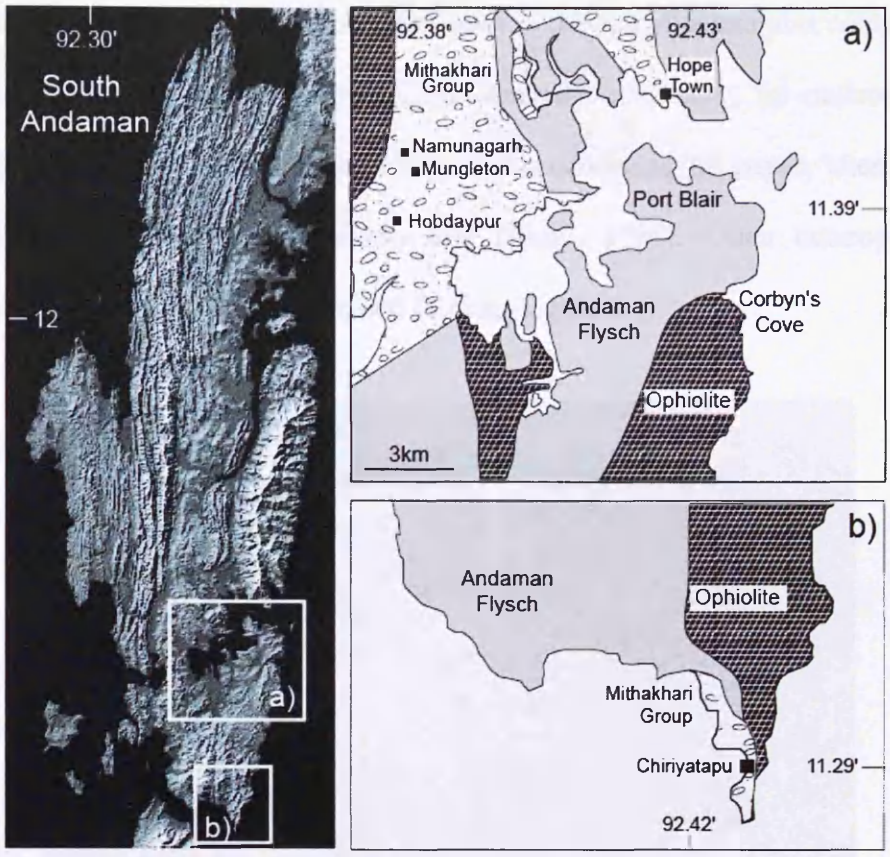

Figure 3.3 General location map of Andaman Islands and local geology (a, and b) for the areas on South Andaman sampled for this study.

Ophiolite: The Andaman ophiolite contains the main components of an ophiolite sequence that includes upper mantle depleted harzburgites and dunites, lower crustal cumulates gabbros and peridotites and upper crustal sheeted dykes, pillow lavas and marine pelagic sediments (Halder, 1985; Ray *et al.* 1988; Roy, 1992). However, the sequence is tectonically disturbed and much of the crustal section is deformed and difficult to identify in the field. Pillow lavas are abundant, but sheeted dykes have only been identified disrupted small-scale faulting and folding. Both massive and layered gabbros are recognized in the preserved ophiolite. South Andaman has the best-preserved and most complete sequence of ophiolite that extends for about 30 km from Corbyn's Cove in the north to Chiriyatapu in the south (Figure 3.3).

Pelagic Sedimentary Rocks: The topmost part of the ophiolite complex contains thin and discontinuous lenses and streaks, and laterally continuous (at outcrop scale) bedded sequences of pelagic sedimentary rocks consisting of jasper, chert, cherty limestone and shales (Bandopadhyay and Ghosh, 1998). Often outcrops show evidence of significant deformation and folding (Figure 3.4).

Figure 3.4 Folded cherts and shales that represent the pelagic cover to the Cretaceous ophiolite exposed on the shore at Chiriyatapu, South Andaman.

***Bedded Chert*:** Rhythmic alternations of cm-thick, milky white chert and mm-to-cm thick reddish brown and purple shale/mudstone beds constitute the bedded chert facies. Chert and shale normally show uniform (0.5–4.0 cm thick) beds that have sharp bases and tops and planar contacts. Occasionally, 10 to 15 cm thick and massive chert beds are present. Soft-sediment deformation is evident in some locations. Radiolaria are preserved to varying degrees in most cherts and indicate a late Cretaceous to Paleocene depositional age, which constrains the underlying ophiolite sequence to an Upper Cretaceous age.

***Shale*:** At outcrop the shale facies form interbedded sequences of extremely variable thickness and lateral continuity. Basaltic volcanic rocks occur as thin intercalations, conformable lenses, and at places, small cross-cutting dikes. Thin beds of fine-grained sandstone, siltstone, and cherty limestone are also present. There is evidence of soft-sediment deformation, slump folds, as well as cutting by normal and thrust faults. Some shales are clearly tuffaceous with plagioclase phenocrysts, vitric fragments, pumice clasts and diagenetically altered volcanic lithic fragments. Chlorite is abundant in the matrix of the altered tuff and tuffaceous shale. Occasionally sharp edged, cuspate or platy, fresh glass shards can be found (Bandopadhyay and Ghosh, 1998).

Mithakhari Group

The Mithakhari Group consists of immature gravels and coarse to fine-grained sandstones, pebbly to fine-grained pyroclastic sandstones and minor thin beds of mudstones and coal. Whilst the Mithakhari Group dominates the outcrop geology of the Andaman Islands, particularly in North and Middle Andaman, a paucity of good exposures and poor access make it difficult to obtain continuous sections and exposures are limited to isolated stone quarries, coastal areas and road cuttings. In South Andaman the Mithakhari Group occurs as a north-south trending outcrop that extends for ~50 km, but the best sections exposing the least weathered outcrops are only found near Hope Town, Mungleton, Namunagarh and Chiriyatapu (Figure 3.3). Karunakaran *et al.* (1968) first introduced the term Mithakhari Group; dividing the Group into lower Lipa Black shale, middle Hope Town Conglomerate, and an upper Namunagarh Grit Formation (Table 1). The Lipa Black shale is a minor unit and not well exposed and so will not be considered any further.

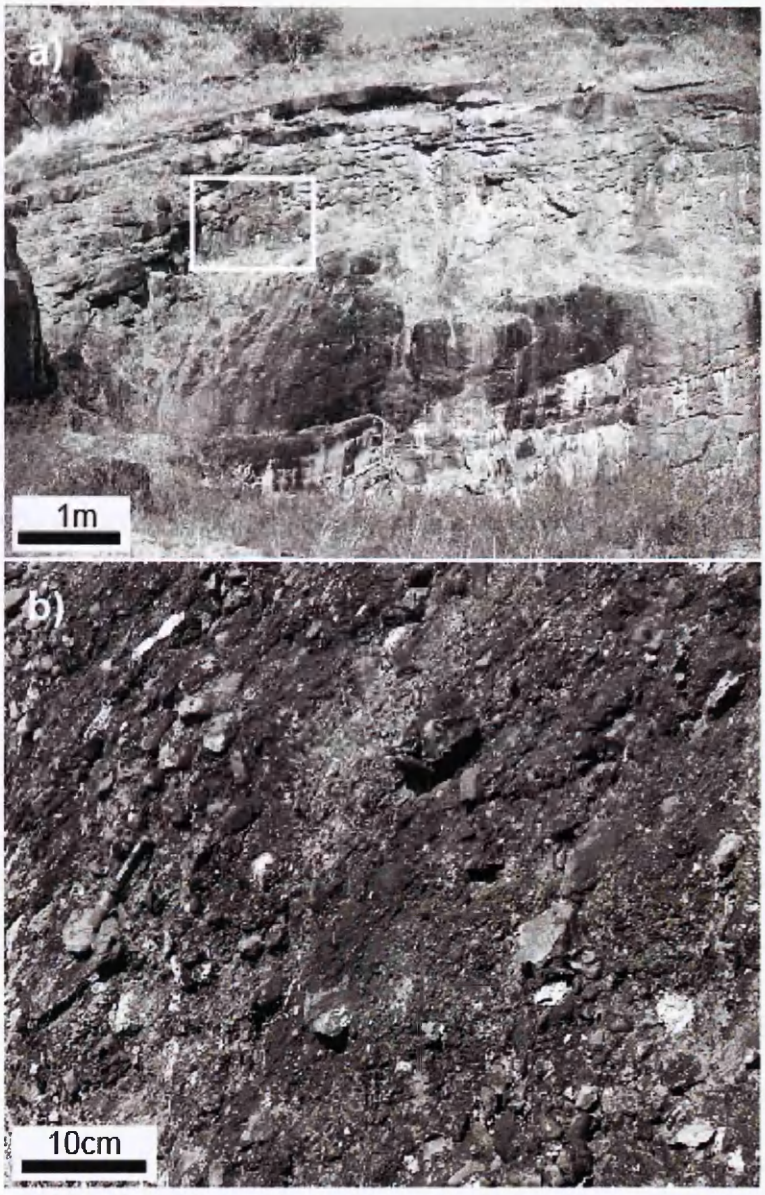

Figure 3.5 Massive polymict conglomerates exposed at Hope Town Quarry (5a), South Andaman. These polymict conglomerates are dominated by basic and ophiolitic clasts (5b) whilst the matrix contains abundant volcanic glass and felsitic volcanic grains, which suggests a dominant volcanic arc source, although zircon FT data also show evidence of continental Mesozoic sources.

Hope Town Conglomerates: This is best seen near Hope Town on South Andaman where there is a good exposure of ~6 m of conglomerates and pebbly sandstones (Figure 3.5) interbedded with thin beds of greenish grey coarse and fine-grained sandstones. The sequence shows fining and thinning upward sequences with evidence of slumping and soft sediment deformation. Bed contacts are generally sharp and planar and some evidence of fluvial channels can be found. Conglomerates are polymict, of mainly basic-ultrabasic sources with subordinate to minor amounts of andesite, sedimentary limestone, cherts with occasional mudstone clasts and metamorphic quartz.

Namunagarh Grit Formation: This unit is characterized by coarse to fine-grained sandstones and siltstone with minor conglomerate occurring at the base. On South Andaman the type section and best exposures are found in quarry sections near Namunagarh village (Figure 3.3). These display 3–5 m thick, green, matrix-supported sandstones. The sandstones are well bedded, laterally persistent along the quarry sections and consist of coarse and fine-grained beds. The coarse-grained beds, occurring at the base of the section, are ≥1 m thick, with sharp non-erosive contacts. The finer-grained beds consist of 4–8 cm thick beds of fine to medium grained volcaniclastic sandstones interbedded with thin mudstones. Large fragments of volcanic rock fragments, including elongated pumice lapilli are sometimes present. These resemble floating clasts in turbidites. For a long time the sandstones exposed at Namunagarh stone quarries have been described as greywacke formed from weathering and erosion of accreted ophiolite (Acharyya *et al.* 1989). Recently Bandopadhyay (2005) identified beds with abundant pyroclasts including vesiculated glass fragments, pumice clasts and shards, euhedral feldspars and angular lithic

fragments diagnostic of tuff, indicating that some of the Namunagargh Grit beds were derived from direct volcanic arc input (Figure 3.6).

The polymict conglomerates (Hope Town Conglomerate) and grits (Namunagarh Grit Formation) are interpreted as derived from the ophiolite and its pelagic-shallow marine cover. The succession, which includes thin coals and gypsum, was deposited in a delta slope setting with facies associations ranging from subaerial alluvial plain to prodelta slope (Chakraborty *et al.* 1999). Its depositional age is not well defined due to the lack of distinct biostratigraphic evidence but shallow benthic foraminifera in the Hope Town Conglomerate including *Nummulites atacicus* constrain the age to between the late Ypresian and early Lutetian (Karunakaran *et al.* 1968) although many foraminifera are broken and abraded (i.e. reworked). The relationship of the Namunagargh Grits to the Hope Town Conglomerates is not clear although the Namunagarth Grits are presumed to be younger.

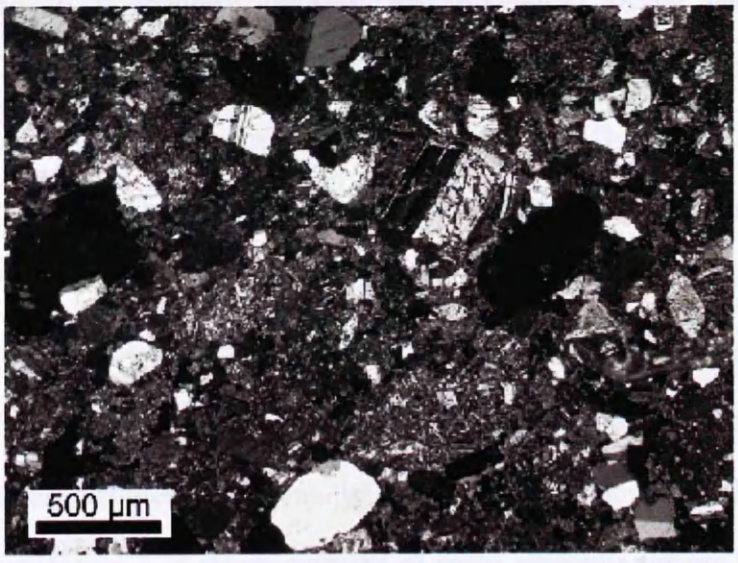

Figure 3.6 Namunagargh Quarry. Thin sections show the sediments are largely tuffaceous showing clear evidence of fresh arc volcanic material including devitrified glass.

Figure 3.7 Outcrop of the Andaman Flysch looking south across Corbyns Cove (see figure 3.3) towards outcrops of pillow basalts and ophiolite.

Andaman Flysch

The Andaman Flysch is a siliciclastic turbidite sequence deposited on a submarine fan. It is bounded between the Mithakhari Group below and the Archipelago Group above. The (misleading) term flysch derives from their resemblance to the classic Bouma turbidites described in the Swiss Alps. Similar looking beds are seen throughout the Andaman Islands; hence the Andaman Flysch is described as outcropping over a N-S strike length of 200 km from the southern part of South Andaman to the northern tip of North Andaman. Overall thickness is not well defined with estimates varying from 750 m (Roy, 1983) to 3000 m (Pal *et al.* 2003). The best and most completely documented exposures are found on South Andaman at Corbyn's Cove (Figure 3.3) where outcrops of steep, westerly-dipping beds are seen adjacent to the pillow basalt of the ophiolite sequence (Figure 3.7), although the nature of the contact is uncertain. Individual sandstone beds can be traced along strike for distances of several kilometers but the total thickness is only 250–300 m. Current

directional structures in sandstone beds include flute casts, groove casts and current bedding. Orientation of flute casts at the base of overturned sandstone beds near Corbyn's Cove reveals southward-directed paleocurrents (Pal *et al.* 2003). The relationship between the turbidites and underlying lithostratigraphic units is unclear. Onlap of the Andaman Flysch with the Mithakhari Group has been reported (Chakraborty and Pal, 2001) but no supporting evidence was found in this study. However, there is a marked change in lithology and provenance with up to 50% quartz in the Andaman Flysch in contrast to the relatively quartz-free Mithakhari Group (Pal *et al.* 2003). Lithic fragments in the Andaman Flysch range from micaceous metamorphic clasts diagnostic of continental sources to cherts, basalts and weathered volcanic glass consistent with derivation from volcanic arc and ophiolite. Biostratigraphic evidence is vague and spans the Oligocene to early Miocene, approximately 36–21 Ma (Pal *et al.* 2003).

Archipelago Group

The Archipelago Group represents the topmost stratigraphic unit of the Tertiary succession. The lower units comprise basal conglomerates and sandstones overlain by calcareous arenites of the Strait Formation. This is followed by chalk and limestone with some argillaceous limestones and shale, described as Melville Limestone (Shell Limestone) Formation. Deposition was mostly in a slope environment (Pal *et al.* 2005; Roy, 1983). These sedimentary rocks most likely covered most of Andaman but recent uplift and erosion means that today only small patches can be found on the main islands, with most exposure confined to Havelock Island and associated smaller islands to the east of South Andaman in Richie's Archipelago (Figure 3.1). Radiolaria, planktonic foraminifera and calcareous nannofossils from John Lawrence

Island (Singh *et al.* 2000) indicate a maximum depositional age for the calcareous chalk Archipelago Formation of 18.3–15.6 Ma (Burdigalian to Serravallian) but elsewhere the Archipelago Group may span anywhere between the Miocene to Pliocene (Pal at al., 2005).

3.4 Methodological Details

The aim of this work is to provide improved understanding of the burial and uplift history of the accretionary wedge and provenance of constituent sedimentary rocks, now exposed on the Andaman Islands though the application of thermochronometry, petrographic and geochemical analysis of the sedimentary rocks. Multiple proxies are used to get the best image of source provenance and to avoid potential bias that may arise by relying on a single type of mineral. For example, mica is generally not present in arc-derived volcanic rocks whilst apatite and zircon are. Sampling is confined to South Andaman where there are accessible exposures of the main type localities, studied by Bandopadhyay and Ghosh, (1998), Chakraborty and Pal (2001), Pal *et al.* (2003, 2005), and Bandopadhyay (2005). Both Middle and North Andaman are less developed and more inaccessible with extensive areas of jungle that includes large tribal reserves that are restricted to aboriginal peoples.

Samples from South Andaman were collected for detrital thermochronometry, heavy mineral studies, biostratigraphy and Sm-Nd whole rock and single grain analysis.

3.4.1 Zircon and apatite fission-track analysis

Apatite and zircon fission-track (FT) analysis are used to define provenance low-temperature histories and where sediments have been subjected to significant (>1.5 km) burial their post-depositional burial and uplift history. Fission tracks in apatite are

sensitive to relatively low temperatures (typically <60–110°C) and ideally suited to constrain levels of post-depositional burial and timing of subsequent rock uplift and exhumation (e.g., Green at al., 1995). Zircon fission-track data record higher temperature cooling histories (typically ~200–310°C) and for sedimentary rocks are more suited to provenance studies recording either volcanic formation ages or post-metamorphic cooling/exhumation ages (Carter, 1999). Samples for FT analysis were irradiated in the well thermalised (Cd ratio for Au >100), Hifar Reactor, at Lucas Heights in Australia. Apatite grain compositions were monitored using etch pits and direct measurement on a JEOL microprobe using a defocused 15 KeV Beam to prevent F and Cl migration. Durango apatite and rock salt were used as standards. Samples with mixed age, indicated by c^2 values <5% and large age dispersion values (>20%) were deconvolved into their principal age components using the approach of Sambridge and Compston (1994) incorporating the method of Galbraith and Green (1990).

3.4.2 Apatite Helium analysis

Apatite helium dating was used to provide additional constraint on rock uplift histories. The method complements FT dating as it is sensitive to closure at ~60°C, the temperatures where FT begin to lose sensitivity to changes in cooling rate. Helium ages were based on replicate analyses of apatite grains hand picked to avoid mineral and fluid inclusions. Each selected grain was first photographed, and its dimensions were recorded for later alpha ejection correction. Samples were loaded into platinum microtubes for helium outgassing and U/Th determination. Outgassing was achieved using an induction furnace at temperatures of 950°C. The abundance of ^{4}He was measured relative to a 99.9% pure ^{3}He spike in a Pfeiffer Prisma 200 quadrupole mass

spectrometer. Quantification of U/Th was performed on an Agilent 7500 quadrupole mass spectrometer using spiked solutions of the dissolved apatite. Repeated analysis of the California Institute of Technology (CIT) laboratory Durango apatite standard gives an age of 31.3 ± 1.2 Ma (2 sigma) based on 39 analyses. This error of the mean (6.7%), combined with the U/Th and He analytical uncertainties is used as a measure of the total uncertainty in sample age.

3.4.3 Ar-Ar age dating of detrital white micas

The $^{40}Ar/^{39}Ar$ age of a detrital muscovite records the timing of cooling and exhumation (or crystallisation) of rocks in its source region, aiding the discrimination of potential source regions for clastic sequences (e.g., Sherlock *et al.* 2002; Haines *et al.* 2004). For this study single-grains were totally fused using an infra-red laser ablation microprobe (IRLAMP). Samples were monitored using the GA1550 biotite standard with an age of 98.8 ± 0.5 Ma (Renne *et al.* 1998). The calculated *J* value for the samples was 0.0138 ± 0.000069. Blanks were measured both before and after each pair of sample analyses, and the mean of the two blanks was used to correct the sample analyses for the measured isotopes. Overall mean blank levels for ^{40}Ar, ^{39}Ar and ^{36}Ar were (378, 6 and 11) x 10^{-12} cm^3 at standard temperature and pressure. The resulting analyses were also corrected for mass spectrometer discrimination, ^{37}Ar decay, and neutron induced interferences. The correction factors used were: $(^{39}Ar/^{37}Ar)_{Ca}$ = 0.00065, $(^{36}Ar/^{39}Ar)_{Ca}$ = 0.000264, and $(^{40}Ar/^{39}Ar)_{K}$ = 0.0085; these were based on analyses of Ca and K salts. Samples were irradiated for 33 hours in the McMaster University reactor (Canada).

3.4.4 U-Pb dating of detrital zircon

Zircon U-Pb dating reflects the time of zircon growth, which in most cases is the rock igneous crystallization age. The U-Pb system is mostly unaffected by high-grade metamorphism and is effectively stable up to ~750°C (Cherniak and Watson, 2001; Carter and Bristow, 2001). Zircon U-Pb ages from detrital grains in a sedimentary rock are therefore expected to be representative of the range of crustal ages within the contributing drainage basin. Samples for this study were analysed at University College London by LA-ICPMS using a New Wave 213 aperture imaged frequency quintupled laser ablation system (213 nm) coupled to an Agilent 750 quadrupole ICPMS. Real time data were processed using GLITTER and repeated measurements of external zircon standard PL (Svojtka *et al.* 2001; TIMS reference age 337.1 ± 0.7 Ma) to correct for instrumental mass bias. The results have not been corrected for common lead or ranked according to degree of discordance as the latter involves choosing an arbitrary value and is therefore open to analyser bias.

3.4.5 Sm-Nd isotope analysis

Whole rock Sm and Nd isotope data in sedimentary rocks are widely used to fingerprint sediment source. $^{143}Nd/^{144}Nd$ ratios are generally normalised and expressed in epsilon units as deviation from a chondritic uniform reservoir, where CHUR $\varepsilon Nd = 0$. A single epsilon unit is equivalent to a difference in $^{143}Nd/^{144}Nd$ ratio at the 4th digit. For clastic sedimentary rocks εNd will in part represent the weighted average of when the sediment sources were extracted from the mantle. When melt is extracted from the mantle it has a lower Sm/Nd ratio than its parent and therefore evolves over time to have a lower εNd than CHUR, the residual has a higher Sm/Nd than CHUR evolving to higher εNd over time.

For this study sandstone and mudstone samples were collected from type locations from the Andaman Flysch and the Mithakhari Group. Whole rock samples were ignited overnight at 900°C to remove any organic material. Dissolution and analytical methods follow Ahmad *et al.* (2000) with the exception that the samples were spiked with a mixed ^{150}Nd-^{149}Sm spike and ^{143}Nd-^{144}Nd ratios measured on the spiked fraction. εNd is calculated relative to the present-day (i.e. at t = 0) using CHUR $^{143}Nd/^{144}Nd = 0.512638$. Sm and Nd blanks were less than 10^{-3} of sample and the laboratory Johnson Mathey Nd internal standard gave $^{143}Nd/^{144}Nd = 0.511119 \pm 5$ (1 sigma=24) over the period of the analyses. As whole rock εNd typically represents the weighted average of sediment sources, further insight into the origin of the Andaman Flysch was achieved by analyzing the Nd isotope character of single apatite grains. This was achieved using a 193 nm homogenized ArF New wave/Merchantek laser ablation system linked to a ThermoFinigan Neptune multicollector mass spectrometer at the University of Cambridge (UK). All ablation was carried out in a He environment and mixed with Ar and N after the ablation cell. Laser spots sizes were 65–90 μm. During the analytical period standards reproduced to better than 0.5 epsilon units, whilst samples typically gave internal precisions of 1–2 epsilon units. The full methodology of this *in situ* approach is detailed in Foster and Vance (2006).

3.4.6 Petrography and heavy minerals

400 points were counted in six selected samples according to the Gazzi-Dickinson method (Dickinson, 1985). A classification scheme of grain types allowed for the collection of fully quantitative information on the sampled sandstones. Transparent dense minerals were counted on grain mounts according to the 'ribbon counting' method, and 200 minerals were counted also to assess the percentage of

etched and corroded grains. Dense minerals were concentrated with sodium metatungstate (density 2.9 g/cm$^{3)}$ using the 63–250 μm fraction treated with hydrogen peroxide, oxalic acid and sodium ditionite to eliminate organic matter, iron oxides and carbonates respectively.

3.5 Results and Interpretation

3.5.1 Biostratigraphy

Attempts to extract new, more robust, biostratigraphic control for the Paleogene sedimentary rocks based on nannofossils failed due to the barren nature of the mudstones. Samples of mudstone were taken from the Archipelago Group, Andaman Flysch Group and the Mithakhari Group. Whilst nannofossils are present in the calcareous Neogene sedimentary rocks (Archipelago Group) (Singh *et al.* 2000), we can only conclude that nannofossils were either never present in the Paleogene sedimentary rocks, have since been dissolved by weathering or dissolution below the carbonate compensation depth. Similarly, the sampled rocks yield few (as yet undated) foraminifera. Those found were either broken or abraded, consistent with reworking. At Chiriyatapu clasts of limestone were present within the coarse grained Mithakhari sedimentary rocks (Figure 3.8a). These were found to have shallow marine reef assemblages including *Nummulites* spp, small miliolids and rare *Morozovella* spp, fragments of rodophytes algae, dasyclads (*Belzungia* spp.) of Thanetian-Ypresian age (~58–49 Ma) (Figure 3.8b).

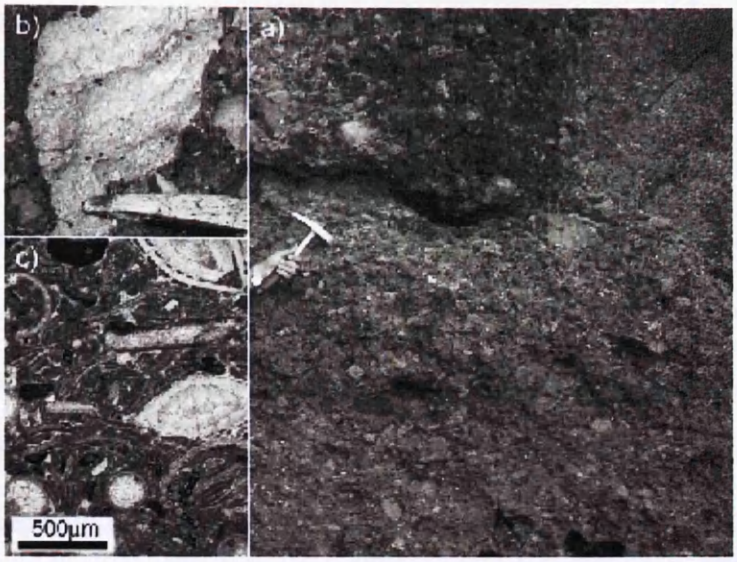

Figure 3.8 a) and b) show clasts of limestone from Mithakhari sediments. These have shallow marine reef assemblages that in thin section (c) are seen to include Nummulites spp, small miliolids and rare Morozovella spp, fragments of rodophytes algae, dasyclads (Belzungia spp.) that indicate an Thanetian–Ypresian depositional age. No in situ outcrops of these beds have been found on South Andaman.

3.5.2 Fission track and (U/Th)-He thermochronometry

Samples from the Mithakhari Group contained relatively low concentrations of heavy minerals and yielded fewer apatites and zircon than Andaman Flysch. For this reason FT datasets from the Mithakhari Group were smaller compared to the Andaman Flysch. Nevertheless the results adequately provide a measure of the underlying detrital FT signatures for each key lithostratigraphic unit. Data are summarised as radial plots in Figures 3.9 and 3.10, and tabulated in Appendix Table 1.

Interpretation of detrital apatite FT data requires comparing youngest ages with sediment depositional age. If all single grain ages are less than depositional age, total resetting took place (generally indicating burial heating to >100–120°C, e.g. Green *et al.* 1995, figure 3.12) whereas if the population of measured single grain ages range from younger to older than depositional age, partial resetting has taken place

(generally indicating burial heating to <100°C). The main issue with interpreting the Andaman FT data is that suitable depositional ages are missing, preventing robust use of FT analysis to determine exhumation rates. Samples from the Hope Town Conglomerate collected at Hope Town quarry (Figure 3.5) yield a single population of apatites with an age of 57 ± 9 Ma. The large uncertainty in age is due to low uranium concentrations. The zircon ages comprise three age modes with the youngest (majority of analysed grains) at 61 ± 2 Ma, within error of the apatite age. The other zircon ages indicate sources with Late Cretaceous and Permian cooling signatures. Given that the zircon grain ages from Hope Town Conglomerate are at or older than the Eocene biostratigraphic age (maximum age due to reworked nature of the fossils), the FT ages must reflect different sources. Furthermore, given that the apatite grains have the same age as the youngest zircon ages, the apatite data must also reflect provenance.

The youngest apatite and zircon ages at ~60 Ma constrain depositional age to being at or after this time for the Hopetown Conglomerate Formation at this location. The apatites are noticeably euhedral, contain variable chlorine and are low in uranium (Figure 3.11), typical of volcanic apatites, consistent with sample petrography that records a dominant flux of volcanic detritus (see below). Similar FT ages and volcanic affinities are seen in the apatite and zircon data from Mungleton quarry (20 km inland from the Hope Town quarry, Figure 3.5) exposing a 6-m-thick sequence of interbedded greenish grey, fine to medium grained sandstones, siltstones and mudstones, underlain by conglomerates. The succession here was described as Namunagarh Grit Formation. In contrast, the apatite FT data from a quarry at Namunagarh village (also mapped as Namunagarh Grit Formation) gave a single population age of 40 ± 4 Ma based on 24 grains. Zircon content of this sample was too low for FT analysis. This quarry studied by Bandopadhyay (2005), comprises

tuffaceous beds with well-preserved pumice fragments and glass shards. The apatites are euhedral and have variable chlorine and low uranium contents typical of volcanic sources. Detrital assemblages in these rocks contain pyroxenes, epidote, sphene, green-brown hornblende, and chrome spinel that is consistent with provenance from a volcanic arc. Major diagenetic dissolution is also evident, so it is questionable whether the apatite age reflects source or resetting. No tracks lengths were measured as a result of the low spontaneous track density. A sample of Namunagargh Grit Formation from Chiriyatapu on the southern coast of South Andaman yielded only zircon that produced three FT provenance age modes at 40 ± 3 Ma, 91 ± 7 Ma and 329 ± Ma. The youngest zircon FT age mode at 40 ± 3 Ma indicates that the Thanetian-Ypresian limestone clasts found in these rocks were derived from erosion of significantly older material (by ~16 Ma). Thus we conclude that the age of Mithakhari Group is constrained to be younger than 60 Ma at two locations, and younger than 40 Ma at a third location. Nevertheless, the volcanic origin of the material, with little sign of reworking, suggests that the rocks were deposited only shortly after the mineral ages were reset. This is consistent with diachronous deposition in local basins as expected in a subduction zone setting (e.g. Draut and Clift, 2006).

Apatite and zircon FT data from four samples collected through the section of Andaman Flysch at Corbyn's Cove are closely similar in age (most are 35–40 Ma) to the youngest age modes in the Namunagargh Grit Formation beds. The youngest ages comprise the majority of analysed grains for zircon and all analysed grains for the apatites. In addition, two of the samples contain zircons age modes at 58–67 Ma similar to the age modes detected in the Mithakhari Group. Three of the samples also contain Mesozoic and Paleozoic FT ages. The Andaman Flysch is widely considered to be Oligocene in age, although biostratigraphic evidence is not robust (Pal *et al.*

2003). Whilst both zircon and apatite FT ages are older than the Oligocene some partial resetting (burial related heating) may have taken place.

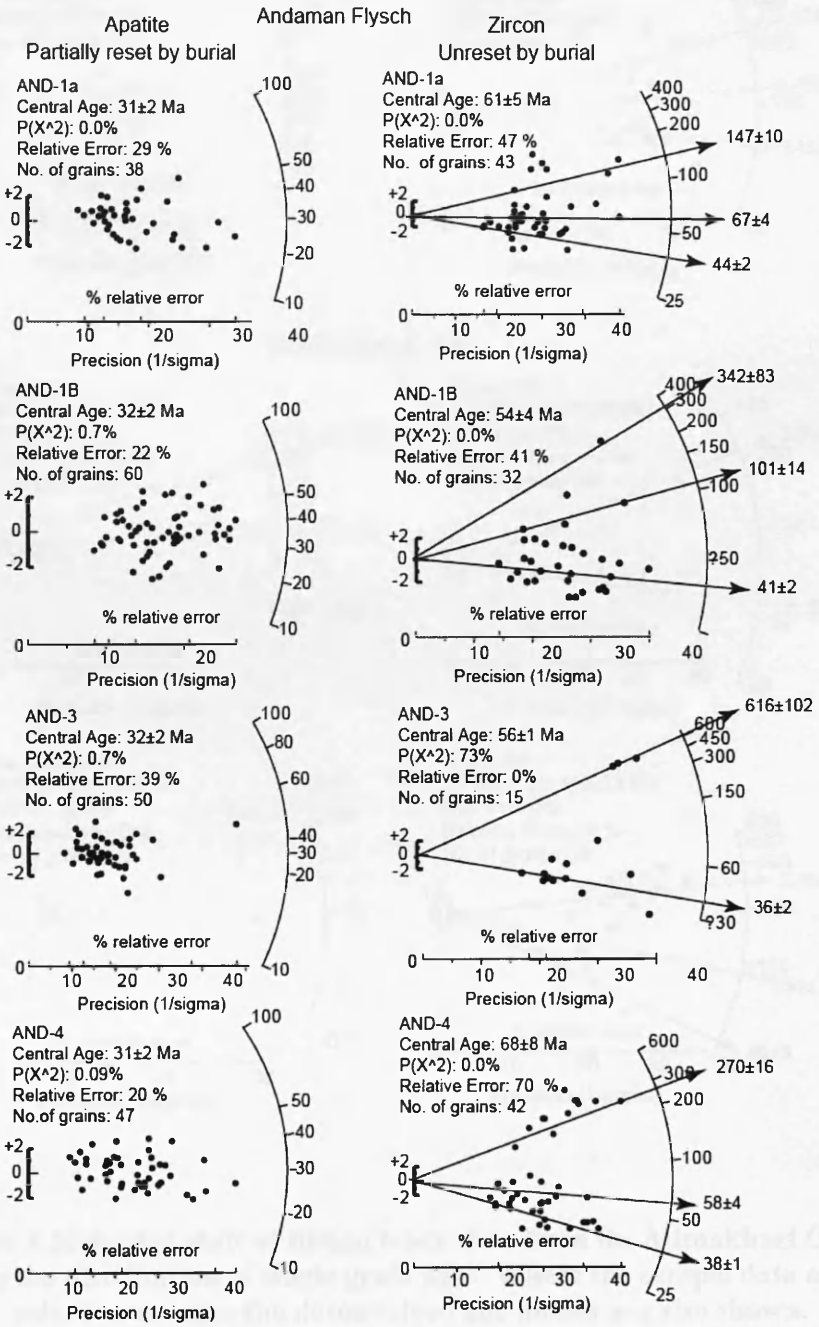

Figure 3.9 Radial plots of fission track data from the Andaman Flysch showing the distribution of single grain ages. Where the sample data comprise mixed grain ages the deconvolved age modes are also shown.

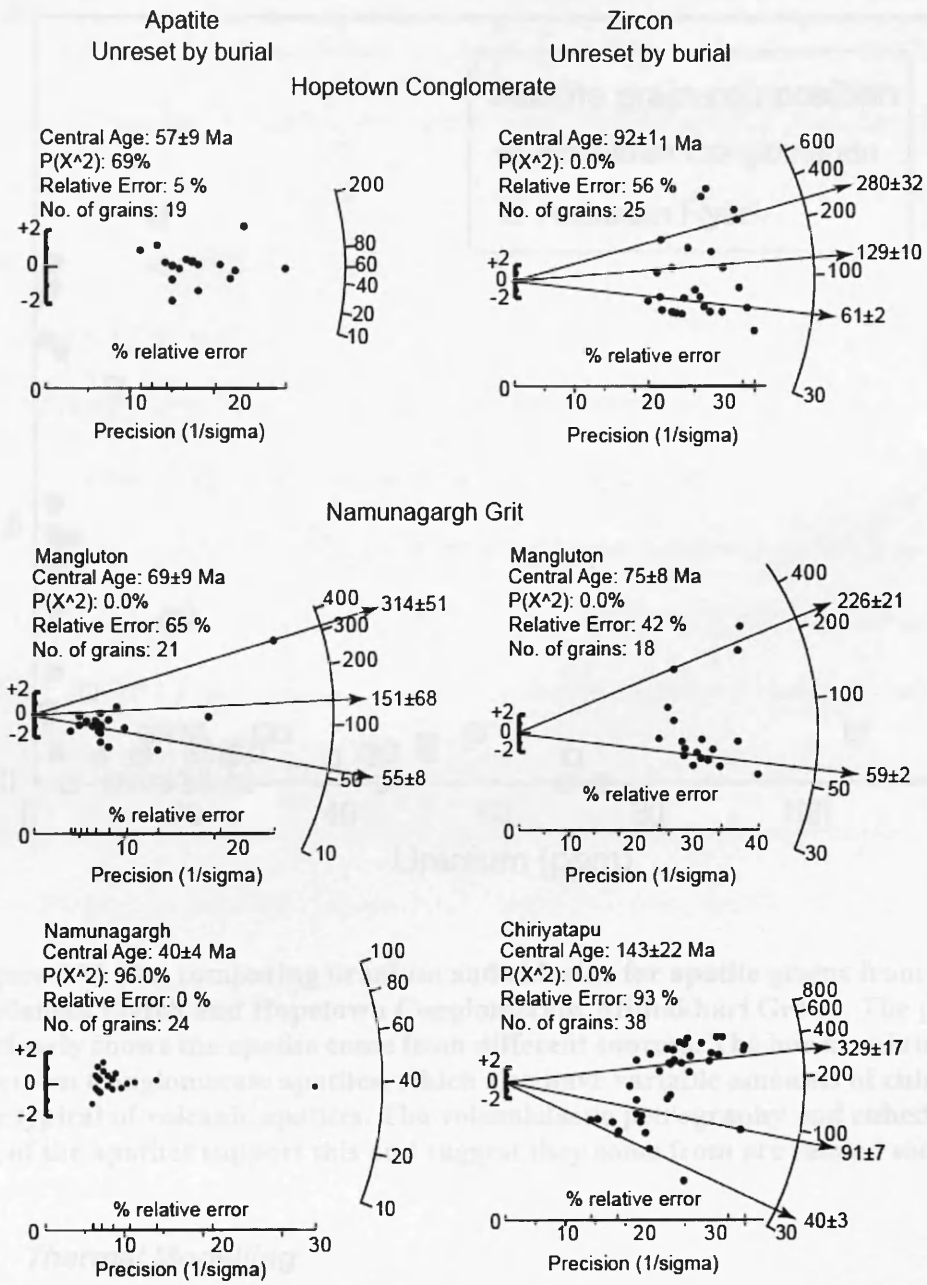

Figure 3.10 Radial plots of fission track data from the Mithakhari Group showing the distribution of single grain ages. Where the sample data comprise mixed grain ages the deconvolved age modes are also shown.

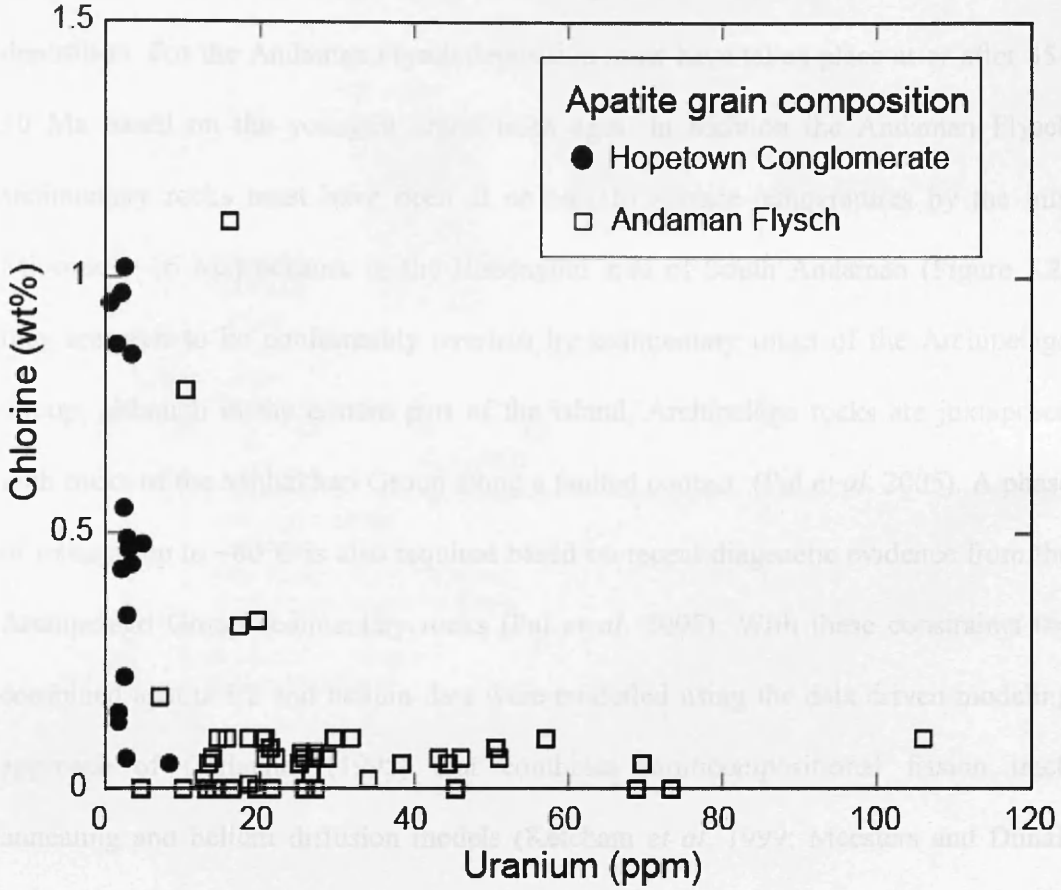

Figure 3.11 Plot comparing uranium and chlorine for apatite grains from the Andaman Flysch and Hopetown Conglomerate, Mithakhari Group. The plot clearly shows the apatite come from different sources. The low uranium Hopetown Conglomerate apatites, which also have variable amounts of chlorine are typical of volcanic apatites. The volcaniclastic petrography and euhedral form of the apatites support this and suggest they come from arc related sources.

3.5.3 Thermal Modelling

To constrain post-depositional thermal history, apatites from one of the samples were analysed by the (U/Th)-He method (Appendix Table 2). Replicates yielded an FT corrected age of 16 ± 1 Ma, crudely representing the time at which the sample cooled to <50 ± 10°C. To define more robustly sample post-depositional thermal history the FT and helium data can be jointly modeled. Ideally this requires incorporating a sample depositional age, but as discussed this is not well defined and

so we resort to using the youngest detrital ages as an upper limit for the time of deposition. For the Andaman Flysch deposition must have taken place at or after 35–30 Ma based on the youngest argon mica ages. In addition the Andaman Flysch sedimentary rocks must have been at or near to surface temperatures by the mid Miocene (~16 Ma) because in the Hobdaypur area of South Andaman (Figure 3.2) they are seen to be conformably overlain by sedimentary rocks of the Archipelago Group, although in the eastern part of the island, Archipelago rocks are juxtaposed with rocks of the Mithakhari Group along a faulted contact (Pal *et al.* 2005). A phase of reburial up to ~60°C is also required based on recent diagenetic evidence from the Archipelago Group sedimentary rocks (Pal *et al.* 2005). With these constraints the combined apatite FT and helium data were modelled using the data driven modeling approach of Gallagher (1995) that combines multicompositional fission track annealing and helium diffusion models (Ketcham *et al.* 1999; Meesters and Dunai, 2002). The best-fit solution (Figure 3.12), highlights three important stages: 1) A requirement for deposition and burial to peak temperatures of ~80–90°C between ~30–25 Ma. 2) Uplift to the surface between ~25–20 Ma. 3) Reburial in the Miocene (~25–5 Ma) to temperatures of 50–60°C (broadly equivalent to depths of ~1–1.5 km, assuming geothermal gradients of 30°C/km).

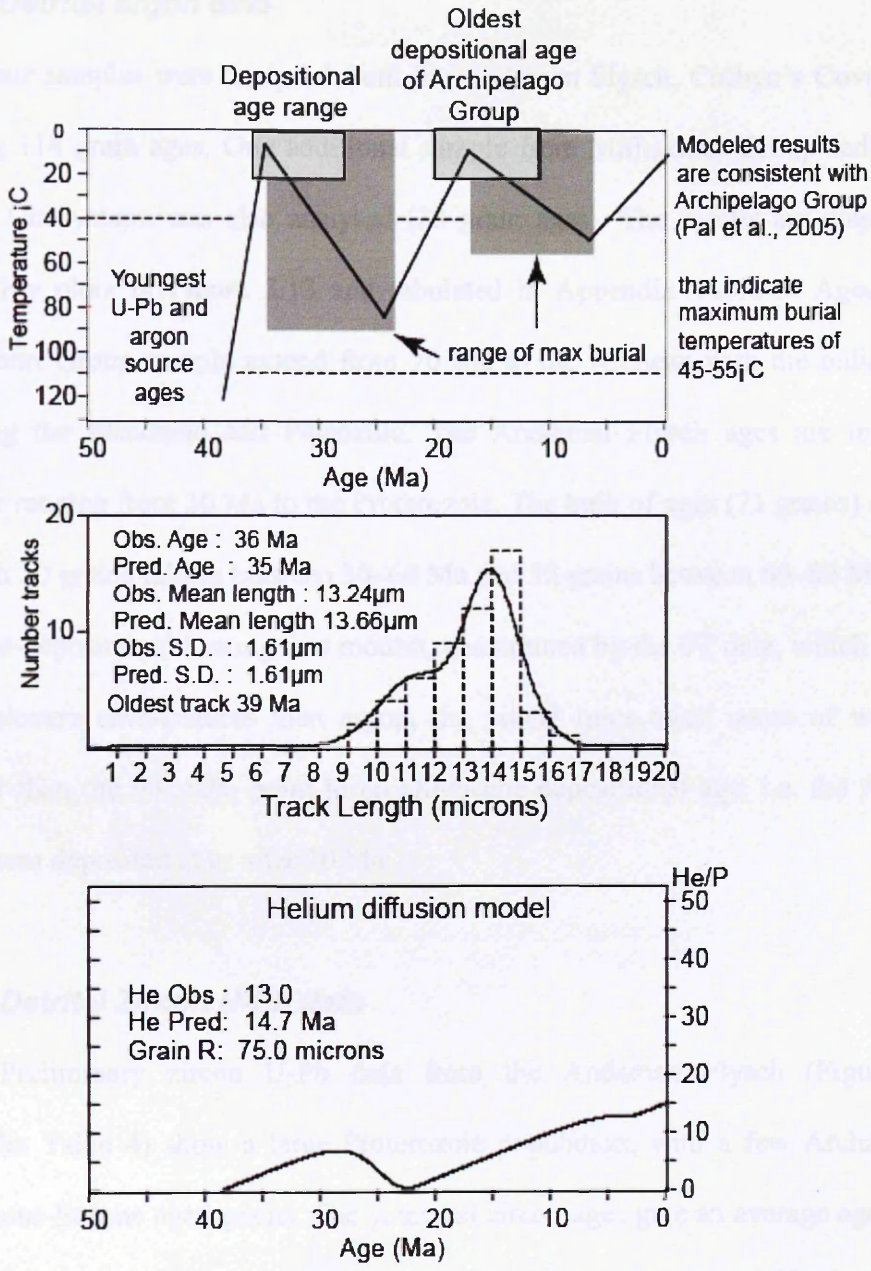

Figure 3.12 Best-fit thermal history model for the apatite fission track and (U-Th)/He data from the Andaman Flysch. Key features are a requirement for maximum burial temperatures between ~20-30 Ma and rapid cooling at ~ 20 Ma.

3.5.4 Detrital argon data

Four samples were analysed from the Andaman Flysch, Corbyn's Cove section yielding 114 grain ages. One additional sample from Mithakhari Group sedimentary rock at Chiriyatapu was also analysed (33 grain ages). The results are displayed as probability plots in Figure 3.13 and tabulated in Appendix Table 3. Ages for the Mithakhari Group sample extend from 70 Ma to the Archean with the bulk of ages spanning the Mesozoic and Paleozoic. The Andaman Flysch ages are in general younger ranging from 30 Ma to the Proterozoic. The bulk of ages (71 grains) are <200 Ma with 20 grains falling between 30–60 Ma and 32 grains between 60–80 Ma. Given that post-depositional heating was modest, constrained by the FT data, which measure lower closure temperatures than argon, the young mica ages, some of which are younger than the FT data, point to an Oligocene depositional age, i.e. the Andaman Flysch was deposited at or after 30 Ma.

3.5.5 Detrital Zircon U-Pb data

Preliminary zircon U-Pb data from the Andaman Flysch (Figure 3.14, Appendix Table 4) show a large Proterozoic population, with a few Archaean and Cretaceous-Eocene aged grains. The youngest zircon ages give an average age of 48 ± 5 Ma (five grains) that overlap with both zircon FT and mica ages. These grains are euhedral and have concentric zoning typical of magmatic zircon that suggests direct input from an Early Eocene igneous source rather than reworking of older sedimentary deposits.

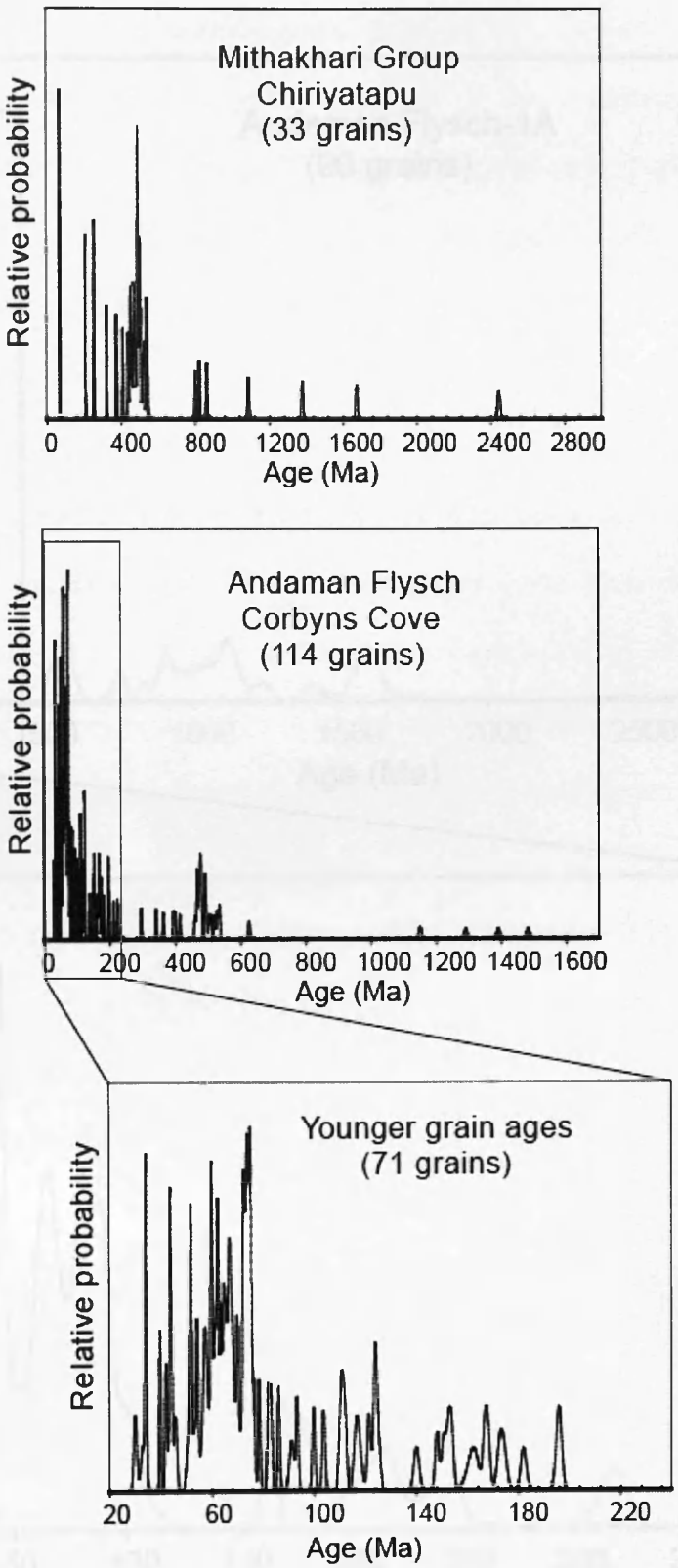

Figure 3.13 Probability plots that show the distribution of detrital argon mica ages

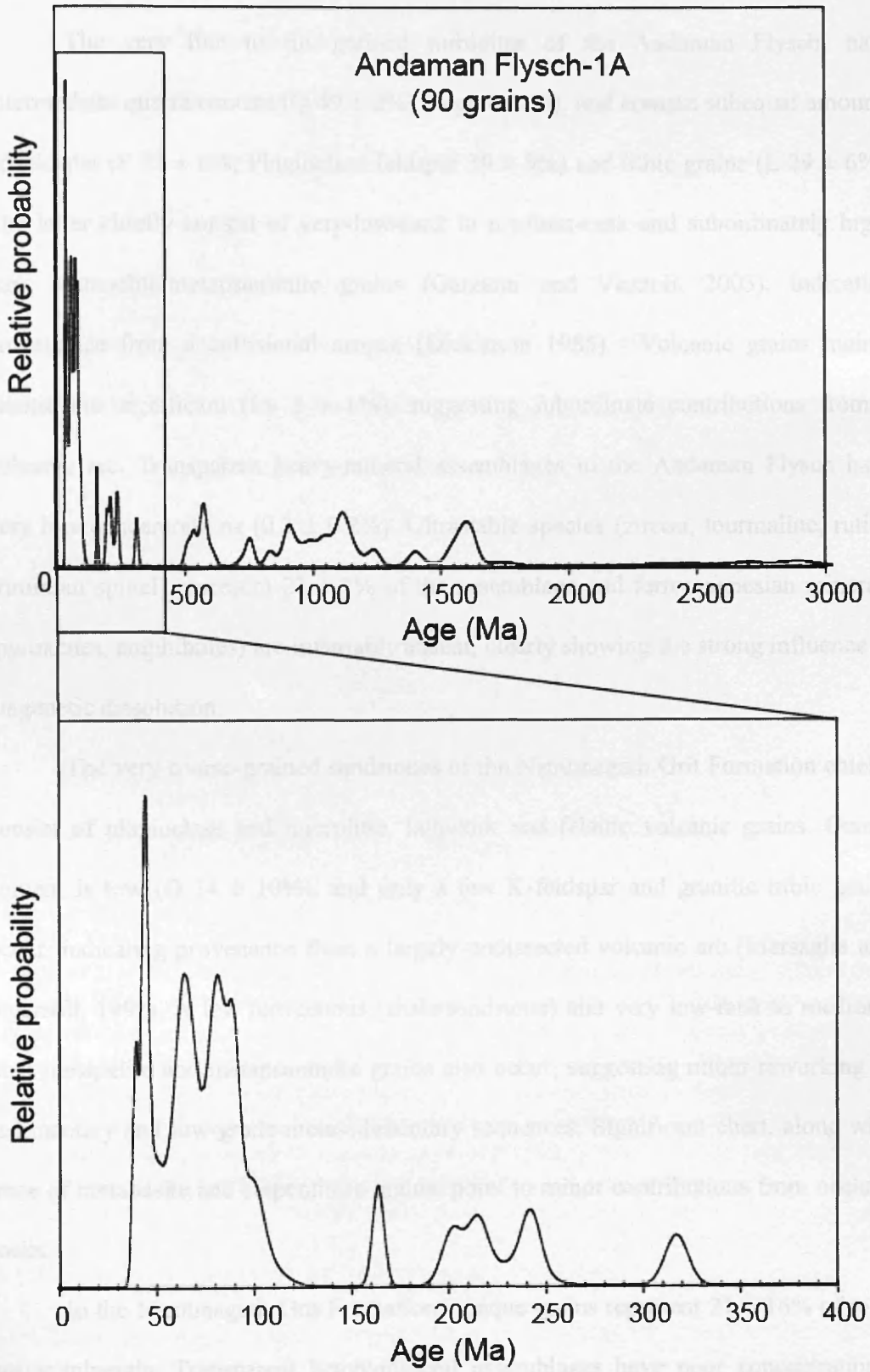

Figure 3.14 Probability plots that show the distribution of concordant detrital zircon U-Pb ages analysed in this study.

3.5.6 Petrography and heavy mineral data

The very fine to fine-grained turbidites of the Andaman Flysch, have intermediate quartz content (Q 49 ± 2%) (Figure 3.15), and contain subequal amounts of feldspar (F 22 ± 6%; Plagioclase feldspar 39 ± 9%) and lithic grains (L 29 ± 6%). The latter chiefly consist of very-low-rank to medium-rank and subordinately high-rank metapelite/metapsammite grains (Garzanti and Vezzoli, 2003), indicating provenance from a collisional orogen (Dickinson 1985). Volcanic grains mainly felsitic are significant (Lv 8 ± 1%), suggesting subordinate contributions from a volcanic arc. Transparent heavy-mineral assemblages in the Andaman Flysch have very low concentrations (0.3 ± 0.2%). Ultrastable species (zircon, tourmaline, rutile, chromian spinel) represent 21 ± 2% of the assemblage and ferromagnesian minerals (pyroxenes, amphiboles) are invariably absent, clearly showing the strong influence of diagenetic dissolution.

The very coarse-grained sandstones of the Namunagarh Grit Formation chiefly consist of plagioclase and microlitic, lathwork and felsitic volcanic grains. Quartz content is low (Q 14 ± 10%), and only a few K-feldspar and granitic lithic grains occur, indicating provenance from a largely undissected volcanic arc (Marsaglia and Ingersoll, 1992). A few terrigenous (shale/sandstone) and very low-rank to medium-rank metapelite and metapsammite grains also occur, suggesting minor reworking of sedimentary and low-grade metasedimentary sequences. Significant chert, along with trace of metabasite and serpentinite grains, point to minor contributions from oceanic rocks.

In the Namunagarh Grit Formation, opaque grains represent 21 ± 16% of total heavy minerals. Transparent heavy-mineral assemblages have poor concentrations, pointing to significant diagenetic dissolution. These mainly include pyroxenes (mostly

green augite; 35 ± 24%) and epidote (34 ± 19%), with subordinate sphene (11 ± 8%), green-brown hornblende (8 ± 8%), chromian spinel (8 ± 8%), minor apatite (2 ± 1%), garnet, rutile and other titanium oxides, consistent with provenance from a volcanic arc. It must be kept in mind, however, that the original composition of the Namunagarh Grit Formation sandstones (abundant volcanic glass and ferromagnesian minerals) was markedly different with respect to orogen-derived turbidites, and therefore that dissolution reactions of ferromagnesian minerals may have progressed at different rates and in the presence of partially buffered or even saturated interstitial waters.

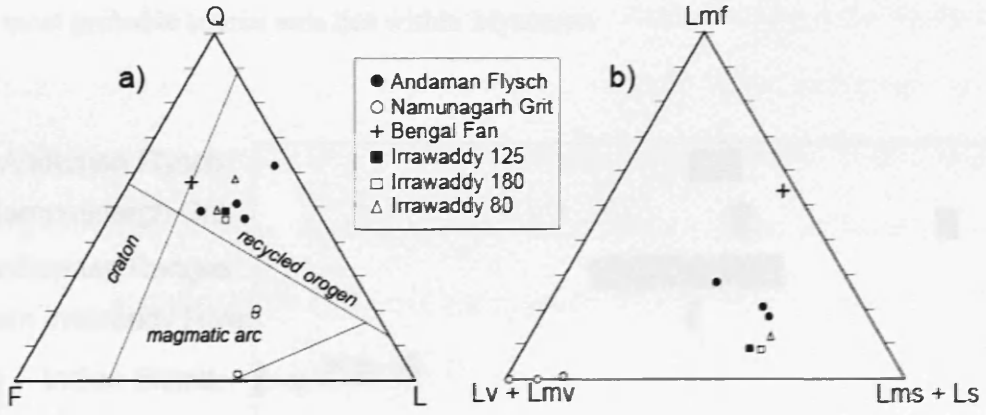

Figure 3.15 Petrography of Tertiary sandstones of South Andaman. Whereas composition of the Namunagarh Grit Formation sandstones points to provenance from an undissected/transitional magmatic arc, a recycled orogenic provenance is clearly indicated for the Andaman Flysch (Dickinson, 1985). These very fine to fine-grained turbidites compare closely with modern sands of homologous grain size from the Irrawaddy delta. Q= quartz; F= feldspars; L= lithic grains (Lv+Lmv= volcanic and low-rank metavolcanic; Ls+Lms= sedimentary and low-rank metasedimentary; Lmf= high-rank metamorphic).

3.5.7 Sm-Nd whole rock and single grain analyses

Sandstone and mudstone samples from the Mithakhari Group yielded whole rock εNd values of −7.2 and 3.1(+) respectively. The Andaman Flysch samples gave whole rock values of εNd −11.1 and −8.2 for the sandstone sample and mudstone

sample respectively. Such values are lower than Himalayan sources, which typically range between εNd –12 and –26 (Galy *et al.* 2001) and inconsistent with Indian Shield sources (Peucat *et al.* 1989). Very little data exists for the relevant Myanmar source regions. Analyses of modern river sediment from the Irrawaddy River give εNd values between -10.7 (Colin *et al.* 1999) and -8.3 (this paper: Table 2). The Western Indo-Burman ranges (Figure 3.16), which may have been exhuming by the Oligocene (Mitchell, 1993) have more negative values (Colin *et al.* 2006; Singh and France Lanord, 2002; this paper – Table 2, (Appendix Table 6). Figure 3.16, which compares the whole rock data from the Andaman Flysch with possible source areas, shows that the most probable source area lies within Myanmar.

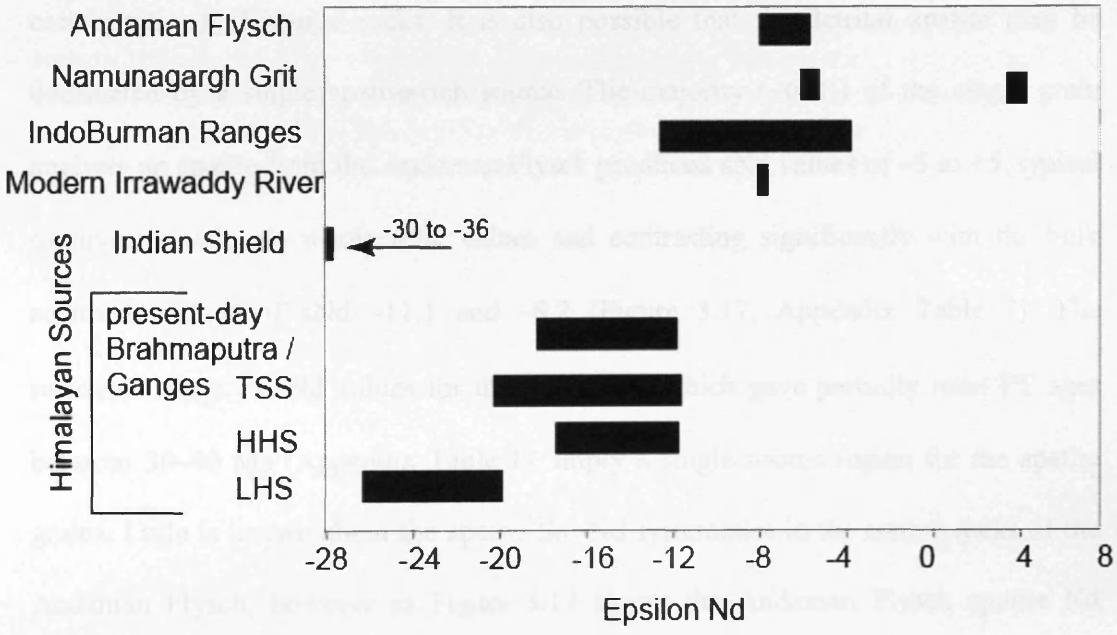

Figure 3.16 Plot comparing Sm-Nd whole rock values from the Namunagargh Grit Formation and Andaman Flysch Formation with data from possible source regions (Colin *et al.* 2006; DeCelles *et al.* 2004; Peucat *et al.* 1989; Singh and France-Lanord, 2002). The data do not support the Himalayan region as the main source.

To understand source in more detail and in particular the significance of apatite from the Andaman Flysch, which appear to come from more distant sources compared to local arc and ophiolite sources in the Mithakhari Group sedimentary rocks, Nd isotope composition was measured on single grains of apatite from the Andaman Flysch. Apatite typically has Sm/Nd ratios of 0.2 to 0.5, therefore for non-age corrected apatite the $^{143}Nd/^{144}Nd$ ratio tends to reflect the Nd isotopic composition of their parent whole rock enabling a direct linkage between thermochronometric data and source in terms of Nd isotopic signature. This approach is particularly effective if the source rocks are young and/or their potential range of Sm-Nd has been quantified. It is also important to note that this approach yields information that is not the same as sediment whole rock values that record an average value (weighted by Nd concentration) of source rocks. It is also possible that the detrital apatite may be dominated by a single apatite-rich source. The majority (~60%) of the single grain analysis on apatite from the Andaman Flysch produced εNd values of –5 to +5, typical of juvenile volcanic whole rock values and contrasting significantly with the bulk sediment values of εNd –11.1 and –8.2 (Figure 3.17, Appendix Table 7). The restricted range of εNd values for these apatites, which gave partially reset FT ages between 30–40 Ma (Appendix Table 1), imply a single source region for the apatite grains. Little is known about the apatite Sm-Nd systematics in the source rocks of the Andaman Flysch, however as Figure 3.17 shows the Andaman Flysch apatite Nd isotope data contrast with apatite Nd data from a Holocene sand dominated by Himalayan sources collected from the Bengal Basin near Joypur, West Bengal. This plot clearly shows that there is little evidence for material eroded from Himalayan sources in this sample.

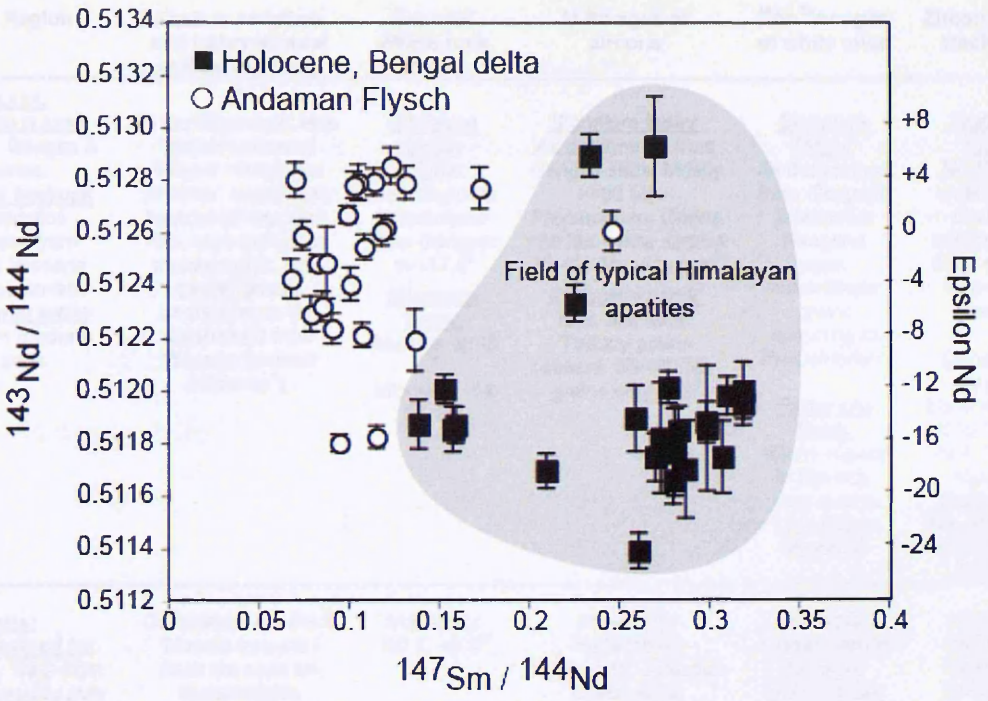

Figure 3.17 Single grain Nd measured on apatite from the Andaman Flysch Formation compared with a Holocene sand from the Bengal Basin known to have been sourced from the Himalayas. The clear difference between these two samples supports the Sm-Nd whole rock data plotted in Figure 3.16.

Source Region	Rock description and heavy Mineral and Petrography	Sm – Nd Whole rock εNd(0).	U-Pb ages of zircons	^{40}Ar-^{39}Ar ages of white mica	Zircon Fission track ages
HIMALAYA, (SOUTHERN FLANK) Drained by Ganges & tributaries. ***Oligocene bedrock*** characteristics interpolated from Eocene & Miocene foreland basin rks. ***Bedrk signal today*** taken from modern river seds	In the Oligocene, less metamorphosed "Higher Himalayan protolith" would likely have been exposed. Rks were low-grade metamorphic, sub-garnet grade, unmicaceous (as determined from Miocene foreland basin rks[1]).	Signature today: Higher Himalayan as determined from *Ganges*: av -17.5[2] Oligocene bedrk: Eocene: av -8[3] Miocene: -14 to -17[4]	Signature today: As determined from *Ganges* seds: Mostly >400 Ma – Precambrian. Grains <30 Ma – rare. Grains 30-400 Ma very rare[5] Oligocene bedrk: Eoc. and Mioc: Tertiary grains absent. 65-400 Ma grains very rare[6]	Signature today: As determined from *Gangetic tributaries:* Neogene peak, subordinate grains spanning to PreCambrian[7] Oligocene bedrk: Micas absent in Eocene, very rare in Late Oligo-Miocene[8]	Signature today: No FT data available for Gangetic sediment. He data: <55 Ma, Plio-Pleist peak.[9] Oliogocene bedrk: Eocene: Peaks at 45 Ma, 119 Ma & 343 Ma[10] Miocene: Peaks at 30 Ma, 60-75 Ma, 117 Ma, 300-370 Ma[11]
BURMA: ***Region drained by Irrawaddy.*** Data from modern Irrawaddy river sediment. Shan-Thai block lies to east, forearc-back arc of Indo-Burman Ranges (IBR) to west. Paleocontinental margin.	Cretaceous arc rks & Triassic fore-arc / back arc seds on metamorphic basement. Mogok schists, gneisses and intrusives, Shan-Thai Proterozoic – Cretaceous sedimentary rks on schist basement. Irrawaddy river sediment plots in "recycled orogenic" province field of QFL plot (Dickinson 1985).[12]	Irrawaddy: -10.7, -8.3[13]	Irrawaddy: Proterozoic, Ordovician, Jurassic-Cretaceous, Paleogene and Neogene grains[14]	Irrawaddy: Cretaceous to Miocene grains, peak 30-55 ma[15]	Irrawaddy: Neogene, Paleogene Cretaceous grains[15]
Western Indo-Burman Ranges; accretionary prism; may have been exhuming and thus a sediment source in L. Eoc-Oligocene. Data determined from Arakan modern river sands (R. Allen *et al.*, unpublished data) unless otherwise stated	Dark grey v. fine grained volcanic arenite of Eocene (Oligocene?) age. Only limited mica and heavy minerals. Many shale & silst lithics.[16]	3 samples give values of -4.0. 1 sample (further north) gives a value of -7.4[16]	Precambrian – Archaean and Proterozoic. Cretaceous and Paleogene (55-65 Ma) grains[16]	No mica present in pre-Miocene sedimentary rks[16]	Cretaceous and Paleocene to Eocene grains[16]
INDIAN SHIELD Dominantly Archaean craton. Subordinate Proterozoic mobile belts	Predom gneisses and granites; Opaques, opx and sillimanite found in rivers draining east craton[17]	Values from south and east craton only. -30 to -36[18]	Dominantly Archaean[19]	No data available	No data available

[1]Najman and Garzanti 2000. [2]: Galy *et al.* 2001.[3&4]Robinson *et al.* 2001; Najman *et al.* 2000. [5]Campbell *et al.* 2005. [6]DeCelles *et al* 2004. [7]Brewer *et al.* 2003; Najman & Pringle unpublished data. [8]DeCelles *et al.* 1998; Najman & Garzanti 2000; [9] Campbell *et al.* 2005 [10]Najman *et al.* 2005 [11]Najman *et al.* 2004, 2005. [12]Mitchell 1993; Pivnik *et al.* 1998; Bertrand *et al.* 1999; R. Allen *et al.* unpublished data [13] Colin *et al.* 1999; R. Allen *et al.* unpublished data,[14]Bodet & Scharer 2000. [15]R. Allen *et al.* unpublished data [16]R. Allen *et al.* unpublished data [17]Mallik 1976. [18] Peucat *et al.* 1989; Saha *et al.* 2004. [19]Mishra *et al.* 1999, Auge *et al* 2003.

Table 2. Typical Signatures of Potential Source regions

3.6 Discussion

3.6.1 Constraints on sedimentation and uplift

New thermochronometric evidence and field observations from type locations on South Andaman combined with existing biostratigraphy and petrography provides an improved chronology for deposition and uplift. The accretionary setting means that sedimentation history will be intimately tied to subduction behavior, offscraping, accretion and uplift. Whilst in such a setting uplift may be viewed as a more or less continuous process, we recognise some distinct uplift events affecting the South Andaman geology.

The earliest conglomerates and grits of the Mithakhari Group record subaerial exposure and erosion of the arc sequence and shallow marine limestone cover, as described above, constraining the age of ophiolite as pre-Mithakhari Formation (early to middle Eocene) and post-shallow marine sedimentation. The petrography of the Mithakhari Group is indicative of an undissected volcanic arc with minor reworking of sedimentary and low-grade metasedimentary sequences and minor contributions from oceanic igneous rocks.

Our data provide maximum and minimum age constraints for deposition of the Andaman Flysch. Detrital Ar-Ar mica and fission track data constrain maximum depositional age to ~30 Ma. Minimum depositional age is constrained by the thermal history modelling, which indicates that burial to maximum temperatures of ~90 ± 5°C was reached around 25–20 Ma, ending with a phase of rapid cooling at ~20 Ma. This implies a discrete episode of major uplift at ~20 Ma consistent with deposition of Archipelago Group shallow marine volcanic-rich sedimentary rock from ~18 Ma onwards (Pal *et al.* 2005; Singh *et al.* 2000) that was deposited on top of the Andaman Flysch. Uplift at ~20 Ma is also regionally significant, coinciding with major

stratigraphic changes in the Irrawaddy Delta, Mergui Basin, (Figure 3.1) in sediments accreted onto the Andaman–Nicobar Ridge (Curray, 2005), and formation of an unconformity in the Indo-Burman Ranges (Acharyya *et al.* 1989). 20 Ma uplift of the Andaman Ridge is also coincident with the uplift of the Owen and Murray ridges in the Arabian Sea (Mountain and Prell, 1990), suggestive of a more wider plate tectonic trigger.

An outstanding question is what was the original maximum thickness of the Andaman Flysch? Hydrocarbon exploration wells drilled to the east and west of Middle Andaman indicate thicknesses of <1000 m (Roy *et al.* 1992), whilst outcrop estimates range from ~750 m up to 3000 m (Pal *et al.* 2003). Results from thermal history modeling indicate burial of the sampled Andaman Flysch beds beneath at least 2.5 km of cover (assuming geothermal gradients in the range 35–30°C). In a growing accretionary wedge, burial is as likely to be due to thrust stacking as it is to sedimentation. Crucially ~2.5 km of burial is incompatible with the unannealed apatite data from the stratigraphically lower Mithakhari Group, highlighting the fact that these different units must have been deposited in different locations (sub-basins?) within the accretionary wedge. Thermal history modeling also shows a phase of accelerated cooling from ~10–5 Ma. This is likely tied to a phase of regional Miocene-Pliocene uplift linked to spreading in the Andaman Sea driven by increases in the subduction rate and dip of the subducted slab (Khan and Chakraborty, 2005). This last phase of uplift, the result of squeezing between subduction in the west and extension in the east is likely responsible for the present topography of Andaman Islands.

The relationship of these episodes of uplift and erosion to regional events can be appreciated when these new constraints are compared against reconstructions of

Indian plate convergence history. Figure 3.18 plots India-Asia convergence rate and convergence angle from the studies of Lee and Lawver (1995) and more recently that of Guillot *et al.* (2003). The graph shows the studied outcrops of Andaman Flysch were deposited at a time of more northerly convergence and ended when subduction shifted to a less oblique angle. Seismic lines taken from across the Andaman arc show how the angle of subduction can influence wedge development where the intensity of deformation, which increases from north to south, changes with obliquity of subduction (Curray, 2005). This relationship may explain the evidence for a discrete episode of uplift, involving the Corbyns Cove Andaman Flysch, at ~20 Ma.

3.6.2 Sediment Provenance

The Mithakhari Group shows clear evidence of dominant contribution from an arc, in keeping with its interpreted forearc basin depositional environment and in line with previous provenance work based on petrography (Bandopadhyay, 2005). The rocks plot in the "Magmatic arc" field on the QFL petrographic plot (Figure 3.15), volcanic fragments and glass shards are common, and mineral grains, for example apatite, are euhedral. A positive whole rock εNd signal (+3) is indicative of derivation from a mafic / juvenile source. The source was likely that of the Cretaceous-Eocene arc that stretched from the Himalaya collision zone through Myanmar to Sumatra (Mitchell, 1993), as reflected in the FT ages of the euhedral apatites. A subordinate continental source is confirmed by petrography and Precambrian-Paleozoic Ar-Ar mineral grain ages. Such a source was likely the continental margin of the Shan-Thai Block (Sibumasu) running down to peninsular Thailand, adjacent to the forearc (Metcalfe, 1996) (Figure 3.19).

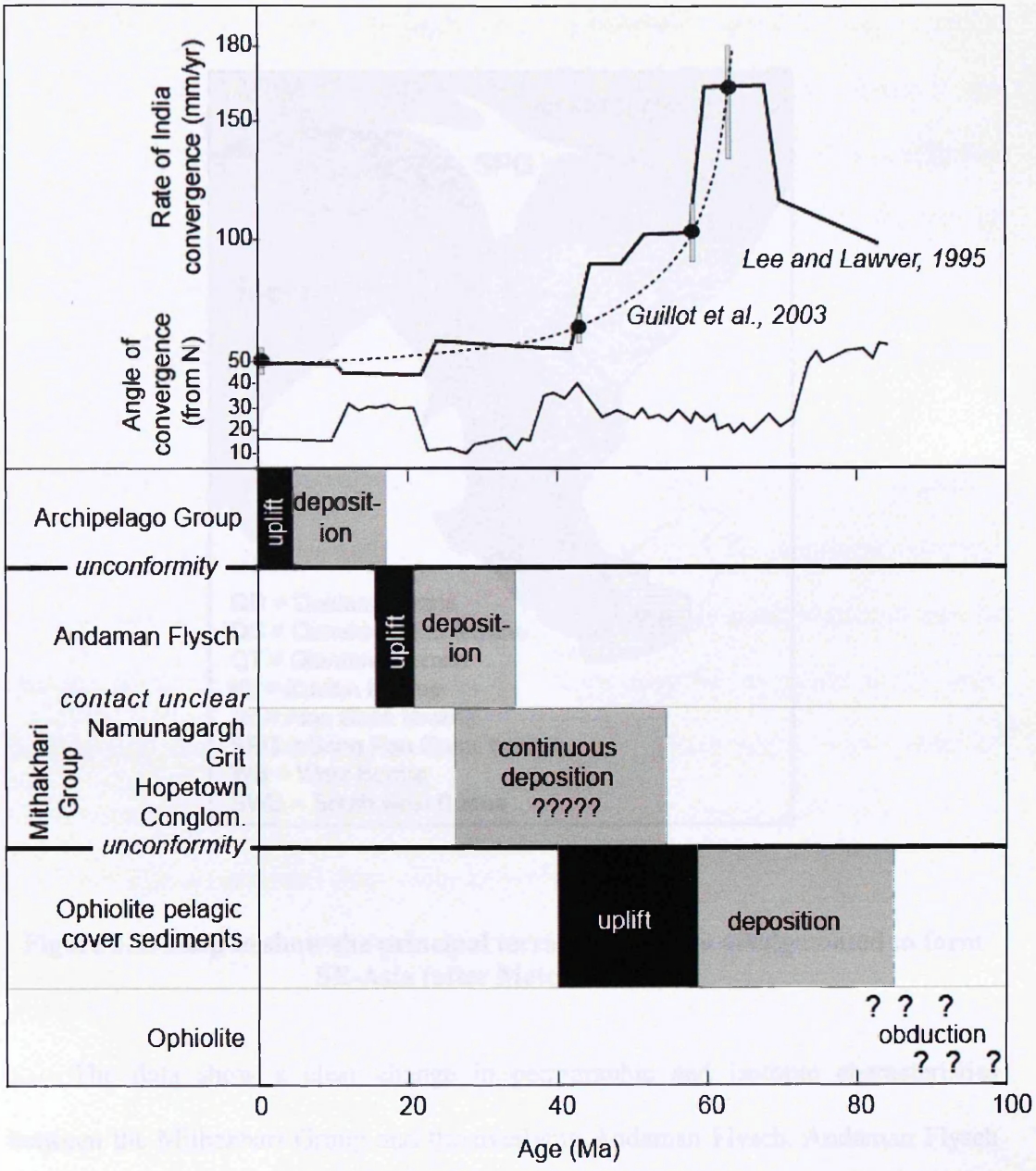

Figure 3.18 A comparison between India convergence history (after Lee and Lawver, 1995 and Guillot *et al.*, 2003) and the uplift and sedimentation history of the studied rocks from South Andaman.

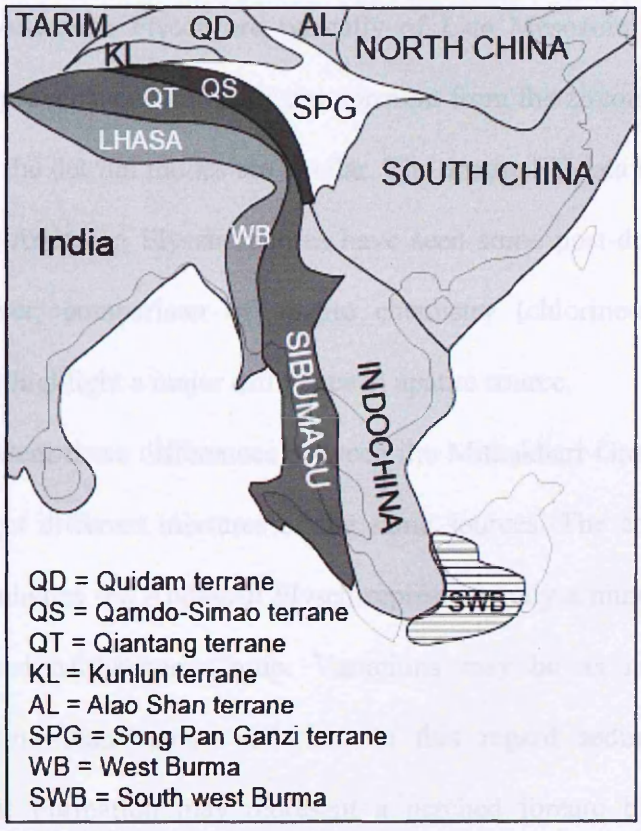

Figure 3.19 Map to show the principal terrains that have amalgamated to form SE-Asia (after Metcalfe, 1996).

The data show a clear change in petrographic and isotopic characteristics between the Mithakhari Group and the overlying Andaman Flysch. Andaman Flysch composition represents the first sedimentary material to plot in the "Recycled Orogenic" province (Figure 3.15). Initial results from the pilot study of Sm-Nd whole rock values differ markedly between the Mithakhari Group and Andaman Flysch, particularly when the finer grained facies are compared. The positive εNd signal of the Mithakhari Group contrasts strongly with the more negative εNd signal (-11), of the Andaman Flysch mudstone, suggestive of a contribution from older continental crustal sources (Figure 3.15). Detrital micas are of radically different ages, with the peak of

ages for the Mithakhari Group falling within Precambrian-Paleozoic spectrum, whilst those from the Andaman Flysch are typically of Late Mesozoic and Tertiary age (Figure 3.13). A provenance contrast is not apparent from the zircon FT data (Figures 3.9 and 3.10), as the detrital modes are similar. The apatite FT data cannot be directly compared as the Andaman Flysch apatites have seen some post-depositional partial resetting. However, comparison of apatite chemistry (chlorine-uranium content, Figure 3.11) does highlight a major difference in apatite source.

To some extent these differences between the Mithakhari Group and Andaman Flysch may reflect different mixtures of the same sources. The continental-derived material that dominates the Andaman Flysch represents only a minor contribution in the arc dominated Mithakhari Group. Variations may be as much to do with depositional setting than source variation. In this regard sedimentary rocks of Namunagarh Grit Formation may represent a perched forearc basin whereas the Andaman Flysch represents deep-water turbidites.

It has been proposed by Karunakaran *et al.* (1964, 1968) and Pal *et al.* (2003) that these "recycled orogenic" Andaman Flysch rocks were sourced by the Irrawaddy River of Myanmar and deposited in a forearc basin. By contrast, Curray *et al.* (1979) consider the Andaman Flysch to be trench sediments offscraped from the Himalayan-derived Bengal Fan on the downgoing Indian slab. Significant contribution from the northward drifting cratonic Greater India can be ruled out by the dissimilar petrography, Sm-Nd signature and mineral cooling ages (Figure 3.16; Table 2) as well as the apatite Nd data (Figure 3.17). No apatites were measured with significantly negative εNd values (e.g. -30) diagnostic of India shield sources. The mica argon ages older than 50 Ma, present in both the Mithakhari Group and Andaman Flysch are consistent with known sources along the western margin of the Shan-Thai Block

(Sibumasu) adjacent to the forearc. The presence in the Andaman Flysch of a small but recognisable population of mica ages between 30–40 Ma, is not consistent with these Sibumasu sources as the youngest granites on the Thai peninsular are ~50 Ma (Charusiri *et al.* 1993). Possible sources for the Tertiary mica ages might instead include a region affected by India-Asia collision at ~50 Ma, possible candidates being either the nascent Himalaya to the north, Transhimalaya or a more north-eastern source, namely Myanmar locations of the Burman-Thai Block, where Tertiary metamorphism, magmatism and grain isotopic characteristics and ages are ascribed to the affects of the India-Asia collision (Bertrand *et al.* 1999; 2001, Bodet and Schäerer, 2000; Barley *et al.* 2003). Isotopic characteristics of these Myanmar rocks are incompletely documented at present. That which are available are taken from bedrock, and analyses of Irrawaddy River sands which drain from the areas under discussion (i.e., the Central Myanmar Basin, to its east the Mogok Belt and Shan Plateau and to its west the Indo-Burman Ranges (Bodet and Schäerer, 2000; Colin *et al.* 2006; Singh and France-Lanord, 2002; Table 2 this study) as verified by 30 Ma Ar-Ar ages in the Irrawaddy which drains this region (Table 2). Discrimination between these two possible sources; the Himalayan or Myanmar region, requires an understanding of the different paleogeography and paleodrainage of the region in the Oligocene compared to present day, as discussed below (Figure 3.20).

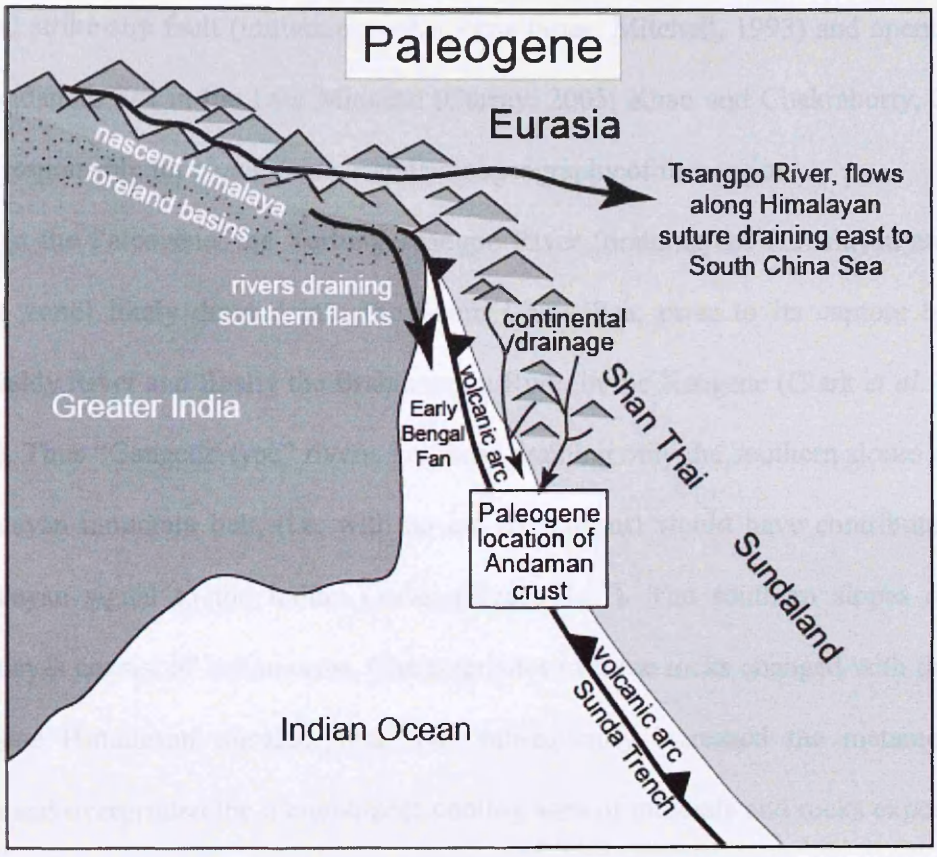

Figure 3.20 Cartoon to illustrate the Paleogene paleogeography and paleodrainage of SE-Asia. Although a simplification, as the location of the subduction zone, Asian margin and Andaman crust would have changed throughout the Paleogene as Greater India moved northwards the cartoon serves to illustrate the general location of continental sources and drainages to the Andaman region.

Prior to India-Asia collision, the northward extension of the Sunda Arc as far as Pakistan permits correlation between the southern margin of Asia in the Himalayan region, with equivalent rocks in Myanmar (Mitchell, 1993) and further south. Subsequent to continental collision at ~50 Ma (Rowley, 1996), the Himalayan thrust belt started to develop in the north whilst the eastern (Myanmar) region remained an active continental margin with, for example, the Central Basin along which the Irrawaddy now drains, the site of the continental margin between the subduction zone to the west and the arc to the east (Pivnik *et al.* 1998). Movement along the Sagaing

dextral strike-slip fault (initiation pre-Miocene times: Mitchell, 1993) and opening of the Andaman Sea in the Late Miocene (Curray, 2005; Khan and Chakraborty, 2005) were responsible for changes in coastal paleogeography of this region.

In the Paleogene, the Yarlung-Tsangpo River (draining the Himalayan arc and suture zone) likely drained into the South China Sea, prior to its capture by the Irrawaddy River and finally the Brahmaputra River in the Neogene (Clark *et al.* 2004, 2005). Thus "Gangetic-type" rivers, i.e. those draining only the southern slopes of the Himalayan mountain belt, (i.e. with no arc component) would have contributed the Himalayan signal to the Indian Ocean (Figure 3.17). The southern slopes of the Himalayas consist of Indian crust. Characteristics of these rocks changed with time as Neogene Himalayan metamorphism has subsequently increased the metamorphic grade and overprinted the metamorphic cooling ages of minerals and rocks exposed at surface today. By contrast, the northeastern Myanmar region was devoid of Indian crustal rocks, and there was no thrust belt to bar the Asian and arc sources from draining south. Prior to opening of the Andaman Sea, rivers draining the Myanmar region would presumably have drained into the trench-forearc system, which acted as a "sink" preventing deposition further west onto the Indian plate.

The Andaman Flysch records mixed orogenic and arc provenance. The young (<100 Ma) U-Pb dated detrital zircons from the Andaman Flysch are consistent with derivation from igneous sources, most likely an eastern (Myanmar) provenance based on similar aged grains found in modern Irrawaddy River sediment (Bodet and Schärer, 2000) since grains with young U-Pb zircon ages are extremely rare in the southern flanks of the Himalaya (Campbell *et al.* 2005; DeCelles *et al.* 1998, 2004).

Myanmar sources can also adequately account for the majority of the "recycled orogenic" component of the detritus in the Andaman Flysch. Both petrography and

εNd whole rock signatures, especially of the fine-grained material, are near identical to that of the modern day Irrawaddy River (Figures 3.15 and 3.16). ^{40}Ar-^{39}Ar and zircon fission track data from the Irrawaddy river also shows a similarity with data obtained from the Andaman Flysch, showing a mica age peak of ~ 30–60 Ma with a population of older Cretaceous grains, and zircon fission track ages of Miocene and Paleogene (20–65 Ma) to Cretaceous (Table 2). Nevertheless, there are some disparities. The lack of zircon grains with Jurassic U-Pb ages in the Andaman Flysch is surprising, considering their prevalence in the Mogok Belt (Barley *et al.* 2003) and their presence in modern Irrawaddy sand (Bodet and Schärer, 2000). Recourse to Himalayan input through the Bengal Fan is not required to explain the "recycled orogenic" component of the Andaman Flysch. However, a minor contribution from the Himalayan thrust belt cannot be ruled out: For example; grains aged 100–1500 Ma in the Andaman Flysch are common to both Himalayan and Myanmar rock types. In addition, the intermediate whole rock εNd values may represent a mixture between a more negative Himalayan source and more positive Myanmar sources, as implied by the single grain apatite analyses. The possibility of dual provenance, with Himalayan-derived Bengal Fan material and Myanmar-derived material meeting and mixing in the trench, is a model that would be consistent with the regional seismic data, which shows folding and uplift of Bengal Fan sediments at the base of the slope (Curray, 2005). Definitive discrimination between Myanmar and Himalayan sources, if possible at all, awaits more information on the source rock geology of Myanmar, in particular that of the Shan Plateau and Mogok Belt, and analysis of, as yet undrilled, Oligocene-aged sediments preserved in the Bengal Fan, and co-eval sedimentary rocks of the Central Myanmar Basin.

3.7 Conclusions

The Mithakhari Group was deposited in the Late Paleocene/Eocene with a maximum age of ~60 Ma. This current study shows that the sedimentary rocks are predominantly arc derived from a proximal source in-keeping with the interpreted forearc depositional environment. A subordinate contribution from an older continental source was most likely to be the western Sibumasu margin, but a Transhimalayan arc unit source cannot be ruled out.

The Oligocene Andaman Flysch was deposited between 30 and 20 Ma, and then uplifted by 20 Ma. It shows a clear change in petrographic and isotopic characteristics from the Mithakhari Group and is comprised mainly of 'recycled orogenic' sources with a subordinate arc provenance. It represents the earliest record in the region of major influx from a continental area. The 'recycled orogenic' component is most simply explained by erosion from the northeastern (Myanmar) continental region. Isotopic and petrographic differences between formations may be explained to some extent by different mixtures and contributions from the same source regions. Whilst, dual provenance is a favourable model for this region, detailed discrimination between Himalayan and Myanmar sources at present, awaits more data from Myanmar source rocks.

Chapter 4: Provenance of the Tertiary sedimentary rocks of the Indo-Burman Ranges, Burma (Myanmar): Burman arc or Himalayan-derived?

Accepted for Publication in the Journal of the Geological Society

4.1 Abstract

The accretionary prism deposits of the Indo-Burman Ranges in western Myanmar extend along the India-Eurasian subduction zone and may be divided into a westward portion of Neogene sedimentary rocks, and an eastward Cretaceous-Palaeogene belt. The sedimentary rocks may preserve a record of Himalayan erosion, although a Burman margin source has also been suggested for the Palaeogene rocks of the Indo-Burman Ranges. Thermochronological analyses on detrital grains, isotopic analyses on bulk rock, and heavy mineral and petrographic data indicate a Himalayan provenance for the Neogene deposits. In contrast, the isotopic and petrographic composition of the Palaeogene deposits contain a significant component of arc-derived detritus interpreted as derived from the Burmese part of the Mesozoic-Tertiary arc to the east. An older crustal component is also identifiable in the Palaeogene Indo-Burman Ranges, which may be sourced from the Himalaya or Burmese margin. Our data suggest that the deposition of the Palaeogene belt continued through the Late Eocene (after 37 Ma). Unequivocal evidence of substantial early Himalayan erosion remains elusive.

4.2 Importance of the erosion record

The Himalayas provide a type example of orogenesis, on which a number of current models of crustal deformation are based (Tapponnier *et al.*, 1982; Grujic *et al.*, 1996, 2002; Beaumont *et al.*, 2001, 2004; Jamieson *et al.*, 2004). A knowledge of the erosional response of the orogen since collision (commonly taken at ca 55-50 Ma

(Garzanti *et al.,* 1987; Klootwijk *et al.,* 1992; Searle *et al.,* 1997)) is important for discriminating between these various models, which differ in the timing and extent of associated erosion (Grujic *et al.,* 1996, 2002; Beaumont *et al.,* 2001, 2004; Jamieson *et al.,* 2004; Tapponier *et al.,* 1982; Replumaz and Tapponier, 2003; Ali and Aitchison, 2007). Knowledge of the timing of the onset of significant erosion is also critical to evaluating the hypotheses that exhumation of the Himalayas influenced Tertiary global cooling (Raymo and Ruddiman, 1992; Molnar *et al.,* 1993) and the marked increase in marine $^{87}Sr/^{86}Sr$ ratios at ~40 Ma (Richter *et al.,* 1992). However, evidence for significant Palaeogene erosion from the southern flanks of the eastern and central Himalayas, particularly to eastern repositories, remains elusive. A large proportion of the Oligocene is represented in the foreland basin by a hiatus (DeCelles *et al.,* 1998; Najman *et al.,* 2004) and whilst a thick Palaeogene sequence of sediments is preserved in the Indus Fan, which may record early Himalayan erosion from the western part of the orogen (Qayyum *et al.,* 1997; Clift *et al.,* 2001), possible Oligocene strata in the Bengal Fan are currently inaccessible, with rocks from the base of the Ocean Drilling Program (ODP) legs 116 and 121 drill holes being dated at ~ 17 Ma (Curray 1994; Galy *et al.,* 1996). This paper seeks to find an early record of Himalayan erosion, preserved in the Indo-Burman Ranges of Western Myanmar (Burma), as suggested by Curray *et al.,* (1979) and others.

The Cretaceous-Palaeogene Indo-Burman Ranges of western Myanmar lie east of the subduction zone that runs from the Himalaya to the north and southward to Sumatra. The Indo-Burman Ranges continue westward as the Neogene Indo-Burman Ranges and the Chittagong Hill Tracts of Bangladesh and sit approximately along the line of the subduction zone (Figure 4.1).

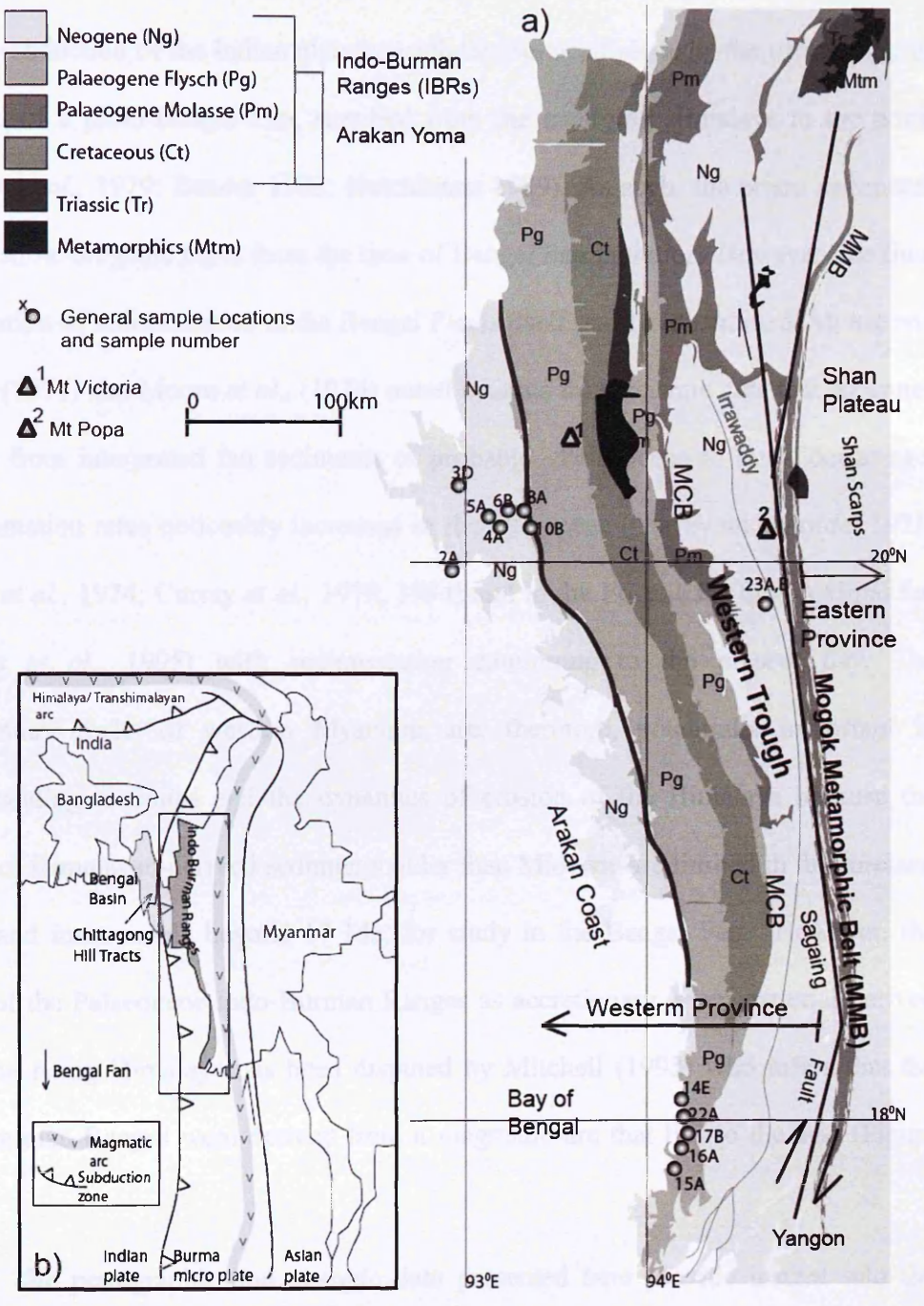

Fig. 4.1 Simplified Geology map of Western Myanmar (a) showing generalized sample locations for which the specific GPS references can be found in Appendix 1. The Mogok Metamorphic Belt (MMB), Myanmar Central Basin (MCB), Irrawaddy River and divide between the Palaeogene and Neogene Indo-Burman Ranges are of note. The major notable and tectonic features of the region (inset b) include the Bengal Fan, plate boundaries, the magmatic arc and the India-Asian subduction zone.

This west-vergent range has been interpreted as an accretionary prism, formed during subduction of the Indian plate beneath the Eurasian plate, by the offscraping of material of a proto-Bengal Fan, supplied from the emerging Himalaya to the north (Curray *et al.,* 1979; Bender 1983; Hutchinson 1989). As such, the prism sediments should show orogenic input from the time of Bengal Fan initiation. However, the time of initiation of sedimentation in the Bengal Fan is itself poorly constrained. Moore and Curray (1971) and Moore *et al.*, (1974) noted a hiatus from seismic data that separates pre-fan from interpreted fan sediments of probable ~Palaeocene to mid-Eocene age. Sedimentation rates noticeably increased in the Oligocene (Curray and Moore, 1971; Moore *et al.,* 1974; Curray *et al.,* 1979, 1994) and in the Eocene for the proximal fan (Davies *et al.,* 1995) with sedimentation continuing to the present day. The sedimentary rocks of western Myanmar are, therefore, potentially important in understanding tectonics and the dynamics of erosion of the Himalaya because the record of Himalayan-derived sediments older than Miocene are limited in the foreland basin, and inaccessible beyond 17 Ma, for study in the Bengal Fan. However, the status of the Palaeogene Indo-Burman Ranges as accretionary prism material derived from the rising Himalaya has been disputed by Mitchell (1993) who infers that the Indo-Burman Ranges were derived from a magmatic arc that lies to the east (Figure 4.1).

The petrographic and isotopic data presented here provide insight into the depositional history, source exhumation and provenance of the sedimentary rocks of western Myanmar. To assess provenance we have compared our data with the approximately coeval foreland and remnant ocean basin deposits of known Himalayan derivation (Robinson *et al.,* 2001; DeCelles *et al.,* 2004; Najman *et al.,* 2005; Najman *et al., In Press*; Bernet *et al.,* 2006, Szulc *et al.,* 2006), Himalayan bedrock data

(DeCelles et al., 1998a,b; 2000) and with data from rocks of the Jurassic-Tertiary magmatic arc of Myanmar (United Nations Report, 1978 b, c; Barley *et al.,* 2003; Searle *et al.,* 2007)

4. 3 Overview of the geology of western Myanmar

Myanmar is located on the eastern edge of the zone of Himalayan convergence, ~600 km south of the eastern Himalayan syntaxis where the north – east striking structures of the Himalayan mountain chain rapidly change strike to a north – south orientation (Figure 4.1). The region represents the transition zone between the Himalayan collision belt and the Indonesian arc where the Indian plate is at present subducting under Asia (Le Dain *et al.,* 1984).

Most of western Myanmar is situated on the Burma microplate, interpreted by some as a forearc sliver (Fitch 1972; Curray *et al.,* 1979; Pivnik *et al.,* 1998; Bertrand *et al.,* 2003) and bordered on the east by the Sagaing dextral strike-slip fault. It is a long-lived active margin, expressed in arcs of the Mogok Belt of Jurassic to Eocene age (Barley *et al.,* 2003) and a younger Miocene to Recent arc of the Mount Popa Region to the west (Figure 4.1), active during recent stages of eastward subduction and associated with the Andaman Sea spreading-centre (Stephenson *et al.,* 1984). The Mogok belt is considered an extension of the Transhimalayan arc and Lhasa terrain (Mitchell 1993; Mitchell *et al.,* 2007; Searle *et al.,* 2007) that runs through the Himalaya to the north marking the ancient Asian active margin, and abruptly changes to a north-south orientation at the eastern Himalayan syntaxis. To the west of the arc in Myanmar, the Western Trough is considered to be a forearc basin (Mitchell 1993; Pivnik *et al.,* 1996; Bertrand *et al.,* 2003) that moves furthest west into the Indo-Burman Ranges, which itself can be divided laterally into two belts. The eastern

Palaeogene belt preserves a sequence of predominantly Palaeogene sediments with Carnian aged feldspathic turbidites, local ophiolite, and metamorphic rocks of Triassic to Cretaceous age and a mica schist belt up to 30 km wide (Brunnschweiler 1966; Bender 1983; Mitchell 1993). The Neogene western belt is predominantly composed of Neogene flysch-type sediments with minor deformed Campanian and Maastrichtian aged (~83-65 Ma) pelagic limestones and shales which outcrop in the furthest western parts of the Ranges as well as on offshore islands of the Arakan coast, and continue along strike into Bangladesh (Bender 1983; Mitchell 1993). The southernmost portion of the Indo-Burman Ranges, and the region from which samples have been collected, is often referred to as the Arakan Yoma and is a name used hereafter (see also Figure 4.1).

4.4 Approach and Methods

The two possible sources for the Palaeogene and Neogene Indo-Burman Ranges are the eastern Himalaya (including Indian crust metamorphosed during the Tertiary orogeny, and the Cretaceous-Palaeogene Transhimalayan arc of the Asian plate) (Mitchell 1974; Curray *et al.,* 1979; Hutchinson 1989) and Burmese Margin dominated by the Burmese arc (Mitchell 1993). Their contrasting ages and lithologies are reflected in different petrographic, mineralological, isotopic and mineral age characteristics. A combination of published Himalayan bedrock data and data from the Himalayan-derived foreland basin and Bengal Basin sediments is used to characterise the signature of material eroded from the southern flanks of the rising Himalayan thrust belt through time. These petrographic and isotopic data show that the Indian crustal material is distinct and easily distinguished from the late Jurassic to Eocene magmatic arc that lies to the east of the Indo-Burman Ranges and stretches south

through Myanmar to Sumatra, as well as northwest into the Himalaya as the Transhimalaya of the Asian plate (Mitchell 1993).

We undertook analyses on a total of 14 samples (Appendix 1) from the Palaeogene and Neogene Indo-Burman Ranges and compared them with published data from the Himalaya and Burma in order to identify provenance of the rocks. Where available, Palaeogene and Neogene bedrock was sampled. However, poor exposure has also necessitated sampling of modern river sands and muds. Modern river sediments provide an efficient average sample of exposed crust in the river catchment even though the precise location of the source rock is unknown.

Multiple proxies are used to get the best image of source provenance and to avoid potential bias that may arise by relying on a single mineral type. All data tables and methodologies are shown in Appendix 2-1 to 2-7. A heavy mineral and petrographic study (Appendix 2-2a, b) was done on all samples from the Palaeogene and Neogene and was used as the first-step in identifying the provenance of the samples. Detrital zircons were used for fission track analysis (Appendix 2-3) and U-Pb dating (Appendix 2-4 and 2-5). Zircons have a closure temperature for fission track analysis of ~200°C-310°C (Hurford 1986). Above this, fission tracks may partially or fully anneal. The relatively higher closure temperature compared to apatite (~120°C) makes this technique suitable for provenance work, as the zircon fission track grain ages are not as susceptible to resetting at burial temperatures. The ages obtained represent thermal cooling of the source region. The U-Pb system has a much higher closure temperature for zircon and is stable to ~750°C (e.g., Spear and Parrish, 1996), beyond which uranium is lost. Zircon U-Pb ages from detrital grains in a sedimentary rock are therefore considered to be primary crystallization / metamorphic ages. ^{40}Ar-^{39}Ar dating of detrital micas was undertaken on Neogene samples (Appendix 2-6), but

not on the unmicaceous Palaeogene samples. White mica has a closure temperature of ~350°C in the Ar-Ar system (e.g., McDougall and Harrison, 1999) and as such also records post-metamorphic cooling in the source region, making ^{40}Ar-^{39}Ar dating and fission track analysis highly compatible for provenance determination of clastic sequences. Modern river muds were used for whole-rock Sm-Nd isotope fingerprinting (Appendix 2-7). The ε_{Nd} value reflects the age and composition of the source rock ranging from very negative values for crustal rocks, to positive values for younger mafic rocks.

4. 5 Results

4. 5. 1 Isotopic and petrographic data from the Palaeogene Indo-Burman Ranges

The data presented in Table 1, and summarized below, were obtained from Palaeogene bedrock, samples of modern rivers draining the Palaeogene Indo-Burman Ranges and pebbles taken from a modern river draining the bedrock at the border between the Palaeogene/Neogene Indo-Burman Ranges (Figure 4.1).

Petrographic point-count data from the pebbles extracted from a modern river, and bedrock data are presented in Figure 4.2. The bedrock petrographic data show a significant proportion of volcanic lithic detritus and on the standard QFL plot of Dickinson (1985) plot within the Magmatic Arc province. The pebbles plot within the Recycled Orogen province of the QFL, however the lithic plot (Figure 4.2b) shows that the pebbles incorporate a mix of sources from orogenic to magmatic arc as indicated by the percentage of low-grade metamorphic lithics and volcanic lithics respectively.

Location	Rock description and Heavy Mineral and Petrography	Whole Rock Sm-Nd εNd(0)	Zircon U-Pb ages	40Ar-39Ar ages of white mica	Zircon Fission Track ages
Palaeogene Indo-Burman Ranges (east) Data from **bedrock** and **modern rivers** draining Palaeogene bedrock.	Fine grained interbedded mudstones, silts and sstn, thin interbedded turbidites and micritic limestones. Bedrock is volcanic lithic and plots within Magmatic arc province of QFL plot (Dickinson 1985) and Modern river samples represent a continuum of arc provenance to recycled orogen with low grade metamorphic to volcanic lithics	-4.0, -4.1 and –4.2	Bedrock and Modern River: Predominant age peaks at 70-150 Ma and 500-2800 Ma with a recurring subordinate population at 42-60 Ma. 2 grains of 12-16 Ma, reflect drainage through isolated Miocene exposure	Unmicaceous	Bedrock and Modern River: Dominant age peaks at 37 Ma, 45-60 Ma and ~85 Ma with smaller populations at 100 Ma and >290 Ma. Rare ages below 25 Ma, likely reflect drainage through isolated Miocene bedrock exposure
Neogene Indo-Burman Ranges (west) Data from **bedrock**	Medium grained interbedded sstn and mdst. Low grade metamorphic lithics plot within Recycled orogen of the QFL plot	-10.7 and –12.2 -7.3 for a sample on the border between the Palaeogene and Neogene Indo-Burman Ranges	Main age peaks 500-2800 Ma (80-96% of all grains) Grains ages <150 Ma make up 0% to a max of 15% of total grains per sample	Main age component <55 Ma (up to 100% of grains)	Dominant age peaks <55 Ma with up to 100% of grains <55 Ma. Older ages of >200 Ma and 60-150 Ma are also present
Irrawaddy River **modern river sediment** (Draining the Burman Margin including the Indo-Burman Ranges, The Mogok Metamorphic belt and the Central Basins, and eastern Himalayan syntaxis)	Plots within Recycled orogen province on QFL plot	-8.3 (see also Table 2)	See Table 2.	<55 Ma grains make up 89% of the sediment. 7% arc-aged grains of between ~70-150 Ma, and 4% >200 Ma.	Tertiary ages make up 74% of the sample. Arc-aged component ~25%

Table 1. Data from the Palaeogene and Neogene Indo-Burman Ranges, and the Irrawaddy River

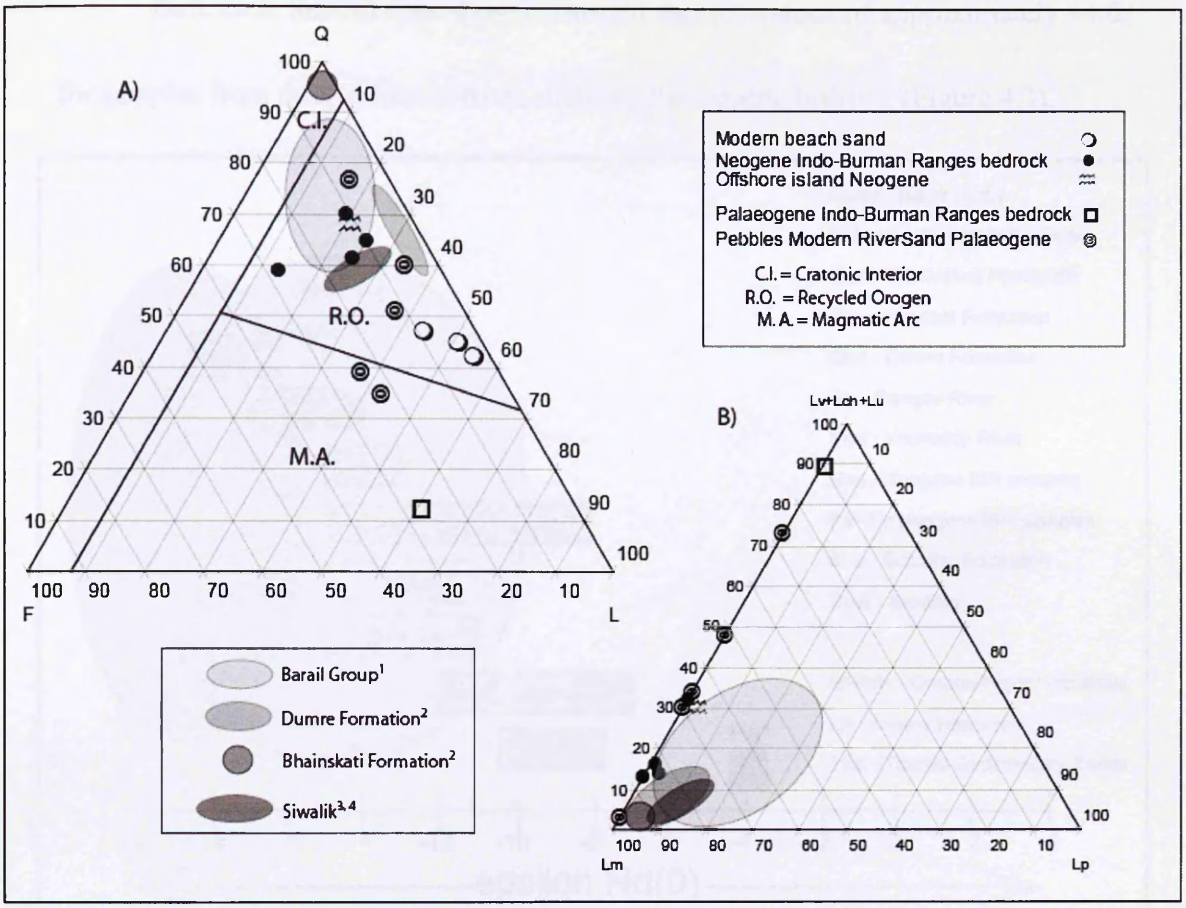

Figure 4.2 (a) QFL and (b) lithic plot for Palaeogene and Neogene samples from the Indo-Burman Ranges compared with petrographic assemblages of the Oligocene Barail Formation of the Bengal Basin, and Himalayan foreland basin rocks of the Eocene Bhainskati Formation, the Miocene Dumre Formation and the Miocene to recent Siwalik Group. Circled regions showing the Bhainskati, Dumre and Siwalik Formations are based on the data for each, incorporating minimum and maximum values, however they are not statistically rigorous in relation to this figure. Q = quartz, F = Feldspar, L = lithics (Lm= metamorphic lithics, Lp= pelagic lithics, Lv= volcanic lithics, Lch=chert lithics, Lu= ultramafic lithics) [1]Najman *et al.,* (in review), [2]Najman *et al.,* (2005), [3]DeCelles *et al.,* (1998a), [4]Szulc *et al.,* (2006)

Bulk rock Sm-Nd data show consistent ε_{Nd} (0) values of approximately –4.0, for samples from three different rivers draining Palaeogene bedrock (Figure 4.3).

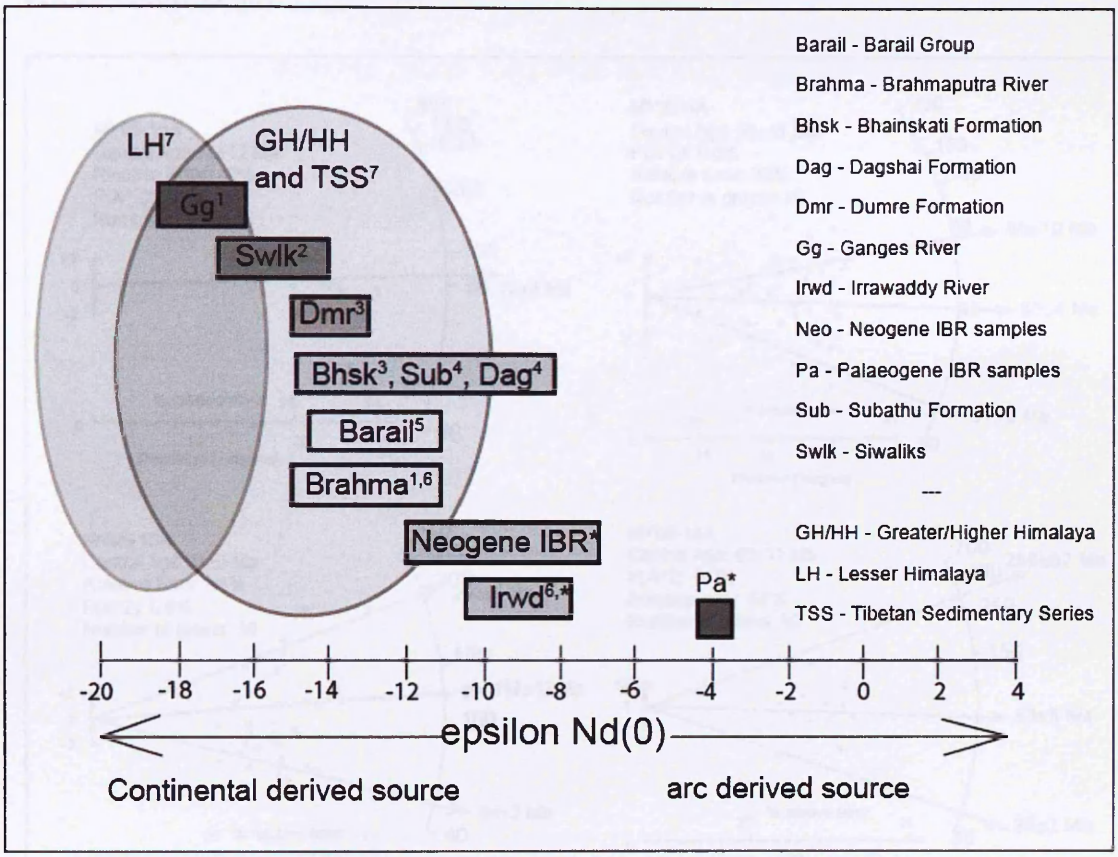

Figure 4.3 ε_{Nd} (0) values for Palaeogene and Neogene samples from the Indo-Burman Ranges compared with data from the Himalayan derived foreland and remnant ocean basin rocks (Bhainskati Formation, Subathu and Dagshai Formations, Dumre Formation, Barail Formation and Siwalik Group) and Himalayan bedrock as well as modern river samples from the Irrawaddy, Ganges and Brahmaputra. A crustal source with a subordinate arc-derived component is indicated by the weakly negative ε_{Nd} values for the Palaeogene Indo-Burman Ranges and is in contrast to our Neogene Indo-Burman Ranges samples, Himalayan bedrock and Himalayan foreland basin detritus which show continental derivation as indicated by their more strongly negative values. One sample (MY05 8A) was taken from the boundary between the Palaeogene and Neogene Indo-Burman Ranges and its epsilon Nd value of –7.3, reflects an intermediate composition between Palaeogene and Neogene samples. [1]Singh and France Lanord, 2002, [2]Szulc *et al.*, 2006, [3]Robinson *et al.*, 2001, [4]Najman *et al.*, 2000, [5]Najman *et al.*, in review, 2002, [6]Colin *et al.*, 1999, [7]DeCelles *et al.*, 2004,*our data, this study

Zircon fission track data (Figure 4.4a) from bedrock and modern river sands show dominant Palaeogene and Cretaceous age populations with minor contribution of Palaeozoic grains.

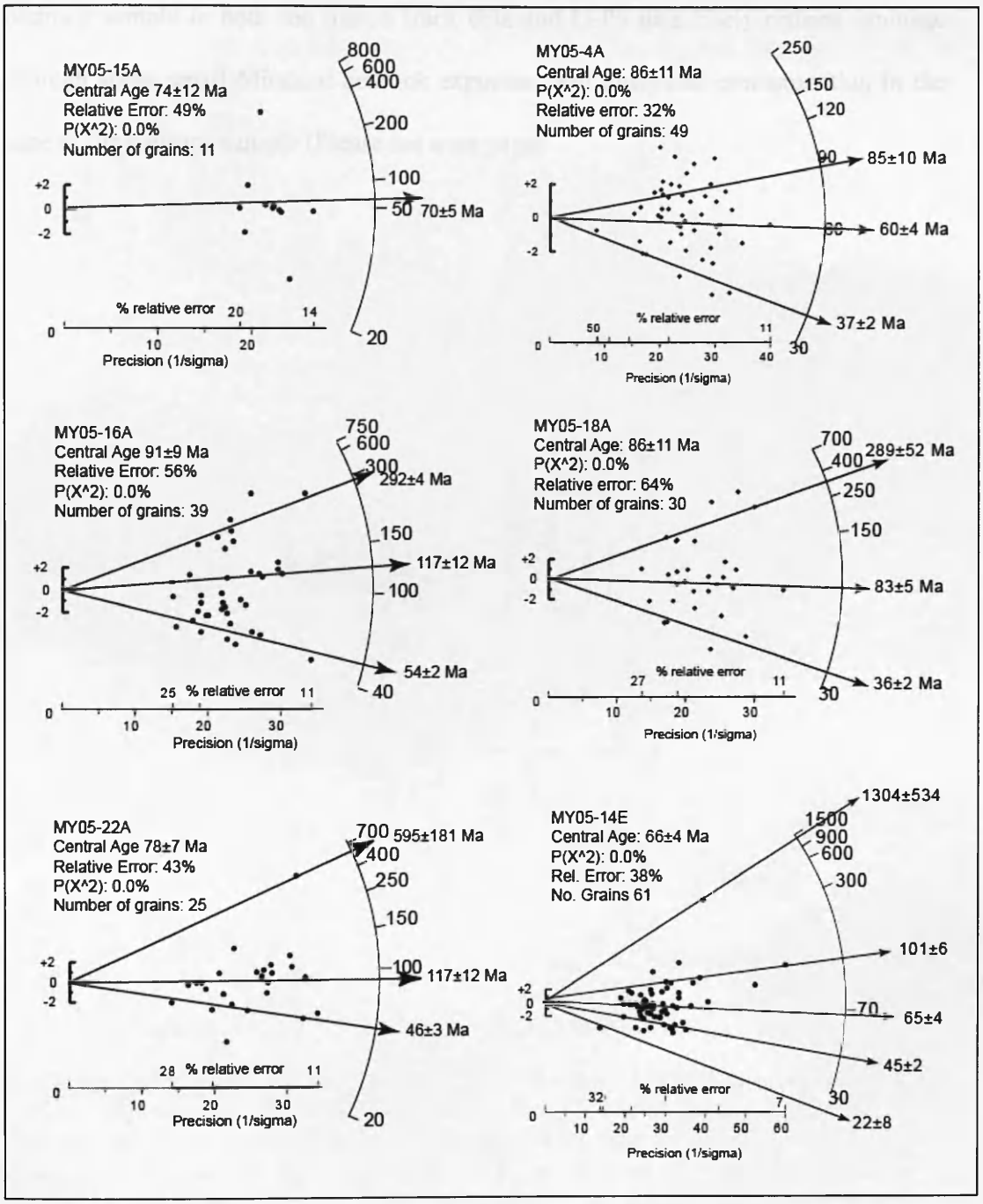

Figure 4.4 (a) Detrital Zircon Fission track radial plots data for the Palaeogene Indo-Burman Ranges with main population modes highlighted. The data show a predominance of arc-aged grains of 75-150 Ma in Palaeogene samples. However, younger populations (down to 20 Ma) as well as small older aged populations of less than 300 Ma are also represented and are attributed to a subordinate continental source.

U-Pb dating on detrital zircons (Figure 4.5) shows predominant zircon populations of Palaeocene/Cretaceous (~55-150 Ma) and Proterozoic (>545 Ma) age. Rare Neogene aged grains appearing in modern river samples and one Palaeogene bedrock sample in both the fission track data and U-Pb data likely reflects drainage through some small Miocene bedrock exposure, and analytical contamination in the case of the bedrock sample (Please see over page).

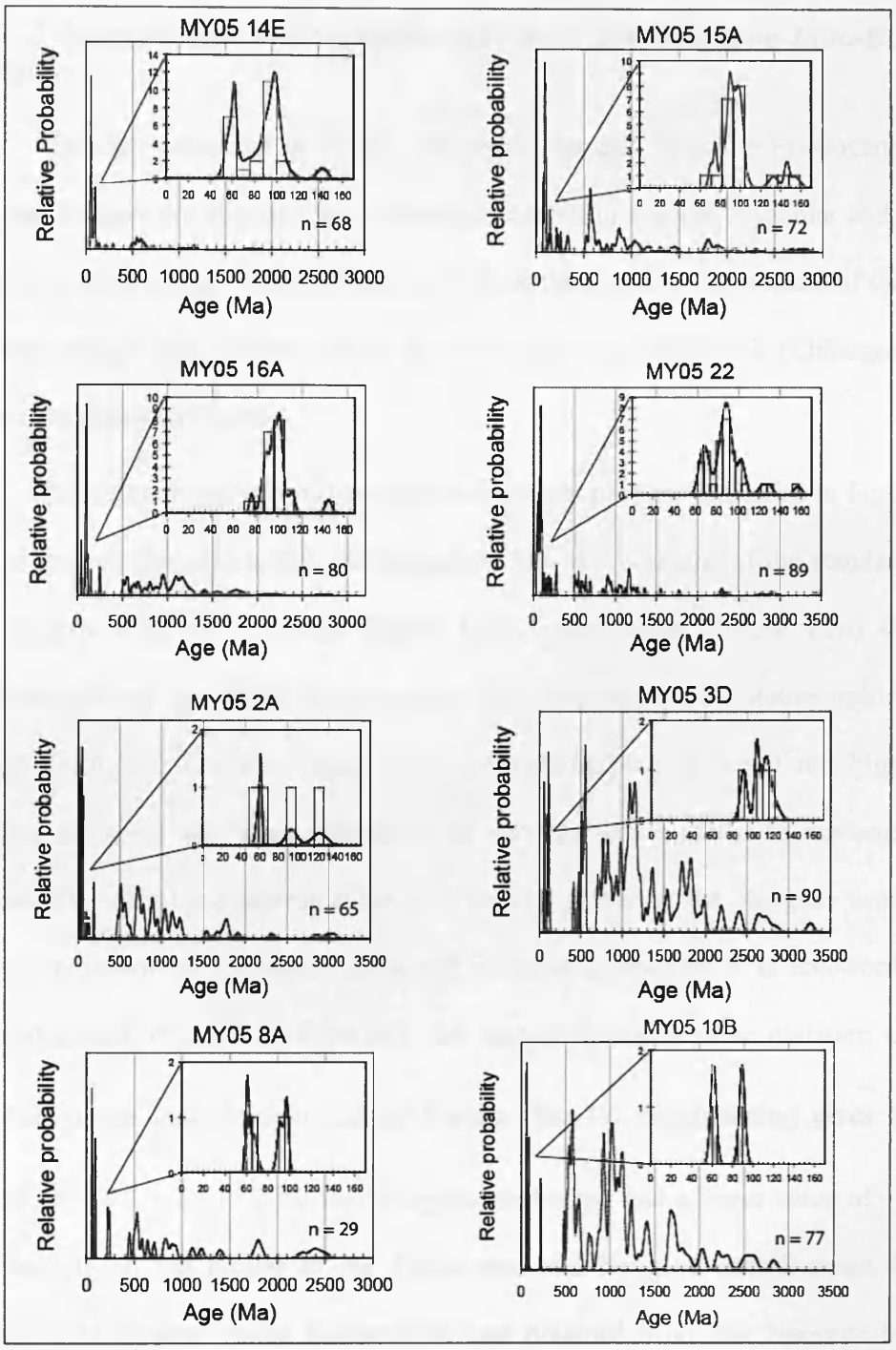

Figure 4.5 Concordant detrital zircon $^{238}U/^{206}Pb$ ages from bedrock and modern river sediments from the Palaeogene and Neogene Indo-Burman Ranges. Significant arc-aged populations of between 70-150 Ma are present within the Palaeogene samples (see insets), as well as a large number of grains between 500-2800 Ma. Whilst these are consistent with a Himalayan signature, as seen in the Eocene foreland basin Bhainskati Formation (DeCelles *et al.*, 2004) they are not exclusive to it. A lack of data from the Burman source region precludes further discrimination between Himalayan and Burman margin derivation. Young grains of <20 Ma in modern river samples likely indicate drainage through small Miocene bedrock exposures. Ages of >300 Ma are present in 3 samples but in very small proportions with less than <8 grains in each sample. Neogene samples show a limited number of grains between 70 and 150 Ma (see insets, maximum of 4 grains per sample), with most ages spanning 500 to 2800 Ma.

4. 5. 2 Isotopic and petrographic data from the Neogene Indo-Burman Ranges

The data presented in Table 1 alongside the data from the Palaeogene Indo-Burman Ranges, are obtained from Neogene bedrock in western Myanmar and from a modern river draining Neogene bedrock, both in the westernmost portion of the Indo-Burman Ranges that extends along strike into eastern Bangladesh (Chittagong Hill Tracts) as shown in Figure 4.1.

Petrographic data from Neogene bedrock samples are presented in Figure 4.2. All of the samples plot within the Recycled Orogenic province of the standard QFL plot (Figure 4.2a) of Dickinson (1985). Lithic composition (Figure 4.2b) shows a predominance of low-grade metamorphic lithic fragments. The Metamorphic Index ranges from 100 to 250 (where 0 is non-metamorphic and 500 are high-grade (Appendix 2a, b) indicating occurrence of very-low-grade (slate) to medium grade (micaceous schist) metamorphic lithics. Plentiful garnet in the Neogene samples is further indication of a medium grade metamorphic component. It is noteworthy that the occurrence of garnet diminishes as the sample locations move eastward towards the Palaeogene Indo-Burman Ranges border. Sm-Nd fingerprinting gives ε_{Nd} (0) values of –10.7 and –12.2 for two Neogene sandstones and a lower value of –7.3 for one sample on the border of the Palaeogene and Neogene Indo-Burman Ranges (Figure 4.3). Detrital zircon fission track data obtained from four Neogene bedrock samples all show dominant age populations of less than 55 Ma. As the sample locations move eastwards towards the Palaeogene Indo-Burman Ranges, the proportion of Tertiary grains decreases in the zircon fission track data and grains >200 Ma increase, as do the proportion of grains aged 56-150 Ma (from 0-40% of total number of grains, figure 4.4b).

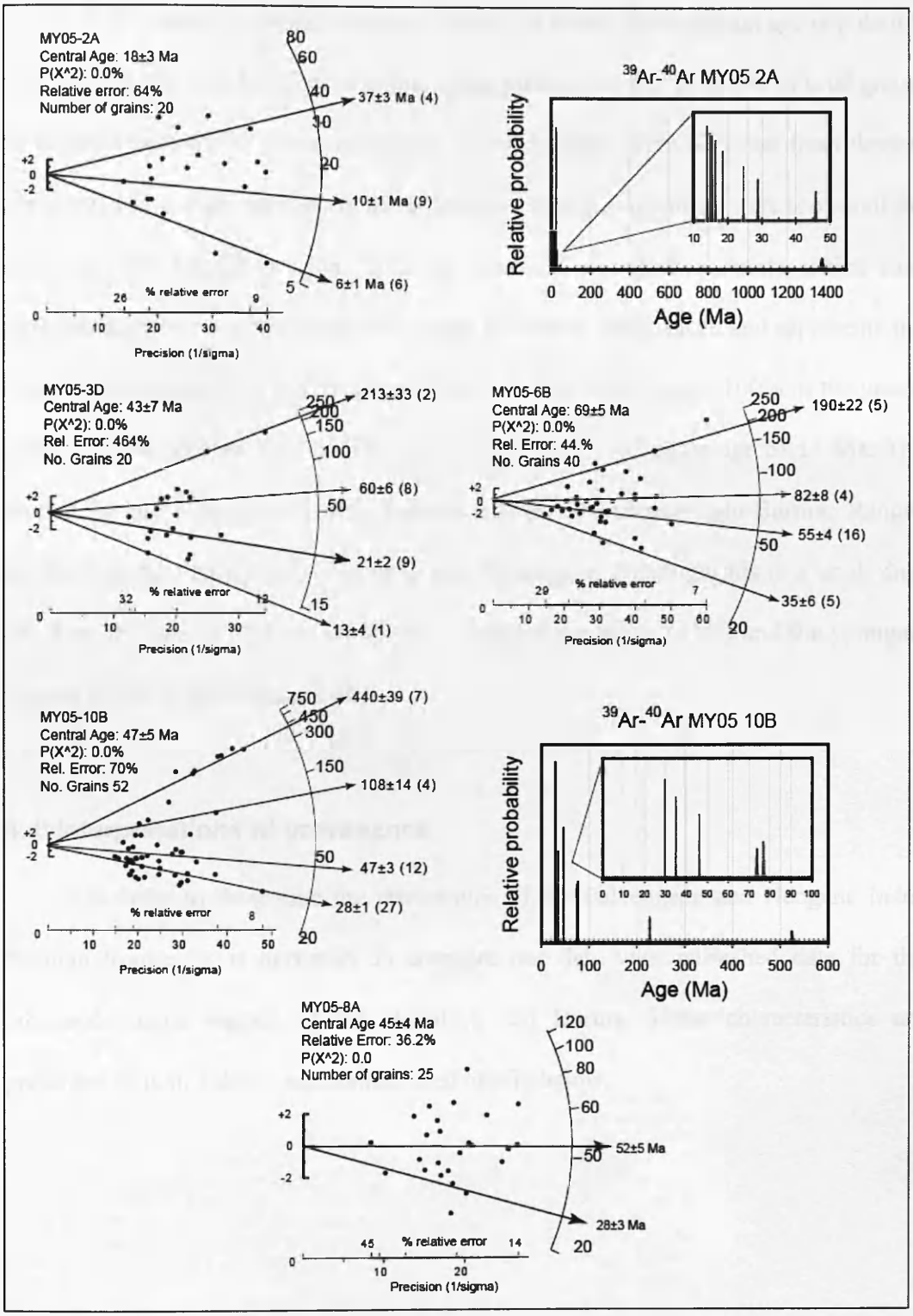

Figure 4.4 (b) Detrital Zircon Fission track radial plots and ^{39}Ar-^{40}Ar for the Neogene Indo-Burman Ranges with main population modes highlighted. The Neogene samples show a predominance of ages less than 55 Ma. ^{39}Ar-^{40}Ar white mica data are presented for samples furthest west (MY05 2A) in the Neogene Indo-Burman Ranges and furthest east (MY05 10B).

U-Pb dating of detrital zircons (Figure 4.5) shows the dominant age population is 500-2800 Ma with Cretaceous grains being present but few (4 to 6% of total grains in samples with 65-90 grains analysed). ^{40}Ar-^{39}Ar dates were obtained from detrital white mica from two samples (in other Neogene samples the micas were too small for analysis). One sample is taken from the Arakan Coast (Sittwe Point), which runs along strike into the Chittagong Hill Tracts of eastern Bangladesh and represents the most westerly sample in the Neogene of the Indo-Burman Ranges. 100% of the grains in this sample yielded ages of less than 55 Ma, with a youngest age of 13 Ma. The second sample is from the sample furthest east in the Neogene Indo-Burman Ranges on the boundary between the Neogene and Palaeogene. Although this is a small data set, Tertiary ages of <55 Ma comprise the largest age mode (43%) and the youngest detrital age is 29 Ma (Figure 4.4b).

4. 6 Interpretations of provenance

In order to determine the provenance of the Palaeogene and Neogene Indo-Burman Ranges, it is necessary to compare our data with published data for the proposed source regions of the Himalaya and Burma. These characteristics are presented fully in Table 2 and summarized briefly below.

Source Region	Rock Description and Heavy Mineral and Petrography	Whole rock Sm-Nd εNd(0)	U-Pb ages of zircon	^{40}Ar-^{39}Ar ages Of detrital white mica	Detrital Zircon Fission Track data
Himalayan Bedrock southern flank (characteristics interpolated from foreland and remnant ocean basin sediments)	-	HH bedrock –15 to –20 and LS bedrock –16 to –25[1,2]	HH bedrock 500-2800 Ma, lack of Cretaceous grains[2, 3]	-	-
Eocene Bhainskati Formation (Nepal)	Quartz arenites[3]	-8 to –14.9[1]	Ages 500-2800 Ma[2]	Unmicaceous	Peaks at ~343 Ma (59%), ~119 Ma (21%) and 45 Ma (20%)[4]
Oligocene Barail (Bangladesh)	Sedimentary/Low grade metamorphics. Recycled orogen[5] on QFL of Dickinson (1985)	-11 to –14.6[5]	Ages 500-2800 Ma[5]	Rare micas until the late Oligocene	Peaks at 23-28 Ma, 37-42 Ma and 250-350 Ma[5]
Oligo-Miocene Dumre Formation (Nepal) (also Subathu and Dagshai) (India)	Metasedimentary lithics. Recycled orogen on QFL plot[3]	-14.5 to –13.1[1] and –9 to –10 and –15 to –16 for Subathu[8] and Dagshai[8] respectively.	Ages 500-2800 Ma[3]	All ages <55 Ma[6]	Peaks at 30 Ma (69-84%), 300-350 Ma (8-18%) and 60-120 Ma (6-8%)[4]
Miocene to Recent Siwaliks	metamorphic lithics, plagioclase and first appearance of high-grade metamorphic minerals in the Siwalik. Plots Recycled orogen[3]	-14 to –30 (average of –17) in the Siwaliks[7]	Ages 500-2800 Ma[9]	All ages <55 Ma. Peaks at 20 Ma and 15 Ma[10]	13-19 Ma (35-95%)[9]
Bedrock Signal Today Modern River sediments Higher Himalaya dominates detritus	Modern River sands and muds	Ganges -16 to –18[11] Brahmaputra -11 to –15[11, 16]	Data from the Ganges shows a dominance of Proterozoic to Palaeozoic ages and no grains between 55-125 Ma[12]	As determined from *Gangetic tributaries:* Neogene peak, subordinate grains spanning to PreCambrian[13]	No FT data available for Gangetic sediment. He data: <55 Ma, Plio-Pleist peak.[12]
Burma The magmatic arc	See below Cretaceous arc rks & Triassic fore-arc / back arc seds on metamorphic	No data available	Zircon U-Pb ages on I-type granitoids give ages of 120-150 Ma	K-Ar mineral dating of batholiths gives cooling ages of 79-100 Ma[15]	No data available
The Burman Margin including region drained by the Irrawaddy River and area intruded by the arc. Data from modern Irrawaddy river sediment. Shan-Thai block lies to east, forearc-back arc of Indo-Burman Ranges (IBR) to west. Paleocontinental margin.	basement. Mogok schists, gneisses and intrusives, Shan-Thai Proterozoic – Cretaceous sedimentary rks on schist basement. Irrawaddy river sediment plots in "recycled orogenic" province field of QFL plot (Dickinson 1985)	Irrawaddy River -10.7[16] also see data in table 1 from this study.	U-Pb dating shows Tertiary ages zircons along the Burma Margin[17] Irrawaddy U-Pb data peaks at <55 Ma (30%) and 56-150 Ma (38%). Older grains present up to 1250 Ma (32%)[19]	Mica ages of 26-16 Ma along Shan Scarp[18] Also See data Table 1 from this study for Irrawaddy data	Data Table 1 from this study

[1]Robinson *et al.*, 2001, [2]DeCelles *et al.*, 2004, [3]DeCelles *et al.*, 1998a,b, [4]Najman *et al.*, 2005, [5]Najman *et al*, in review, [6]DeCelles *et al.*, 2001, [7]Szulc *et al.*, 2006, [8]Najman *et al.*, 2000, [9]Bernet *et al.*, 2006, [10]Szulc *et al.*, in press, [11]Singh and France-Lanord, 2002, [12]Campbell *et al.*, 2005, [13]Brewer *et al.*, 2003, [14]Barley *et al*, 2003, [15]United Nations Report 1978b, c (*in* Mitchell, 1993), [16]Colin *et al.*, 1999, [17]Searle *et al.*, 2007, [18]Bertrand *et al.*, 1999, [19]Bodet *et al.*, 2000

Table 2. Possible source region provenance characteristics

4. 6. 1 Characteristics of the proposed source regions for the Indo-Burman Range sedimentary rocks: Himalayan and Burman Margin.

Data from the peripheral foreland basin provide the source signature of detritus eroded from the southern flank of the Himalaya and is a valuable source of information on erosion of the hinterland that has been lost in the hinterland itself due to metamorphic overprinting. The Himalayan detritus from the peripheral foreland and remnant ocean basins in India, Nepal and Bangladesh contains minerals with predominantly Tertiary but subordinate pre-Tertiary cooling age populations as seen in ^{39}Ar-^{40}Ar ages of detrital white micas and zircon fission track ages from the Eocene Bhainskati (Sakai 1983; Najman *et al.,* 2005), Oligocene Barail (Reimann 1993; Najman *et al.,* in review), Oligo-Miocene Dumre (DeCelles *et al.,* 1998a; 2001) and mid Miocene to recent Siwalik (Bhatia 1982; Gautam and Fujiwara, 2000; Szulc *et al.,* 2003; Bernet *et al.,* 2006) Formations, representing erosion from metamorphosed core and unmetamorphosed cover of the Himalaya. U-Pb data for all Formations show that the majority of zircon grains are between 500-2800 Ma and are consistent with data from Himalayan bedrock (DeCelles *et al.,* 1998a, b) as well as data from the Ganges River that drains the Himalaya (Campbell *et al.,* 2005). ε_{Nd} values from the peripheral foreland basin span –8 (Eocene Bhainskati Formation) to –16 (Miocene-Recent Siwalik Group) confirming a continental-influenced source region with greater input from the suture zone during early stages of orogenesis (Robinson *et al.,* 2001; DeCelles *et al.,* 2004).

The Cretaceous-Tertiary Transhimalayan batholith (Singh *et al.,* 2006) running north of the suture zone and representing the ancient Asian active margin, made only a minor contribution to basins south of the orogen, as evidenced from the relative paucity of arc-derived material in the basin detritus as seen in Table 2 (Najman *et al.,*

2005, Najman *et al.,* in review; DeCelles *et al.,* 2001, 2004; Szulc *et al.,* 2006). This ancient active margin continues south into Burma. United Nations Report 1978 (b, c) documents the typical age signature of Cretaceous arc magmatism based on K-Ar mineral dating of batholiths (Table 2). Barley *et al.,* (2003) report zircon U-Pb ages from I-type granitoids that confirm Andean-type granite magmatism was widespread along the Burma margin throughout the pre-collisional period in the Tertiary.

Although dominated by the Cretaceous-Eocene arc, the Burmese Margin also contains material from crustal sources, which pre-date and were intruded by the arc and minerals reset by Tertiary magmatism and metamorphism. This includes the high ground of the Indo-Burman Ranges in the eastern belt comprised of Triassic flysch and mica schists (Mitchell 1993). Data from the Burman Margin, including our new data for the Irrawaddy River is presented in Tables 1 and 2. Bertrand *et al.,* (1999) report mica ages spanning the Oligocene to middle Miocene from the Shan Scarp alongside the Mogok Metamorphic Belt and U-Pb data (Barley *et al.,* 2003; Searle *et al.,* 2007) identifies Tertiary aged zircons. This confirms the presence of two distinct metamorphic events on the Burman margin, one at approximately 59 Ma and a later phase that over printed the former between ~ 43 Ma to 29 Ma. ^{39}Ar-^{40}Ar white mica data (Table 1, 2 and Figure 4.6) from the Irrawaddy River, which drains the tip of the Himalayan eastern syntaxis as well as the Central Myanmar Basin, Mogok Belt and Indo-Burman Ranges, show that Tertiary aged mica grains make up the bulk of the sediment (the majority of which are Palaeogene). The remainder comprise Mesozoic arc-aged grains and grains older than 200 Ma. Over 70% of detrital zircon fission track dates from the Irrawaddy bed load give Tertiary ages, whilst the arc-aged component represents ~25% of total grains (Figure 4.6). U-Pb zircon data from the Irrawaddy (Bodet *et al.,* 2000) also gives Tertiary aged grains, with a similar

proportion of ages falling in the arc-aged bracket of 56-150 Ma. Old grains up to a maximum of ~1250 Ma are also present. Epsilon Nd values of ca. –8 to –10 in the Irrawaddy River reflects mixed input from continental-derived (Himalayan and/or Burman margin) and arc-derived bedrock (Table 1 and 2 and Figure 4.3).

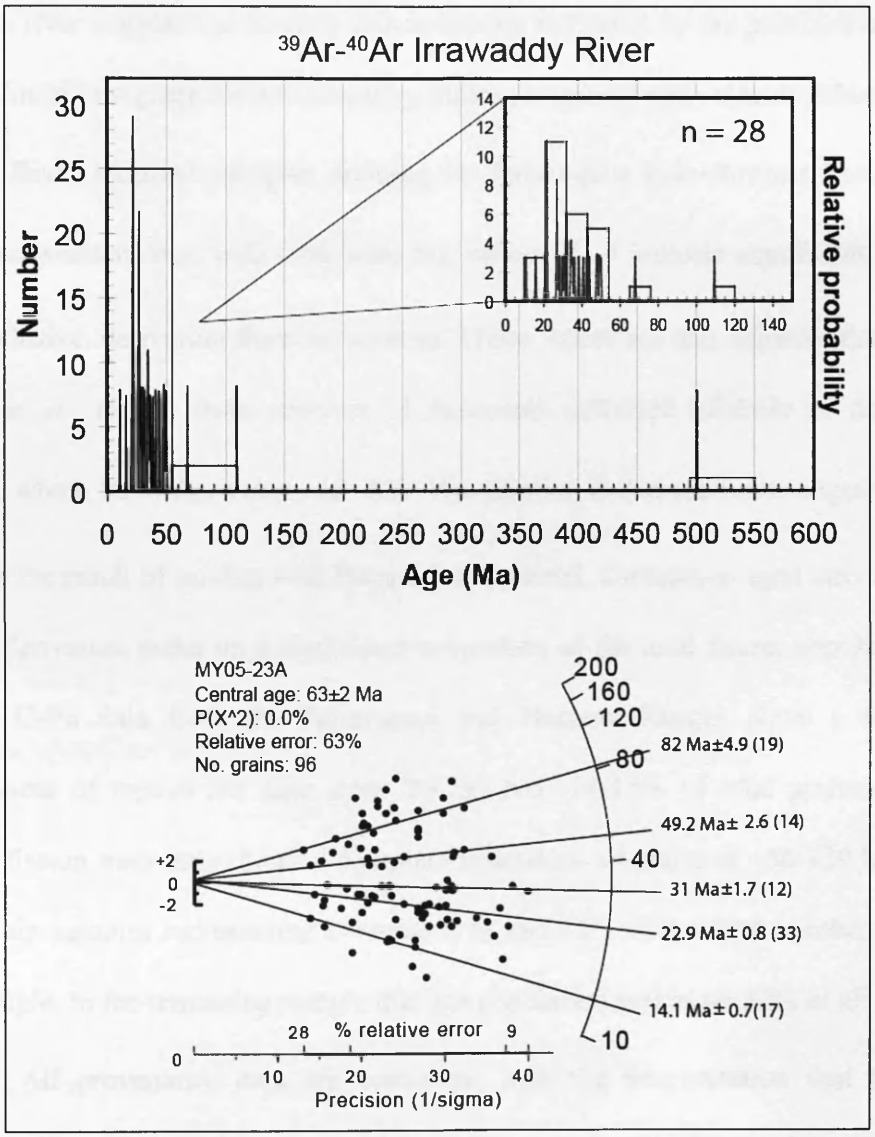

Figure 4.6 ^{39}Ar-^{40}Ar white mica and zircon fission track data for the modern Irrawaddy River. Both data sets show dominant Tertiary aged grains that make up 80-89% of the sample. The majority of these grains are Palaeogene with subordinate Neogene ages. A smaller but notable "arc-aged" (~60-150 Ma) component is also present in the Ar-Ar white mica and zircon fission track data (7-20% respectively) which is comparable to U-Pb data by Bodet *et al.*, (2000) where the arc aged component is dominant and significant but subordinate Tertiary ages are also present. These data are to be expected in a large river that drains the corner of the eastern Himalayan syntaxis as well as the Mogok metamorphic belt, Myanmar Central Basin and Indo-Burman Ranges on the Burman Margin.

4. 6. 2 Provenance of the Palaeogene rocks of the Indo-Burman Ranges

Evidence of Cretaceous arc detritus in the Palaeogene Indo-Burman Ranges

The significant proportion of volcanic detritus in the bedrock sample as seen on the QFL plot (Figure 4.2) is consistent with arc derivation. The pebbles from a modern river suggest that there is source mixing indicated by the presence of pebbles with a lot of low-grade metasedimentary lithics (orogenic) and volcanic lithics (arc).

River sediment samples draining the Palaeogene Indo-Burman Ranges along the southwestern coast with consistent ε_{Nd} values of –4 indicate significant, although not exclusive, derivation from arc sources. These values are less negative than data by Colin *et al.,* (1999) from analyses of sediments collected offshore of the Arakan Yoma, which have ε_{Nd} values of –8.6. We surmise that these more negative values may be the result of mixing with Bengal Fan material. Cretaceous aged zircons typical of arc-derivation make up a significant proportion of the total zircon population. The zircon U-Pb data from the Palaeogene Indo-Burman Ranges show a significant component of typical arc ages from 70-150 Ma (14-36% of total grains). Detrital zircon fission track data shows a dominant population of grains at ~56-120 Ma in five out of six samples representing between 57% and 82% of the total number of grains per sample. In the remaining sample this age population makes up 32% of all grains.

All provenance data are consistent with the interpretation that the Indo-Burman Ranges contains a significant component of detritus derived from a Cretaceous-Palaeogene arc. This Cretaceous-Tertiary arc forms the Transhimalaya and then bends southward, through Myanmar to Sumatra (although the arc is not identified in the northeast syntaxis, it reappears in Burma). The Burman extension of this arc is the most likely source to the Palaeogene Arakan Yoma (Indo-Burman

Ranges) sedimentary rocks, in view of its proximity to the region. The possibility that the Yarlung Tsangpo (which drains the northern side of the Himalaya and Transhimalaya) may have routed to the South China Sea during this period (Clark *et al.,* 2004) and the fact that in contrast to the Palaeogene Indo-Burman Ranges, the Palaeogene Himalayan foreland and remnant ocean Bengal Basin Barail deposits show evidence of only minor arc-derived input (Table 2; ε_{Nd} values of the foreland and remnant ocean basins are more negative compared to the Palaeogene IndoBurman Ranges (Najman *et al* in review, Robinson *et al.,* 2001) and the arc-aged component of the zircon population is subordinate [DeCelles *et al.,* 2004; Najman *et al.,* 2005; Najman *et al.,* in review]) is inconsistent with substantial Transhimalayan material being transported south of the orogen to eastern repositories at this time. An arc-derived component to the Indo-Burman Ranges detritus is in partial agreement with Chhibber (1934b) and Mitchell (1993) who consider the Palaeogene Indo-Burman Ranges to be an equivalent/extension to the Western Trough forearc sediments of Western Myanmar. Pivnik *et al.,* (1998) believe this was later separated by the rising Mt. Popa arc, whereas Mitchell (1993) believes this separation was caused by the emplacement of older rocks in the east of the ranges in late Eocene or early Oligocene.

Subordinate component of crustal-derived detritus in the Palaeogene Indo-Burman Ranges rocks

As well as the significant arc-derived component represented in the petrography, zircon U-Pb and fission track data, and bulk rock Sm-Nd, our data clearly show an additional continental source as identified in petrography by low grade metamorphic and siltstone lithic fragments, by more negative epsilon Nd values than expected for arc-derived rocks, and by zircons with U-Pb ages of 500-2800 Ma,

and fission track ages older than 300 Ma. This contribution makes up to between 2 and 71% of the detritus (2-15% zircons with such ZFT ages, and 35-71% zircons with such U-Pb ages).

It could be argued that these grains are of Himalayan origin, since such age ranges (Table 2) are found in grains of the foreland basin Bhainskati Formation, whereas zircons from the modern Irrawaddy River, which drains the Burman Margin and Indo-Burman Ranges, Central Myanmar Basins and Mogok Belt (as well as parts of the eastern Himalayan syntaxis), do not show evidence of U-Pb detrital zircon grains older than 1300 Ma (Bodet *et al.,* 2000). Furthermore, the modern Irrawaddy River lacks the older fission track age mode of >300 Ma. In a sample of 95 grains 74% are less than 55 Ma and 24% of grains are arc-aged between 59 and 130 Ma and the remaining 2% of grains are between 130 and 190 Ma. However, the isotopic characteristics of the Asian margin into which the arc intruded are incompletely characterised and differences between the terrains as currently proposed may be the result of sparse sampling. For example, 600 Ma grains have been found on the Burman margin and grains older than 1300 Ma in the Irrawaddy River sand (Liang *et al.,* in press). Thus, on available data, it is not possible to definitively differentiate between a Burmese margin and Indian Himalayan source for this older continental derived component.

4. 6. 3 Provenance of the Neogene Indo-Burman Ranges

Comparison of our samples with the approximately coeval Dumre Formation (21-16 Ma) and the Siwaliks (15 Ma – recent) of the peripheral Nepalese foreland basin allows an assessment of potential Himalayan provenance for the Neogene Indo-Burman Ranges.

Sediments from both the Dumre Formation and the Siwaliks plot within the Recycled Orogen province of the standard QFL plot. The predominance of metasedimentary lithic clasts provides evidence of derivation from the rising metamorphosed Himalayan fold thrust belt, at first seen in the Dumre Formation and then in the Siwaliks (DeCelles *et al.,* 1998a, Szulc *et al.,* 2006). This is comparable to the petrographic data from the Indo-Burman Ranges Neogene samples, although potassium feldspar is noticeably higher in our samples (Figure 4.2). ε_{Nd} (0) values of –10.7 and –12.2 are indicative of a continental derived source region and fall within the typical range of values for the modern Brahmaputra River, which drains the Himalaya (Colin *et al.,* 1999; Singh and France-Lanord, 2002). Values are less negative than those from Miocene foreland basin rocks (Robinson *et al.,* 2001), presumably due to a higher proportion of arc-derived detritus in the Neogene Indo-Burman Ranges. U-Pb zircon data from the Dumre Formation and the Siwaliks (section 3) are comparable with that from the Neogene Indo-Burman Ranges (Figure 4.5). Zircon fission track and white mica ^{39}Ar-^{40}Ar ages in the Dumre Formation (DeCelles *et al.,* 2001; Najman *et al.,* 2005) and the Siwaliks (Bernet *et al.,* 2006; Szulc *et al.,* 2006) both show a predominance of grains less than <55 Ma, which represent metamorphic cooling ages in the source region typical of the metamorphosed Higher Himalaya. This dominant age component of <55 Ma as seen in the Neogene foreland basin sediments is comparable to our data from the Neogene Indo-Burman Ranges (Figures 4.4 and 4.6).

Our data are thus consistent with that from both Himalayan bedrock and sediments of known Himalayan derivation in the peripheral foreland basin. In this scenario, the source region for the Neogene Indo-Burman Ranges was the rising Himalaya during the Miocene, detritus from which was incorporated into the proto-

Bengal Fan, susequently forming an accretionary prism at the subduction zone between the Indian and Asian plate. By contrast, we consider an eastern, Burman, source unlikely. The unmicaceous very fine-grained sandstones and mudstones of the Palaeogene Indo-Burman Ranges have a dissimilar thermochronological, isotopic and petrographic signature to the rocks of the Neogene Indo-Burman Ranges (as described in section 5a) and could not have sourced the Neogene rocks. Further east, the Burmese arc margin is of Cretaceous age but nevertheless shows evidence of some grain age populations of both Tertiary and Paleozoic-Proterozoic age, similar to those found in the Himalaya and Neogene Indo-Burman Ranges (see section 4). However, it is unlikely that the Burma arc source to the east was a source to the Neogene Indo-Burman Ranges in view of the extremely limited extent of arc derived material in the Neogene Indo-Burman Ranges (4-6% of zircon U-Pb ages, 0-40% zircon fission track ages) and the fact that the Palaeogene Indo-Burman Ranges would have provided a barrier to transport of Burmese margin material west by this time.

4.7 Constraints to the depositional age and time of exhumation of the Indo-Burman Ranges

4.7.1 The Palaeogene Indo Burman Ranges

Fission track dating on modern river sediments draining the Palaeogene Indo-Burman Ranges reveals a persistent youngest population of ~37 Ma. This indicates that the depositional age and subsequent exhumation of the sediment extends to younger than ~37 Ma. This gives tighter constraint on previous estimations of late Eocene-Oligocene age and exhumation of the Arakan Yoma (Indo-Burman Ranges) (Mitchell 1993) although we note that the youngest population of modern river sand need not be representative of its entire drainage basin and earlier exhumation of some rocks may well have occurred. Moving westwards, as the succession youngs into the

Neogene Chittagong Hill Tracts (as described below) the maximum age of deposition is constrained at younger than 6 Ma and likely reflects the diachronous uplift history of the region.

4.7.2 The Neogene Indo-Burman Ranges

Fission track data on detrital zircons from Neogene bedrock samples reveal a youngest age of 6 Ma in one sample furthest west, and 13 Ma to 29 Ma moving eastwards towards the Palaeogene Indo-Burman Ranges as indicated in the ^{39}Ar-^{40}Ar white mica data. This indicates that the depositional age of the sediment furthest west in Myanmar was post 6 Ma – latest Miocene, but moving eastwards to the border with the Palaeogene the maximum depositional age increases to post 29 Ma. These data are consistent with the westward younging of the whole sequence from the Palaeogene Indo-Burman Ranges through to the west vergent Chittagong Hill Tracts, and their equivalent along the Arakan coast.

4. 8 Discussion and Conclusions

Youngest zircon fission track populations constrain the sampled Palaeogene deposits as post 37 Ma, with exhumation occurring thereafter (with older deposits also possibly occurring). In contrast, youngest zircon fission track and U-Pb ages constrain the most western Neogene deposits at younger than 6 Ma. Westward younging of the youngest ZFT population is consistent with progressive exhumation of the Indo-Burman Ranges from the Palaeogene in the east to the Neogene in westernmost Myanmar.

The Neogene rocks of the Indo-Burman Ranges show close affinity with signatures from the foreland basin Dumre Formation and Siwaliks, which record

erosion from the Himalaya since the Miocene. As such, the Neogene Indo-Burman Ranges most likely represents accretionary prism sediments of the Himalayan derived palaeo-Bengal Fan.

By contrast, the Palaeogene rocks of the Indo-Burman Ranges show clear evidence of significant arc-derived input. This is in contrast to the approximately coeval Himalayan derived Bhainskati and Barail Formations of the foreland and remnant ocean basins. As there is no evidence of such substantial input of Transhimalayan (arc) detritus to any basins south of the eastern Himalaya during this period, we suggest that the source of this detritus in the Indo-Burman Ranges is the Burmese portion of the arc, to the east of the Indo-Burman Ranges. The source of the older crustal component in the Palaeogene Indo-Burman rocks is ambiguous and may represent erosion from the rising southern flanks of the Himalaya, or the Burmese terrains along the Burman margin into which the arc is intruded. If the continental source is Himalayan, then the palaeogeographic environment of deposition of the Indo-Burman Ranges sediments most likely involved mixing in the subduction trench, with Burmese arc detritus bypassing the forearc and outer arc high through a series of canyons, as seen for example in the Tonga trench (Draut *et al.,* 2006). If the Burman margin is the older source, then forearc deposition on the Asian plate is the more likely depositional setting as suggested by Mitchell (1993).

The systematic difference between Palaeogene and Neogene signature of the Indo-Burman Ranges may be explained either by their potentially different palaeogeographical location as outlined above, or by onset of substantial erosion of the Himalayas in the Neogene that initiated a swamping of the arc signal. Regardless, it appears that there is evidence of major, substantial, erosion from the Himalaya in the Neogene. However, significant erosion of the Himalayan mountain range during

the Palaeogene remains equivocal. Our data are therefore consistent with models of crustal deformation that favour insignificant early erosion (Beaumont *et al.,* 2001, 2004; Jamieson *et al.,* 2004; Replumaz and Tapponier, 2003)

Chapter 5: New seismic, biostratigraphic and isotopic constraints to the geological evolution and sedimentary provenance of the SE Bengal Basin, Bangladesh

Submitted for publication to Basin Research

Abstract

The offshore Hatia Trough and adjacent onshore Chittagong Hill Tracts to the east (a belt of north-south trending thrust-bounded linear anticlines, interpreted as an accretionary prism) in the SE Bengal Basin, may preserve an archive of Himalayan erosion since the Miocene. However, a Burman and Indian cratonic source for these rocks has also been suggested and the use of this potential record is hampered by poor stratigraphic control. Here, we establish a basin-wide stratigraphy and provenance for the Bengal Basin Tertiary sediments.

2D seismic mapping of the southeast Bengal Basin splits the Tertiary succession into three seismically–distinct, regionally–correlatable sedimentary packages (termed Megasequences; MS1, 2 and 3, dated at ~5 Ma, ~3.25 Ma and ~1.55 Ma respectively) that show deposition within a prograding delta. Reorganisation of the geology of the Chittagong Hill Tracts into a seismic stratigraphic framework that is calibrated by well penetrations and biostratigraphic data, has shown that the rocks at surface are younger than previously thought.

Seismic mapping of the Bengal palaeoshelf shows that the input direction shifted from the north-east, to the north through time. Thermochronological analyses on detrital grains, isotopic analysis on bulk rock and heavy mineral and petrographic data have identified the Himalaya as the primary source of the sediments of the Hatia Trough and Chittagong Hill Tracts throughout the Neogene. An Indian cratonic and Burman source is ruled out on the basis of dissimilarity of isotopic and petrographic data.

Our seismic data indicate that deformation of the CHT began at ~2 Ma with diachroneity across strike typical of a west-vergent accretionary prism. We consider that it is encroachment and final abutment of the Chittagong Hill Tracts onto the already-uplifted Shillong Plateau that caused diversion of the palaeo-Brahmaputra to the west of the plateau as the north-east route closed.

5.1 Introduction

Spanning 2400 km over six nations, the Himalaya are a type example for studying the processes involved in orogenesis, including the coupling and feedback between tectonics and erosion. Understanding the processes of erosion since collision of India and Eurasia at ca. 50 - 55 Ma (Garzanti *et al.,* 1987; Klootwijk *et al.,* 1992; Searle *et al.,* 1997) is vital for discriminating between different models of crustal deformation, which differ in the timing and extent of required or resultant erosion (Tapponier *et al.,* 1982; Dewey *et al.,* 1988; Grujic *et al.,* 1996, 2002; Chemenda *et al.,* 2000; Beaumont *et al,* 2001, 2004; Jamieson *et al.,* 2006). Studying the erosion record, and erosion pathways, is also important for evaluating the role of the uplifting Himalaya on global climate (Raymo and Ruddiman, 1992; Molnar *et al.,* 1993), seawater chemistry (Richter *et al.,* 1992) and palaeodrainage over time (e.g., Clark *et al.,* 2004). The major sediment repositories of the Himalaya where such an erosion record is preserved, include remnant ocean basins (Katawaz, Makran, Bengal Basins) and deep sea fans (Indus and Bengal), as well as basins on land of which the foreland basin (Pakistan to eastern India), and the Indus suture zone (Zanskar, South Tibet (e.g. Najman, 2006) and north Pakistan (Zeilinger *et al.,* 2007)) are the most significant. Often they provide the only remaining archive of mountain belt evolution, when the

record of early orogenesis in the hinterland itself is lost due to metamorphic overprinting and erosion.

The Bengal Basin is bound to the north by the Precambrian basement of the Shillong Plateau, to the east by the Burman Margin and to the west by the Indian shield, whilst the south of the basin (Faridpur and Hatia Troughs) is open and empties into the Bengal Fan via the 'Swatch of No Ground' (Figure 5.1).

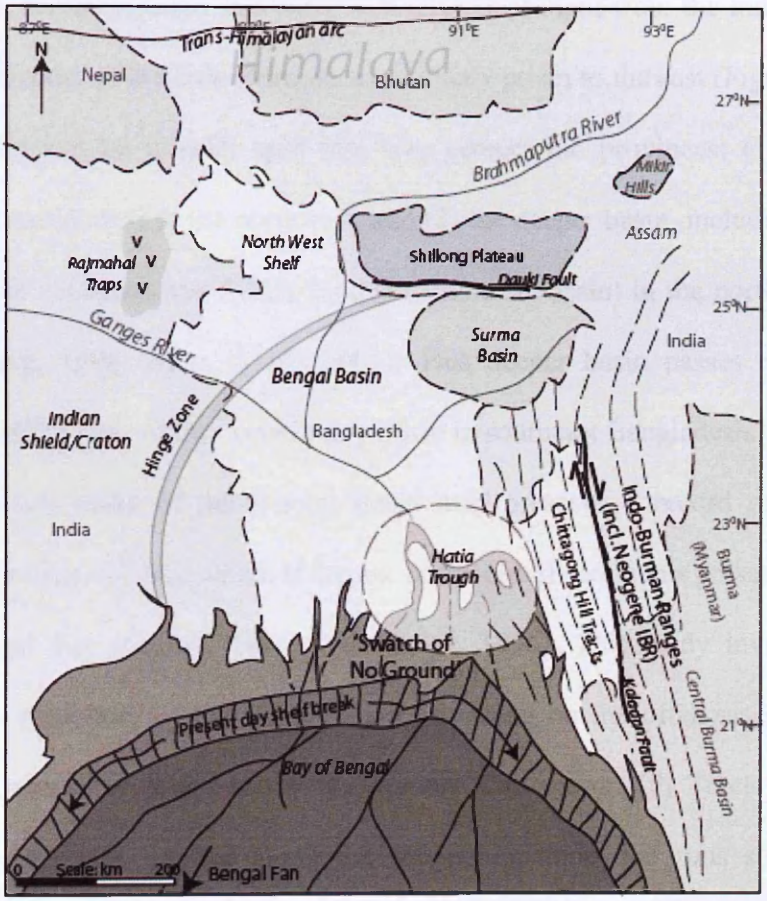

Figure 5.1 Regional map of the Bengal Basin showing sub-basins Surma Basin and Hatia Trough and the Chittagong Hill Tracts, which abut the Indo-Burman Ranges of western Myanmar and are separated by the dextral Kaladan fault. Location of the Himalaya, Indian Craton and Shillong Plateau are also shown. The hinge zone marks the change from the North West shelf of the Bengal Basin to the Bengal Basin Depocentre.

The sediment repository preserved in the Bengal Basin of Bangladesh is predominantly a delta complex comprised of the coalesced Ganges and Brahmaputra rivers, and with a present coverage of approximately 144,000 km^2 onshore and 63,000 km^2 offshore (Uddin and Lundberg, 1998). It preserves a Tertiary sequence of sediments with a thickness of up to ~16-22 km (Curray and Moore, 1971; Curray, 1983; Gani and Alam, 1999; Uddin and Lundberg, 2004) sourced principally from the Himalaya to the distal north and west, with additional input from the Indian shield to the west and rocks of the Indo-Burman accretionary prism to the east (Figure 5.1). The Bengal Basin can be broadly split into two geotectonic provinces; (1) the Indian platform or stable shelf in the northwest, and (2) the deeper basin, including the Hatia Trough in the southeast and Sylhet Trough (Surma subbasin) in the northeast (Uddin and Lundberg, 1998; Alam *et al.,* 2003). This deeper basin passes east into the Chittagong Hill Tracts of the accretionary prism in southeast Bangladesh.

Sedimentary rocks of the Bengal Basin may preserve a record of Himalayan erosion older than ~17 Ma, which is the age of the oldest sediments presently accessed in the Bengal Fan (Curray, 1994; Galy *et al.,* 1996). This study investigates the sedimentary repository of the Bengal Basin, focusing on the offshore eastern Hatia Trough and the more easily accessible onshore Chittagong Hill Tracts (SE Bengal Basin). The latter is situated along the subduction zone that runs south through western Myanmar and the Andaman Islands to Sumatra, where the Indian oceanic plate is being subducted beneath the Burma platelet (Gani and Alam, 1999). Whilst the Hatia Trough currently remains a site of sedimentation, the Chittagong Hill Tracts (also called the Chittagong-Tripura Fold Belt or Eastern Fold Belt), consist of sediments deposited in the Bengal Basin and subsequently incorporated into the accretionary prism as material progressively offscraped during subduction.

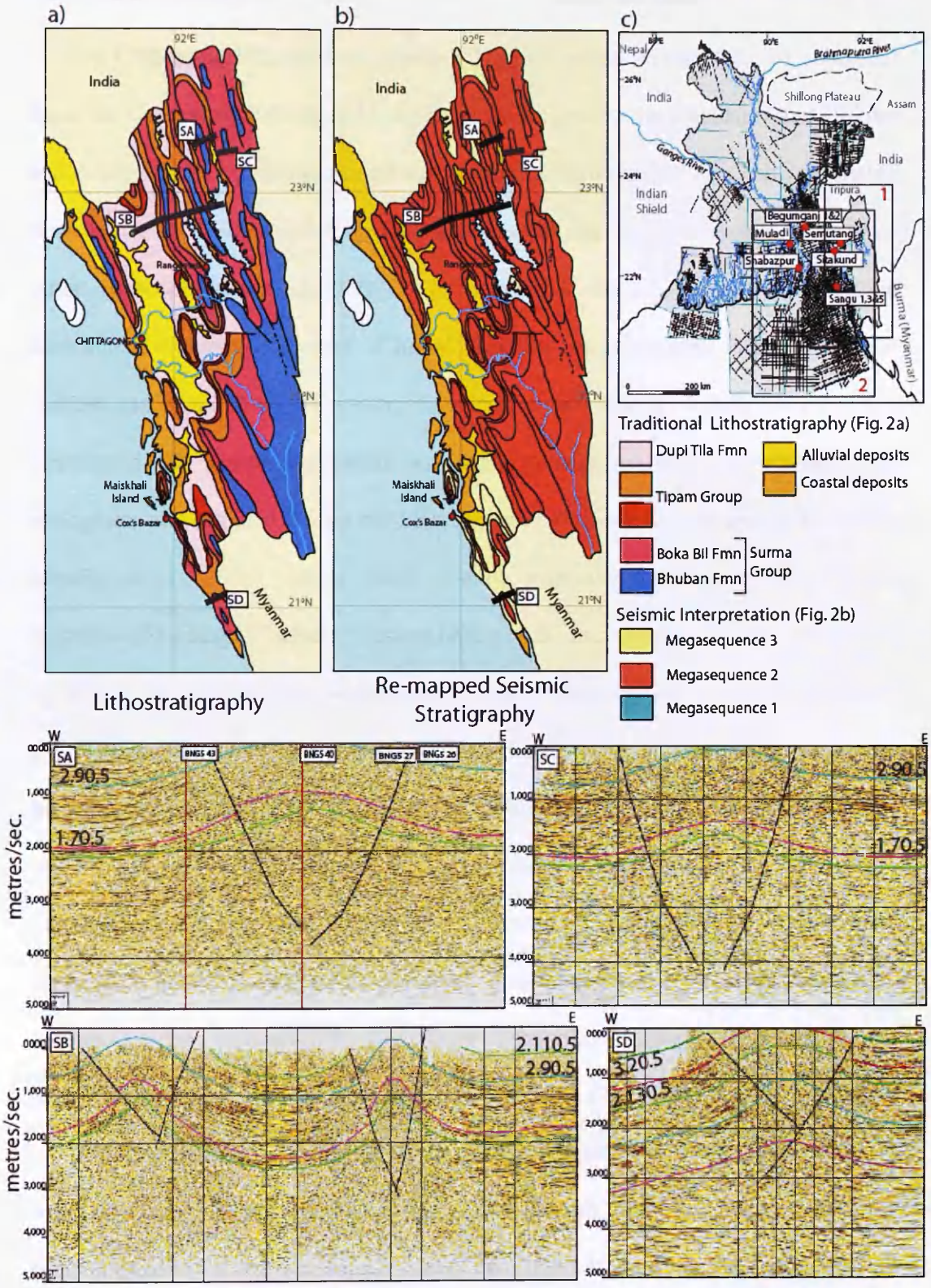

Figure 5.2a shows the published lithostratigraphy geology map of the Chittagong Hill Tracts (after data from Evans, 1932; Uddin and Lundberg, 1998). Figure 5.2b is the remapped seismic stratigraphy developed in this study using a Megasequence framework. The location of maps A and B are shown in inset 1 of 2c. Remapping of the region using seismic data has resulted in a younger geology at surface than previously thought, with widespread exposure of MS2. Examples of the seismic lines used to constrain the stratigraphic framework in this area are labelled SA-SD. Seismic line A shows down-lines which indicate the presence of a sample at surface. Figure 5.2c is a basemap of all seismic data available for the Bengal Basin, the boxed area (boxes 1 and 2) and represents seismic interpreted and mapped for this study. The well penetrations are also indicated.

The Chittagong Hill Tracts is a belt of Neogene strata (Figure 5.2a, b), separated from the Cretaceous-Palaeogene Indo-Burman Ranges by the Kaladan Fault (Sikder and Alam, 2003). Compressive east-west tectonics have resulted in a belt comprising en-echelon, north-south oriented, folded strata with mainly east-dipping, high-angle thrust packets (Gani *et al.,* 1999). The region may have developed on a folded detachment at depth as a result of initial buckling and subsequent fault propagation (Sikder and Alam, 2003) However, the initiation and timing of deformation of the Chittagong Hill Tracts is disputed, with some authors suggesting deformation was multiphase and initiated during the Miocene-early Pliocene (Sikder and Alam, 2003; Mandal *et al.,* 2006), whilst others dispute extensive diachroneity and suggest initiation of folding in the Late Pliocene (Allen *et al., this study*).

Whilst the Bengal Basin sediments provide a major repository within which the Himalayan erosion record is preserved, its potential use is currently limited by our inadequate knowledge of the stratigraphic evolution of the basin. Poor biostratigraphic control has resulted in usage of a stratigraphic framework based on tenuous lithostratigraphic correlation with rocks in Assam, as first described by Evans (1932), in spite of the time-transgressive nature of sedimentation in a prograding delta. Previous workers recognised the limitations of the lithostratigraphic approach (Salt *et al.,* 1986; Reimann, 1993; Uddin and Lundberg, 1999; Gani and Alam, 1999, Alam *et al.,* 2003), and whilst a sequence stratigraphic approach was suggested in order to overcome the problem (Gani and Alam, 2003), its use for long distance correlation was hampered by a lack of regional marker beds and adequate biostratigraphic control in the area under study.

Notwithstanding the inability to accurately date deposition or structural evolution of the area, provenance studies have been carried out on the basin sediments. Input

directions have been determined using lithofacies maps (Uddin and Lundberg, 1999), isopach maps constructed from well data (Uddin and Lundberg, 2004), and possible sources discussed on the basis of petrographic, heavy mineral and Ar-Ar dating of bulk micas (Uddin and Lundberg, 1998a,b; Rahman and Faupl, 2003). A dominant northern Himalayan versus mixed Himalayan and eastern Indo-Burman (Uddin and Lundberg, 1999, 2004; Gani and Alam 1999, 2003) source input to the sediments of the Chittagong Hill Tracts region through time is debated. A Shillong Plateau provenance is considered for the Pliocene sediments of the Bengal Basin (Johnson and Nur Alam, 1991). In addition, a subordinate contribution from a western cratonic source is also possible.

We bring to the study of this region a new and extensive seismic reflection database (Figure 5.2c) calibrated to well and biostratigraphic data, and various isotopic analyses on single grain and bulk rock samples (locations are shown on Figure 5.3). With this information we, in conjunction with previous work undertaken at Cairn Energy, have constructed the first basin-wide regionally applicable sequence stratigraphic framework and determined sediment input directions based on seismically defined clinoform data that is drill-well and biostratigraphically calibrated. We assign provenance based on a multi-technique approach, which mitigates ambiguities that arise when using only a single method. Our objective is to provide a robust stratigraphic framework and basin evolutionary history for the region in order that further work on the Himalayan erosion record preserved in this repository can be interpreted in its correct context.

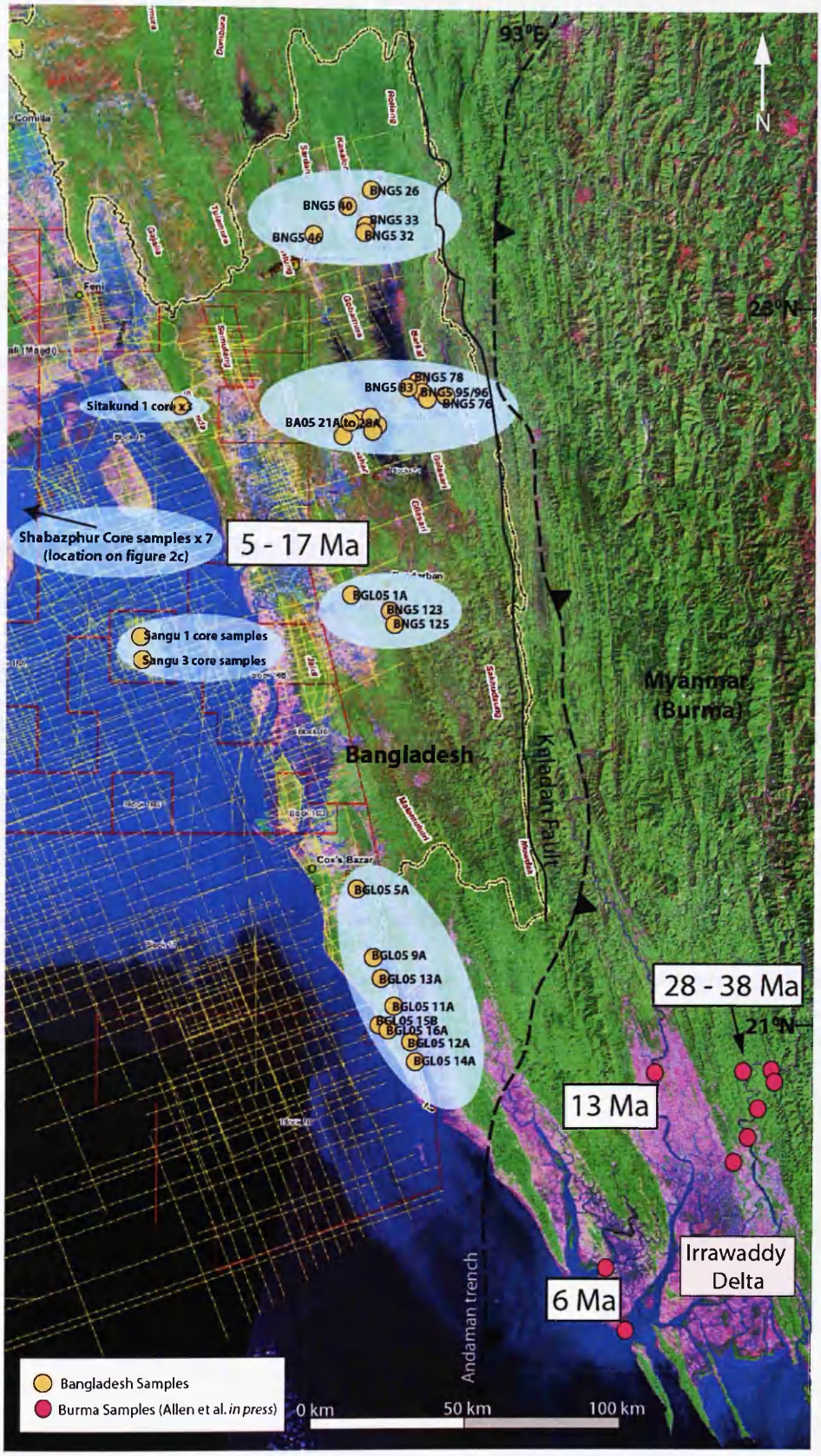

Figure 5.3 Satellite map of the Chittagong Hill Tracts showing location of all samples analysed from Bangladesh (Orange) and Burma (Pink) (Burmese samples from Allen et al. in press). Boxed ages show the youngest detrital zircon fission track ages from Neogene samples in the regions of eastern and western Indo-Burman Ranges/Chittagong Hill Tracts. Data show westward younging, consistent with deposition in a west vergent accretionary prism. Samples with a total of less than 10 grains analysed are excluded since the youngest age in these cases are highly unlikely to be representative.

5.2 Stratigraphy of the Tertiary rocks of Bangladesh

5.2.1 Traditional Lithostratigraphic framework versus Seismic Stratigraphy

The present lithostratigraphic nomenclature utilised for the stratigraphy of Bangladesh, and on which the published surface geology map is based (Khan and Muminullah, 1980. Figure 5.2a), is extrapolated by correlation with formations in Assam Basin in India (Evans, 1932) on the basis of loosely defined lithofacies descriptions of the rock types in both regions.

In the Hatia Trough and Chittagong Hill Tracts, the lithostratigraphy comprises the Oligocene Barail Formation, which is not exposed at surface and the overlying Neogene Formations comprised of the Surma Group (divided into the Bhuban and Boka Bil Formations) and overlain by the Tipam and Dupi Tila Formations (Uddin and Lundberg, 1998a, Gani and Alam, 1999). Elsewhere in the Bengal Basin the Oligocene Barail Formation overlies the Eocene Sylhet Limestone and Kopili Formation (Uddin and Lundberg, 1998a). However, it is unclear to what extent these formations are present in the Hatia Trough and Chittagong Hill Tracts. Figure 5.4 shows the lithostratigraphy for the Hatia Trough, Chittagong Hill Tracts and Surma Basin.

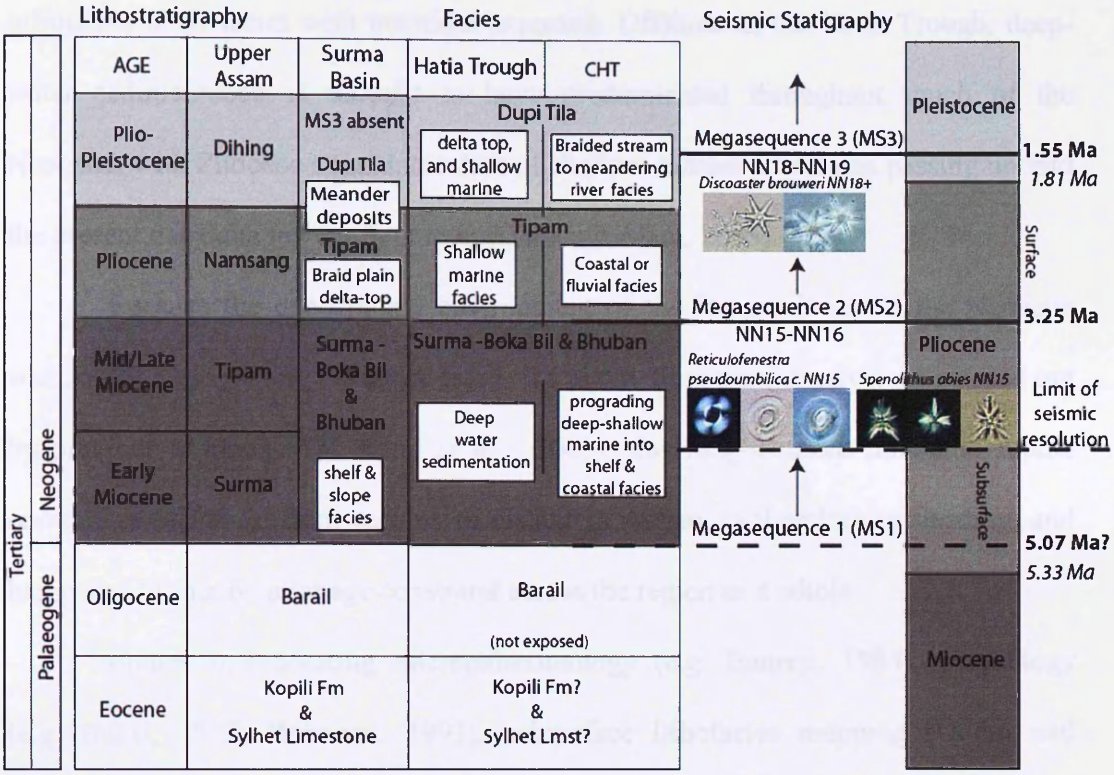

Figure 5.4 The traditional lithostratigraphy is presented with a description of the associated facies for the Surma Basin and the Chittagong Hill Tracts (CHT)/Hatia Trough (HT). Note that the Tipam Group in the Surma Basin is deposited in a fluvial delta-top environment, whilst the Tipam in the CHT/HT are tide-dominated facies. This discrepancy is a result of correlating the geology over a large area (Assam to Bengal) based on the age of the rocks, and assuming that the facies are the same at any given time. This is not the case in a highly time-transgressive delta environment. The new seismic Megasequence stratigraphy is shown. The Surma Group correlates to MS1, The Tipam and Lower Dupi Tila are time-equivalent to MS2 and the Upper Dupi Tila corresponds with MS3. Biostratigraphic constraint is indicated and shown in detail in figure 5.7

In the Chittagong Hill Tract region, Gani and Alam (1999) split the Neogene succession of the Chittagong Hill Tracts into three groups, which correlate to the lower Surma Group (prograding deep-shallow marine delta facies), the upper Surma Group (shelf-coastal facies) and the joint Tipam/Dupi Tila Formations, which shows first evidence of continental facies with the transition from braided fluvial facies to meandering facies in the delta with time. By contrast, Davies *et al.,* (2003) consider the upper part of the Surma Group and the Tipam Formation to represent tidally

influenced shelf facies with intertidal exposure. Offshore in the Hatia Trough, deep-water sedimentation is thought to have predominated throughout much of the Neogene, with Pliocene strata indicative of shallow-marine conditions passing up into the present day delta top configuration (Gani and Alam, 2003).

Because the depositional environment of the Bengal Basin in the Neogene was that of a prograding delta, the facies are highly time-transgressive. As pointed out by previous workers (e.g. Alam *et al.,,* 2003), this long-distance lithostratigraphic correlation of facies, from regions as distant as Assam, is therefore misleading, and hampered further by poor age constraint across the region as a whole.

Studies incorporating micropalaeontology (e.g. Banerji, 1984), palynology (e.g. Baksi, 1972; Reimann, 1993), subsurface lithofacies mapping (Uddin and Lundberg, 1999) and sequence/seismic stratigraphy (e.g. Salt *et al.,,* 1986; Lindsay *et al.,* 1991; Gani *et al.,* 2003, Alam *et al.,* 2003) have gone some way in refining the stratigraphy and describing depositional variations across the basin. Gani *et al.,* (2003) provide an in-depth sequence stratigraphic framework for two anticlines in the Chittagong fold belt. However, the framework was not regionally correlatable across the Bengal Basin due to the small study area and lack of regionally correlatable marker horizons; a problem that could be overcome with more surface and subsurface data. Furthermore, the authors acknowledged the lack of biostratigraphic constraint.

The basin-wide sequence stratigraphic approach employed by Cairn Energy Plc. has further eroded the limitations of the aforementioned methods by dividing the rocks of the upper Neogene into three geometric packages termed megasequences (MS1, 2 and 3), each with its own distinct seismic character and bounded by unconformities (Figure 5.5; Cairn Energy Internal Report 2000).

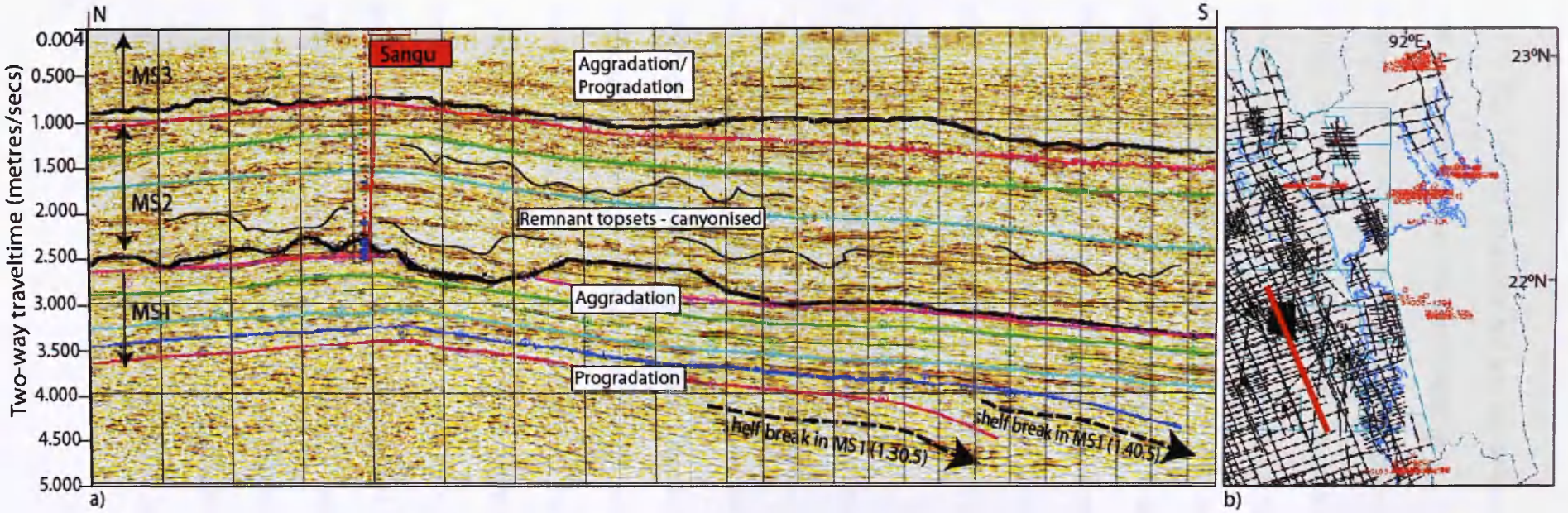

Figure 5.5 Figure 5a is a seismic line from the Hatia Trough region of the Bengal Basin (red line located in Figure 5b), which is a type example of the generic nature of all three Megasequences in the subsurface of the southern Bengal Basin. The drill well Sangu is shown for reference and the biostratigraphy from this well used, along with other drill welis, to constrain the Megasequence framework presented in Appendix 8. Figure 5a also shows clinoforms dropping basinward within MS1 which have been interpreted as the palaeoshelf break at MS1 1.30.5 (~ 5.26 Ma) and MS1 1.40.5 (~4.9 Ma).

The seismic character reflects the influence of delta morphology, shelf-edge position, sedimentation rates and relative sea level. Older Tertiary rocks are not included in the scheme due to a lack of seismic resolution with increasing depth. Within the Megasequences, topset and foreset horizons can be dated with biostratigraphic data from wells drilled in the Bengal Basin, and are considered as timelines. The sequence stratigraphic units are correlatable over thousands of kilometres. The framework has been applied to the Surma and Hatia Basins by Cairn Energy (Cairn Energy Internal Report 2000, reproduced for publication in the open literature for the first time in this paper), and for this study was also extended onshore into the Chittagong Hill Tracts of eastern Bangladesh (see Figure 5.4).

5.2.2 Seismic Stratigraphy: The Megasequences

MS1, 2 and 3 in the Hatia Trough are each defined by regional unconformities, which separate the upper Neogene sedimentary section of the Bengal Basin into major, discrete phases of basin evolution. *Megasequence 1* is the deepest and therefore oldest unit and is time equivalent to the lithostratigraphic Surma Group comprised of the Boka Bil and Bhuban Formations. In both the Surma Basin and Hatia Trough, the facies are marine and characterised by a forestepping, progradational sequence stack. Figure 5.5 illustrates the progradation of the shelf-slope break, resulting from increasing sediment supply or relative sea level fall. Across Bangladesh, the shelf succession is characterised by laterally continuous sub-parallel topset seismic reflectors, whilst the slope environment is defined by steeply dipping clinoforms. The top of MS1 is defined by the last major marine flooding event across NE Bangladesh, a sub-regional correlative event recorded in the Upper Marine Shale (Figure 5.7)

The boundary with *Megasequence 2* reflects a major change in conditions across the whole of Bangladesh. In the Surma Basin the seismic character of Megasequence 2 is that of a transparent, opaque, reflection–free package representing braided fluvial facies of the Tipam Formation, overlain by a more heterogeneous package reflecting a change to the more meandering facies of the Dupi Tila Formation. In the Surma Basin, the boundary therefore marks a major basinward shift in coastal facies. In the Hatia Trough Megasequence 2 is characterised by discontinuous geological outliers (sequence remnants) preserved between large, multiple, downcutting, submarine canyon erosion surfaces which incise into MS1 below with considerable relief. The canyon fill is seismically opaque, grading vertically into stronger sub-parallel reflectors, of the canyon spill-over facies which onlap and overstep the canyon margins. Canyonisation resulted from relative sea level fall. The repeated cut and fill indicates fluctuating relative sea levels during the megasequence, superimposed on an overall relative sea level rise which allowed fills to be preserved and topsets to be stacked.

Megasequence 3, present in the Hatia Trough but absent from the Surma Basin, is time equivalent to the upper part of Dupi Tila to Recent sediments, and is recognisable by a return to a package of laterally continuous seismic reflectors, and an absence of canyons, representing a delta top environment, where sedimentation and accommodation are generally in equilibrium. Figure 5.6 demonstrates the aggradational nature of the shelf slope break during this period, consistent with relative sea level rise.

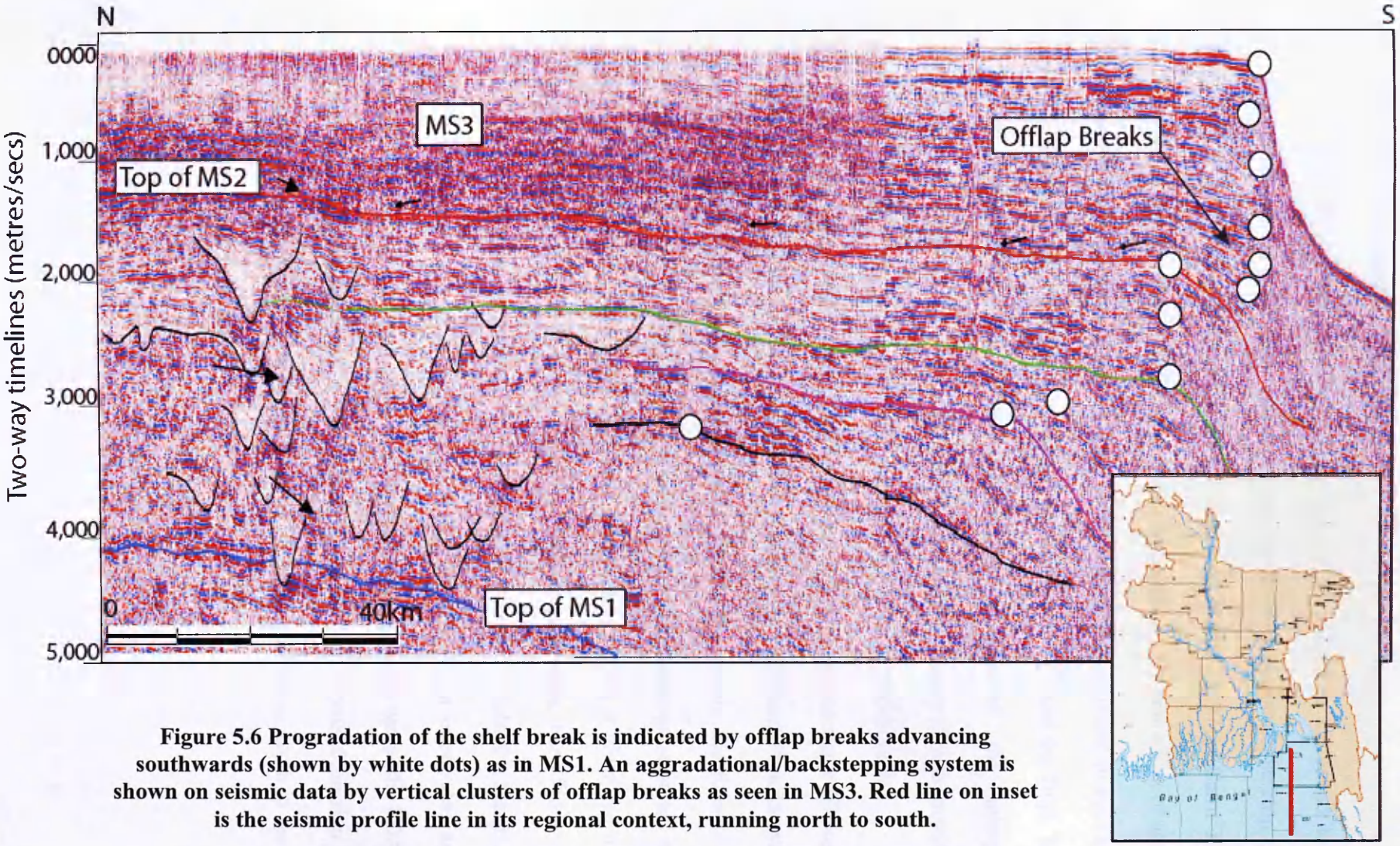

Figure 5.6 Progradation of the shelf break is indicated by offlap breaks advancing southwards (shown by white dots) as in MS1. An aggradational/backstepping system is shown on seismic data by vertical clusters of offlap breaks as seen in MS3. Red line on inset is the seismic profile line in its regional context, running north to south.

5.2.3 Biostratigraphic Calibration

The sequence stratigraphic Megasequence framework is calibrated to well penetrations across the Bengal Basin and age constrained by nannoplankton dating based on the Nannoplankton Zonation Scheme of Martini (1971) (Cairn Energy Internal Reports No. 26020, 27810 and 27903, Appendix 8). Despite a lack of age data on the region, the Surma Group has long been considered as Miocene in age (Evans, 1932; Reimann, 1993), the Tipam Formation as Pliocene age and the Dupi Tila as Plio-Pleistocene age. Nannofossil dating has constrained the interpreted Megasequence framework as Late Miocene to Pleistocene. An overview is provided in Figure 5.4 and 5.7 and detailed biostratigraphy is presented in Appendix 8.

Whilst the age of nannoplankton species with a long time range (*Discoaster quinqueramus*, *Discoaster asymmetricus*, *Helicosphaera sellii*, *and Pseudoemiliania lacunose ovata*) cannot be used to precisely date a succession, the time of their extinctions can still provide a tool for dating where a continuous sediment record exists. In Bangladesh, their First Downhole Appearances (FDA) is identified in well core and thus has been used to date the Megasequence succession. The FDA of forms used in the wells Begumganj 1 and 2, Sitakund 1, Shabazpur 1, Muladi 1, Sangu 1 to 5 and South Sangu 1 and 2 (Figure 5.2c and Appendix 8) are interpreted as true extinction events due to their stepped appearance throughout the wells (the FDA may sometimes be associated with a hiatus in the well and not a true extinction event which is indicated by the FDA for all forms recorded at the same depth in the well. This is not seen in these data).

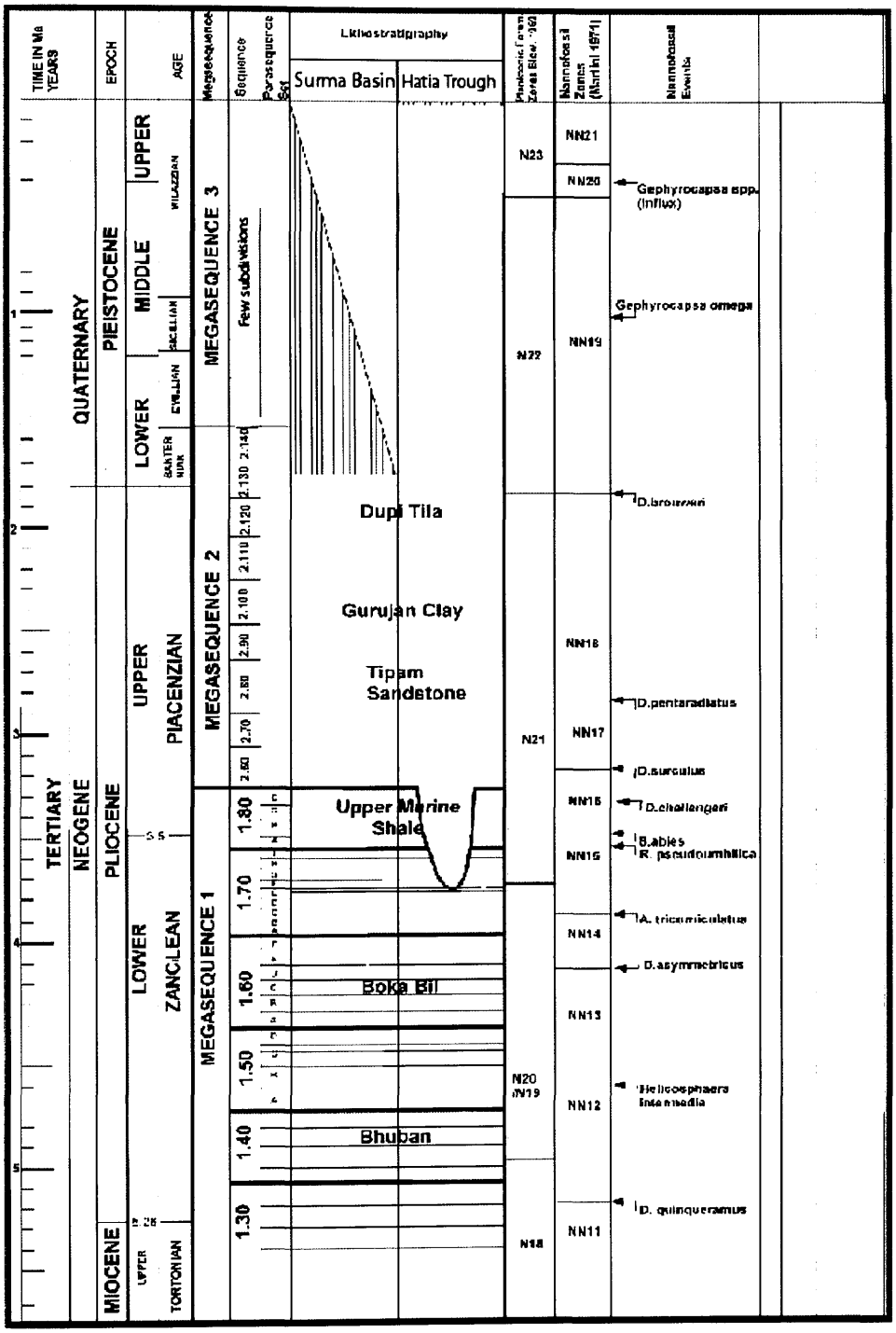

Figure 5.7 After Cairn Internal Report ED/BAN/GEN/GEO/04/05/1698 showing the Megasequence correlation with the old lithostratigraphy, and detailed biostratigraphy used to constrain the seismic stratigraphy, from which it is possible to date the two-way time horizons. Biostratigrapic correlation was achieved by nannofossil assemblage from a series of offshore and onshore drill wells (Appendix 8).

These data, combined with short range species (*Discoaster quinqueramus, Discoaster asymmetricus, Helicosphaera sellii*), have allowed the top of MS1, terminating at the Upper Marine Shale (NN15-NN16), to be dated at 3.25 Ma (Martini, 1971), with the boundary situated within Nannoplankton Zone NN16. Megasequence 2 extends through NN17-NN19, with the boundary between MS2 and MS3 in NN19 at ~1.55 Ma (Pleistocene). MS3 continues through the Pleistocene into present times (Figure 5.7). These data are in agreement with magnetostratigraphic data by Worm *et al.,* (1998) from the Surma Basin, where the Neogene succession is allocated younger ages than previously reported (Reimann, 1993).

5.2.4 Correlation of the offshore geology with the onshore Chittagong Hill Tracts, SE Bangladesh

Once the sequence stratigraphic framework was created for the offshore portion of the Bengal Basin and calibrated with biostratigraphic data from various well penetrations, the offshore geology was correlated with the onshore stratigraphy of the Chittagong Hill Tracts. This was achieved by mapping nine seismic timelines/horizons across the region from the southern Hatia Trough, eastwards in the Chittagong Hill Tracts and offshore towards the proximal parts of the Bengal Fan (Table 1). Five time horizons were interpreted and mapped from within MS1, three from MS2 and one from MS3 (one horizon from each megasequence was converted to two-way time structure maps in order to study changes in the palaeoshelf over time – see Section 5.4). Our correlation shows that the published geological map of the Chittagong Hill Tracts based on lithofacies correlation attributes an older age and rock unit to outcrop at surface. Figure 5.8 illustrates a location where the published geology map shows the Surma Group (MS1 time equivalent) outcropping at surface, whereas

the seismic mapping shows that the outcropping strata are in fact upper MS2 and MS3.

Horizon colour	Horizon name*	Mega sequence	Age (Ma)**
	Reg 3.20.5	3	~ 1.45 Ma
	Reg 2.130.5	2	~ 1.75 Ma
	Reg 2.110.5	2	~ 2.2 Ma
	Reg 2.90.5	2	~ 2.6 Ma
	Reg 1.70.5	1	~ 3.8 Ma
	Reg 1.60.5	1	~ 4.2 Ma
	Reg 1.50.5	1	~ 4.5 Ma
	Reg 1.40.5	1	~ 4.9 Ma
	Reg 1.30.5	1	~ 5.26 Ma

*The horizon name is made up of 3 parts. The first number denotes the Megasequence, whilst the second and third number set relates to further subdivision of the megasequence. MS1 runs from 1.30 - 1.80, MS2 runs from 2.60 to 2.140 and MS3 has one main marker at 3.20.5 with the rest of the megasequence left undivided.

** Ages are based on Biostratigraphy from Cairn Energy Internal Reports no. 27903, 26026 and 27810

Table 1. Key for seismic horizons mapped and their corresponding ages (Ma)

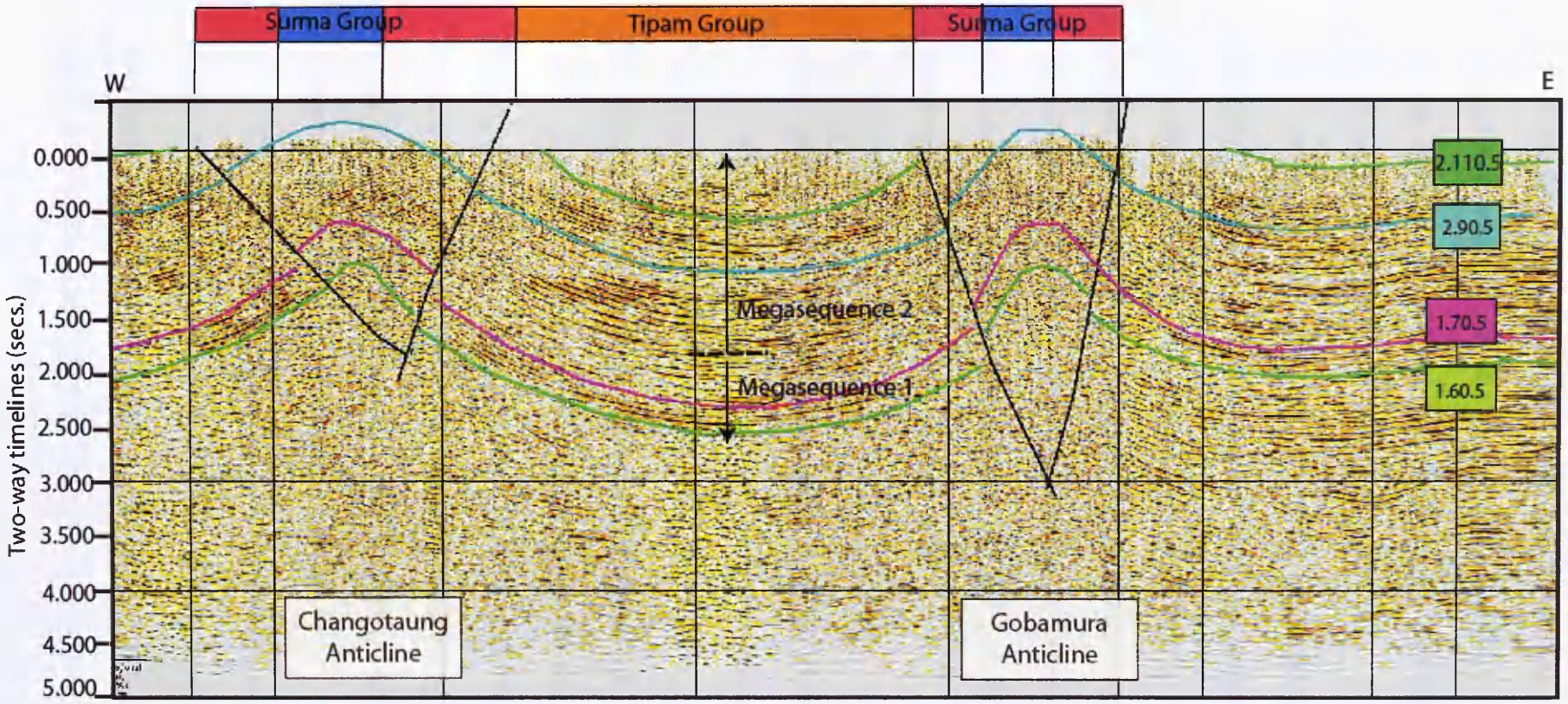

Figure 5.8 Shows a seismic line shot across two anticlines in the Chittagong Hill Tracts – Changotaung and Gobamura (shown on Figure 5.2 Line SB). Mapping and correlating the time horizons over the region reveals that the boundary between MS1 and MS2 lies within the subsurface, with MS2 sediments exposed at surface in the antiforms, and upper MS2/MS3 in the synforms. This is different to the published lithostratigraphy (shown in the bar along the top of the seismic line) that shows the Surma Group (MS1) exposed at surface in the crests of the anticlines (see also Fig 5.2a). This discrepancy is seen throughout the Chittagong Hill Tracts. Our new correlations allow us to remap the area using seismic data, as shown in Figure 5.2b.

We therefore used the seismic data to remap the area, as shown in Fig 5.2b. It is possible that Megasequence 1 may however crop out in areas further east in the Chittagong Hill Tracts or in the Indo-Burma Ranges where there is no coverage from our available seismic data.

Because of this discrepancy between the published map and our map, it was necessary to reclassify all surface samples taken for analysis into the megasequence stratigraphic framework. The samples, the anticlines or wells they have been taken from and their lithostratigraphic nomenclature, as well as their new Megasequence classification, are listed in Appendix 3.1 and shown on Figure 5.3. The samples used for analysis in this study will thus be referred to by their Megasequence terminology and not by their lithostratigraphic nomenclature.

5.3 Deformation of the Chittagong Hill Tracts - Hatia Trough

Hiller (1988) and Lohmann (1995) considered folding of the Chittagong Hill Tracts to have taken place in the Late Miocene-Pliocene. By using two-dimensional modelling over three anticlines in western Chittagong Hill Tracts, Sikder and Alam (2003) argue for multiphase fold development as the direct consequence of E-W compression, buckling and fault propagation on a decollement at depth. Three main phases are identified starting with a main deformation phase during deposition of the Tipam Formation, which is then followed by two further phases after deposition of the Tipam Formation and the Dupi Tila Group respectively.

We provide further constraint to the timing of deformation of the accretionary prism as deduced from evidence of strata thinning over anticlines and onlap of synformal sediments onto flanks of antiforms, which are biostratigraphically calibrated. We also expand the database further offshore into the Hatia Trough (Figure

5.9). In the east, thinning of MS3 strata over anticlines and onlap of MS3 sediments onto MS2 sediments, as shown over Feni anticline (Figure 5.9a) and Jaldi (Figure 5.9b) in the Chittagong Hill Tracts, suggests that deformation started during late MS2 (~ 2 Ma onwards), which is broadly consistent with Sikder and Alam (2003). Further west offshore, deformation appears to have started during initial deposition of MS3 sediments (~1.55 Ma). This is indicated by thinning of MS3 sediments over MS2 sediments. In the Sangu anticline the sediments do not onlap to the flanks of the anticline as seen in Jaldi, which implies that folding/deformation is either synchronous with or postdates initial deposition of MS3 sediments (Figure 5.9b). Therefore, in the Chittagong Hill Tracts of Bangladesh, deformation began very recently from ca. 2 Ma, and is of limited east-west diachroneity.

Dating deformation still further east in the Chittagong Hill Tracts is hampered (1) by erosion on the anticline crest that has removed the record of thinning and onlapping sediments and (2) by the quality of seismic data which precludes the identification of any onlap surfaces within MS2 that would provide concrete evidence of any early exhumation and deformation.

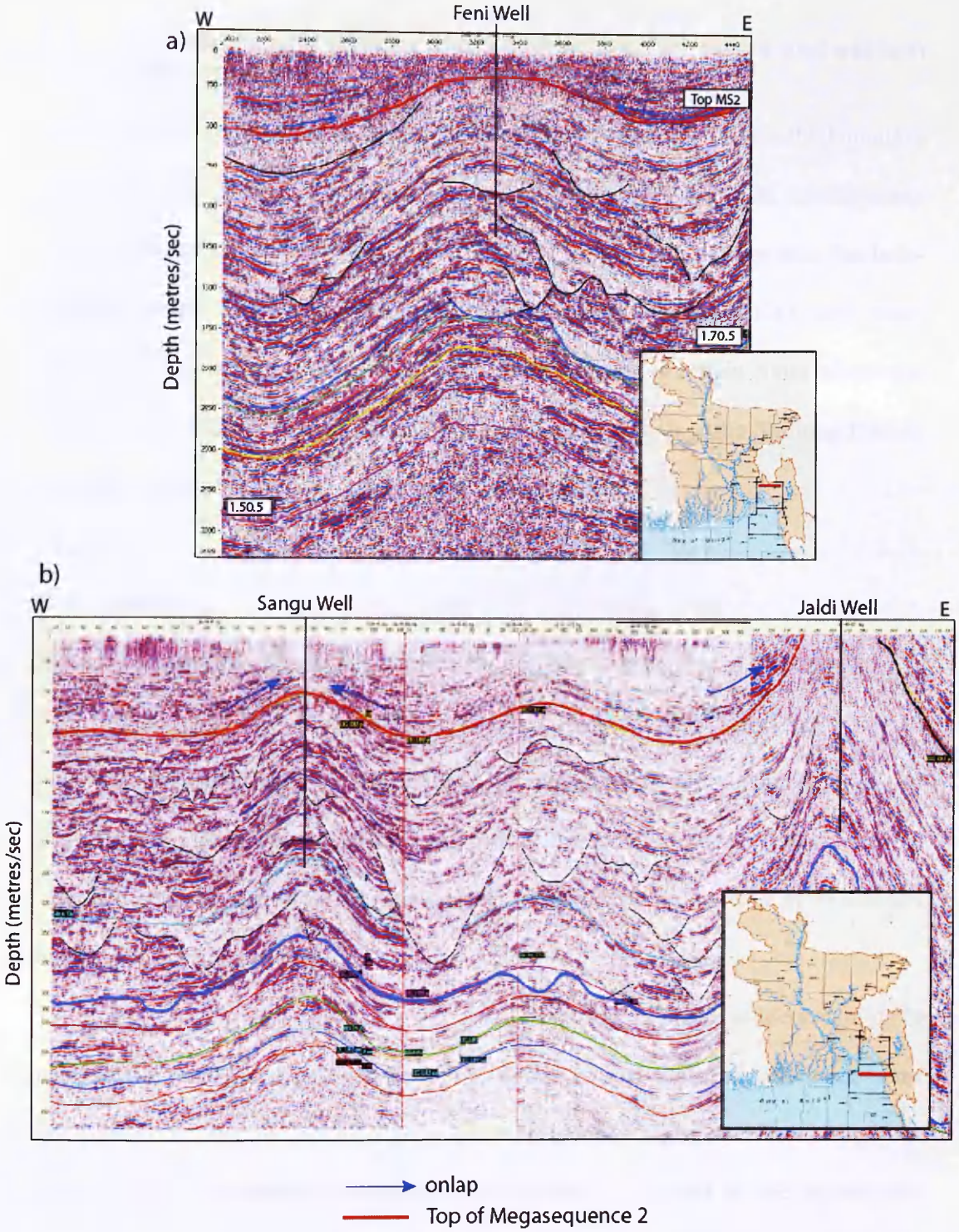

Figure 5.9 Shows two seismic lines from a) Feni (onshore) and b) Sangu to Jaldi. (offshore-onshore) from the Chittagong Hill Tracts. Marked thinning of MS3 strata over the anticlines and onlap (as indicated by the blue arrows) of MS3 sediments onto MS2 over onshore Feni anticline and Jaldi, suggests that deformation started during late MS2 (~ 2 Ma onwards). Further west offshore deformation appears to have started in earliest MS3 (~1.55 Ma) as indicated by sediments of MS3 thinning but not onlapping MS2 as seen in Sangu (offshore) as incipient deformation occurs.

5.4 Provenance of the rocks of the Chittagong Hill Tracts and eastern Hatia Trough

Whilst the principal input to the Bengal Basin overall is clearly the Himalaya during Neogene time (e.g., Uddin and Lundberg, 1999; Davies *et al.,* 2003), some previous workers have considered input to the eastern part of the basin from the Indo-Burman Ranges to be significant (Uddin and Lundberg, 1999; 2004), with some researchers considering that such an input was dominant at certain times (Gani and Alam 2003). Additional input from the Indian craton, including the Shillong Plateau (Johnson and Nur Alam, 1991) also needs to be considered.

5.4.1 Data

Seismic Palaeoshelf Mapping; determination of sediment input directions

Uddin and Lundberg (1999, 2004) used isopach and lithofacies maps to determine two sediment input directions to the Bengal Basin: a dominant source from the northeast and a second subordinate source from the northwest. Our approach, integrating the interpretation and mapping of 2D seismic lines, allows a more detailed analysis of this subject.

Palaeoshelf mapping and clinoform orientation provides evidence of delta progradation and clastic input direction through time. Seismic reflectors were interpreted and mapped across a geographical region on a grid of 2D seismic lines (Figure 5.2c). The reflectors mapped regionally are interpreted as the topsets and foresets of a prograding shelf delta. Consequently, these two-way time surfaces each represent a specific time horizon and have been dated using biostratigraphy (Figure 5.7). Mapping clinoforms across the region defines the position of the shelf slope break and its progradation with time.

From a total of nine horizons used to correlate offshore stratigraphy with the onshore (Section 2 and Table 1), three were chosen as representative of the position of the palaeoshelf during deposition of MS1, MS2 and MS3 at approximately 3.8 Ma, 2.6 Ma and 1.45 Ma respectively. Figure 5.10a, b, c is a sequence of two-way time structure maps generated for these time intervals that show the overall southward migration of the shelf-slope break from MS1 to MS3 reflecting delta progradation and subtle changes in sediment input direction across the Bengal Basin since Miocene times. From MS1 ~3.8 Ma (line 1.70.5) to MS3 ~1.45 Ma (3.20.5) there is a southward migration of the shelf-slope break reflecting delta progradation as sediment is continually supplied to the Bengal Fan, via the Bengal Basin (Figure 5.10a,b,c). During MS1 there is a rapid progradation of the shelf break. During MS2 the relative sea level fluctuates and allows for the development of canyons during relative sea level fall, which then become filled during relative sea level rise, causing the delta to both prograde and aggrade during MS2. The shelf slope then becomes aggradational during MS3 as shown by static offlap breaks (Figure 5.6).

Our palaeoshelf mapping commenced with a seismic horizon in late MS1 time. Seismic data quality was insufficient to map the palaeoshelf break before this time. During this time period (MS1, line 1.70.5 ~3.8 Ma) the palaeoshelf orientation was WNW-ESE, indicative of an input direction from the NNE (Figure 5.10a). During the deposition of the lower part of MS1 on the Northwest shelf (Figure 5.5 and 5.10d) a northwest input direction is also observed from clinoform data suggesting separate build outs of two rivers in that region. However, by upper MS1 (i.e. by ~3.8 Ma; line 1.70.5 as seen on Figure 5.10a) palaeoshelf mapping records the area below the confluence of the two inputs. During MS2 times (~2.6 Ma, line 2.90.5 – Figure 5.10b - map) the orientation of the palaeoshelf was still WNW-ESE.

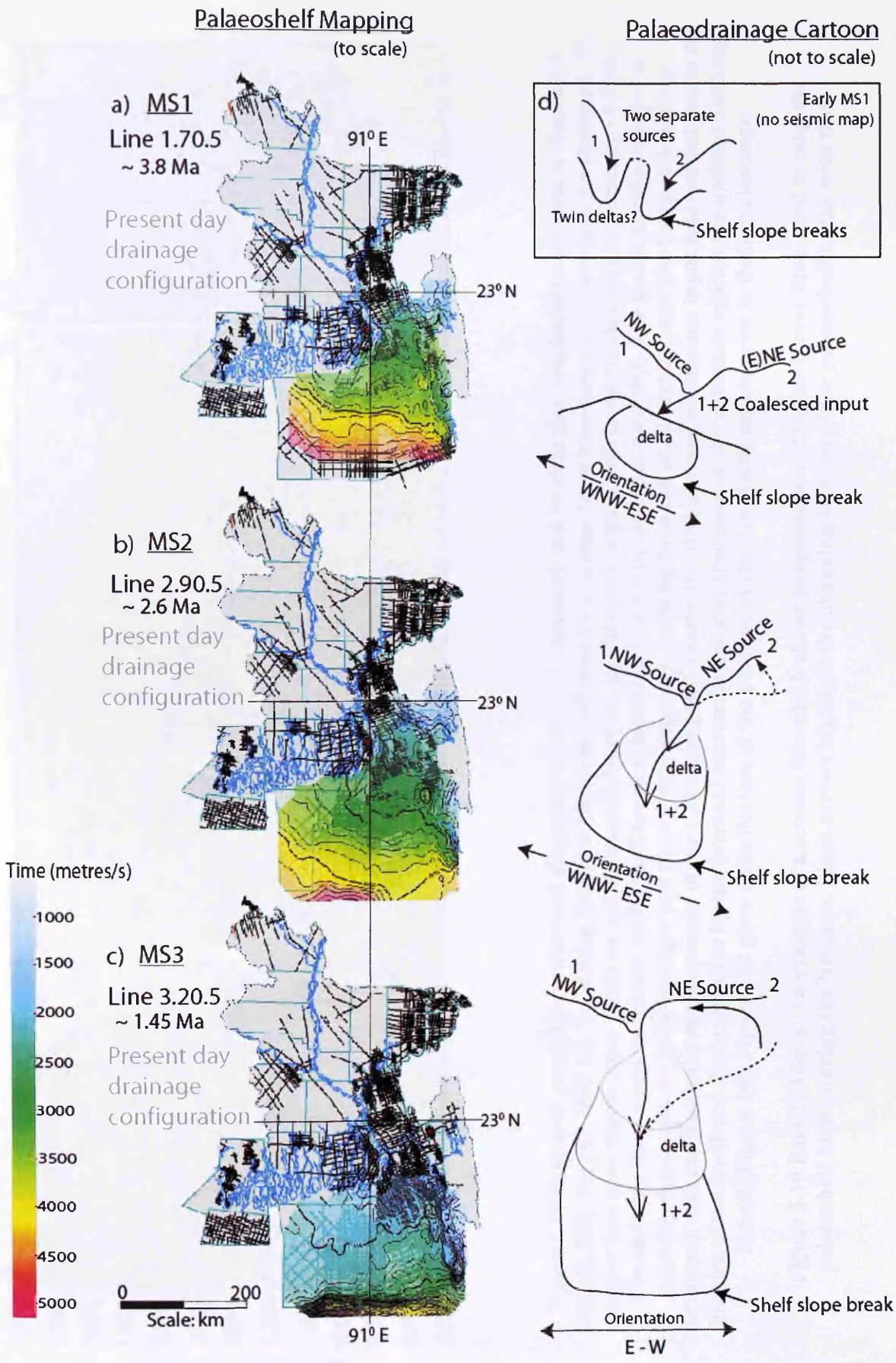
Palaeoshelf Mapping
(to scale)
Palaeodrainage Cartoon
(not to scale)
a) MS1
Line 1.70.5
~ 3.8 Ma
Present day drainage configuration
91° E
23° N
d)
Early MS1
(no seismic map)
Two separate sources
1
2
Twin deltas?
Shelf slope breaks
NW Source
1
(E)NE Source
2
1+2 Coalesced input
delta
Orientation
WNW-ESE
Shelf slope break
b) MS2
Line 2.90.5
~ 2.6 Ma
Present day drainage configuration
23° N
1 NW Source
NE Source
2
delta
1+2
Orientation
WNW- ESE
Shelf slope break
Time (metres/s)
1000
1500
2000
2500
3000
3500
4000
4500
5000
c) MS3
Line 3.20.5
~ 1.45 Ma
Present day drainage configuration
23° N
0
200
Scale: km
91° E
1
NW Source
NE Source
2
delta
1+2
Shelf slope break
Orientation
E - W

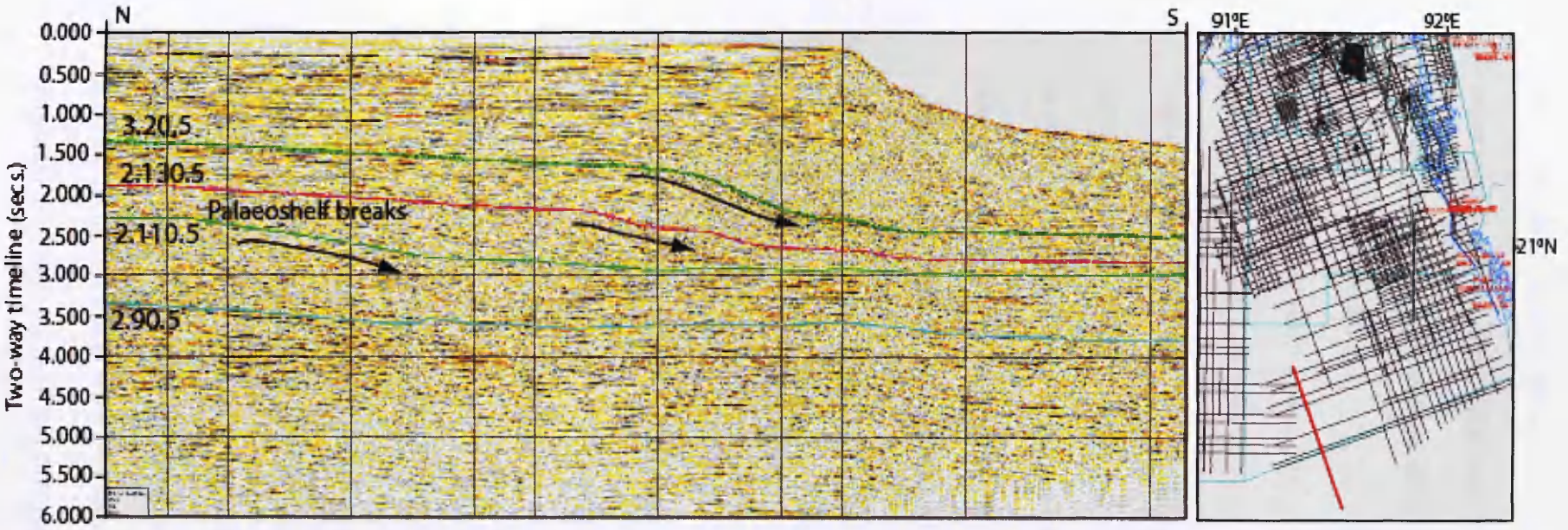

Figure 5.10 (previous page) The southward progradation of the palaeoshelf and its changing orientation over time is shown for MS1(a), MS2 (b) and MS3 (c). Increasing thickness/depth is indicated by a change from blue-green to yellow-pink on the maps. We suggest that a northeast input direction is dominant throughout the Neogene, with a shift to northern input direction by ~1.5 Ma. The cartoons show a representation of the shelf break orientation relative to the input direction. The clastic northeast input is considered to be the coalesced Ganges and palaeo-Brahmaputra draining from the northeast through the basin and shifting northward with the westward encroachment of the Chittagong Hill Tracts. By MS3 a strong northward input is identified due to the closure of the northeast drainage route by the eventual encroachment and abutment of the anticlines against the uplifted Shillong Massif (Figure 16). Figure 10d gives an indication of the position of the two clastic inputs prior to their coalescence.

Figure 5.10 Part 2 (Above) An example of a seismic line which shows progradation of the shelf over time, used to map the palaeoshelf break during the Neogene. Black arrows highlight the changing location of the palaeoshelf break with time.

However, by MS3 times (~1.45 Ma; line 3.20.5 Figure 5.10c) the palaeoshelf orientation lies E-W. More time lines would need to be mapped in order to assess whether the shifting orientation of the palaeoshelf is progressive over time or whether the change occurred abruptly.

Provenance can be investigated further using the isotopic and single grain thermochronological data from samples taken from the Chittagong Hill Tracts and Hatia Trough. These data are compared with data from Himalayan bedrock and detritus of known Himalayan derivation in order to assess a potential northern source, as well as with data from the Indo-Burman ranges and the Indian craton, which have also been proposed as sources for the Chittagong Hill Tracts and Hatia Trough (Johnson and Nur Alam, 1991; Uddin and Lundberg, 1998, 1999).

Isotopic data from the Neogene Chittagong Hill Tracts and Hatia Trough, SE Bangladesh

The data presented are from Neogene rocks of the onshore Chittagong Hill Tracts (surface samples, and drill core) and offshore drill cores in the Hatia Trough (Figure 5.2c). A total of 50 samples were used (Figure 5.3) and where possible these were tied with seismic lines in order to fit them within the seismic stratigraphic/Megasequence framework (Appendix 1): The GPS co-ordinates for all samples were loaded into Geoframe 4.3 (IESX module) to tie in with seismic lines on an HPxw8200 workstation. Seismic mapping of the palaeoshelf break across the Bengal Basin and offshore into the Bengal Fan gave an initial understanding of sediment distribution and source direction across the region. A variety of isotopic techniques were then applied in order to establish provenance of the Neogene rocks of the Chittagong Hill Tracts and their offshore equivalents in the Hatia Trough. Data are presented for heavy mineral and petrographic analysis, ^{40}Ar-^{39}Ar on detrital white

mica, detrital zircon fission track and zircon U-Pb dating and Sm-Nd isotope fingerprinting on mudstones and siltstones. XRD analysis was also used to assess the likelihood that mineral ages could reflect the time of post-depositional resetting rather than the time of cooling through closure temperature in the source region. The data are summarised in Table 2.

Age	Rock description, heavy mineral and petrography	Sm-Nd isotope fingerprinting on mudstones and siltstones	^{40}Ar-^{39}Ar on detrital white mica	Fission Track on detrital zircon	U-Pb on detrital zircons
Surface samples – Neogene	Medium to coarse grained micaceous sandstones, interbedded with rare mudstones and siltstones. Plots within Recycled Orogen of the QFL plot (Dickinson, 1985). Low-medium grade metamorphic mineral assemblage with abundant garnet and staurolite	Epsilon Nd values of -11.1 to –12.9	10 Samples – 79-100% of grains < 55 Ma, with the majority of those ages Neogene with subordinate Palaeogene ages. Rare older grains present of Cretaceous, and Palaeozoic-Proterozoic age. Typically make up <21% of the total sample.	17 samples –main populations are 17-40 Ma with rare grains at ~65Ma, 100-150 Ma and 200 and 550 Ma.	Dominant age populations of 500-2800 Ma makes up 50-66% of the total sample, with subordinate age populations making up the remainder. Populations at <55 Ma (~0-18% of total grains), 60-120 Ma (~8-13%) and 150-500 Ma (~18-21%)
Drill core samples – onshore CHT and offshore (Hatia Trough)	Fine grained grey sandstone with siltstone, plots within Recycled Orogen of QFL plot and an abundance of low-medium grade metamorphic minerals such as garnet and staurolite	Epsilon Nd values for MS1 –13.6 to –15.2, MS2 –12.6 to –13.1 and MS3 –13.4	100% of grains less than 29 Ma. Youngest age present 1 Ma.	majority of ages are <55 Ma with rare Mesozoic grains. 1 sample has no Tertiary ages with populations at 131, 288 and 526 Ma.	No data

Table 2. Provenance data for Neogene samples of the Chittagong Hill Tracts (surface and drill core) and offshore Hatia trough

X-Ray Diffraction:

An X-ray diffraction (XRD) illite crystallinity study was performed on 48 samples from 6 drill core/cut locations, which cover the full stratigraphy from MS1 to MS3 in the Chittagong Hill Tracts offshore (Hatia Trough), to determine whether the post-burial temperatures exceeded detrital mineral closure temperatures. Mudstone is ideal

for this analysis due to its clay content and the consequent abundance of illite relative to detrital mica (that interferes with measured illite peaks). However, mudstones in these samples are rare and as such siltstones have been used. Procedural details and the data table are presented in Appendix 2. A summary of the results follows.

Hb_{rel} values of ~147-278 (accounting for a precision of ± 20%) for all samples from MS1 – MS3 indicate the burial temperatures corresponding to the anchizone and epizone facies metamorphic grade (Blenkinsop, 1988). However, XRD analysis of the clay–sized fraction from these siltstones identifies mixtures of kaolinite, illite and mixed layer chlorite/smectite and illite/smectite in all boreholes which are diagnostic of the diagenetic zone of burial and temperatures up to 200°C. This discrepancy resulted from contamination of the clay mineral fraction by detrital micas, which are abundant in the siltstone samples. The separation procedure had not sufficiently separated the clay fraction from the mica, and as such the mica appears to be swamping the clay illite peaks at the 10Å position giving Hb_{rel} values, which are a mixture of minor illite and major detrital mica. However, one mudstone sample from Shabazphur (3290m) gave a diagnostic Hb_{rel} value of 303 and as such it is possible to suggest that based on XRD analyses of clay mineralogy the samples have not been reheated above 200°C (diagenetic zone of burial). Therefore, the zircon fission track ages and ^{40}Ar-^{39}Ar ages used in this study are interpreted to reflect the timing of cooling in the source region and do not show post-burial resetting.

Heavy mineral and petrographic study:

A heavy mineral and petrographic study was conducted on a total of nine drill core samples (seven offshore, two onshore) and 13 surface samples. This was augmented by analyses on two wells (Sangu and Sonadia) already documented in

Cairn Internal Reports (HMA/99/01 and J978/052). The full methodology is presented along with the data in Appendix 3, which is summarized below. Petrographic point-count data is shown in Figure 5.11.

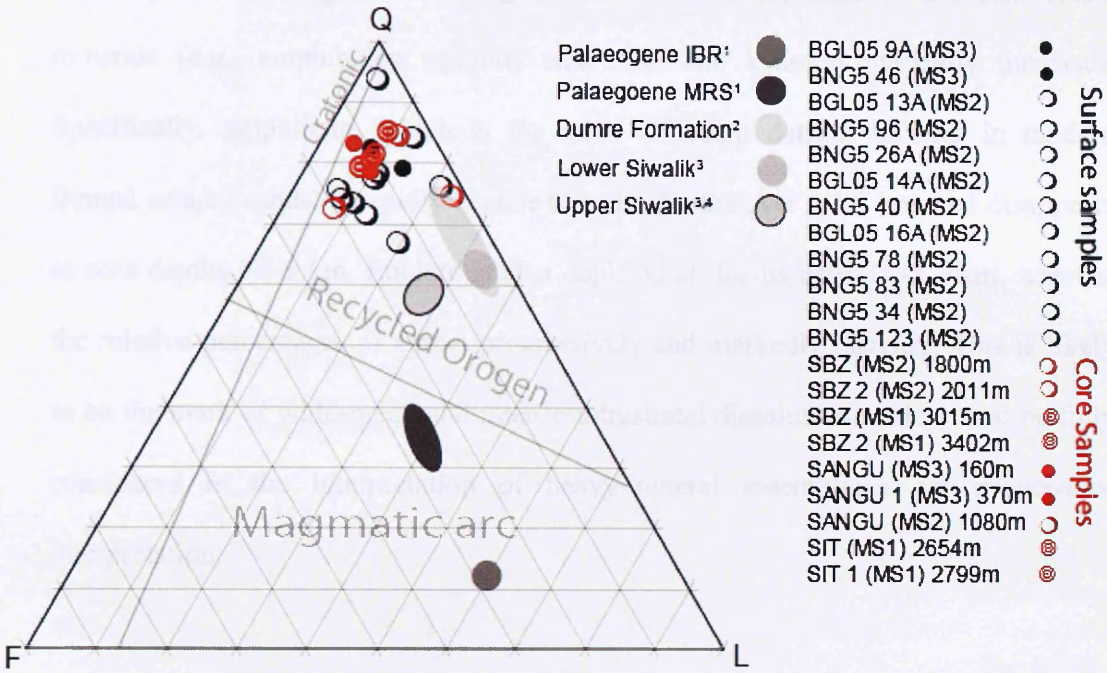

Figure 5.11 QFL plot for core and surface samples from the Hatia Trough and Chittagong Hill Tracts, respectively. Q= quartz, L= lithics and F=feldspars. All samples plot within the Recycled Orogen field. Also shown are coeval data from the Himalayan foreland basin including the Dumre Formation and Siwaliks, and data from the Palaeogene Indo-Burman Ranges and Palaeogene modern river sands draining the Indo-Burman Ranges. [1]Allen *et al.* In Press, [2]Najman *et al.* 2005, [3]DeCelles *et al.* 1998a, [4]Szulc *et al.* 2006

All core and surface samples plot within the Recycled Orogen field of the standard QFL plot of Dickinson (1985) except for one sample that lies on the boundary with continental interior derivation. The core and surface samples are characterized by significant potassium feldspar, which increases up-section, and a high proportion of low-medium grade metamorphic minerals, such as garnet, which is present in all samples and particularly prevalent in core samples of MS1 age (Mio-Pliocene). The higher-grade metamorphic minerals staurolite and kyanite become

more common in upper MS2 and MS3 samples (four surface samples and core samples) higher in the section (Cairn Energy Internal Reports HMA/99/01; J978/052). In core samples, heavy mineral abundance and variety was found to decrease notably with depth, while degree of etching and alteration of the unstable and semi-stable minerals (e.g., amphiboles, epidote, staurolite, and kyanite) markedly increases. Specifically, amphibole, which is the most abundant detrital mineral in modern Bengal estuary sands, is rapidly depleted at core depths over 1-1.5 km, and disappears at core depths >2-3 km. Epidote is also depleted at depths below 2-2.2 km, whereas the relative percentages of garnet progressively and markedly increase. This is likely to be the mark of widespread and intense intrastratal dissolution, which must be fully considered in the interpretation of heavy-mineral assemblages for provenance interpretation.

Bulk rock Sm-Nd study

10 drill core siltstones (eight offshore, two onshore) representing MS1, MS2 and MS3, and six modern river muds from rivers draining Neogene rocks of MS2 and MS3 were analysed for whole rock Sm-Nd isotope compositions using Thermal Ionisation Mass Spectrometry at Cambridge University. Isotope ratios were analysed on a T40 Sector 54 VG mass spectrometer using a triple filament assembly. The modern river samples were used to characterize the isotopic signature of the Hatia Trough and Chittagong Hill Tracts. These data were augmented by data from the Sangu well documented in Cairn Internal Report J978/052. The full method and data tables are presented in Appendix 4, and results summarised below.

Surface samples from formations of MS2 and MS3 all show consistent ε_{Nd} values of between –11 to –12.9. Six drill core/cut samples of equivalent

megasequence in the Hatia Trough show values ranging from –12.6 to –13.4. In four samples from MS1 (Surma Group) values are slightly higher and range from –13.6 to –15.2 (Figure 5.12).

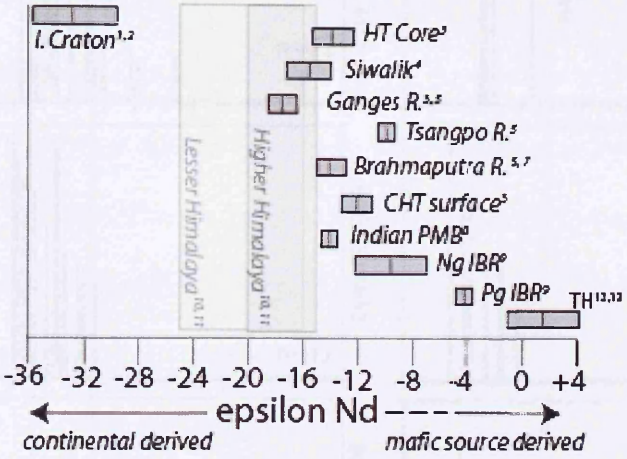

Figure 5.12 Bulk rock Epsilon Nd values are indicated for Neogene samples of the onshore and offshore CHT, and compared with published data from the possible source regions. [1]Peucat *et al.* 1989, [2]Saha *et al.* 2004, [3]This Study, [4]Szulc *et al.* 2006, [5]Singh and France-Lanord 2002, [7]Colin *et al.* 1999, [8]Najman *et al.* In press, [9]Allen *et al.* 2007, [10]DeCelles *et al.* 1998a,b, [11]Robinson *et al.* 2001, [12]Allegre and Benothman (1980), [13]Clift *et al.* (2002) I. Craton= Indian Craton, Indian PMB= Indian Proterozoic Mobile Belt, Ng IBR= Neogene Indo-Burman Ranges, Pg IBR= Palaeogene Indo-Burman Ranges, TH=Transhimalaya

^{40}Ar-^{39}Ar dating of detrital white micas

Detrital white mica from 10 Neogene surface bedrock sandstones sampled from the Chittagong Hill Tracts and three drill core sandstone samples from the Hatia Trough, representing MS1, 2 and 3 respectively, were used for ^{40}Ar-^{39}Ar dating. Most data were collected on a GVi Instruments Argus multi-collector mass spectrometer (SUERC, Glasgow) using a variable sensitivity faraday collector array in static (non-peak hopping) mode. However, additional samples were run on a Balzers 217 SEM detector. The full laser fusion method and data tables are presented in Appendix 5 and results summarised briefly below (Figure 5. 13)

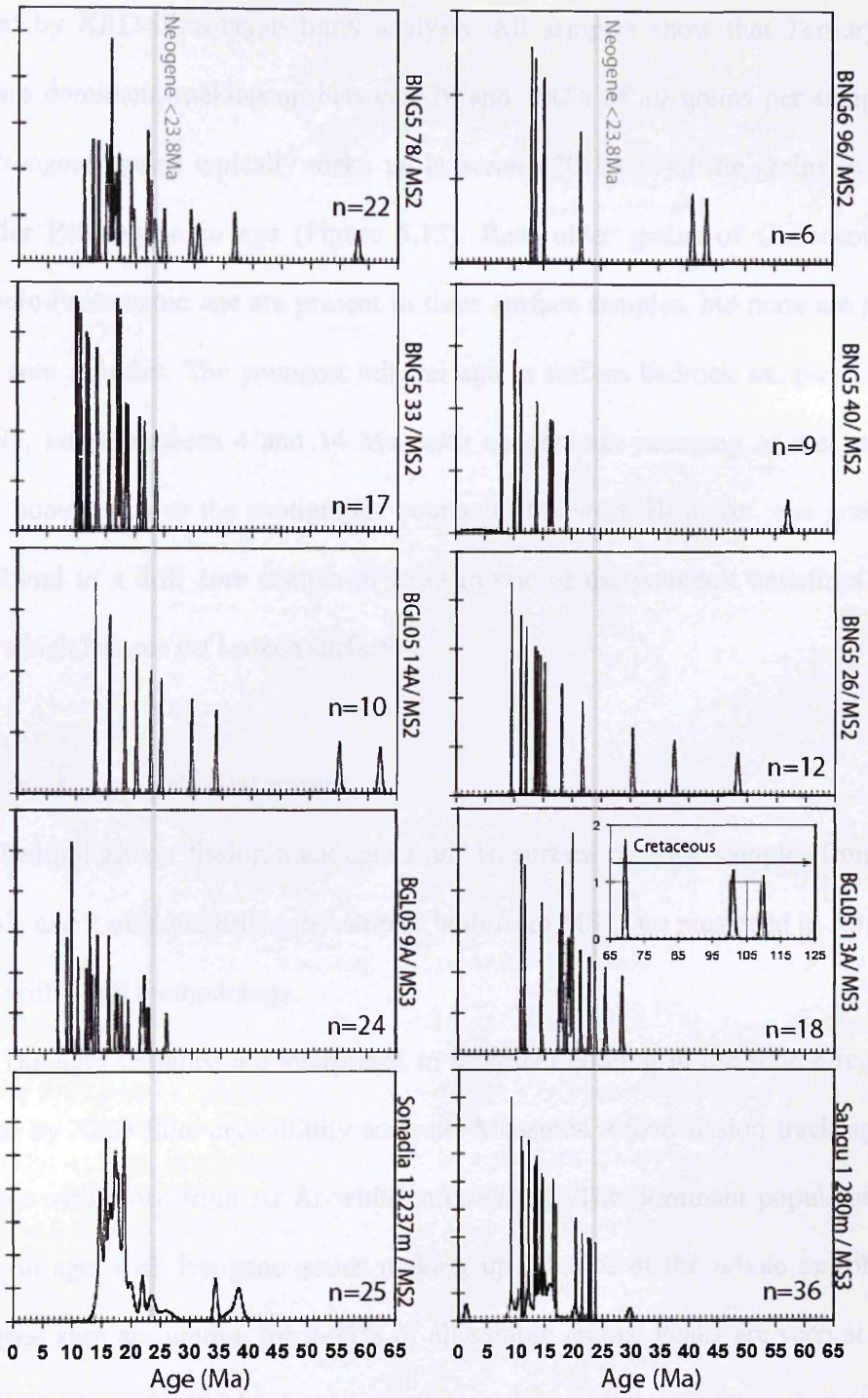

Figure 5.13 Probability density plot for ^{40}Ar-^{39}Ar detrital white mica data. The ages are reported with uncertainties at 1-sigma level. Two offshore core samples and eight surface samples show a dominance of Neogene aged grains. Palaeogene grains are present but limited as well as rare Cretaceous aged grains.

The ages obtained are interpreted to represent cooling in the source region as indicated by XRD illite crystallinity analysis. All samples show that Tertiary aged grains are dominant, making up between 79 and 100% of all grains per sample. Of these, Neogene grains typically make up between ~70-100% of the grains, with the remainder Palaeogene in age (Figure 5.13). Rare older grains of Cretaceous and Palaeozoic-Proterozoic age are present in three surface samples, but none are present in drill core samples. The youngest mineral age in surface bedrock samples of MS2 and MS3, range between 4 and 14 Ma, with no obvious younging of the youngest mineral populations as the stratigraphy youngs to the west. However, one grain of 1 Ma is found in a drill core sample of MS3 in one of the youngest anticlines in the region, which has not yet broken surface.

Fission track ages of detrital zircons

Detrital zircon fission track data from 16 surface bedrock samples from MS2 and MS3, and 2 offshore drill core samples both from MS1, are presented in Appendix 6 along with a full methodology.

The ages obtained are interpreted to represent cooling in the source region as indicated by XRD Illite crystallinity analysis. Measured zircon fission track ages are consistent with those from Ar-Ar white mica dating. The dominant populations are Tertiary in age, with Neogene grains making up 30-96% of the whole sample, and Palaeogene ages accounting for 0-65% of all sample grains. Peaks are seen at ~5-16 Ma, ~18-30 Ma, and ~40 Ma. A subordinate population of sample grains have ages of ~65 Ma, 100-150 Ma and 200-550 Ma, but where present these grains typically make up 2-23% of the sample (Figure 5.14). The youngest age obtained from surface sampling is 5 Ma in a sample of MS3, but varies from 6 Ma to 21 Ma. There is no

evidence of younging mineral populations moving westwards to the youngest anticlines.

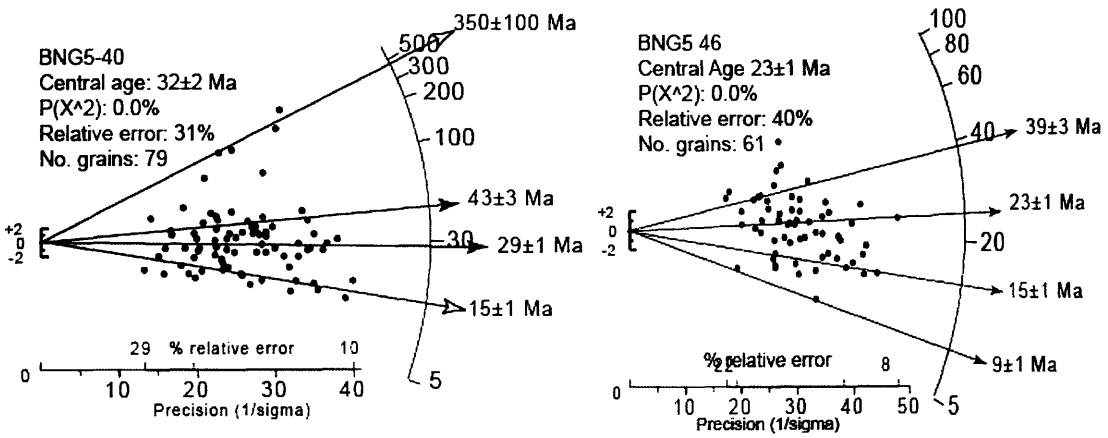

Sample #		No of samples	Central age (Ma) ±1σ	Age Components 1st	2nd	3rd	4th	5th
SB 3016	MS1	63	23.6±1.7	13±1 (13)	18±1 (40)	31±2 (12)	99±18 (2)	190±21 (2)
Sangu 3840	MS1	43	30.9±3.1	13±1 (7)	23±1 (17)	36±2 (17)	210±38 (2)	
BGL05-12A	MS2	9	22.9±6.8	6.1±0.8 (3)	29.6±2.0 (5)	225±119 (1)		
BGL05-14A	MS2	33	27.5±4.0	12.5±0.5 (13)	24.6±1.3 (16)	64.0±7.3 (1)	423.7±90.5 (2)	
BGL05-5A	MS2	26	31.1±5.2	14.8±0.5 (10)	26.9±1.1 (8)	64.7±5.5 (3)	205.9±28.4 (3)	
BGL05-6A	MS2	28	27.0±3.6	9.0±0.5 (4)	18.7±1.1 (10)	31.2±1.3 (8)	67.9±7.7 (5)	388±101 (1)
BNG5 123	MS2	50	25.1±1.7	16.5±0.8 (15)	23.2±0.8 (24)	42.1±2.8 (9)	242±39 (1)	
BA05-21A	MS2	46	35.0±4.1	12.8±0.8 (9)	23.4±0.8 (18)	41.0±1.7 (13)	355.7±39.5 (4)	
BA05-22A	MS2	23	26.3±3.4	15.2±0.8 (8)	25.9±1.2 (8)	45.1±4.0 (2)	125±14 (2)	
BA05-23A	MS2	51	17.2±1.6	7.0±0.5 (3)	10.5±0.9 (14)	14.6±0.9 (13)	25.6±0.9 (13)	133.5±14 (5)
BNG5 33	MS2	63	25.5±1.7	16.6±0.5 (30)	28.7±0.9 (24)	48.1±4.0 (6)	110±15 (3)	
BNG5 40	MS2	79	31.5±2.4	15.0±0.3 (24)	28.5±1.1 (30)	42.6±2.6 (21)	146±23 (3)	
BA05-27A	MS2	31	29.0±2.6	9.9±1.5 (3)	19.2±1.7 (7)	30.7±1.9 (13)	51.2±5.0 (6)	
BA05-28A	MS2	24	24.1±2.8	14.5±1.3 (8)	23.7±0.9 (15)	531±173 (1)		
BGL05-11A	MS3	8	39.7±8.8	21.3±1.7 (3)	42.9±4.0 (3)	181±46 (1)		
BNG5 46	MS3	61	23.1±1.3	9.3±0.9 (2)	14.7±0.5 (16)	23.0±0.7 (30)	39.3±3.1 (12)	
BA05-25A	MS3	53	21.4±2.2	5.3±0.4 (7)	13.8±0.7 (14)	21.8±0.8 (16)	32.8±1.2 (12)	85.4±13.2(2) 228±28 (2)
BA05-24A	MS3	20	26.3±5.0	9.5±0.6 (8)	28.8±1.6 (9)	264.9±27.3 (2)		

Figure 5.14 Detrital zircon fission track data are presented in the lower table with representative radial plots above. Component populations are shown. The dominant age populations are Tertiary in age, with Neogene grains making up 30-96% of the whole sample, and Palaeogene ages accounting for 0-65% of all grains. A subordinate population of grains have ages of ~65Ma, 100-150 Ma and 200-550 Ma, but where present these grains typically make up 2-23% of the sample.

U-Pb dating of detrital zircons:

The data and method for U-Pb dating on detrital zircons from three surface bedrock sandstone samples is presented in Appendix 7. Samples were analysed by

LA-ICPMS using a New Wave 213 aperture–imaged frequency–quintupled laser ablation system (213 nm) coupled to an Agilent 750 quadrupole-based ICP–MS.

73-98% of zircons fall between 500-2800 Ma with subordinate Tertiary aged populations (0-13%) and Cretaceous aged grains (1-8%) making up the remainder of each sample (Figure 5.15).

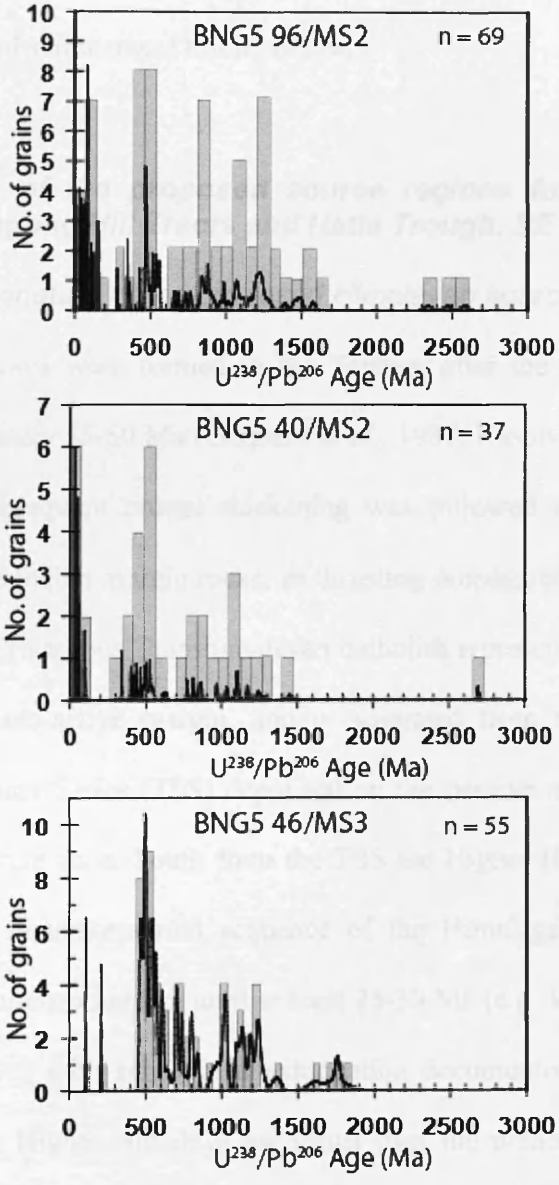

Figure 5.15 Detrital zircon U^{238}-Pb^{206} probability density plots with overlain histograms for 3 surface samples from MS2 and MS3 shows 73-98% of zircons fall between 500-2800 Ma with subordinate Tertiary aged populations (0-13%) and Cretaceous aged grains (1-8%) making up the remainder of each sample.

5.4.2 Interpretations

To determine the provenance of the Neogene sediments from the Chittagong Hill Tracts and Hatia Trough, taken from onshore surface and core and offshore core, our data are compared with published data of the proposed source regions of the Himalaya and the Palaeogene Indo-Burman Ranges of Myanmar. A subordinate source from the Indian Shield is also considered. These characteristics are presented fully in Table 3 and summarized briefly below.

Characteristics of the proposed source regions for the rocks of the Neogene Chittagong Hill Tracts and Hatia Trough, SE Bangladesh

Characteristic signature of the proposed Himalayan source

The Himalaya were formed in the Tertiary after the collision of India and Eurasia approximately 55-50 Ma (Garzanti *et al.,* 1987; Klootwijk *et al.,* 1992, Searle *et al.,* 1997). Subsequent crustal thickening was followed by metamorphism and exhumation of the Indian margin rocks, as thrusting propagated southward with time. In the north, the Cretaceous Transhimalayan batholith represents the Andean-type arc of the Asian palaeo-active margin, and is separated from the Palaeozoic-Eocene Tethyan Sedimentary Series (TSS) deposited on the passive margin of India, by the Indus-Yarlung Suture zone. South from the TSS the Higher Himalaya represents the rapidly exhumed metamorphosed sequence of the Himalaya. Mineral P-T-t paths indicate prograde metamorphism until at least 25-30 Ma (e.g. Vance and Harris 1999; Godin *et al.,,* 1999) with subsequent exhumation documented by Neogene mineral cooling ages. The Higher Himalaya are thrust over the predominantly low-grade to unmetamorphosed sedimentary rocks of the Lesser Himalaya, which is itself thrust over the sub-Himalaya/foreland basin syn-Himalayan sediments.

Source region And age	Rock description, Heavy Mineral and Petrography	Sm – Nd Whole rock εNd(0)	^{40}Ar-^{39}Ar ages of white mica	Zircon Fission track ages	U-Pb ages of zircons
Himalayan Bedrock (southern flank) extrapolated from foreland basin sediments	Varies across tectonic units. Metamorphosed and sedimentary terrains	HH bedrock –15 to –20 and LS bedrock –16 to –25[1,2]	<55 Ma in Higher Himalaya, Proterozoic ages in Lesser Himalaya[3]	See foreland basin below[4,5]	Ages 500-2800 Ma, lack of Cretaceous grains[1]
Transhimalaya / Yarlung Tsangpo	High epidote and hornblende, batholith souces[6]	Transhimalaya -1[7] to (+)5[8] And Tsangpo -10[8]	No available mica data but Palaeogene biotite ages[10]	Cretaceous Batholith with Neogene and Palaeogene populations[10,11]	No data for Tsangpo. Jurassic to Cretaceous in Transhimalaya[12].
Miocene to Recent Siwaliks	metamorphic lithics, and first appearance of high grade metamorphic minerals in the Siwalik. Plots Recycled orogen[1]	-14 to –30 (average of –17) in the Siwaliks[13]	All ages <55 Ma. Peaks at 20 Ma and 15 Ma[4]	13-19 Ma (35-95%)[5]	Ages 500-2800 Ma[1,5]
Himalayan Bedrock Signal Today Modern River sediments Higher Himalaya dominates detritus from the Ganges and Brahmaputra	Brahmaputra: high in quartz, epidote, hornblende, feldspar and white mica as well as medium to high grade metamorphic mineral[6,14] Ganges: similar rock types as Brahmaputra but but lower hornblende and epidote	Ganges -16 to –18 *,9 Brahmaputra -11 to –15 [9, 15]	As determined from *Gangetic tributaries:* Neogene peak, subordinate grains spanning to PreCambrian[16]	Ganges tributaries dominant Neogene popns with older grains >100-220Ma[17] He data: <55 Ma, Plio-Pleist peak.[18]	Data from the Ganges shows a dominance of Proterozoic to Palaeozoic ages and no grains between 55-125 Ma[18]
Burman – Indo-Burman Ranges (Palaeogene), drained by the Irrawaddy River	Fine grained interbedded mdts, silts and sstn, thin interbedded turbidites and micritic limestones. Bedrock and MRS plots within Magmatic arc and Recycled orogen province of QFL plot[19] (Dickenson 1985)	-4.0, -4.1 and –4.2[19]	Unmicaceous	Dominant age peaks at 37 Ma, 45-60 Ma and ~85 Ma with smaller populations at 100 Ma and >290 Ma[19]. Rare ages below 25 Ma	Predominant age peaks at 70-150 Ma and 500-2800 Ma with a recurring subordinate population at 42-60 Ma[19].
Indian Shield – Dominantly Archaean craton. Subordinate Proterozoic mobile belts and Gondwanan sedimentary cover.	Predominantly gneisses and granites; Opaques, opx and sillimanite found in rivers draining east craton[20] Mobile belt is supracrustal clastic arkose with rare lithics[21,22]	Values from south and east craton. -30 to -36[23,24], values from rivers draining the proterozoic mobile belt -14[25]	Palaeozoic and Proterozoic[23] ages from the Proterozoic mobile belt	Lowest Palaeozoic and Proterozoic[23]	Dominantly Archaean[26, 27] in the craton, but younger proterozoic ages found in mobile belt[23]

[1]DeCelles *et al.,* 1998a,b. [2]Robinson *et al.,* 2001, e.g.[3]Copeland *et al.,* 1991, [4]Szulc *et al.,* in press, [5]Bernet *et al.,* 2006, *Allen *et al.,* this study, [6]Garzanti *et al.,* 2004, [7]Clift *et al.,* 2002, [8]Allegre and Benotham, 1980, [9]Singh and France-Lanord, 2002, [10]Schlup *et al.,* 2003, [11]Kumar *et al.,* 2007, [12]Chu *et al.,* 2006, [13]Szulc *et al.,* 2006, [14]Heroy *et al.,* 2003, [15]Colin *et al.,* 1999, [16]Brewer *et al.,* 2003, [17]Bernet *et al.,* 2006, [18]Campbell *et al.,* 2005, [19]Allen *et al., in review,* [20]Mallik 1976, [21]Misra et al., 2005, [22]Acharyya, 2005, [23]Peucat *et al.,* 1989, [24]Saha *et al.,* 2004, [25]Najman *et al., In review,* [26]Mishra *et al.,* 1999, [27]Auge *et al.,* 2003.

Table 3. Typical signatures for possible source regions

In addition to bedrock, the rocks of the Himalayan foreland basin and modern river sediments draining the orogen provide a source signature of detritus eroded from the southern flank of the Himalaya through time. In the foreland basin, the rocks approximately coeval to those in the Chittagong Hill Tracts and Hatia Trough are the mid-Miocene to Recent Siwaliks (Bhatia, 1982; Gautam and Fujiwara, 2000). These, and rivers draining the southern flanks of the mountain belt, show clear derivation from low-medium grade metamorphic rocks of the rising Himalaya: the rocks and modern river sands show a petrographic assemblage with abundant metamorphic lithic grains and minerals (DeCelles *et al.,* 1998b; 2003b Szulc, 2006); ^{40}Ar-^{39}Ar ages of detrital white micas and fission track ages of detrital zircons show a dominance of Neogene ages with subordinate pre-Tertiary cooling ages (DeCelles *et al.,* 2001; Szulc *et al.,* 2006; Brewer *et al.,* 2003; Brewer and Burbank, 2006; Ruhl and Hodges, 2005; Bernet *et al.,* 2006). U-Pb ages of detrital zircons and ε_{Nd} bulk rock values are also consistent with bedrock Himalayan signature. The vast majority of zircons have U-Pb ages which fall between 500-2800 Ma, as seen in bedrock (DeCelles *et al.,* 1998a, b), Siwalik rocks (DeCelles *et al.,* 1998b; Bernet *et al.,* 2006) and Ganges modern river sediments (Campbell *et al.,* 2005). Cretaceous grains are notably absent whilst the occurrence of occasional Neogene grains are indicative of Himalayan leucrogranites sources. ε_{Nd} values are also consistent between bedrock and detrital material with High Himalayan bedrock displaying a signature between –15 to –20, Lesser Himalaya –16 to –25 (DeCelles *et al.,* 1998a, b; Robinson *et al.,* 2001) foreland basin Siwaliks between -14 to -30 (average -17) (Szulc *et al.,* 2006) and Gangetic sediment values of –16 to –18 (Singh and France-Lanord, 2002).

The characteristics of the Brahmaputra River differ somewhat from those of the Ganges and tributaries draining the Himalayan southern flanks. The Brahmaputra

has a higher proportion of epidote and hornblende compared to the Ganges (Garzanti *et al.,* 2004; Heroy *et al.,* 2003), and less negative ε_{Nd} values of -11 to -15 (Colin *et al.* 1999; Singh and France-Lanord, 2002). This difference is due to its drainage basin, which extends north of the Himalaya, thus receiving additional input from the suture zone and Cretaceous Transhimalayan batholith to the north in addition to detritus eroded from the Himalaya's southern slopes. The Yarlung Tsangpo, which flows along the suture zone draining the TSS and Trans-Himalaya, characterises this part of the drainage basin. Consistent with its influence on the Brahmaputra signature, it has epidote and hornblende content higher than that of the Ganges (Garzanti *et al.,* 2004), and a ε_{Nd} value that is less negative (-10; Singh and France Lanord 2002). The Transhimalaya has a positive ε_{Nd} of 1–5 typical of an arc setting (Allegre and Benothman, 1980) and the Ladakh batholith shows values of c. -1 (Clift *et al.,*, 2002). Although no published work documents the U-Pb ages of detrital zircons in the Yarlung Tsangpo or Brahmaputra, U-Pb ages of zircons from the Transhimalayan bedrock clearly show the dominance of Jurassic-Cretaceous ages (Chu *et al.,*, 2006).

Characteristic signature of the proposed Palaeogene Indo-Burman Ranges source

A second potential source for the Chittagong Hill Tracts and Hatia Trough is that of the Cretaceous-Palaeogene Indo-Burman Ranges of western Burma, exhumed after 37 Ma. The data summarised below are taken from Allen *et al.,* (*in press*). The rocks are typically unmicaceous very fine grained sandstone and siltstones, which show evidence of input from the Cretaceous Burmese arc to the east.

The petrographic assemblage of bedrock from the Palaeogene Indo-Burman Ranges is predominantly analysed from pebbles in modern rivers, due to scarcity of in

situ bedrock exposure. The samples vary in their assemblage from showing predominantly low grade metamorphic lithics in some samples, which plot within the Recycled Orogen province of the QFL diagram, to others that are composed of mainly lithics, and plot within the magmatic arc field. The modern river samples show a minor proportion of volcanic detritus, whereby volcanic-derived lithic clasts total a few percent of the whole sand sample. ε_{Nd} values of ~ -4.0 in the modern river samples are consistent with the petrographic data reflecting a mix of mafic igneous and continental sources. The dominant zircon fission track age populations in the modern river sands are greater than 55 Ma, with common age components at ~ 60, 85, 100 and >290 Ma. Tertiary ages are present as subordinate populations. Analyses of U-Pb in detrital zircons shows predominant populations at 70-150 Ma, and 500-2800 Ma. No ^{40}Ar-^{39}Ar data are available since the Palaeogene bedrock, and hence the modern river samples, lack mica.

Characteristic signature of the proposed Indian cratonic source

A third possible source which may have contributed material to the Neogene Chittagong Hill Tract and Hatia Trough sediments is the Indian Shield, which is dominantly an Archaean craton with Proterozoic mobile belts and Gondwanan sedimentary cover. The geology of the craton largely consists of gneisses and granites, and the ε_{Nd} values are strongly negative at between –30 and –36 (Peucat *et al.,* 1989; Saha *et al.,* 2004). Archaean ages dominate the detrital zircon U-Pb data (Mishra *et al.,* 1999; Auge *et al.,* 2003) but there is little other data published, and none for ^{40}Ar-^{39}Ar age of detrital micas or fission track analyses of detrital zircon. The Chotangpur Proterozoic mobile belt is adjacent to the Bengal Basin and is drained by the Damodar River (Acharyya, 2003; Mishra and Johnson, 2005) and its extension north of the

Bengal Basin, the Shillong Plateau, is drained by the Jadhu Kata and Dauki River. The detrital load in these rivers (Najman *et al.,* in press) provides the source signature of the Proterozoic mobile belt. Sediments are quartzofeldspathic with rare lithics and have ε_{Nd} values of ~ -14 and detrital zircon U-Pb, zircon fission track and white mica Ar-Ar ages are mostly lowest Palaeozoic and Proterozoic (~500-2500 Ma) with only extremely scarce Tertiary ages present.

Therefore, in summary, the three potential source regions are distinct in their petrogaphic, thermochronological and isotopic signatures. Whilst Tertiary Ar-Ar and zircon fission track mineral cooling ages accompanied by metamorphic detritus, is distinctive of Himalayan provenance, quartzofeldspathic material with grains of predominantly Pre-Tertiary cooling age are distinctive of erosion from the Indian craton. By contrast, isotopic composition and mineral grains typical of appreciable derivation from the Cretaceous Burmese magmatic arc characterise the Indo-Burman Ranges.

Provenance of the Neogene Chittagong Hill Tracts, Bangladesh

The significant proportion of low to medium-grade metamorphic grains and metamorphic minerals such as garnet, staurolite and kyanite present in the Neogene samples of the Chittagong Hill Tracts and Hatia Trough is consistent with orogenic provenance and similar to the characteristics of the Himalayan-derived foreland basin deposits. Similar petrography and heavy mineral assemblages characterise coeval sediments of the Sylhet Trough, and have previously been attributed to unroofing of the Himalaya since the Miocene (Uddin and Lundberg, 1998a, b).

Tertiary (dominantly Neogene <23 Ma, with subordinate Palaeogene) and rare older ages in the zircon fission track and white mica Ar-Ar isotopic data of the

Neogene samples from the Hatia Trough and Chittagong Hill Tracts are also similar to those found in the peripheral foreland basin and reflects metamorphic cooling ages in the source region of the Himalaya. Ar-Ar mica data from Neogene samples in the Hatia Trough and Chittagong Hill Tracts are similar to comparable Neogene data from the Surma Basin (Sylhet Trough) of coeval age, and are attributed to derivation from the High Himalayan (Rahman and Faupl, 2003).

Rare Tertiary ages and a dominance of grains dated to between 500-2800 Ma, in the zircon U-Pb age populations from the Neogene Chittagong Hill Tracts is consistent with data from the foreland basin, Himalayan bedrock and modern river sediments from the Ganges. Whilst the subordinate Cretaceous population in the Chittagong Hill Tracts samples is not reflected in bedrock data from the Himalaya's southern slopes, or its detritus, it is consistent with derivation from the Transhimalaya. ε_{Nd} values from surface and drill core samples of –11 to –15 also reflect additional input from the Transhimalaya. Such data are consistent with values from the Brahmaputra. These values are notably less negative than the average signature of the coeval foreland basin Siwaliks (Table 3), which contains detritus derived exclusively from the southern flanks of the Himalaya.

Palaeoshelf mapping, which indicates a northern clastic input direction to the Bengal Basin since Miocene-Pliocene times, is consistent with the interpretation that detrital mineral populations indicate Himalayan sources.

By contrast, the Archean mineral ages and very negative ε_{Nd} values > -30 of much of the Indian Craton (Peucat *et al.,* 1989; Mishra et al, 1999; Auge *et al.,* 2003; Saha *et al.,* 2004), are unlike that of the Bengal Basin sediments under study. Petrographically, samples from the Indian Craton, including the Proterozoic mobile belt, are distinctly different from the Neogene samples of the Bengal Basin and, unlike

the Bengal Basin sediments, there is an absence in cratonic detritus of Tertiary aged mica and zircons revealed in Ar-Ar dating and zircon fission track, respectively (Najman *et al.,* in press). The orientation of the palaeoshelf indicating a source to the north or northeast also indicates that the Indian Craton is not likely to be the dominant source to the Hatia Trough and the Chittagong Hill Tracts during the mid-late Neogene (figure 5.9a, b).

The source direction with flow from the northeast to north into the Bengal Basin during the Neogene would be consistent with input from the Palaeogene Indo-Burman Ranges (Uddin and Lundberg, 1998a, b, 1999, 2004; Gani and Alam, 2003). However, rock type, petrography and isotopic data from the Indo-Burman Ranges are incompatible with the concept that the Chittagong Hill Tracts and Hatia Trough sediments were sourced from this region. The Palaeogene Indo-Burman Ranges are mica-free very fine-grained sandstones, siltstones and shales with petrography, ε_{Nd} values and U-Pb zircon ages all attesting to arc input from the Burman margin along with recycled orogenic material. It is therefore impossible that these sedimentary rocks sourced the coarser grained micaceous sandstones of the Neogene Chittagong Hill Tracts and Hatia Trough, which have considerably more negative ε_{Nd} values, and a preponderance of zircons with Neogene fission track ages, which are exceedingly rare in the Palaeogene Indo-Burman Ranges.

All provenance data are thus consistent with the interpretation that the Neogene sediments of the Chittagong Hill Tracts and Hatia Trough are sourced by the rising Himalaya, and as such represent a Neogene accretionary prism, whereby the eroded sediments were incorporated into the proto-Bengal Fan and then subducted and accreted along the zone of convergence between India and Asia, as suggested by Curray *et al.,* (1979). We rule out significant recycling of older (MS1) Bengal Basin

sediments into the Chittagong Hill Tracts and Hatia Trough, on the basis that deformation did not start until late MS2 times, therefore making it unlikely that the sediments would have been recycled into their proposed time-equivalent sediments in the western anticlines. Whilst both palaeoshelf mapping and isotopic provenance data indicate a dominant source consistent with Himalayan derivation, subordinate contribution from the Indo-Burman Ranges and a minor contribution from the Indian craton cannot be ruled out.

5.5 Regional Implications

5.5.1 Palaeodrainage in the Bengal Basin

Seismic palaeoshelf mapping and interpretation of seismic lines of the Hatia Trough and Chittagong Hill Tracts highlight input from a clastic source to the northeast during deposition of MS1 and MS2, shifting more north by deposition of MS3 (Figure 5.10a, b, c). Given the present configuration of major drainage in the region today and consensus with previous work using isopach maps and lithofacies maps (Uddin and Lundberg, 1999; 2004) it seems likely that the NE input in the Miocene-Pliocene is from the coalesced palaeo-Brahmaputra and palaeo-Ganges river system, dominated by input from the Brahmaputra as is the case today (Islam *et al.,* 1999; Singh and France-Lanord, 2002; Garzanti *et al.,* 2004).

Previous workers have proposed that uplift of the Shillong Plateau by 3-4 Ma (Biswas *et al.,* in press), caused diversion of the palaeo-Brahmaputra to the west of the plateau (Johnson and Nur Alam, 1991). This is not easily reconcilable with our palaeoshelf mapping which shows a NE input from the palaeo-Brahmaputra continuing into MS2 times (<3.25 Ma). We propose that it was westward encroachment and final abutment of the Chittagong Hill Tracts accretionary prism

against the already uplifted Shillong Plateau that resulted in the closure of the northeast drainage route and consequent diversion of the palaeo-Brahmaputra west of the Shillong Plateau (Figure 5.16).

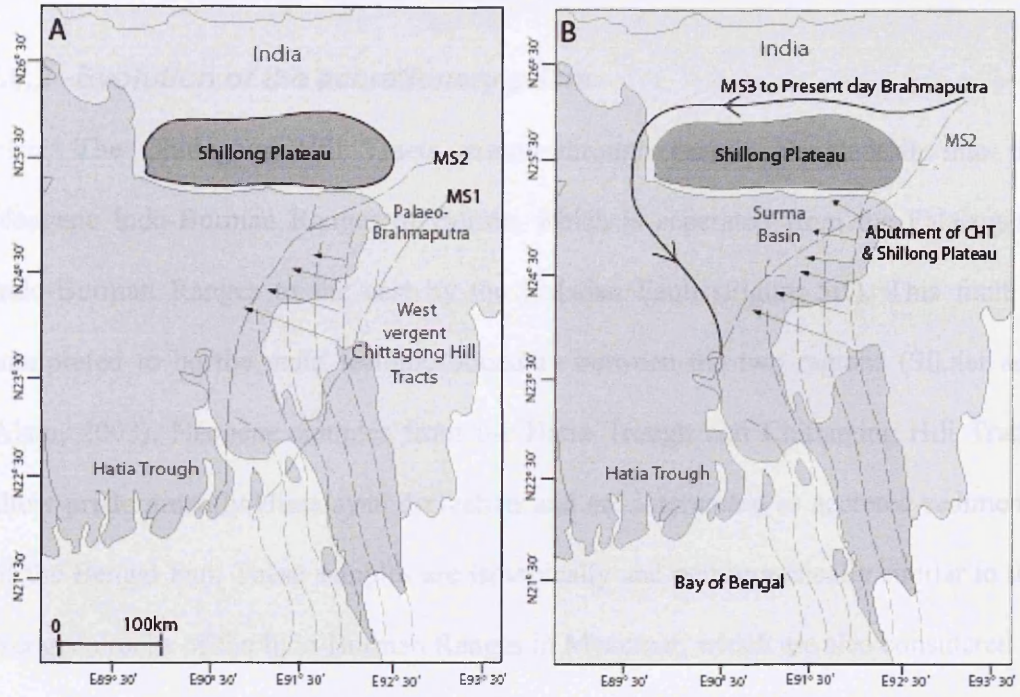

Figure 5.16 The progressive closure of the northeast drainage route for the palaeo-Brahmaputra is caused by the westward encroachment of the Chittagong Hill Tracts (A) onto the already uplifted Shillong Plateau (B) causing its ultimate diversion around the northern edge of the massif in latest MS2-MS3 times (<2 Ma). Our data suggest that the uplift of the Shillong Plateau was not the trigger for the palaeo-Brahmaputra diversion, as the river was still draining through the Bengal Basin from the northeast post 3-4 Ma when it is suggested the Shillong Plateau was uplifted.

We constrain the timing of this diversion from the date that the youngest emergent anticlines at the leading edge of the westward propagating accretionary prism in the study area of the Chittagong Hill Tracts /Hatia Trough were uplifted (~1.55 Ma; latest MS2) (section 3). This is coeval with the timing of the observed shift in clastic input direction from NE to North between MS2 and MS3 (Figure 5.10),

which may be an expression of this river diversion, although such a shift could also have been caused solely by gradual progressive encroachment of the Chittagong Hill Tract into the area.

5.5.2 Evolution of the accretionary prism

The Chittagong Hill Tracts extend through eastern Bangladesh, into the Neogene Indo-Burman Ranges of Burma, which is separated from the Palaeogene Indo-Burman Ranges to the east by the Kaladan Fault (Figure 5.1). This fault is interpreted to be the main tectonic boundary between the two regions (Sikder and Alam, 2003). Neogene samples from the Hatia Trough and Chittagong Hill Tracts show predominantly Himalayan derivation and are interpreted as accreted sediments of the Bengal Fan. These samples are isotopically and petrographically similar to the Neogene rocks of the Indo-Burman Ranges in Myanmar, which are also considered to be of Himalayan derivation (Allen *et al., in Press*). However, east of the Kaladan Fault the Palaeogene rocks of the Indo-Burman Ranges (Arakan Yoma, Figure 5.1) are petrographically and isotopically distinct from their Neogene neighbours. They are interpreted to be predominantly Burman margin derived, but deposition in a forearc setting or accretionary prism setting is equivocal (Allen *et al., in Press*).

Detrital mineral cooling ages provide a maximum depositional age of the host sediment. Combining youngest depositional ages from both the Neogene samples of the Chittagong Hill Tracts and the Neogene Indo-Burman Ranges, deposition of the Neogene Indo-Burman Ranges can be seen to occur after 29 Ma in the east (Allen *et al., in Press*) and after 1 Ma in the west. Taking the youngest mineral population from each sample produces an overall trend of younging in a westward direction, consistent with deposition in a west-vergent accretionary prism (Figure 5.3). Considering the

youthfulness of age of deformation and exhumation in the west (~2 Ma), diachroneity of exhumation is assumed, in line with typical evolution of an accretionary prism, but current lack of data on the exhumation and deformation history of the Burmese section of the Neogene Indo-Burman Ranges precludes further assessment at this time.

Whilst all data from the Neogene Indo-Burman Ranges are consistent with an accretionary prism environment, the abrupt change in provenance of rocks across the Kaladan Fault, and the possibility that the Palaeogene rocks to the east of the fault may be forearc rather than accretionary prism deposits (Allen *et al., in press*), complicates the tectonic interpretation. The Kaladan Fault must represent a significant tectonic boundary juxtaposing either accretionary prism and forearc tectonic facies, or the Palaeogene and Neogene parts of an accretionary prism.

5.6 Conclusions

The Tertiary sedimentary sequence preserved within the Chittagong Hill Tracts and Hatia Trough was previously subdivided on a lithostratigraphic framework based on matching of like-for-like facies with rocks in Assam, despite their differing ages. We present a new sequence stratigraphic framework for the Bengal Basin that is regionally applicable, correlatable and biostratigraphically constrained. On the basis of this seismic stratigraphy we find that the surface rocks in the Chittagong Hill Tracts have previously been ascribed inaccurate old ages. We find no evidence of the traditional Surma Group (time equivalent to MS1) at surface in the studied region and instead suggest the widespread exposure of MS2 aged sediments that correspond to the lithostratigraphic Tipam Formation and lower Dupi Tila Formation (<3.25 Ma).

Petrographic and isotopic analyses confirm Himalayan provenance that is consistent with derivation from the offscraped (palaeo-) Bengal Fan during the

Neogene, which supports the accretionary prism model of deposition. We rule out major derivation from the Indo-Burman Ranges and the Indian craton (Shillong Plateau) based on dissimilar petrography and palaeoshelf mapping. Isotopic data and seismic interpretation reveal that deformation in the Chittagong Hill Tracts started ~2 Ma and continues at present offshore in the Hatia Trough, typical of a west-vergent accretionary prism.

Mapping of the evolving palaeoshelf slope break during the Neogene has revealed a dominant input direction from the northeast and this is consistent with major input from the palaeo-Brahmaputra (which had coalesced with the palaeo-Ganges by this time). Palaeoshelf mapping combined with the timing of deformation suggests that the palaeo-Brahmaputra drained from the northeast until ~1.55 Ma when the encroachment of the emerging Chittagong Hill Tracts on to the already uplifted Shillong Plateau resulted in the Brahmaputra shifting its drainage course around the back of the massif, entering the Bengal Basin from a more northerly position, as seen in MS3 times (1.55 Ma onwards).

Chapter 6: Conclusions and Discussion

6.1 Introduction

This chapter firstly summarises the evidence for Himalayan provenance, or otherwise, of the sedimentary rocks of the Andaman Islands, Burma and Bangladesh. The novel aspects of the thesis are then considered, followed by a discussion of the broader context and implications of this study of the erosion record.

6.2 Conclusions

In order to address the principle question of this thesis: '*Do the sediments of the Sunda subduction zone from Bangladesh, Burma and Andaman Islands, preserve a record of early Himalayan erosion?*' it was necessary to characterise the provenance of each field area using a multi-proxy approach that combined thermochronological analysis with petrographic and isotope data and seismic data where available (Appendices 1 to 3). The areas studied had previously been suggested as a potential repository for Himalayan sediments by offscraping of the Bengal Fan (Curray *et al.* 1979, 2005; Bender, 1983), however this had been disputed (e.g. Mitchell, 1993; Pal *et al.* 2003).

The existing stratigraphy of each region is poorly understood and its age often poorly constrained, mainly due to the inaccessibility of the field areas (Indo-Burman Ranges, Chapter 4), but also due to the complex geology of each region, which is also typically heavily weathered (Andaman Islands, Chapter 3), lacks adequate biostratigraphic control or incorrectly correlated with the regional geology elsewhere (Chittagong Hill Tracts, Chapter 5). For this reason, the stratigraphy of the Chittagong Hill Tracts first had to be resolved within a robust regional sequence stratigraphic framework, which led to the reclassification of the geology and assignment of a

younger age for the outcropping sediments than had previously been suggested. The main conclusions from this work are as follows:

Conclusion 1

The Palaeogene sedimentary rocks of both South Andaman and the Indo-Burman Ranges (Burma) show appreciable magmatic arc derivation with additional orogenic input. Although a subordinate continental source to these regions is observable from the data it is most likely that this source is the Burman continental margin and not the Himalaya. However, I do not altogether rule out the possibility of minor Himalayan contribution. I do not find unambiguous evidence of Himalayan derivation in the region until ~ 38 Ma in the Bengal Basin (see co-authored paper by Najman *et al.* in press). In younger Palaeogene to Neogene sedimentary rocks of the Andaman Islands (30-20 Ma) a provenance change to dominantly recycled orogen with minor arc sources is seen. This is most easily explained by derivation from Burman continental margin sources and not from the Himalaya.

Deposition of the Palaeogene sedimentary rocks cannot easily be explained by the accretionary prism model unless trench bypass is invoked (e.g. Draut and Clift, 2004). Instead we suggest deposition may have occurred in a forearc setting. However, the evidence for both remains elusive and debate continues for both options.

Conclusion 2

The Neogene rocks deposited along the line of India-Eurasia subduction in both the Indo-Burman Ranges and the Chittagong Hill Tracts are separated from Palaeogene formations in Burma by the Kaladan Fault. West of this tectonic divide the evidence for Himalayan derivation is compelling. The rocks in the westernmost Indo-Burman

Ranges and the Chittagong Hill Tracts/Hatia Trough are isotopically and petrographically distinct from their Palaeogene counterparts, but similar to coeval rocks of known Himalayan derivation in the orogen's foreland basin. The sedimentary rocks of the Neogene Hatia Trough and Chittagong Hill Tracts (Figure 5.1), which extend south into westernmost predominantly coastal areas of the Indo-Burman Ranges, support a typical accretionary prism depositional setting whereby Himalayan sediments are eroded and transported to this region deposited in the Bengal Fan and ultimately subducted and offscraped onto the leading edge of the Asian plate.

In addition, seismic mapping of the Neogene sedimentary rocks have given new insight to palaeodrainage of the Brahmaputra ~2 Ma. New seismic data suggests that it was not the uplift of the Shillong Plateau at ~3.5 Ma that caused the deflection of the Brahmaputra around the northern flank of the massif, but instead the encroachment of the leading edge of the growing Chittagong Hill Tracts onto the already uplifted plateau at ~1.5 Ma, that closed the northeast drainage route to the Brahmaputra, forcing it to divert its course.

In consideration of the question posed it is therefore reasonable to infer that there is no clear evidence of substantial amounts of early Himalayan erosion in the sedimentary rocks studied along the subduction zone spanning Bangladesh to the Andaman Islands. From which point Himalayan derivation to the region is substantial, distinct and unequivocal throughout the Neogene in Bangladesh and Burma, and likely represents deposition in an accretionary prism setting due to the offscraping of sediments of the Bengal Fan. Elsewhere in the Bengal Basin the earliest record of Himalayan erosion is at ~38 Ma (Najman *et al., in press*).

6.3 Novel aspects of this thesis

- A multi-proxy approach to the problem of provenance discrimination in the studies regions across Southeast Asia, moving away from a reliance on one or two methods: increasing robustness and reliability of the data (Chapter 2)
- Established convincing evidence for the provenance of three regions: South Andaman, the Indo-Burman Ranges and Chittagong Hill Tracts, whose provenance had previously been disputed.
- A quantitative 'pilot study' of the complete stratigraphy and thermal history of South Andaman, first suggested as a possible record of Himalayan erosion since the Palaeogene by Curray and Moore (1971) (Chapter 3)
- Extension and development of a basin evolution history for the southern Bengal Basin, including;
    - A sequence stratigraphic framework for the sedimentary rocks of the Hatia Trough and Chittagong Hill Tracts, leading to the reclassification of the poorly constrained geology of this area, assigning the outcropping and exposed rocks a younger age (Pliocene) than previously suggested (Chapter 5)
    - Development of a palaeogeography and palaeodrainage history for the basin
    - Better, precise constraint (post 2 Ma) to the timing of tectonic evolution of the Chittagong Hill Tracts.
- A reappraisal of the depositional setting for the Indo-Burman Ranges (Chapter 4)

6.4 Discussion

6.4.1 Erosion and crustal deformation

Good evidence exists for India – Asia collision at 55-50 Ma (Patrait and Achache, 1984; Klootwijk *et al.* 1992; Garzanti *et al.* 1987; Searle *et al.* 1997). However, in the central-eastern Himalaya there is no record of erosion from the Himalayan southern flank until ~38 Ma (Najman *et al.* in press). The results of this study show unequivocal evidence of Himalayan erosion during the Neogene, however these distal regions do not present a convincing record of Himalayan erosion in the Palaeogene. Early erosion of the Himalaya can be found in the western Himalayan sedimentary repositories as early as mid-Eocene in the Indus Fan (Clift *et al.* 2001b; Daley and Alam, 2002) and as early as collision before 49 Ma in the Suture Zone (Clift *et al.* 2001). However, detritus from the Indus Fan cannot be dated more precisely than mid-Eocene and represents material eroded from the Transhimalaya to the north, and not from the southern flank. The same is true for molasses of the Indus Suture Zone, which are well constrained but not sourced from the rising southern flanks of the Himalaya. Moreover, suggested Palaeogene sediments of the Katawaz basin (Qayyum *et al.* 2001) that may record Himalayan provenance are also poorly age constrained, to at best the Early Eocene.

The first widespread appearance of material eroded from the southern flank of the Himalaya is found in the Miocene in sedimentary repositories south of the Himalaya including the Bengal Basin, Bengal Fan, Indus Fan, Katawaz Basin and the Makran (Qayyum, 1996; Clift *et al.* 2001; Aitchison, 2002).

Evidence for erosion since collision in sediments preserved in western Himalayan sedimentary repositories are currently poorly age constrained. Tighter age constraint and more data will confirm in the future whether these sediments are

derived from the eroding southern Himalaya. Elsewhere, it may be possible that early eroded sediments have been incorporated into the south–propagating thrust belt. If an early record of erosion is confirmed in the western Himalaya then it will have important repercussions on models of palaeodrainage in the Tertiary and will require a reappraisal of major drainage patterns and directions and the role of the largest rivers such as the Brahmaputra, Ganges, Indus and Yarlung Tsangpo.

In the case that no older eroded material is found from the southern flank of the Himalaya in the east or west, then it becomes increasingly important to reconcile collision at 55-50 Ma without any appreciable or substantial erosion until ~38 Ma. Some questions to consider include;

- Can collision result in topographic relief without erosion?
- Can convergence be accommodated without topographic relief and hence little or no erosion?
- Does a lack of early erosion indicate that collision did not take place at 55 Ma but later when clear and unambiguous Himalayan input is first seen?

Lack of early erosion can be explained by a suggested early arid climate (Guillot *et al.* 2003), accommodation of initial convergence by lateral extrusion (e.g. Tapponier *et al.* 1982), early subdued topography, a low angle continental subducting plate (Guillot *et al.* 2003) and even later collision of India and Eurasia (Ali and Aitchinson, 2007). In the most popular models crustal deformation can occur and be accommodated in a variety of ways that either do not require early erosion immediately after collision, or indeed favour delayed erosion.

In the increasingly popular Channel Flow model (e.g. Grujic *et al.* 1996; Beaumont *et al.* 2001) erosion is modest in order to maintain sufficient overburden at surface in order to drive the self-radiative heating and melting required to initiate

ductile flow in mid-crustal levels. Erosion at surface later causes the dynamic coupling of surface with the crustal channel, and the channel is exhumed at the denudation front. Early models were optimised to produce results that were compatible with observed geological features of the Himalaya, and initiated erosion at 30 Ma (Beaumont *et al.* 2001; Jamieson *et al.* 2004). However, recent revisions of the model (Jamieson *et al.* 2007) that input moderate erosion from the start of the model runs (i.e. from collision) cause a later onset of channel flow and plateau uplift and result in inconsistencies with observed geological data. Advancing the onset of erosion to 38 Ma will no doubt require input parameters to the current and best models that both maintain channel flow and are still compatible with geological data.

Other models may also explain a delay in erosion. The lithospheric delamination model (Dewey *et al.* 1998) explains a delay in erosion whereby the heavy thick crustal root of the mountain belt is progressively delaminated from its underside until tectonically induced uplift occurs and rebound results in erosion at surface. In the cold dense root model the dense down-going slab maintains limited topography at the surface until slab-break off when buoyancy driven uplift increases the amount of erosion at the surface (Chemenda *et al.* 2000). In this model erosion is directly related to deeper crustal processes. In the lateral extrusion model (Tapponnier *et al.* 1982; Replumaz and Tapponnier, 2003) convergence is accommodated by the lateral extrusion of crustal blocks of finite strength along zones of displacement such as strike skip faults. In this sense, there is no requirement for extensive vertical topography (although a negligible amount was likely to have occurred due to a small degree of uplift) in early stages of collision because the convergence is mainly accommodated laterally over a large area.

Understanding the timing of erosion is therefore vital to constraining the various models of Himalayan evolution.

6.4.2 Tectonics, erosion and climate interactions

This discussion is not intended to be exhaustive, but a context by which to understand the importance of the work done in this thesis. Many researchers have extensively investigated the controls and climatic effects of erosion (e. g. Raymo and Ruddiman, 1992; Molnar *et al.* 1993; Fielding, 1996; Zhang *et al.* 2001; Vance *et al.* 2003; Clift *et al.* 2004, Huyghe *et al.* 2005; Grujic *et al.* 2006; Clift and Blusztajn, 2005; Clift, 2006 to name a few).

The feedback between climate, tectonics and erosion is dynamic and complicated and invariably involves one process impacting on another in order to create complex negative or positive feedback loops. The prevailing climate may increase or decrease erosion rates and likewise erosion will serve to negate or exacerbate climatic conditions. Similarly, erosion may force tectonics through the dynamic loading and unloading of the Earth's crust and mantle lithosphere (e.g. Willett 1999) and tectonics may force erosion, providing the topographic contrast required for effective erosion by, e.g., gorge incision by fluvial erosion. Dynamic coupling between tectonics and surface processes such as erosion is illustrated by the fact that denudation is shown to cause the exponential decay of topography with a typical time constant of ~2.5 million years (Burov *et al.,* 2007). In the *absence* of a strong tectonic feedback a mountain belt would erode itself flat in a few millions years (Burov *et al.* 2007 and references therein). However, it is clear that on expansive and elevated mountain belts such as the Himalaya, Alps and Andes, this is not the case. Isostatic reaction and continued convergence are two tectonic feedback mechanisms

required to keep a mountain belt in dynamic equilibrium (e.g. Beaumont 1981, Willett 1999, Simpson and Schluneggar, 2003). This has led to much debate as to the true control on erosion. When asking the question 'What drives erosion?' then beyond the control of gravity it is important to consider forcing factors such as tectonic rock uplift, precipitation and climate variability.

As discussed in Chapter 1, a continuing understanding of the volume, location and timing of erosion from a mountain belt is important for constraining models of crustal deformation as well as understanding the role of orogenesis in changes to ocean geochemistry and to observed climatic changes. The influence of erosion on crustal deformation is discussed above (Section 6.4.1).

The coupling of climate and erosion is complex; with erosion suggested as a cause for climate change as well as the result of it. Erosion is particularly important in the drawdown of carbon dioxide through silicate weathering, riverine transport and the subsequent burial of organic carbon. The Himalaya is thought to be a major contributor to the drawdown of carbon dioxide from the atmosphere, and the Bengal Fan is thought to have stored ~15% of the global carbon budget in the last 15 million years alone (Galy *et al.* 2007). The efficient burial of carbon in Himalayan offshore repositories has led to the theory that the uplift of the Himalaya and subsequent erosion, has caused Cenozoic global cooling since 45-50 Ma (e.g. Raymo and Ruddiman, 1992). Moreover, the uplift of the Tibetan Plateau and subsequent increase in erosion, is thought to have intensified the Asian monsoon, instigated continental aridification elsewhere and further increased erosion since ~34 Ma (Dupont-Nivet *et al.* 2007).

Erosion is also suggested as the primary cause of changes to ocean geochemistry in the worlds' oceans. The Himalaya is an important source of strontium

to global oceans, and both the Ganges and Brahmaputra are characterized by high $^{87}Sr/^{86}Sr$ ratios. Richter *et al.* (1992) first observed that significant erosion from the nascent Himalaya may have caused the rise in marine $^{87}Sr/^{86}Sr$ values since ~40 Ma.

6.4.3 Significance of the data

In order to validate the abounding theories that Himalayan erosion can directly force changes to the global climate, ocean geochemistry and to tectonic processes within an actively converging mountain belt, it is clearly necessary to have an accurate picture of when erosion was initiated in the Himalaya, how much erosion has taken place and any periods of quiescence.

In the sediments of the Sunda subduction zone accretionary prism stretching from Bangladesh, through Burma to the Andaman Islands, there is no compelling evidence of substantial Himalayan erosion until the Neogene. Older Palaeogene sediments do not show provenance characteristics consistent with Himalayan sources. Elsewhere in the Bengal Basin, Himalayan erosion is seen earlier at ~38 Ma (Najman *et al. In review*). Whilst possible evidence for early erosion has been suggested for sediments of the Indus Fan and suture zone in the western Himalaya, beneath the main thrust belt of the Himalaya (which in any case will remain inaccessible) or in offshore repositories (when drilling capabilities improve), the data is either poorly age constrained or represents erosion from the northern flank of the Himalaya, which never reaches the southern repositories due to the topographic boundaries and drainage orientation, and not from the south. In the east-central Himalaya there is as yet no convincing evidence of major erosion prior to ~38 Ma. Importantly, evidence for delayed erosion is supported by regional evidence for a widespread transition from slow mass sediment accumulation in the offshore basins surrounding the collision

zone, to exponentially increased accumulation at the start of the Oligocene (e.g. Clift, 2006).

Our data is consistent with the hypothesis that erosion of the Himalaya could have caused an increase in global ocean $^{87}Sr/^{86}Sr$ ratios since ~40 Ma (Richter *et al.* 1992). Despite potential evidence for early erosion in the western Himalaya these rocks are less radiogenic than those in the east, and would not have affected the global ocean strontium budget (Pande *et al.* 1994). Our data does not appear to be consistent with the theory that onset of substantial erosion from the Himalaya at ~55 Ma caused global cooling, due to the lack of any substantial evidence as yet, of erosion since collision. The results of this thesis support models of crustal deformation which require a delay in erosion or do not require erosion at all in early stages of convergence. Replumaz and Tapponier (2003) suggest that lateral extrusion can account on average for 30% of convergence of India and Asia. Perhaps combined with models such as Channel Flow it is possible to reason for a delay in erosion as a result of both initial lateral extrusion and Channel Flow.

Chittagong Division, Bangladesh – Spring 05

General References

Acharyya, S. K., 2005, The nature of mesoproterozoic Central Indian Tectonic Zone with exhumed and reworked older granulites, Gondwana Research, 6, 2, pp197-214.

Acharyya, S. K., 2003, The Nature of Mesoproterozoic Central Indian Tectonic Zone with Exhumed and Reworked Older Granulites, Gondwana Research, 6, pp197-214.

Acharyya, S. K., Ray, K. K. and Roy, D. K., 1989, Tectonic stratigraphy and emplacement History of the Ophiolite assemblage from Naga Hills and Andaman island arc, India, Journal of the Geological Society of India, 33, pp4–18.

Acharyya, S.K., Ray, K.K. and Sengupta, S., 1990, Tectonics of the ophiolite belt from Naga Hills and Andaman Islands, India: Proceedings Indian Academy Science (Earth Planetary Science), 99, pp187–199.

Ahmad, T., Harris, N., Bickle, M., Chapman, H., Bunbury, J. and Prince, C., 2000, Isotopic constraints on the structural relationships between the Lesser Himalayan Series and the High Himalayan Crystalline Series, Garhwal Himalaya: Geological Society of America Bulletin, 112, pp467-477.

Aitchison, J. C., Ali, J. R. and Davis, A. M., 2007, When and where did India and Asia collide? Journal of Geophysical Research, 112, B05423, doi:10.1029/2006JB004706, 2007.

Aitchison, J. C., Davies, A. M., Badengzhu, B., and Luo, H. 2002, New constraints on the India-Asia collision: the lower Miocene Gangrinboche conglomerates, Yarlung Tsangpo suture zone, SE Tibet. Journal of Asian Earth Sciences, 21, pp251-263

Alam, M., Mlam, M. M., Curray, J. R., Chowdhury, A. L. R. and Gani, M. R. (2003) An overview of the sedimentary geology of the Bengal Basin in relation to the regional tectonic framework and basin-fill history, Sedimentary Geology, 155, 3-4, pp179-208.

Allegre, C. J. and BenOthman, D., 1980, Nd-Sr isotopic relationship in granitoid rocks and continental crust development: a chemical approach to orogenesis, Nature, 286, pp325-342.

Allen, R., Carter, A., Najman, Y., Bandopadhyay, P. C., Chapman, H. J., Bickle, M. J. Garzanti, E. , Vezzoli, G., Andò, S., Foster, G. L., Gerring, C. (2008) New Constraints on the sedimentation and uplift history of the Andaman-Nicobar accretionary prism, South Andaman Island. GSA Special Publication 436, *In Press.*

Allen, R., Najman, Y., Carter, A., Barfod, D., Bickle, M. J., Chapman, H. J., E. Garzanti, E., Vezzoli, G., Ando, S., and Parrish, R., *In Press*, Provenance of the Tertiary sedimentary rocks of the Indo-Burman Ranges, Burma (Myanmar): Burman arc or Himalayan-derived? Journal of the Geological Society, London.

Argand, E., 1924, La tectonique de l' Asie. Proceedings of the 13th International Geological Congress, 7, pp171-372

Auge, T., Cocherie, A., Genna, A., Armstrong, R., Guerrot, C., Mukherjee, M.M., and Patra, R. N., 2003, Age of the Baula PGE mineralization (Orissa, India) and its implications concerning the Singhbhum Archaean nucleus, Precambrian Research, 121, 1-2, pp85-101.

Avouac, J. P., and Burov, E. B., 1996, Erosion as a driving mechanism of intracontinental mountain growth, Journal of Geophysical Research, 101, pp.17,747-17,769

Baksi, S. K., Deb, U., 1981, Palynology of the Upper Cretaceous of the Bengal Basin, India, Reviews in Palaeobotany and Palynology, 31, 3-4, pp335-365.

Bandopadhyay, P.C., 2005, Discovery of abundant pyroclasts in Namunagarh Grit, South Andaman; evidence for arc volcanism and active subduction during the Palaeogene in the Andaman area: Journal of Asian Earth Sciences, 25, pp95–107.

Bandopadhyay, P.C., and Ghosh, M., 1999, Facies, petrology and depositional environment of the Tertiary sedimentary rocks around Port Blair, South Andaman: Journal of the Geological Society of India, 52, pp53–66.

Banerji, R. K., 1984, Post-Eocene biofacies, palaeoenvironments and palaeogeography of the Bengal Basin, India, Palaeogeography, Palaeoclimatology and Palaeoecology, 45, pp49-73.

Barley, M.E., Pickard, A.L., Zaw, K., Rak, P., and Doyle, M.G. 2003. Jurassic to Miocene magmatism and metamorphism in the Mogok metamorphic belt and the India-Eurasia collision in Myanmar. Tectonics, 22, 1019, doi:10.1029/2002TC001398.

Barrow, G., 1893, On an intrusion of muscovite-biotite gneiss in the southeastern highlands of Scotland and its accompanying metamorphism, Journal of the Geological Society, London, 49, pp. 320-360

Batra, R. S., 1989, A reinterpretation of the geology and biostratigraphy of the lower Tertiary formations exposed along the Bilaspur-Shimla Highway, Himachal Pradesh, India, Journal of the Geological Society of India, 33, pp503-523.

Beaumont, C. 1981, Foreland Basins, Geophysical Journal of the Royal Astronomical Society, 65, pp291-329.

Beaumont, C., Jamieson, R. A., Nguyen, M. H. & Lee, B., 2001, Himalayan tectonics explained by extrusion of a low-viscosity, crustal channel coupled to focused surface denudation. Nature, 414, pp738-742.

Beaumont, C., Jamieson, R. A., Nguyen, M. H. & Medvedev, S. 2004. Crustal channel flows: 1. Numerical models with applications to the tectonics of the Himalayan-Tibetan orogen. Journal of Geophysical Research, 109, B06406

Bender, F., 1983, Geology of Burma, Gebruder Borntraeger. Berlin.

Bernet, M., Van der Beek, P., Pik, R., Huyghe, P., Mugnier, J. L., Labrin, E., Szulc, A., 2006, Miocene to Recent exhumation of the central Himalaya determined from combined detrital zircon fission track and U-Pb analysis of Siwalik sediments, western Nepal, Basin Research, 18, 4, pp393-412.

Bertrand, G. & Rangin, C., 2003. Tectonics of the western margin of the Shan plateau (central Myanmar): implication for the India-Indochina oblique convergence since the Oligocene. Journal of Asian Earth Sciences, 21, 10, pp1139-1157.

Bertrand, G., Rangin, C., Maluski, H., and Bellon, H., 2001, Diachronous cooling along the Mogok Metamorphic Belt (Shan scarp, Myanmar): the trace of the northward migration of the Indian syntaxis: Journal of Asian Earth Sciences, 19, pp649–659.

Bertrand, G., Rangin, C., Maluski, H., Han, T.A., Thein, M., Myint, O., Maw, W., and Lwin, S., 1999, Cenozoic metamorphism along the Shan scarp (Myanmar): evidences for ductile shear along the Sagaing fault or the northward migration of the eastern Himalayan syntaxis? : Geophysical Research Letters, 26, pp915–918.

Besse, J. and Courtillot, V., 1988, Palaeogeographic maps of the continents bordering the Indian Ocean since the Early Jurassic, Journal of Geological Physical Research Bulletin, 93, pp1791-1808.

Bhatia, S. B.,1982, Facies, Flora and fauna in the lower Tertiary formations of northwestern Himalayas: a synthesis. The Palaeontological Society of India Special Publication, 1, pp8-20.

Bird, P., 1991, Lateral extrusion of lower crust from under high topography, in the isostatic limit. Journal of Geophysical Research, 91, pp10275–10286.

Biswas, S., Coutand, I., Grujic, D., Hager, C., Stockli, D., and Grasemann, B., 2007, Exhumation and uplift of the Shillong plateau and its influence on the eastern Himalayas: new constraints from apatite and zircon (U-Th-[Sm])/He and apatite fission track analyses, Tectonics, In Press.

Blenkinsop, T.G., 1988, Definition of low grade metamorphic zones using illite crystallinity, Journal of Metamorphic Geology, 6, pp623-636.

Bodet, F., and Schärer, U., 2000, Evolution of the SE-Asian continent from U-Pb and Hf isotopes in single grains of zircon and baddeleyite from large rivers: Geochimica Cosmochimica Acta, 64, pp2067–209.

Brewer, I. D. and Burbank, D. W., 2006, Thermal and kinematic modelling of bedrock and detrital cooling ages in the central Himalaya, Journal of Geophysical Research 111 (B9), Article No. B09409.

Brewer, I.D., Burbank, D.W., and Hodges, K.V., 2003, Modelling detrital cooling-age populations: insights from two Himalayan catchments: Basin Research, 15, pp305–320.

Brookfield, M. E., 1998, The evolution of the great river systems of southern Asia during the Cenozoic India-Asia collision: Rivers draining southwards, Geomorphology, 22, pp285-312.

Brunnschweiler, R. O., 1966. On the Geology of the Indoburman Ranges. Journal of the Geological Society, Australia, 13, pp137-194.

Burbank, D. W., 2002, Rates of erosion and their implications for exhumation, Mineralogical Magazine, 66, 1, pp25-52.

Burbank, D. W., Leland, J., Fielding, E. Anderson, R. S., Brozovic, N., Reid, M. R., and Duncan, C., 1996, Bedrock incision, rock uplift and threshold hillsopes in the northwestern Himalaya, Nature, 379, 6565 , pp505-510.

Burov, E. and Toussaint, G., 2007, Surface processes and tectonics: Forcing of continental subduction and deep processes, Global and Planetary Changes, 58, pp141-164.

Burov, E.B. and Diament, M., 1995, The effective elastic thickness (Te) of continental lithosphere: what does it really mean? Journal of Geophysical Research, 100, pp3905–3927.

Cairn Energy PLC (Edinburgh, Scotland), 1998, Provenance and correlations of Oligocene to Recent sediments, Bay of Bengal, Bangladesh: Constraints from Neodymium isotope and heavy mineral stratigraphy of Sangu-3 and Sangu-3z wells, Internal Report, J978/052.

Cairn Energy PLC (Edinburgh, Scotland), 1999, Heavy mineral assemblages from the Miocene-Recent sequence in Sonadia-1, Bay of Bengal, Bangladesh: Implications for correlation and provenance, Internal Report, HMA/99/01.

Cairn Energy PLC (Edinburgh, Scotland), 2000, A sequence stratigraphic model for the Bengal Basin, Bangladesh, Internal Report, EDEX01176/Oct 2000.

Cairn Energy PLC (Edinburgh, Scotland) SAN-GEO-04-61 Nannofossil Biostrat of Shell Ban Wells, VAROL, 27810

Cairn Energy PLC. (Edinburgh, Scotland), 2005, A Sequence Stratigraphic framework for the Bengal Foredeep, with observations on palaeogeography and palaeoclimate, Internal Report, ED/BANG/GEN/GEO/04/05/1698

Campbell, I.H., Reiners, P.W., Allen, C.M., Nicolescu, S., and Upadhyay, R., 2005, He-Pb double dating of detrital zircons from the Ganges and Indus Rivers: Implication for quantifying sediment recycling and provenance studies: Earth and Planetary Science Letters, 237, pp402–432.

Carter, A. & Bristow, C. S., 2000, Detrital zircon chronology: enhancing the quality of sedimentary source information through improved methodology and combined U-Pb and fission track techniques, Basin Research, 12, 1, pp47-57.

Carter, A., 1999, Present status and future avenues of source region discrimination and characterization using fission track analysis, Sedimentary Geology, 124, 1-4, pp31-45.

Chakraborty, P.P. and Pal, T., 2001. Anatomy of a forearc submarine fan: Upper Eocene-Oligocene Andaman Flysch Group, Andaman Islands, India: Gondwana Research, 4, pp. 477-487.

Chakraborty, P.P. Pal, T., Dutta Gupta, T. and Gupta, K.S., 1999, Facies pattern and depositional motif in an immature trench-slope basin, Eocene Mithakhari Group, Middle Andaman, India: Journal of the Geological Society of India, 53, pp271-284.

Charusiri, P., Clark, A. H., Farrar, E., Archibald, D,. and Charusiri, B., 1993, Granite belts in Thailand: evidence from the $^{40}Ar/^{39}Ar$ geochronological and geological syntheses: Journal of Southeast Asian Earth Sciences: 8, pp127–136.

Chemenda, A.I., Burg, J.-P. and Mattauer, M., 2000, Evolutionary model of the Himalaya–Tibetan system: geopoem based on new modelling, geological and geophysical data, Earth and Planetary Science Letters, 174, pp397–409.

Cherniak, D.J.. and Watson E.B., 2001, Pb diffusion in zircon: Chemical Geology, 172, pp5–24.

Chhibber, H. L., 1934. The Geology of Burma, Macmillan, London.

Chu, M. F., Chung, S. L., Song, B. A., Liu, D. Y., O'Reilly, S. Y., Pearson, N. J., Ji, Y. Q. and Wen, D. J., 2006, Zircon U-Pb and Hf isotope constraints on the Mesozoic tectonics and crustal evolution of southern Tibet, Geology, 34, 9, pp745-748.

Clark, B., 2001, The Structural Evolution of Coastal Eastern Bangladesh, Cairn Energy PLC, Internal Report (Edinburgh, Scotland).

Clark, M.K., House, M.A.,Royden, L.H., Whipple, K.X., Burchfiel, B.C., and Zhang, X.,Tang, W. 2005, Late Cenozoic uplift of southeastern Tibet: Geology, 33, pp525–528.

Clark, M.K., Schoenbaum, L.M., Royden, L., Whipple, K.X., Burchfield, B.C., Zhang, X., Tang, W., Wang, E., and Chen, L. 2004. Surface uplift, tectonics, and erosion of eastern Tibet from large-scale drainage patterns. Tectonics, 23, TC1006doi:10.1029/2002TC001402.

Clift, P. D. and Blusztajn, J., 2005, Reorganisation of the western Himalayan river system after 5 million years ago, Nature, 438, 7070, pp1001-1003.

Clift, P. D., 2006, Controls on the erosion of Cenozoic Asia and the flux of clastic sediment to the ocean, Earth and Planetary Science Letters, 241, 3-4, pp571-580.

Clift, P. D., Campbell, I. H., Pringle, M. S., Carter, A., Zhang, X. F., Hodges, K. V., Khan, A. A. and Allen, C. M., 2004, Thermochronology of the modern Indus River bedload: New insight into the controls on the marine stratigraphic record, Tectonics, 23, 5, Art. No. TC5013.

Clift, P. D., Carter, A., Krol, M., and Kirby, E., 2002a, Constraints on India-Asia collision in the Arabian Sea Region taken from the Indus Group, Ladakh Himalaya, India. In: Clift, P. D., Kroon, D., Craig, J., Gaedicke, C. (Eds.) The Tectonic and climatic evolution of the Arabian Sea region, Geological Society of London, Special Publication, 195, pp97-116.

Clift, P. D., Degnan, P. J., Hannigan, R., and Blusztajn, J., 2000, Sedimentary and geochemical evolution of the Dras forearc basin, Indus suture, Ladakh Himalaya, India, Geological Society of America Bulletin, 112, 3, pp450-466.

Clift, P. D., Lee, J., Hildebrand, P, Shimizu, N., Layne, G. D., Blusztajn, J., Blum, J., Garzanti, E., Khan, A. A., 2002, Nd and Pb isotope variability in the Indus River system: implications for sediment provenance and crustal heterogeneity in the Western Himalaya, Earth and Planetary Science Letter, 200, pp91-106.

Clift, P. D., Gaedicke C., Edwards, R., Lee, J. I., Hildebrand, P., Amjad, S., White, R. S., and Schluter, H. U., 2002b, The stratigraphic evolution of the Indus Fan and the history of sedimentation in the Arabian Sea, Marine Geophysical Researches, 23, 3, pp223-245.

Clift, P. D., Shimizu, N., Layne, G. D., and Blusztajn, J., 2001a, tracing patterns of erosion and drainage in the Palaeogene Himalaya through ion probe Pb isotope analysis of detrital K-feldspars in the Indus Molasse, India, Earth and Planetary Science Letters, 188, 3-4, pp475-491.

Clift, P. D., Shimizu, N., Layne, G. D., Blusztajn, J., Gaedicke, C., Schluter, H.-U., Clark, M. K., and Amjad, S., 2001b, Development of the Indus Fan and its significance for the erosional history of the western Himalaya and the Karakoram, Geological Society of America Bulletin, 113, pp1039-1051.

Cochen, M., Le Fort, P and Pecher, A., 1986, Annapurna-Manaslu-Ganesh Himal: Paris, Centre National de la Recherche Scientifique, pp136.

Cochran, J. R., 1990, Himalayan uplift, sea level, and the record of Bengal Fan sedimentation at the ODP leg 116 sites. In: Cochran, J. R., Stow, D. A. V. et al. (eds), Proceedings of the Ocean Drilling Program. Scientific Results, 116, pp397-414.

Colin, C., Bertaux, J., Turpin, L., and Kissel, C., 2001, Dynamics of the erosion in the Irrawaddy River basin during the last two climatic cycles (280-0 ka): Comptes Rendus De L Academie Des Sciences Serie Ii Fascicule a-Sciences de la Terre et des Planetes, 332, pp483-489.

Colin, C., Turpin, L., Bertaux, J., Desprairies, A., and Kissel, C., 1999, Erosional history of the Himalayan and Burman ranges during the last two glacial-interglacial cycles: Earth and Planetary Science Letters, 171, pp647–660.

Colin, C., Turpin, L., Bertaux, J., Frank, N., Kissel, C., and Duchamp, S., 2006, Evolution of weathering patterns in the Indo-Burman Ranges over the last 280 kyr:

Effects of sediment provenance on $^{87}Sr/^{86}Sr$ ratios tracer: Geochemistry, Geophysics, Geosystems, v7. doi:10.1029/2005GC000962.
Copeland, P. and Harrison, T. M., 1990, Episodic rapid uplift in the Himalaya revealed by $^{40}Ar/^{39}Ar$ analysis of detrital K-feldspar and muscovite, Bengal Fan, Geology, 18, pp354-357.

Copeland, P., Harrison, T. M., Hodges, K. V., Maraejol, P., Le Fort, P and Pecher, P., 1991, An early Pliocene thermal disturbance of the main central thrust, Central Nepal: implications for Himalayan tectonics, Journal of Geophysical Research, 96, pp8475-8500.

Critelli, S. and Garzanti, E., 1994, Provenance of the Lower Tertiary Murree redbeds (Hazara-Kashmir Syntaxis, Pakistan) and initial rising of the Himalayas, Sedimentary Geology, 89, pp265-284.

Critelli, S. and Ingersoll, R. V., 1994, Sandstone petrology and provenance of the Siwalik Group (northwestern Pakistan and western-southeastern Nepal, Journal of Sedimentary Research A- Sedimentary Petrology and Processes, 64, 4, pp815-823.

Critelli, S., De Rosa, R. and Platt, J. P., 1990, Sandstone detrital modes in the Makran Accretionary prism, southwest Pakistan: implications for tectonic setting and long distance turbidite transportation, Sedimentary Geology, 68, pp241-260.

Curray, J. R. and Moore, D. G., 1971, Growth of Bengal Deep-Sea Fan and denudation in Himalayas, Geological Society of America Bulletin, 82, 3, pp563.

Curray, J. R. and Moore, D. G., 1974, Sedimentary and Tectonic processes in Bengal deep-sea fan and geosyncline. In: Burk, C. A., Drake, C. L. (Eds.), The Geology of Continental Margins, Springer, New York, pp.617-628.

Curray, J.R., Moore, D.G., Lawver, L.A., Emmel, F.J., Raitt, R.W., Henry, M. and Kieckhefer, R., 1979. Tectonics of the Andaman Sea and Burma. In: Watkins, J., Montadert, L., Dickerson, P.W. (Eds.), Geological and Geophysical Investigations of Continental Margins: American Association Petroleum Geologists, Memoir, 29, pp189–198.

Curray, J. R., Emmel, F. J., Moore, D. G., and Raitt, R. W., 1982, Structure, tectonics and geological history of the northeastern Indian Ocean. In: Nairn, A. E. M., Stehli, F. G. (Eds.) The Ocean Basins and Margins, The Indian Ocean, 6, Plenum Press, New York, pp399-450.

Curray, J. R., 1994, Sediment volume and mass beneath the Bay of Bengal, Earth and Planetary Science Letters, 125, pp371-383.

Curray, J. R., Emmel, F. J., and Moore, D. G., 2003, The Bengal Fan: Morphology, geometry, stratigraphy, history and processes, Marine and Petreoleum Geology, 19, pp1191-1223.

Curray, J. R., 2005, Tectonics and history of the Andaman Sea region, Journal of Asian Earth Sciences, 25, 1, pp187-232.

Daley, T. and Alam, Z., 2002, Seismic stratigraphy of the offshore Indus Basin, Geological Society Special Publication, 195, pp259-271.

Davies, C., Best, J. and Collier, R., 2003, Sedimentology of the Bengal shelf, Bangladesh: comparison of Late Miocene sediments, Sitakund anticline, with the modern tidally dominated shelf, Sedimentary Geology, 155, pp271-300.

Davies, T. A., Kidd, R. B. and Ramsey, A. T. S. 1995. A time-slice approach to the history of Cenozoic sedimentation in the Indian Ocean, Sedimentary Geology, 96, pp157-179.

Debon, F., Le Fort, P., Sheppard, S. M. F. and Sonet, J., 1986, The four plutonic belts of the Transhimalaya-Himalaya: a chemical, mineralogical, isotopic and chronological synthesis along a Tibet-Nepal section, Journal of Petrology, 27, 1, pp219-250.

DeCelles, P. G., Gehrels, G. E., Quade, J., and Ojha, T. P., 1998a, Eocene-early Miocene foreland basin development and the History of Himalayan thrusting, western and central Nepal, Tectonics, 17, pp741-765.

DeCelles, P. G., Gehrels, G. E., Quade, J., Ojha, T. P., Kapp, P. A., and Upreti, B. N., 1998b, Neogene foreland basin deposits, erosional unroofing, and the kinematic history of the Himalayan fold-thrust belt, western Nepal, Geological Society of America Bulletin, 110, 1, pp2-21.

DeCelles, P.G., Gehrels, G.E., Quade, J., LaReau, B. and Spurlin, M. 2000. Tectonic implications of U-Pb zircon ages of the Himalayan orogenic belt in Nepal, Science, 288, 5465, pp497-499.

DeCelles, P. G., Robinson, D. M., Quade, J., Ojha, T. P., Garzione, C. N., Copeland, P., and Upreti, B. N., 2001, Stratigraphy, structure, and tectonic evolution of the Himalayan fold-thrust belt in western Nepal, Tectonics, 20, 4, pp487-509.

DeCelles, P. G., Gehrels, G. E., Najman, Y., Martin, A. J., Garzanti, E., 2004, Detrital geochronology and geochemistry of Cretaceous-Early Miocene strata of Nepal: implications for timing and diachroneity of initial Himalayan orogenesis, Earth and Planetary Science Letters, 227, pp313-330.

Dewey, J. F., Shackleton, R. M., Chang, Chenga, ad Sun, Yiyin, 1988, The Tectonic Evolution of the Tibetan Plateau, Philosophical Transactions of the Royal Society of London, 327, pp379-413.

Dickinson, W.R,. 1985. Interpreting provenance relations from detrital modes of sandstones: Provenance of arenites, G.G. Zuffa, ed., NATO ASI , Reidel, Dordrecht, 148, pp333–361.

Ding, L., Kapp, P., and Wan, X., 2005, Palaeocene-Eocene record of ophiolite obduction and initial India-Asia collision, south central Tibet, Tectonics, 24, TC3001, doi:10.1029/2004TC001729.

Draut, A.E., and Clift, P.D., 2006, Sedimentary processes in modern and ancient oceanic arc settings; Evidence from the Jurassic Talkeetna Formation of Alaska and the Mariana and Tonga Arcs, western Pacific: Journal of Sedimentary Research, 76, pp493–514.

England, P. and Searle, M. 1986, The Cretaceous-Tertiary deformation of the Lhasa block and its implications for crustal thickening in Tibet, Tectonics, 5, pp1-14.

Evans, P., 1932, Tertiary Succession in Assam, Transactions of the Mining and Geological Institute of India, 27, pp155-260.

Farley, K. A., 2000, Helium diffusion from apatite: General behavior as illustrated by Durango fluorapatite, Journal of Geophysical Research-Solid Earth, 105, pp2903-2914.

Fielding, E. J., 1996, Tibet Uplift and erosion, Tectonophysics, 260, 1-3, pp55-84.

Fitch, T. J. 1972. Plate convergence, transcurrent faults, and internal deformation adjacent to Southeast Asia and western pacific, Journal of Geophysical Research, 77, 23, pp4432-

Foster, G., Kinny, B., Vance, D., Prince, C., Harris, N., 2000, The significance of monazite U-Th-Pb age data in metamorphic assemblages; a combined study of monazite and garnet chronometry, Earth and Planetary Science Letters, 181, pp327-340.

Foster, G.L., and Vance, D. 2006. In situ Nd isotopic analysis of geological materials by laser ablation MC-ICP-MS: Journal of Analytical Atomic Spectrometry, 21, pp288-296.

France-Lanord, C. and Derry, L. A., 1997, Organic carbon burial forcing of the carbon cycle from Himalayan erosion, Nature, 390, pp65-67.

Gaetani, M., Garzanti, E., 1991, Multicyclic history of the northern India continental margin (northwestern Himalaya), The American Association of Petroleum Geologists Bulletin, 75, pp1427-1446.

Galbraith R.F. and Green, P.F., 1990, Estimating the component ages in a finite mixture: Nuclear Tracks and Radiation Measurement, 17, pp197–206.

Galbraith, R.F. and Laslett, G.M., 1993, Statistical models for mixed fission track ages: Nuclear. Tracks and Radiation Measurement, 21, pp459–470.

Gallagher, K., 1995, Evolving temperature histories from apatite FT data: Earth Planetary Science Letters, 136, pp421–435.

Galy, A. and France-Lanord, C., 2001, Higher erosion rates in the Himalaya: Geochemical constraints on riverine fluxes, Geology, 29, pp23–26.

Galy, A., France-Lanord, C. and Derry, L. A., 1996. The late Oligocene-early Miocene Himalayan belt constraints deduced from isotopic compositions of early Miocene turbidites in the Bengal Fan, Tectonophysics, 260, pp109-118.

Galy, A., France-Lanord, C. and Derry, L. A., 1999, The strontium isotopic budget of Himalayan Rivers in Nepal and Bangladesh, Geochimica et Cosmochimica Acta, 63, No. 13/14, pp1905–1925.

Galy, V., France-Lanord, C., Beyssac, O, Faure, P., Kudrass, H., Palhol, F., 2007, Efficient organic carbon burial in the Bengal fan sustained by the Himalayan erosional system, Nature, 450, pp407-411.

Gani, M. R. And Alam, M. M., 1999, Trench-slope controlled deep-sea clastics in the exposed lower Surma Group in the southeastern fold belt of the Bengal Basin, Bangladesh, Sedimentary Geology, 127, 3-4, pp221-236.

Gani, M. R. and Alam, M. M., 2003, Sedimentation and basin-fill history of the Neogene clastic succession exposed in the southeastern fold belt of the Bengal Basin Bangladesh: a high-resolution sequence stratigraphic approach, Sedimentary Geology, 155, 3-4, pp227-+

Gani, M. R. and Alam, M. M., 2004, Fluvial facies architecture in small-scale river systems in the Upper Dupi Tila Formation, northeast Bengal Basin, Bangladesh, Journal of Asian Earth Sciences, 24, 2, pp225-236.

Gansser, A., 1964, Geology of the Himalayas, Interscience Publishers, London.

Garzanti E., and Vezzoli, G., 2003, A classification of metamorphic grade in sands based on their composition and grade: Journal of Sedimentary Research, 73, pp830–837.

Garzanti, E and Van Haver, T., 1988, The Indus Clastics, fore-arc basin sedimentation in the Ladakh Himalaya (India), Sedimentary Geology, 59, 3-4, pp237-249.

Garzanti, E., Baud, A. and Mascle, G., 1987. Sedimentary record of the northward flight of India and its collision with Eurasia (Ladakh Himalaya, India), Geodinamica Acta 1, pp297-312.

Garzanti, E., Vezzoli, G., Ando, S., France-Lanord, C., Singh, S. K. and Foster, G., 2004, Sand petrology and focused erosion in collision orogens: the Brahmaputra case, Earth and Planetary Science Letters, 220, 1-2, pp157-174.

Garzanti, E., Vezzoli, G., Ando, S., Lave, J., Attal, M., France-Lanord, C., DeCelles,P., 2007, Quantifying sand provenance and erosion (Marsyandi River, Nepal Himalaya), Earth and Planetary Science Letters, 258, 3-4, pp500-515.

Gautam, P. & Fujiwara, Y. 2000. Magnetic polarity stratigraphy of the Siwalik group sediments of Karnali River section in western Nepal, Geophysical Journal International, 142, pp812-824.

Godin, L., Brown, R. L., Hanmer, S. and Parrish, R. R., 1999, Back folds I the core of the Himalayan orogen: an alternative interpretation, Geology, 27, pp151-154.

Green, P.F., Duddy, I.R., and Bray, R.J., 1995, Applications of thermal history reconstruction in inverted basins: In: Buchanan, J. G. and Buchanan, P. G. (eds.), Basin Inversion. Geological Society of London Special Publication No. 88, pp149–165.

Grujic, D., Casey, M., Davidson, C., Hollister, L. S., Kundig, R., Pavlis, T. and Schmid, S. 1996. Ductile extrusion of the Higher Himalayan Crystalline in Bhutan: evidence from quartz microfabrics, Tectonophysics, 260, pp21-43.

Grujic, D., Coutand, I., Bookhagen, B., Bonnet, S. and Blythe, A., 2006, Climatic forcing of erosion, landscape, and tectonics in the Bhutan Himalayas, Geology, 34, 10, pp801-804.

Grujic, D., Hollister, L. S. and Parrish, R. R., 2002. Himalayan metamorphic sequence as an orogenic channel: insight from Bhutan, Earth and Planetary Science Letters, 198, pp177-191.

Guha, D. K., and Mohan, M., 1965, On the Ostracod from the Neogene of Andaman Island: Journal of the Geological Survey of India, 9, pp58–66.

Guillot, S., Garzanti, E., Baratoux, D., Marquer,D., Mahéo, G. and de Sigoyer, J., 2003, Reconstructing the total shortening history of the NW Himalaya: Geochemistry, Geophysics, Geosystems, 4, pp1064, doi:10.1029/2002GC000484.

Haines P.W., Turner S.P., Kelley S.P, Wartho J-A., and Sherlock S.C., 2004, Ar/Ar dating of detrital muscovite in provenance investigations: A case study from the Adelaide Rift Complex, South Australia: Earth and Planetary Science Letters, 227, pp297–311.

Halder, D., 1985. Some Aspects of the Andaman Ophiolite Complex: Geological Survey of India, 115, pp1–11.

Harris, N., 2007, Channel flow and the Himalayan-Tibetan orogen: a critical review, Journal of the Geological Society, 164, pp511-523.

Harrison, T.M., 2004, Did molten Tibetan middle crust create the Himalaya via channel flow?, *in* Searle, M.P., et al., eds., Channel fl ow, ductile extrusion and exhumation of lower-mid crust in continental collision zones [abstract]: Geological Society [London], 6–7 December 2004, pp16–17.

Hayes, J. M., Strauss, H and Kaufman, A. J., 1999, The abundance of ^{13}C in marine organic matter and isotopic fractionation in the global biogeochemical cycle of carbon during the past 800 Ma, Chemical Geology, 161, pp103-125.

Heroy, D. C., Kuehl, S. A. and Goodbred, S. L., 2003, Mineralogy of the Ganges and Brahmaputra Rivers: Implications for river switching and late Quaternary climate change, Sedimentary Geology, 155, pp343-359.

Hiller, K., 1988, On the petroleum geology of Bangladesh. Geol. Jahrb. D, 90, pp3–322.

Hodges, K. V., 2000, Tectonics of the Himalaya and southern Tibet from two perspectives, Geological Society of America Bulletin, 112, pp 324-350.

Hodges, K. V., Parrish, R. R., Searle, M. P., 1996, Tectonic evolution of the central Annapurna Range, Nepalese Himalaya, Tectonics, 15, pp1264-1291.

Hovius, N., 1998, Controls on sediment supply by large rivers, in Climate and tectonics in continental rocks, Shanley, K. W., McCabe, P. J., S. E. P. M. Special Publication, 59, pp3-16.

Hurford, A. J. 1986. Cooling and uplift patterns in the Lepontine Alps, South Central Switzerland and an age of vertical movement on the Insubric fault line, Contrib Mineral Petrol, 92, pp413-427.

Hurford, A.J., 1990, Standardization of fission track dating calibration: recommendation by the Fission Track Working Group of the IUGS Subcommission on geochronology: Chemical Geology, 80, pp177–178.

Hutchinson, C. S., 1989. Geological Evolution of South-East Asia, Oxford University Press, New York.

Huyghe P., Mugnier, J. L., Gajurel, A. P. and Delcaillau, B., 2005, Tectonic and climatic control of the changes in the sedimentary record of the Karnali River section (Siwaliks of western Nepal), Island Arc, 14, 4, pp311-327.

Ingersoll, R. V., Graham, S. A. and Dickinson, W. R., 1995, Remnant Ocean Basins. In: Busby, C. J., Ingersoll, R. V. (Eds.) Tectonics of Sedimentary Basins, Blackwell Science, Oxford, pp363-391.

Ingersoll, R.V and Suczek, C.A., 1979, Petrology and provenance of Neogene sand from Nicobar and Bengla Fans, DSDP sites 211 and 218: Journal of Sedimentary Petrology, 49, pp1217–1228.

M.R. Islam, S.F. Begum, Y. Yamaguchi, K. Ogawa, 1999, The Ganges and Brahmaputra rivers in Bangladesh: basin denudation and sedimentation, Hydrological Processes, 13, 2907-2923.

Jamieson, R. A., Beaumont, C., Medvedev, S., Nguyen, M. H. 2004. Crustal channel flows: 2. Numerical models with implications for metamorphism in the Himalayan-Tibetan orogen, Journal of Geophysical Research, 109, B06407

Jamieson, R. A., Beaumont, C., Nguyen, M. H. and Grujic, D., 2006, Channel flow, ductile extrusion and exhumation in continental collision zones, Geological Society Special Publication, 268, pp165-182.

Johnson, S. Y. and Nur Alam, A. M., 1991, Sedimentation and Tectonics of the Sylhet Trough, Bangladesh, Geological Society of America Bulletin, 103, 11, pp1513-1527.

Karunakaran, C. Ray, K. K., and Saha, S. S., 1968, Tertiary sedimentation in Andaman-Nicobar geosyncline: Journal of the Geological Society of India, 9 pp32–39.

Kelley, S.P., 1995, Ar-Ar dating by laser microprobe. In: Potts, P.J., Bowles, J.F.W., Reed, S.J.B. and Cave, M.R. (eds). Microprobe Techniques in the Earth Sciences. Chapman & Hall, London.

Ketcham, R.A., Donelick, R.A., and Carlson, W.D., 1999, Variability of apatite fission-track annealing kinetics: III Extrapolation to geological time-scales: American Mineralogist, 84, pp1235–1255.

Khan, M. R. and Muminullah, M., 1980, Stratigraphy of Bangladesh. Proceedings of Petroleum and Mineral Resources of Bangladesh. Ministry of Petroleum and Mineral Resources, Government of Bangaldesh, pp35-40.

Khan, P.K., and Chakraborty, P, P., 2005, Two-phase opening of Andaman Sea: a new seismotectonic insight: Earth and Planetary Science Letters, 229, pp259-271.

Kitoh, A., 2004, Effects of mountain uplift on East Asian summer climate investigated by a coupled Atmosphere – Ocean GCM, Journal of Climate, 17, 4, pp783-802.

Klootwijk, C. T., Gee, J. S., Peirce, J. W., Smith, G. M. and Mcfadden, P. L. 1992. A early India-Asia contact: Palaeomagnetic constraints from Ninetyeast Ridge, ODP Leg 121, Geology, 20, pp395-398.

Kubler, B., 1967, La crystallinite de l'illite et les zones tout a fait superieurs du metamorphisme: Colloque sur les 'Etages tectoniques'. Neuchatel, Festschrift, pp105-122.

Kumar, R., Lal, N., Singh, S., and Jain, A. K., 2007, Cooling and exhumation of the Transhimalayan batholith as constrained by fission track apatite and zircon ages, Current Science, 92, 4, pp490-496.

Lee, T.T., and Lawver, L.A., 1995, Cenozoic plate reconstruction of Southeast Asia: Tectonophysics, 251, pp85–138.

Liang, Y. H., Chung, S. L., Liu, D., Xu, Y., Wu, F.-Y., Yang, J.-H., Wang, Y. and Lo, C.-H., Detrital zircon evidence from Burma for reorganization of the eastern Himalayan river system, American Journal of Science, in press subject to revision.

Lindsay, J. F., Holliday, D. W., Hulbert, A. G., 1991, Sequence Stratigraphy and the evolution of the Ganges-Brahmaputra Delta Complex, The American Association of Petroleum Geologists Bulletin, 75, pp1233-1254.

Lohmann, H. H., 1995, On the tectonics of Bangladesh, Swiss Assoc. Pet. Geol. Eng. Bull., 62, 140, pp29– 48.

Mallik, T.K., 1976, Shelf sediments of the Ganges delta with special emphasis on the mineralogy of the western part, Bay of Bengal, Indian Ocean: Marine Geology, 22, pp1–32.

Mandal, B. C. and Woobaidullah, A. S. M., 2006, Sedimentary tectonics of the Eastern Fold Belt of the Bengal Basin, Bangladesh, Journal of the Geological Society of India, 68, 1, pp115-128.

Marsaglia, K.M., and Ingersoll, R.V., 1992, Compositional trends in arc-related, deep-marine sand and sandstone; a reassessment of magmatic-arc provenance, Geological Society of America Bulletin: 104, pp1637–1649.

Mathur, N. S., 1978, Biostratigraphical aspects of the Subathu Formation, Kumaun Himalaya, Recent Researches in Geology, 5, pp96-112.

Maung, H., 1987, Transcurrent movement in the Burma-Andaman Sea region, Geology, 15, 10, pp911-912.

Martini, E., 1971, Standard Tertiary and Quaternary calcareous nannoplankton zonation, in Farinacci, A. (Ed.) Proceedings II Planktonic Conference, Rome, 1970, 2, 739-785.

Maung, H., 1987, Transcurrent movements in the Burma-Andaman Sea region, Geology, 15, 10, pp911-912.

McDougall, I and Harrison, T. M., 1999, Geochronology and Thermochronology by the $^{40}Ar/^{39}Ar$ method, Oxford University Press, Oxford, pp 269.

Meesters A. G. C. A., and Dunai T. J., 2002, Solving the production diffusion equation for finite diffusion domains of various shapes; Part II, Application to cases with alpha -ejection and nonhomogeneous distribution of the source: Chemical Geology, 186, pp57–73.

Metcalfe, I., 1996, Pre-Cretaceous evolution of SE Asian terranes. In: Hall, R. and. Blundell, D. (eds.) Tectonic Evolution of Southeast Asia. Geological Society Special Publication, 106, pp97–122.

Metivier, F., Gaudermer, Y., Tapponier, P. and Klein, M., 1999, Mass accumulation rates in Asia during the Cenozoic, Geophysical Journal International, 137, 2, pp280-318.

Mishra sS., Deomurari m.p., Wiedenbeck m., Goswami J.n., Ray s. and Saha a.k., 1999, pb-207/pb-206 zircon ages and the evolution of the Singhbhum Craton, eastern India: an ion microprobe study, Precambrian Research, 93, 2-3, pp139-151.

Mishra, M. and Rajamani, V. 1999, Significance of the Archaean bimodal volcanics from the Ramagiri schist belt in the formation of the Eastern Dharwar craton: Journal of the Geological Society of India, 54, pp563-583.

Misra, S. and Johnson, P.T., 2005, Geochronological constraints on evolution of Singhbhum Mobile Belt and associated basic volcanics of eastern Indian shield,Gondwana Research, 8, 2, pp129-142.

Mitchell, A. H. G., 1974. Flysch-ophiolite successions: polarity indicators in arc and collision type orogens, Nature, 248, pp747-749.

Mitchell, A. H. G., Htay, M. T., Htun, K. M., Win, M. N., Oo, T. and Hlaing, T., 2007. Rock relationships in the Mogok metamorphic belt, Tatkon to Mandalay, central Myanmar, Journal of Asian Earth Sciences, 29, 5-6, pp891-910.

Mitchell, A.H.G., 1993, Cretaceous–Cenozoic tectonic events in the western Myanmar (Burma)–Assam region, Journal of the Geological Society, 150, pp1089–1102.

Molnar, P. and Tapponier, P., 1975, Cenozoic tectonics of Asia: Effects of a continental collision, Science, 189, pp419-426.

Molnar, P., England, P. and Martinod, J., 1993, Mantle dynamics, uplift of the Tibetan Plateau, and the Indian Monsoon, Reviews in Geophysics, 31, 4, pp357-396.

Moore, D. G., Curray, J. R., Raitt, R. W. and Emmel, F. J., 1974. Stratigraphic-seismic section correlations and implications to Bengal Fan history, *Initial Reports of the Deep Sea Drilling Project*, pp211-218 (sites)

Mountain, G. S. and Prell, W. L., 1990, A multiphase plate tectonic history of the southeast continental margin of Oman, *in* Robertson, A. H. F., Searle, M. P., Reis, A. C., eds., The geology and tectonics of the Oman region: Geological Society (London) Special Publication 49, pp725–743.

Najman, Y. and Garzanti, E., 2000, Reconstructing early Himalayan tectonic evolution and palaeogeography from Tertiary foreland basin sedimentary rocks, northern India, Geological Society of America Bulletin, 112, 3, pp435-449.

Najman, Y., 2006, The detrital record of orogenesis: A review of approaches and techniques used in the Himalayan sedimentary basins, Earth Science Reviews, 74, 1-2, pp1-72.

Najman, Y., Bickle, M., and Chapman, H., 2000, Early Himalayan exhumation: Isotopic constraints from the Indian foreland basin: Terra Nova, 12, pp28–34.

Najman, Y., Bickle, M., Boudagher-Fadel, M., Carter, A., Garzanti, E., Paul, M., Wijbrans, J., Willett, E., Oliver, G., Parrish, R., Akhter, H., Allen, R., Ando, S., Christy, E., Reisberg, L. and Vezzoli, G., 2008, The 'missing' record of Himalayan erosion, Bengal Basin, Bangladesh, Earth and Planetary Science Letters, In Press.

Najman, Y., Carter, A., Oliver, G. and Garzanti, E., 2005, Provenance of early foreland basin sediments, Nepal: constraints to the timing and diachroneity of early Himalayan orogenesis, Geology, 33, pp309-312.

Najman, Y., Garzanti, E., Pringle, M., Bickle, M., Stix, J. and Khan, I., 2003, Early-Middle Miocene palaeodrainage and tectonics in the Pakistan Himalaya, Geological Society of America Bulletin, 115, 10, pp1265-1277.

Najman, Y., Johnson, C., White, N. W. and Oliver, G., 2004, Constraints on foreland basin and orogenic evolution from detrital mineral fission track analyses and sediment facies of the Himalayan foreland basin, NW India, Basin Research, 16, pp1-24.

Najman, Y., Pringle, M. S., Johnson, M. R. W., Robertson, A. H. F., Wijbrans, J. R., 1997, Laser 40Ar/39Ar dating of single grains from early foreland basin sediments in India: implications for early Himalayan evolution, Geology, 25, pp535-538.

Najman, Y., Pringle, M., Bickle, M., Garzanti, E., Burbank, D., Ando, S. & Brozovic, N., 2003b, Non-steady-state exhumation of the Higher Himalaya, N. W. India: insights from a combined isotopic and sedimentological approach, Geophysical Research Abstracts, 5, abstr 04551.

Najman, Y., Pringle, M., Godin, L. and Oliver, G., 2001, Dating of the oldest continental sediments from the Himalayan foreland basin, Nature, 410, pp194-197.

Najman, Y., Pringle, M., Godin, L. and Oliver, G., 2002a, A reinterpretation of the Balakot Formation: implications for the tectonics of the NW Himalaya, Pakistan, Tectonics, 21, pp7-18.

Nelson, K. D., Zhao, W., Brown, L. D., Kuo, J., Che, J., Liu, X., 1996, Partially molten middle crust beneath Southern Tibet: synthesis of project INDEPTH results, Science, 274, 5293, pp1684-1688.

Ni, J. F., Guzman-Speziale, M., Bevis, M., Holt, W. E., Wallace, T. C. and Seager, W. R., 1989, Accretionary tectonics of Burma and the 3D geometry of the Burma Subduction zone, Geology, 17, pp.68-71.

Oldham, R. D, 1885. Notes on the geology of Andaman Islands: Record of the Geological Survey of India. 18 (3), pp135–145.

Pal, T., Chakraborty, P.P., Gupta, T.D., and Singh, C.D., 2003, Geodynamic evolution of the outer-arc-forearc belt in the Andaman Islands, the central part of the Burma-Java subduction complex: Geology Magazine, 140, pp289–307.

Pal, T., Gupta, T.D., Chakraborty, P.P., and Gupta, S.C.D., 2005, Pyroclastic deposits of Mio-Pliocene age in the Arakan Yoma-Andaman-Java subduction complex, Andaman Islands, Bay of Bengal, India: Geochemical Journal, 39, pp69–82.

Pande, K., Sarin, M. M., Trivedi, J. R., Krishnaswami and Sharma, K. K., 1994, The Indus River system (India-Pakistan): Major-ion chemistry, uranium and strontium isotopes, Chemical Geology, 116, pp245-259.

Parrish, R. R. and Hodges, K. V., 1996, Isotopic constraints on the age and provenance of the Lesser and Greater Himalayan sequences, Nepalese Himalaya, Geological Society of America Bulletin, 108, 7, pp904-911.

Patriat, P. and Achache, J., 1984, India-Eurasia collision chronology has implications for crustal shortening and driving mechanisms of plates, Nature, 311, pp 615-621.

Peltzer, F. and Saucier, F., 1996, Present-day kinematics of Asia, derived from geologic fault rates, Journal of Geophysical Research, 101, 27, pp.27,943-27,956.
Peucat, J.J., Vidal, P., Bernard-Griffiths J., and Condie, K.C., 1989, Sr, Nd and Pb isotopic systematics in the Archaean low-to-high-grade transition zone of southern India:Syn-accretion granulites: Journal of Geology, 97, pp537–550.

Pivnik, D.A., Nahm, J., Tucker, R.S., Smith, G.O., Nyein, K., Nyunt, M., and Maung, P.H., 1998, Polyphase deformation in a fore-arc/back-arc basin, Salin sub-basin, Myanmar (Burma): American Association of Petroleum Geologists Bulletin, 82, pp1837–1856.

Prell, W. W. and Kutzbach, J. E., 1992, Sensitivity of the Indian monsoon to forcing parameters and implications for its evolution, Nature, 5, pp66-92.

Qayyum, M., Niem, A. R. and Lawrence, R. D., 1997, Newly discovered Palaeogene deltaic sequence in Katawaz basin, Pakistan, and it's tectonic implications, Geology, 24, pp835-838.

Quade, J., Cater, J. M. L., Ojha, T. P., Adam, J. and Harrison, T. M., 1995, Late Miocene environmental change in Nepal and the northern Indian subcontinent: stable isotope evidence from paleosols, Geological Society of America Bulletin, 107, pp1381-1397.

Rahman, M. J. J. and Faupl, P., 2003, Ar-Ar multigrain dating of detrital white mica of sandstones of the Surma Group in the Sylhet Trough, Bengal Basin, Bangladesh, Sedimentary Geology, 155, pp383-392.

Ratschbacher, L., Frisch, W., Liu, G. and Chen, C., 1994, Distributed deformation in southern and western Tibet during and after India-Eurasia collision, Journal of Geophysical Research, 99, pp19917-19945.

Ray, K. K., Sengupta, S. and Van Den Hul, H. J., 1988, Chemical characters of volcanic rocks from Andaman ophiolite, India: Journal of the Geological Society of London, 145, pp392–400.

Raymo, M. E. and Ruddinman, W. F., 1992, Tectonic forcing of late Cenozoic climate, Nature, 359, pp117-122.

Reimann, K.-U., 1993, Geology of Bangladesh, Borntraegar, Berlin, pp 154.

Renne, P.R., Swisher, C.C., Deino, A.L., Karner, D.B., Owens, T.L., and DePaolo, D.J., 1998, Intercalibration of standards, absolute ages and uncertainties in $^{40}Ar/^{39}Ar$ dating: Chemical Geology, 145, pp117–152.

Replumaz, A. and Tapponier, P., Reconstruction of the deformed collision zone between India and Asia by backward motion of lithospheric blocks, Journal of Geophysical Research-Solid Earth, 108, Art. No. 2285

Richter, F. M., Rowley, D. B. and DePaolo, D. J., 1992. Sr isotope evolution of seawater: the role of tectonics, Earth and Planetary Science Letters, 109, pp11-23.

Robinson, D. M., DeCelles, D. G. and Copeland, P., 2006, Tectonic evolution of the Himalayan thrust belt in western Nepal: Implications for channel flow models, Geological Society of America Bulletin, 118, 7/8, pp.865-885

Robinson, D. M., DeCelles, P. G., Patchett, P. J. and Garzione, C. N., 2001, The kinematic evolution of the Nepalese Himalaya interpreted from Nd isotopes, Earth and Planetary Science Letters, 192, pp507-521.

Rowley, D. B., 1996, Age of initiation of collision between India and Asia: A review of stratigraphic data: Earth and Planetary Science Letters, 145, pp1–13.

Rowley, D. B., 1998, Miminum age of inititation of collision between India and Asia north of Everest based on the subsidence history of the Zhepure mountain section, Journal of Geology, 106, pp229-235.

Roy, S.K., 1992, Accretionary prism in Andaman forearc: Geological Survey India Special Publication, 29, pp273–278.

Roy, T.K., 1983. Geology and hydrocarbon prospects of Andaman–Nicobar basin: In: Bhandari, L.L. (Ed.), Petroliferous Basins of India Petroleum Asia Journal, pp37–50.

Ruhl, K. W. and Hodges, K. V., 2005, The use of detrital mineral cooling ages to evaluate steady state assumptions in active orogens: An example from the central Nepalese Himalaya, Tectonics, 24, 4, Art No. TC4015

Saha, A., Basu, A.R., Garzione, C.N., Bandyopadhyay P.K., and Chakrabarti, A., 2004, Geochemical and petrological evidence for subduction-accretion processes in the Archean Eastern Indian Craton: Earth and Planetary Science Letters, 220, pp91–106.

Sakai, H., 1983. Geology of the Tansen Group of the Lesser Himalaya in Nepal, Memoirs of the Faculty of Science, Kyushu University, Series D, 25, pp27-74

Sakai, H., 1989, Rifting of the Gondwanaland and uplifting og the Himalaya recorded in Mesozoic and Tertiary fluvial sediments in Nepal Himalayas, In: Taira, A. and Masuda, F. (eds) Sedimentary facies in the Active Plate Margin, Terra Pub. Co., Tokyo, pp723-732.

Salt, C. A., Alam, M. M. and Hossain, M. M., 1986, Bengal Basin: Current exploration of the Hinge Zone of southwestern Bangladesh, Proceedings of the 6th Offshore southeast Asia conference, Singapore, pp55-67.

Sambridge, M. S., and Compston, W., 1994, Mixture modelling of multi-component data sets with application to ion-probe zircons: Earth and Planetary Science Letters, 128, pp373–390.

Satyabala, S. P., 2003, Oblique plate convergence in the Indo-Burma (Myanmar) subduction region, Pure Applied Geophysics, 160, 9, pp1611-1650.

Schlup, M., Carter, A., Cosca, M. and Steck, A., 2003, Exhumation history of eastern Ladakh revealed by ^{40}Ar-^{39}Ar and fission track ages: the Indus River-Tso Morari transect, NW Himalaya, Journal of the Geological Society, 160, pp385-399.

Searle, M. P. and Tirrul, R., 1991, Structural and thermal evolution of the Karakoram crust, Journal of the Geological Society, London, 148, pp65-82.

Searle, M. P., 1996, Cooling historym erosion, exhumation and kinematics of the Himalaya-Karakoram-Tibet orogenic belt. In: Harrison, T. M., Yin, A., (eds.), The Tectonic Evolution of Asia, Cambridge University Press, pp110-137.

Searle, M. P., Corfield, R. I., Stephenson, B. and Mccarron, J. 1997. Structure of the north Indian continental margin in the Ladakh-Zanskar Himalayas: implications for the timing and obduction of the Spontang Ophiolte, India-Asia collision and deformation events in the Himalaya, Geological Magazine, 134, pp297-316.

Searle, M. P., Noble, S. R., Cottle, J. M., Waters, D. J., Mitchell, A. H. G., Hiang, T. and Horstwood, M. S. A. 2007. Tectonic evolution of the Mogok Metamorphic Belt, Burma (Myanmar) constrained by U-Th-Pb dating of metamorphic and magmatic rocks, Tectonics, 26, 3, Art no. TC3014

Searle, M., Noble, S. R., Hurford, A. J. and Rex, D. C., 1999a, Age of crustal melting, emplacement and exhumation history of the Shivling Leucogranite, Garwhal Himalaya, Geological Magazine, 136, 5, pp513-525.

Searle, M., 1983, On the tectonics of the western Himalaya, Episodes, 4, pp21-26.

Sherlock S.C., and Kelley S.P., 2002, Excess argon in HP-LT rocks: a UV laserprobe study of phengite and K-free minerals: Chemical Geology, 182, pp619–636.

Sikder, A. M. and Alam, M. M., 2003, 2-D modelling of the anticlinal structures and structural development of the eastern fold belt of the Bengal Basin, Bangladesh, Sedimentary Geology, 155, 3-4, pp209-226.

Simpson, G. and Schlunegger, F., 2003, Topographic evolution and morphology of surfaces evolving in response to coupled fluvial and hillslope sediment transport, Journal of Geophysical Research, 108 (B6) doi:10.1029/2002JB002162.

Sinclair, H. D. and Jaffey, N., 2001, Sedimentology of the Indus Group, Ladakh, northern India; implications for the timing of the initiation of the palaeo-Indus River, Journal of the Geological Society (London), 158, pp151-162.

Singh, O.P., Subramanya, S.M., and Sharma, V., 2000, Early Neogene multiple microfossil biostratigraphy, John Lawrence Island, Andaman Sea: Micropalaeontology, 46, pp343–352.

Singh, S., Kumar, R., Barley, M. E. & Jain, A. K. 2006. SHRIMP U-Pb ages and depth of emplacement of Ladakh Batholith, Eastern Ladakh, India, Journal of Asian Earth Sciences, 30 3-4, pp490-503.

Singh, S.K., and France-Lanord, C., 2002, Tracing the distribution of erosion in the Brahmaputra watershed from isotopic compositions of stream sediments: Earth and Planetary Science Letters, 202, pp645–662.

Spear, F. S. and Parrish, R. R., 1996, Petrology and cooling rates of the Valhalla-complex, British-Columbia, Canada, Journal of Petrology, 37, pp733-765.

Stephenson, D. and Marshall, T. R., 1984. the petrology and mineralogy of Mt Popa volcano and the nature of the late Cainozoic Burma volcanic arc, Journal of the Geological Society, London, 141, pp747-762.

Svojtka, M., Ko, J. and Venera, Z., 2001, Dating granulite-facies structures and the exhumation of lower crust in the Moldanubian Zone of the Bohemian Massif: International Journal of Earth Sciences, 91, pp373–385.

Szulc, A., Najman, Y., Sinclair, H. D., Pringle, M., Bickle, M., Chapman, H., Garzanti, E., Ando, S., Huyghe, P., Mugnier, J. L., Ojha, T. and DeCelles, P., 2006, Tectonic evolution of the Himalaya constrained by detrital Ar-40-Ar-39, Sm-Nd and petrographic data from the Siwalik foreland basin succession, SW Nepal, Basin Research, 18, 4, pp375-391.

Tagami, T., Galbraith, R. F., Yamada, R. and Laslett, G. M., 1998, Revised annealing kinetics of fission tracks in zircon and geologic implications. *In:* Advances in Fission-Track Geochronology. Van den Haute, P., De Corte, F. (eds) Kluwer Academic Publishers, Dordrecht, pp99-112.

Tapponier, P., Peltzer, G., Le Dain, A. Y., Armijo, R. and Cobbold, P., 1982, Propogating extrusion tectonics in Asia: new insights from simple experiments with plasticine, Geology, 10, pp611-616.

Thiede, R. C., Arrowsmith, J. R., Bookhagen, B., McWilliams, M. O., Sobel, E. R. and Strecker, M. R., 2005, From tectonically to erosionally controlled development of the Himalayan Orogen, Geology, 33, 8, pp689-692.

Uddin, A. and Lundberg, N., 1998a, Cenozoic history of the Himalaya-Bengal system: sand composition in the Bengal Basin, Bangladesh, Geological Society of America Bulletin, 110, 4, pp497-511.

Uddin, A. and Lungberg, N., 1998b, Unroofing history of the eastern Himalaya and the Indo-Burman Ranges: Heavy-mineral study of Cenozoic sediments from the Bengal Basin, Bangladesh, Journal of Sedimentary Research, 68, 3, pp465-472.

Uddin, A. and Lundberg, N., 1999, A paleo-Brahmaputra? Subsurface lithofacies analysis of Miocene deltaic sediments in the Himalayan-Bengal system, Bangladesh, Sediment Geology, 123, 3-4, pp239-254.

Uddin, A. and Lundberg, N., 2004, Miocene sedimentation and subsidence during continent-continent collision, Bengal Basin, Bangladesh, Sedimentary Geology, 164, 1-2, pp131-146.

United Nations, 1978b. Geology and exploration geochemistry of the Pinlebu-Banmauk area. Sagaing division, northern Burma. Technical Report, UN/BUR/72/002, No. 2. United Nations Development Programme, New York.

United Nations, 1978c, Geology and exploration geochemistry of the Salingyi-Shinmataung area, Central Burma, Technical Report, UN/BUR/72/002, No. 5, United Nations Development Programme, New York.

Van der Beek, P., Robert, X., Mugnier, J-L., Bernet, M., Huyghe, P. and Labrin, E., 2006, Late Miocene – Recent exhumation of the central Himalaya and recycling in the foreland basin assessed by apatite fission-track thermochronology of Siwalik sediments, Nepal, Basin Research, 18, pp413-434.

Vance, D., Bickle, M., Ivy-Ochs, S. and Kubik, P. W., 2003, Erosion and exhumation in the Himalaya from cosmogenic isotope inventories of river sediments, Earth and Planetary Science Letters, 206, 3-4, pp273-288.

Vohra, C. P., Halder, D., and Ghosh Roy, A. K., 1989, The Andaman-Nicobar ophiolite complex and associated mineral resources -current appraisal: In. Phanerozoic ophiolites of India, N. C. Ghosh (Ed.) Summary Publication. Patna, pp281–315.

Weber, K., 1972a, Notes on the determination of illite crystallinity, Neues Jahrb. Mineral. Monatsch., 6, pp267-276.

White, N. M., Parrish, R. R., Bickle, M. J., Najman, Y., Burbank, D. and Maithani, A., 2001, metamorphism and exhumation of the NW Himalaya constrained by U-Th-Pb analyses of detrital monazite grains from early foreland basin sediments, Journal of the Geological Society (London), 158, pp625-635.

White, N. M., Pringle, M., Garzanti, E., Bickle, M., Najman, Y., Chapman, H. and Friend, P., 2002, Constraints on the exhumation and erosion of the High Himalayan Slab, NW India, from foreland basin sediments, Earth and Science Planetary Letters, 195, pp29-44.

Whitmarsh, R. B., Weser, O. E. and Ross, D. A. 1974, Initial results of the Deep Sea Drilling Project, vol. 23, U. S. Government Printing Office, Washington DC, pp 1180.

Willett, S.D., 1999, Orogeny and orography: the effects of erosion on the structure of mountain belts, Journal of Geophysical Research 104 (B12), 28, 957–28, 982.164

Wobus, C. W., Hodges, K. V. and Whipple, K. X., 2003, Has focused denudation sustained active thrusting at the Himalayan topographic front? Geology, 31, 10, pp861-864.

Worm, H.-U., Ahmed, A. M. M., Ahmed, N. U., Islam, H. O., Huq, M. M., Hambach, U. and Lietz, J. (1998) Large sedimentation rate in the Bengal Delta: Magnetostratigraphic dating of Cenozoic sediments from northeastern Bangladesh, Geology, 26, 6, pp487-490.

Wu, F. Y., Clift, P. D. and Yang, J. H., 2007, Zircon Hf isotopic constraints on the sources of the Indus Molasse, Ladakh Himalaya, India, Tectonics, 26, 2, Art. No. TC2014

Yin, A., and Harrison, T. M., 2000, Geological evolution of the Himalayan-Tibetan orogen, Annual Review of Earth and Planetary Science, 28, pp211-280.

Zeilinger, G., Seward, D., Burg, J. P., 2007, Exhumation across the Indus Suture Zone: a record of back sliding of the hanging wall, Terra Nova, 19, 6, pp425-431.

Zeitler, P. K., Meltzer, A. S., Koons, P. O., Craw, D., Hallet, B., Chamberlain, C. P., Kidd, W. S. F., Park, S. K., Seeber, L., Bishop, M., and Schroder, J., 2001, Erosion, Himalayan geodynamics and the geomorphology of metamorphism, GSA Today, 11, 1, pp4-9.

Zhang, P. Z., Molnar, P., Downs, W. R., 2001, Increased sedimentation rates and grain sizes 2-4 Myr ago due to the influence of climate change on erosion rates, Nature, 410, (6831), pp891-897.

Zhou, H. W. and Murphy, M. A., 2005, Tomographic evidence for wholesale underthrusting of India beneath the entire Tibetan plateau, Journal of Asian Earth Sciences, 25, pp445-457.

Appendices

Appendix 1: Supplementary Information for Chapter 3 (published by GSA Bulletin Spec. Pub.)

Appendix 2: Supplementary Information for Chapter 4 (accepted for publication with Journal of the Geological Society)

Appendix 3: Supplementary Information for Chapter 5 (submitted to Basin Research)

Appendix 4: Seismic Data including biostratigraphic calibration appendix for Chapter 5 (CD included)

Appendix 5: Abstracts and co-authored publications

Sample	Latitude Longitude	Mineral	No. of grains	ρd Nd	ρs Ns	ρi Ni	Dispersion $P\chi^2$	RE%	Central Age ±1 σ (Ma)	Age Components		Mean track length (μm)	S.d.	No tracks
MITHAKHARI GROUP														
Hopetown Conglomerate Fm.														
Hopetown Quarry	N11°41.407' E92°43.501'	*Zircon*	*25*	*0.528 (3450)*	*12.16 (4942)*	*4.32 (1756)*	*0.0*	*56.2*	91.8±10.8	***61±2 (16)***	***129±10 (5)***	***280±32 (4)***		
		Apatite	19	1.106 (6131	0.064 (58)	0.209 (191)	0.03	69.1	56.5±8.5	**57±9 (19)**				
Namunagarh Grit Fm.														
Mungleton Quarry	N11°34.223' E92°39.541'	*Zircon*	*18*	*0.535 (3450)*	*10.972 (4182)*	*4.872 (1857)*	*0.0*	*42.3*	75.1±7.9	***59±2 (15)***		***226±21(3)***		
		Apatite	21	1.106 (6131)	0.150 (322)	0.246 (946)	0.0	64.5	68.9	**55±8 (19)**	**151±68 (1)**	**314±51 (1)**		
Namunagarh Quarry	N11°41.339, E92°41.106	Apatite	24	1.106 (6131	0.060 (108)	0.282 (506)	99.6	0.0	39.8±4.2	**40±4 (24)**				
Chiriyatapu	N11°42.005 E93°32.301'	*Zircon*	38	0.525 (3450)	12.53 (7468)	2.255 (1344)	0.0	92.6	143.0±22	**40±3 (9)**	**91±7 (8)**	**329±17 (22)**		
ANDAMAN FLYSCH														
AND-1A	N11°38.430' E92°45.292'	Apatite	38	1.106 (6131	0.264 (497)	1.653 (3116)	0.02	28.8	30.8±2.2	**31±2 (38)**		13.25±0.17	1.51	76
		Zircon	*43*	*0.516 (3450)*	*8.341 (6439)*	*4.07 (3147)*	*0.0*	*44.5*	62.1±4.6	***44±2 (24)***	***67±4 (12)***	***147±10 (6)***		
AND-1B	N11°38.457 E92°45'318	Apatite	57	1.106 (6131	0.499 (738)	2.499 (3696)	7.3	16.3	37.1±1.8	**37±2 (57)**		13.06±0.20	1.75	75
		Zircon	*32*	*0.515 (3450)*	*6.115 (3085)*	*3.685 (1859)*	*0.0*	*41.5*	53.7±4.4	***41±2 (26)***	***101±14 (6)***			
AND-3	N11°38.459' E92°45.368'	Apatite	50	1.106 (6131	0.497 (852)	2.556 (4739)	0.03	22.6	35.8±1.9	**36±2 (50)**		13.24±0.22	1.61	54
		Zircon	*15*	*0.10 (3450)8*	*10.24 (1930)*	*4.828 (910)*	*0*	*73.0*	58.5±11.3	***36±2 (12)***		***616±102 (3)***		
AND-4	N11°39.461' E92°45.417'	Apatite	47	11.106 (6131	0.427 (923)	2.652 (5733)	0.04	20.2	30.7±1.5	**31±2 (47)**		13.42±0.23	1.80	62
		Zircon	*42*	*0.505 (3450)*	*10.63 (7575)*	*4.506 (3210)*	*0*	*70.1*	67.9±7.6	***38±1 (20)***	***58±4 (10)***	***270±16 (12)***		

Appendix 1 - 1: Fission track analytical data for Andaman Islands – South Andaman

(i). Track densities are ($x10^6$ tr cm^{-2}) numbers of tracks counted (N) shown in brackets;
(ii). analyses by external detector method using 0.5 for the $4\pi/2\pi$ geometry correction factor;
(iii). ages calculated using dosimeter glass CN-5; (apatite) ζ_{CN5} =338±4; CN-2 (zircon) ζ_{CN2} =127±4
calibrated by multiple analyses of IUGS apatite and zircon age standards (see Hurford 1990);
(iv). $P\chi^2$ is probability for obtaining χ^2 value for v degrees of freedom, where v = no. crystals - 1;
(v). Central age is a modal age, weighted for different precisions of individual crystals (see Galbraith 1992);
(vi) Age modes deconvolved using approach of Sambridge and Compston (1994) and Galbraith and Green (1993)

Appendix 1 – 2: Apatite-Helium data

Sample	Location	4He (ncc)	HB (ncc)	4He-HB (ncc)	%SD in Q +/-	4He (atoms)	absolute +/-	238U (ng)	+/- (%)	232Th (ng)	+/- (%)	He* age (Ma)	Error +/- 7%	Grain Radius	FT Corr	FT Corr Age (Ma)
AND-A	N11 38.430' E92 45.292'	0.356	0.023	0.333	0.452	8.95E+09	4.04E+07	0.108	1.2	0.537	1.33	**11.704**	0.819	77	0.81	14.4
AND-B	N11 38.457' E92 45.318'	0.209	0.021	0.188	0.119	5.05E+09	6.01E+06	0.062	2.18	0.215	1.8	**13.756**	0.962	66	0.76	18.1
AND-C	N11 38.459' E92 45.368'	0.222	0.018	0.204	0.119	5.48E+09	6.52E+06	0.058	1.98	0.315	1.4	**12.664**	0.886	82	0.81	15.6

All samples are taken from the Andaman Flysch formation at Corbyn's Cove.
* = uncorrected helium age

Notes
Helium ages are based on replicate analyses of apatite grains

The total uncertainty in sample age is based on the reproducibility of 39 analyses of the Californian Institute of technology (CIT) laboratory Durango apatite standard (this error of the mean = 6.7%) combined with the U/Th and He analytical uncertainties.

Method:
Each selected grain was first photographed, and then its dimensions were recorded for later alpha-ejection correction. Samples were loaded into platinum microtubes for helium outgassing and U/Th determination. Outgassing was achieved using an induction furnace at a temperature of 950°C. The abundance of ^{4}He was measured relative to a 99.9% pure ^{3}He spike in a Pfeiffer Prisma 200 quadrupole mass spectrometer. The quantification of U/Th was performed on an Agilent 7500 quadrupole mass spectrometer using spiked solutions of the dissolved apatite. Repeated analysis of the California Institute of Technology (CIT) laboratory Durango apatite standard gives an age of 31.3 ± 1.2 Ma (2σ), based on 39 analyses. This error of the mean (6.7%), combined with the U/Th and He analytical uncertainties, is used as a measure of the total uncertainty in sample age.

Appendix 1 – 3: Raw Argon data

Andaman Flysch (Corbyns Cove section) A 1b.

A1B	40Ar	39Ar	38Ar	37Ar	36Ar	40Ar*/39Ar	+-	Age (Ma)	+-
Ms 1	0.680680	0.213559	0.003536	0.005284	0.000779	2.109962	0.020067	**51.8**	**0.5**
Ms 2	0.203759	0.060257	0.000705	0.000626	6.48E-05	3.063559	0.006231	**74.7**	**0.4**
Ms 3	0.451179	0.185698	0.002571	0.002597	0.000354	1.865821	0.022963	**45.9**	**0.6**
Ms 4	0.329659	0.110714	0.001661	0.002407	0.000334	2.085147	0.038311	**51.2**	**1.0**
Ms 5	0.37799	0.046614	0.000787	0.000994	0.00013	7.286482	0.032957	**172.9**	**1.1**
Ms 6	0.269821	0.037161	0.000531	0.000573	5.98E-05	6.784923	0.089994	**161.5**	**2.2**
Ms 8	2.277688	0.11746	0.001906	0.002831	0.000274	18.7013	0.031643	**414.2**	**2.0**
Ms 9	2.143176	0.070945	0.000931	0.000402	2.99E-05	30.08465	0.047492	**626.5**	**2.8**
Ms 10	1.384602	0.074126	0.001043	0.001053	0.00018	17.96253	0.023198	**399.5**	**1.9**
Ms 11	0.253605	0.015673	0.000291	5.75E-05	0	16.18154	0.035317	**363.6**	**1.8**
Ms 12	0.259847	0.082319	0.001170	0.000824	7.98E-05	2.870187	0.003993	**70.1**	**0.4**
Ms 13	3.391288	0.385463	0.004783	0.003164	0.000389	8.499624	0.011701	**200.1**	**1.0**
Ms 15	0.790418	0.252174	0.003255	0.003477	0.000284	2.801527	0.02637	**68.4**	**0.7**
Ms 16	0.531821	0.070046	0.000772	0.000291	5.49E-05	7.360776	0.036057	**174.5**	**1.2**
Ms 17	0.323132	0.105295	0.001329	0.001905	0.000189	2.537016	0.031682	**62.1**	**0.8**
Ms 18	0.832588	0.098415	0.001318	0.000894	4.98E-05	8.310543	0.035372	**195.9**	**1.2**
Ms 19	0.176399	0.061786	0.000710	0.000428	7.99E-05	2.472932	0.067916	**60.5**	**1.7**
Ms 20	0.458665	0.086807	0.001068	0.00179	0.00013	4.842794	0.034779	**116.7**	**1.0**
Ms 21	0.269899	0.070387	0.000792	0.000117	0.0002	2.994993	0.047513	**73.1**	**1.2**
Ms 22	1.721992	0.356929	0.004472	0.009619	0.000637	4.296717	0.010036	**103.9**	**0.6**
Ms 23	1.216759	0.459022	0.005575	0.00187	0.00031	2.451514	0.006712	**60.0**	**0.3**
Ms 24	0.085958	0.027352	0.000404	0.000195	0	3.142686	0.011197	**76.6**	**0.5**
Ms 25	0.130443	0.038038	0.000618	0.002262	0.000284	1.219882	0.023433	**30.1**	**0.6**
Ms 26	2.371162	0.106391	0.001354	0.001404	0.000115	21.96896	0.014042	**477.7**	**2.1**
Ms 27	0.314057	0.064276	0.000828	0.000507	4.99E-05	4.656836	0.012754	**112.4**	**0.6**
Ms 28	0.336883	0.064142	0.000767	0.000156	8E-05	4.883813	0.04699	**117.7**	**1.2**
Ms 29	0.999109	0.106174	0.001329	0.00041	0.000125	9.062499	0.029797	**212.6**	**1.2**
Ms 30	0.124323	0.075656	0.000961	0.000488	7.49E-05	1.350842	0.039184	**33.3**	**1.0**
Ms 31	1.604755	0.163177	0.001993	0.000528	0.000145	9.572115	0.020485	**223.8**	**1.1**
Ms 32	0.176028	0.107915	0.001318	0.000411	8.49E-05	1.398714	0.006655	**34.5**	**0.2**
Ms 33	0.094113	0.056227	0.000787	0.000782	5.48E-05	1.385834	0.005724	**34.2**	**0.2**

Andaman Flysch (Corbyns Cove section) A3.

A3	40Ar	39Ar	38Ar	37Ar	36Ar	40Ar*/39Ar	+-	Age (Ma)	+-
Ms 1	0.274897	0.083084	0.000981	0.00039	0.000145	2.793324	0.037215	**68.2**	**1.0**
Ms 2	0.444523	0.143237	0.001850	0.001424	0.000445	2.186142	0.029916	**53.6**	**0.8**
Ms 3	0.297818	0.112368	0.0014	0.000746	0.000115	2.348489	0.038715	**57.5**	**1.0**
Ms 4	1.308190	0.466538	0.005703	0.002087	0.000109	2.734713	0.013397	**66.8**	**0.5**
Ms 5	0.346651	0.128071	0.001671	0.000476	0.000155	2.349362	0.023267	**57.6**	**0.6**
Ms 6	3.632999	0.500069	0.006087	0.001156	0.000305	7.084947	0.012826	**168.3**	**0.9**
Ms 8	0.311219	0.100244	0.001252	0.000476	0.000185	2.55964	0.004776	**62.6**	**0.3**
Ms 9	0.281996	0.054435	0.000680	0.000511	0.000105	4.611138	0.010622	**111.3**	**0.6**
Ms 10	0.180333	0.044863	0.000593	0.000392	2.49E-05	3.855628	0.00766	**93.5**	**0.5**
Ms 11	0.518299	0.095269	0.001186	0.000528	0.000125	5.053064	0.006582	**121.6**	**0.6**
Ms 12	0.604087	0.186293	0.002397	0.000648	0.000155	2.997079	0.016331	**73.1**	**0.5**

Ms 13	0.514859	0.086648	0.001109	0.000392	2.49E-05	5.857044	0.034464	**140.2**	**1.0**
Ms 15	0.190225	0.061068	0.000797	0.000672	0.000145	2.414197	0.048452	**59.1**	**1.2**
Ms 16	0.138431	0.029423	0.000409	0.000534	0.000115	3.551304	0.003826	**86.3**	**0.4**
Ms 17	0.560451	0.085584	0.001022	6.89E-05	6.5E-05	6.324168	0.019494	**151.0**	**0.9**
Ms 18	1.927513	0.246058	0.003455	0.002792	0.000814	6.855692	0.06817	**163.1**	**1.7**
Ms 19	0.549605	0.188385	0.002402	0.001380	0.000265	2.502356	0.018307	**61.2**	**0.5**
Ms 20	0.199519	0.062808	0.000767	0.000897	0.000185	2.307352	0.05385	**56.5**	**1.3**
Ms 21	0.792813	0.159513	0.002090	0.002278	0.000214	4.573025	0.019797	**110.4**	**0.7**
Ms 22	0.531614	0.155877	0.002090	0.001657	0.000385	2.681443	0.009091	**65.6**	**0.4**
Ms 23	0.290937	0.092139	0.001272	0.000881	7.98E-05	2.901768	0.033228	**70.8**	**0.9**
Ms 24	0.481724	0.087635	0.000905	0.000389	9.99E-05	5.160096	0.036978	**124.1**	**1.0**
Ms 25	1.163152	0.352631	0.004461	0.001418	0.00038	2.980373	0.009667	**72.7**	**0.4**
Ms 26	0.272653	0.094083	0.001191	0.005552	8.85E-05	2.619921	0.032203	**64.1**	**0.8**
Ms 27	0.422343	0.128727	0.001610	0.000571	0.00011	3.028746	0.023467	**73.9**	**0.7**
Ms 28	0.24212	0.086183	0.001145	0.000242	9.94E-06	2.775297	0.03496	**67.8**	**0.9**
Ms 29	0.358268	0.11507	0.001441	0.000277	2.99E-05	3.036643	0.005754	**74.1**	**0.4**
Ms 30	0.178945	0.044807	0.000537	0.000211	3.49E-05	3.763259	0.033264	**91.3**	**0.9**
Ms 31	0.273151	0.093756	0.001232	0.000316	0.000115	2.551233	0.016583	**62.4**	**0.5**
Ms 32	0.173772	0.089489	0.00115	1.76E-05	5E-05	1.776730	0.016944	**43.7**	**0.5**

Andaman Flysch (Corbyns Cove section) A4.

A4	40Ar	39Ar	38Ar	37Ar	36Ar	40Ar*/39Ar	+-	Age (Ma)	+-
Ms 1	1.757257	0.228175	0.003051	0.001952	0.000479	7.080388	0.0316	**168.2**	**1.1**
Ms 2	0.350481	0.117885	0.001625	0.000598	0.000135	2.63508	0.030076	**64.4**	**0.8**
Ms 3	0.226229	0.086674	0.001165	0.000669	0.000115	2.218651	0.038875	**54.4**	**1.0**
Ms 4	0.84056	0.203536	0.00254	0.000722	0.000305	3.687254	0.018742	**89.5**	**0.6**
Ms 5	0.387886	0.075170	0.001007	0.000476	3.49E-05	5.023023	0.044232	**120.9**	**1.2**
Ms 6	0.827359	0.256024	0.00326	0.001164	0.00039	2.781793	0.00436	**68.0**	**0.3**
Ms 8	0.124755	0.077014	0.001012	0.000247	0.00011	1.198084	0.007833	**29.6**	**0.2**
Ms 9	3.009747	0.428003	0.005417	0.000953	0.000195	6.897607	0.010471	**164.0**	**0.8**
Ms 10	1.209192	0.187151	0.00232	0.000706	0.000105	6.29557	0.006128	**150.3**	**0.7**
Ms 11	0.497906	0.161033	0.00184	0.000212	7.49E-05	2.954419	0.018552	**72.1**	**0.6**
Ms 12	3.00958	0.046496	0.000608	0.000395	7.99E-05	64.22046	0.067476	**1144.9**	**4.3**
Ms 13	0.239454	0.097718	0.001129	0.000897	0.00013	2.058057	0.005784	**50.5**	**0.3**
Ms 15	1.727941	0.097393	0.001247	3.59E-05	7.5E-05	17.51444	0.014541	**390.6**	**1.8**
Ms 16	0.259758	0.122808	0.001441	0.000395	3.49E-05	2.0312	0.024229	**49.9**	**0.6**
Ms 17	0.102435	0.029899	0.000307	0	1.5E-05	3.277664	0.007241	**79.8**	**0.4**
Ms 18	0.565702	0.067938	0.000869	0.000198	3.49E-05	8.174691	0.007531	**192.8**	**0.9**
Ms 19	0.461503	0.030601	0.000363	0	5E-06	15.03286	0.049761	**340.1**	**1.9**
Ms 20	0.084844	0.03198	0.000358	3.6E-05	9.99E-06	2.560674	0.046289	**62.7**	**1.2**
Ms 21	0.051231	0.028354	0.000327	0.000144	9.96E-06	1.70302	0.116858	**41.9**	**2.9**
Ms 22	0.539888	0.175027	0.002034	0.000648	0.000225	2.705021	0.007126	**66.1**	**0.4**
Ms 23	0.224278	0.125809	0.001584	0.000793	0.000115	1.513072	0.003637	**37.3**	**0.2**
Ms 24	2.435008	0.115560	0.001303	0.000343	8.99E-05	20.84143	0.030878	**456.1**	**2.1**
Ms 25	0.28137	0.043934	0.000537	0.000162	3E-05	6.202931	0.034616	**148.2**	**1.1**
Ms 26	1.447467	0.066026	0.00092	0.001368	0.000185	21.09624	0.0327	**461.0**	**2.1**
Ms 27	0.131921	0.043514	0.000777	0.001825	0.000255	1.303279	0.01007	**32.2**	**0.3**
Ms 28	0.381247	0.061408	0.000899	0.001902	0.000264	4.935659	0.026829	**118.9**	**0.8**
Ms 29	0.400761	0.030962	0.000603	0.001484	0.000155	11.46811	0.056235	**265.1**	**1.7**
Ms 30	0.124287	0.055912	0.000761	0.001294	0.000205	1.141272	0.059711	**28.2**	**1.5**
Ms 31	0.077119	0.024908	0.000368	0.000686	8.98E-05	2.030571	0.013455	**49.9**	**0.4**

Ms 32	0.042558	0.024805	0.000409	0.000952	4.97E-05	1.123077	0.119683	**27.7**	**2.9**
Ms 33	0.057102	0.020714	0.000225	0.000305	5.99E-05	1.901885	0.160137	**46.7**	**3.9**

Mithakhari Group, Chiriytapu

	40Ar	39Ar	38Ar	37Ar	36Ar	40Ar*/39Ar	+-	Age (Ma)	+-
Ms 1	0.8284261	0.0365259	0.0004242	0.0004699	0.0000000	22.6805064	0.0750144	**491.3**	**2.6**
Ms 2	0.7446774	0.0323472	0.0003628	0.0000000	0.0000550	22.5188268	0.0957791	**488.2**	**2.8**
Ms 3	0.7987535	0.0472551	0.0006388	0.0002743	0.0000249	16.7471471	0.0197808	**375.1**	**1.7**
Ms 4	0.3026851	0.0938337	0.0011243	0.0001764	0.0000750	2.9897197	0.0315933	**72.9**	**0.8**
Ms 5	0.6288437	0.0690488	0.0008483	0.0003334	0.0000449	8.9150267	0.0157014	**209.3**	**1.0**
Ms 6	0.2056404	0.0084045	0.0001022	0.0000000	0.0000000	24.4679238	0.0604556	**524.8**	**2.5**
Ms 8	2.0267770	0.0181880	0.0002760	0.0003637	0.0000349	110.8679577	0.1272294	**1674.6**	**5.6**
Ms 9	1.3058958	0.0589862	0.0007666	0.0002830	0.0000949	21.6634575	0.0479489	**471.9**	**2.3**
Ms 10	1.0895856	0.0467023	0.0006133	0.0004044	0.0000849	22.7933251	0.0380826	**493.4**	**2.3**
Ms 11	1.7582128	0.0745294	0.0008279	0.0005462	0.0000899	23.2345815	0.0322423	**501.7**	**2.3**
Ms 12	0.7200124	0.0307043	0.0004191	0.0003844	0.0001499	22.0072636	0.1088272	**478.5**	**3.0**
Ms 13	0.7633280	0.0327602	0.0004344	0.0003442	0.0000499	22.8502553	0.0157553	**494.5**	**2.2**
Ms 15	1.4321915	0.0604223	0.0007308	0.0002229	0.0000499	23.4587880	0.0323211	**506.0**	**2.3**
Ms 16	3.1189393	0.0694722	0.0008943	0.0007095	0.0000998	44.4702431	0.0356104	**863.3**	**3.5**
Ms 17	0.5782068	0.0518422	0.0006746	0.0002434	0.0000349	10.9540815	0.0577358	**254.0**	**1.7**
Ms 18	1.2848422	0.0599626	0.0007052	0.0001623	0.0000750	21.0580001	0.0540885	**460.2**	**2.3**
Ms 19	0.5290525	0.0217523	0.0003015	0.0002639	0.0000199	24.0509065	0.1038536	**517.1**	**3.0**
Ms 20	5.1561196	0.0246141	0.0003628	0.0002639	0.0000799	208.5188362	0.2883512	**2444.9**	**6.9**
Ms 21	0.6433217	0.0339743	0.0003577	0.0001625	0.0000500	18.5010347	0.0472177	**410.2**	**2.1**
Ms 22	1.1030049	0.0956311	0.0011039	0.0005283	0.0001499	11.0708902	0.0175933	**256.5**	**1.3**
Ms 23	0.3852341	0.0186428	0.0002044	0.0000000	0.0000000	20.6639642	0.0133670	**452.6**	**2.0**
Ms 24	0.8201835	0.0345528	0.0004804	0.0002349	0.0000499	23.3100383	0.0867000	**503.2**	**2.7**
Ms 25	0.2651809	0.0818851	0.0009965	0.0008358	0.0001048	2.8603315	0.0027919	**69.8**	**0.3**
Ms 26	0.4454907	0.0287515	0.0004242	0.0007315	0.0001248	14.2118131	0.0282976	**323.1**	**1.6**
Ms 27	0.2823107	0.0124546	0.0001073	0.0000000	0.0000000	22.6671453	0.0457513	**491.0**	**2.3**
Ms 28	7.5439887	0.1794691	0.0021310	0.0008891	0.0001048	41.8625264	0.0295576	**822.6**	**3.3**
Ms 29	0.4338841	0.0171655	0.0002402	0.0000000	0.0000000	25.2765779	0.0434406	**539.8**	**2.5**
Ms 30	0.9228281	0.0225529	0.0003373	0.0004192	0.0000299	40.5267640	0.1467725	**801.4**	**4.0**
Ms 31	2.4734857	0.0295677	0.0004191	0.0005765	0.0000398	83.2566784	0.1423053	**1380.1**	**5.1**
Ms 32	1.5381052	0.0256109	0.0003475	0.0004719	0.0000000	60.0566236	0.1661772	**1089.0**	**4.7**
Ms 33	0.3426377	0.0155174	0.0001942	0.0002623	0.0000299	21.5108920	0.0746433	**469.0**	**2.5**

Method:

For this study, single grains were totally fused using an infrared laser ablation microprobe (IRLAMP). Samples were monitored using the GA1550 biotite standard with an age of 98.8 ± 0.5 Ma (Renne et al., 1998). The calculated *J* value for the samples was 0.0138 ± 0.000069. Blanks were measured both before and after each pair of sample analyses, and the mean of the two blanks was used to correct the sample analyses for the measured isotopes. Overall mean blank levels for ^{40}Ar, ^{39}Ar, and ^{36}Ar were (378, 6, and 11) × $10^{-12}cm^3$ at a standard temperature and pressure. The resulting analyses were also corrected for mass spectrometer discrimination, ^{37}Ar decay, and neutron induced interferences. The correction factors used were $(^{39}Ar/^{37}Ar)_{Ca}$ = 0.00065, $(^{36}Ar/^{39}Ar)_{Ca}$ = 0.000264, and $(^{40}Ar/^{39}Ar)_{K}$ = 0.0085; these were based on analyses of Ca and K salts. Samples were irradiated for 33 h in the McMaster University reactor (Canada).

Appendix 1 – 4: Zircon U-Pb data (uncorrected ages) for Andaman Flysch sample 1A.

Grain #		$^{206}Pb/^{238}U$ ratio	±	$^{207}Pb/^{235}U$ ratio	±	$^{207}Pb/^{206}Pb$ ratio	±	$^{206}Pb/^{238}U$ Age (Ma)	±1sigma	$^{207}Pb/^{235}U$ Age (Mε)	±1sigma	$^{207}Pb/^{206}Pb$ Age (Ma)	±1sigma
8		0.56820	0.01491	18.27837	0.00211	0.23368	0.01172	2900.4	61.3	3004.5	46.4	3077.4	77.9
21		0.52114	0.01876	17.80391	0.00319	0.24751	0.01869	2704.0	79.5	2979.2	72.0	3168.9	114.9
18		0.45548	0.02377	10.17671	0.00390	0.16214	0.01534	2419.6	105.3	2451.0	83.7	2478.1	151.3
28		0.30919	0.01417	5.34072	0.00228	0.12476	0.01304	1736.7	69.8	1875.4	88.2	2025.4	174.4
1		0.25134	0.01476	3.17496	0.00192	0.09164	0.01199	1445.4	76.0	1451.1	95.3	1459.9	230.3
37		2.68537	0.14191	0.23801	0.00394	0.08188	0.00394	1376.4	20.5	1324.4	39.1	1242.7	99.7
7		0.20471	0.00761	2.27006	0.00089	0.08055	0.00685	1200.5	40.7	1203.0	56.6	1210.5	158.8
13		0.19499	0.00490	2.12506	0.00101	0.07915	0.00497	1148.4	26.5	1157.0	42.0	1175.9	119.3
31		2.04475	0.18301	0.19077	0.00536	0.07779	0.00536	1125.6	29.0	1130.5	61.0	1141.5	172.8
16		0.19076	0.00770	2.00881	0.00087	0.07645	0.00752	1125.5	41.7	1118.5	63.8	1106.9	184.9
23		0.19007	0.00612	2.22350	0.00114	0.08469	0.00712	1121.8	33.2	1188.5	58.4	1308.4	154.9
2		0.18013	0.00766	2.41204	0.00081	0.09716	0.00881	1067.7	41.8	1246.2	60.4	1570.4	160.9
9		0.17942	0.00506	1.81366	0.00083	0.07343	0.00503	1063.8	27.7	1050.4	42.7	1025.9	132.6
5		0.17514	0.00495	1.78122	0.00078	0.07384	0.00488	1040.3	27.1	1038.6	40.6	1037.0	128.1
3		0.15851	0.00357	1.66696	0.00100	0.07632	0.00404	948.5	19.8	996.0	31.7	1103.5	102.3
35		1.54569	0.07373	0.15281	0.00239	0.07342	0.00239	916.7	13.4	948.8	29.4	1025.7	94.7
4		0.15069	0.00383	1.56797	0.00082	0.07553	0.00458	904.8	21.5	957.6	35.5	1082.6	117.0
29		0.15001	0.00490	1.70213	0.00107	0.08191	0.00734	901.0	27.5	1009.3	58.2	1243.4	166.2
12		0.13848	0.00336	1.34274	0.00107	0.07044	0.00431	836.1	19.1	864.4	34.2	941.1	120.5
39		1.43337	0.20932	0.12528	0.00491	0.08302	0.00491	760.9	28.2	903.0	87.3	1269.6	266.2
26		0.12184	0.00484	1.12034	0.00076	0.06648	0.00719	741.2	27.8	763.1	57.1	821.5	210.9
6		0.11741	0.00687	0.91179	0.00108	0.05641	0.00919	715.6	39.6	658.0	75.1	467.6	325.9
22		0.09140	0.00258	0.76164	0.00058	0.06035	0.00473	563.8	15.2	575.0	34.3	616.3	160.8
11		0.08908	0.00363	0.96494	0.00048	0.07869	0.00822	550.1	21.5	685.8	49.1	1164.5	194.1
32		0.70554	0.09115	0.08743	0.00262	0.05857	0.00262	540.3	15.6	542.1	54.3	551.3	264.1
25		0.08390	0.00418	0.73573	0.00076	0.06343	0.00948	519.4	24.8	559.9	62.5	722.7	288.8
34		0.54771	0.03128	0.06830	0.00115	0.05821	0.00115	425.9	6.9	443.5	20.5	537.1	122.9
10		0.03673	0.00221	0.25590	0.00024	0.05061	0.01065	232.5	13.7	231.4	41.9	223.1	425.1
40		0.16376	0.10117	0.02074	0.00132	0.05728	0.00132	132.3	8.4	154.0	88.3	501.8	982.4
19		0.01567	0.00179	0.10372	0.00025	0.04802	0.02354	100.2	11.3	100.2	45.6	99.0	874.6
27		0.01427	0.00191	0.10618	0.00022	0.05378	0.03759	91.3	12.1	102.5	67.0	361.9	1092.3
33		0.09256	0.01678	0.01397	0.00047	0.04809	0.00047	89.4	3.0	89.9	15.6	103.5	384.6
17		0.01183	0.00088	0.07776	0.00012	0.04771	0.01416	75.8	5.6	76.0	21.1	84.0	585.7
30		0.09413	0.02893	0.01041	0.00056	0.06564	0.00056	66.7	3.5	91.3	26.9	795.0	545.5
24		0.00927	0.00087	0.06214	0.00010	0.04851	0.01680	59.5	5.5	61.2	19.9	124.2	660.0
20		0.00910	0.00077	0.11849	0.00010	0.09449	0.02208	58.4	4.9	113.7	23.6	1518.0	386.4
38		0.05721	0.00743	0.00799	0.00020	0.05193	0.00020	51.3	1.3	56.5	7.1	282.3	275.3
15		0.00778	0.00052	0.05499	0.00005	0.05135	0.01135	49.9	3.3	54.4	11.2	256.6	441.6
36		0.13338	0.08419	0.00723	0.00081	0.13385	0.00081	46.5	5.2	127.1	75.4	2149.0	828.8
14		0.00705	0.00024	0.04889	0.00004	0.05037	0.00528	45.3	1.6	48.5	4.8	212.2	225.9

Method:

Samples for this study were analysed by laser ablation-inductively-coupled-plasma mass spectrometry (LA-ICP-MS) using a New Wave 213 aperture imaged frequency quintupled laser ablation system (213 nm) coupled to an Agilent 750 quadrupole ICP-MS. Real-time data were processed using GLITTER and repeated measurements of the external zircon standard PL (Svojtka et al., 2001; TIMS reference age 337.1 ± 0.7 Ma) to correct for instrumental mass bias. The results have not been corrected for common lead or ranked according to degree of discordance, as the latter involves choosing an arbitrary value and is therefore open to analyser bias.

Svojtka, M., Ko, J., and Venera, Z., 2001, Dating granulite-facies structures and the exhumation of lower crust in the Moldanubian Zone of the Bohemian Massif: International Journal of Earth Sciences, 91, pp373–385.

Appendix 1 – 5a: Petrography

Site	Formation	Region	Sample	grain size (microns)	Q	KF	P	Lv	Lc	Lp	Lch	Lm	micas	heavy minerals	TOTAL	MI Index
Corbyns cove section N11°38'43.0" E92°45'29.2"	Andaman Flysch	S Andaman	FT1B	115	50	13	5	4	0	1	0	25	1	1	100.0	175
Corbyns cove section -~100m up section from 1A	Andaman Flysch	S Andaman	FT3	140	48	17	11	3	0	2	0	16	2	1	100.0	160
Corbyns cove section below hotel	Andaman Flysch	S Andaman	FT4	130	47	10	9	5	0	3	1	24	1	0	100.0	150
Namunagarh Quarry	Namunagarh Grit	S Andaman	NAM 3D	1500	2	1	41	52	0	0	0	1	0	2	100.0	2
Hopetow n Quarry N11°41'40.7" E92°43'50.1"	Namunagarh Grit	S Andaman	NAM 25A	850	21	2	27	40	0	2	2	5	0	1	100.0	15
Mungleton Quarry N11°34'22.3" E92°39'54.1"	Namunagarh Grit	S Andaman	NAM 26	1800	19	1	30	45	0	1	1	3	0	0	100.0	11
Irraw addy River ~ Nyaungdoun	Modern river sand	Myanmar	MY05 23A	-	47	11	11	6	0	6	1	15	2	1	100.0	112

Q= quartz; KF= K-feldspar; P= plagioclase; Lv= volcanic lithics; Lc= carbonate lithics; Lp= terrigenous (shale/siltstone) lithics; Lch= chert lithics; Lm= metamorphic lithics; MI= Metamorphic Index.

The MI Index ("Metamorphic Index"; Garzanti and Vezzoli 2003) expresses the average rank of metamorphic rock fragments in the studied samples, and varies from 0 in detritus from sedimentary and volcanic cover rocks to 500 in detritus from high-grade basement rocks.

Method:
A total of 400 points were counted in six selected samples according to the Gazzi-Dickinson method (Dickinson, 1985). Aclassification scheme of grain types allowed for the collection of fully quantitative information on the sampled sandstones. Transparent dense minerals were counted on grain mounts according to the "ribbon counting" method, and 200 minerals were counted also to assess the percentage of etched and corroded grains. Dense minerals were concentrated with sodium metatungstate (density, 2.9 g/cm^3) using the 63–250 μm fraction treated with hydrogen peroxide, oxalic acid, and sodium ditionite to eliminate organic matter, iron oxides, and carbonates, respectively.

Appendix 1 – 5b: Heavy mineral data (for method see 1 – 5a)

Site	Formation	Sample	HM% VFS-FS	HM% transp.	% transparent	% opaque	% turbid	Total	zircon	dravite	schorlite	rutile	sagenite	sphene	anatase	brookite	Ti aggregates	apatite	xenotime	monazite	barite	others	blue-green hornblende	green hornblende	green-brown hornblende	brown hornblende
Corbyns cove section N11°38'43.0" E92°45'29.2"	Andaman Flysch	FT1B	0.9	0.5	54	9	37	100	3	4	4	5	0	3	0	0	24	10	0	0	0	0	0	0	0	0
Corbyns cove section -~100m up section from 1A	Andaman Flysch	FT3	0.4	0.2	44	7	49	100	4	4	5	5	2	2	0	0	30	17	0	1	0	0	0	0	0	0
Corbyns cove section below hotel	Andaman Flysch	FT4	0.6	0.2	35	8	57	100	4	3	6	7	1	0	0	0	24	11	0	0	0	0	0	0	0	0
Namunagarh Quarry	Namunagarh Grit	NAM 3D	4.0	1.5	37	38	25	100	0	0	0	0	0	1	0	0	0	3	0	0	0	0	1	2	20	0
Hopetow n Quarry N11°41'40.7" E92°43'50.1"	Namunagarh Grit	NAM 25A	1.3	0.6	42	16	42	100	1	0	0	1	0	15	0	0	3	1	0	0	0	0	0	0	0	0
Mungleton Quarry N11°34'22.3" E92°39'54.1"	Namunagarh Grit	NAM 26	1.0	0.5	53	7	40	100	0	0	0	1	0	16	0	0	1	3	0	0	0	0	0	0	0	0
Irraw addy River ~ Nyaungdoun	River sand	MY05 23A	5 .0	4 .0	79	3	17	100	0	0	0	0	0	3	0	0	0	0	0	0	0	0	44	2	2	1

Sample	oxy-hornblende	glaucophane	sodic amphiboles	tremolite	actinolite	antofillite	other amphiboles	hypersthene	olivine	spinel	epidote	clinozoisite	zoisite	other epidotes	prehnite	pumpellyite	chloritoid	lawsonite	carpholite	garnet	staurolite	andalusite	kyanite	sillimanite	Total Transparent
FT1B	0	0	0	0	0	0	0	0	0	2	18	0	0	0	0	0	12	0	0	14	0	0	0	0	100
FT3	0	0	0	0	0	0	0	0	0	3	2	0	0	0	0	0	12	0	0	13	0	0	0	0	100
FT4	0	0	0	0	0	0	0	0	0	2	0	0	0	0	0	0	25	0	0	15	1	0	0	0	100
NAM 3D	0	0	0	0	0	0	0	0	0	0	11	0	0	0	0	0	0	0	0	0	0	0	0	0	100
NAM 25A	0	0	0	0	0	0	0	0	0	16	43	0	0	2	0	0	0	0	0	0	0	0	0	0	100
NAM 26	0	0	0	0	0	0	0	0	0	7	44	0	0	0	0	0	0	0	0	1	0	0	0	0	100
MY05 23A	0	0	0	0	0	2	0	0	0	0	33	0	0	1	0	0	0	0	0	6	0	0	0	0	100

Appendix 1 – 6a: Bulk rock Sm-Nd analysis

Sample	Location	GPS/ formation	Lithology	Sm	Nd	Sm/Nd	147Sm/144Nd	143Nd/144Nd	1s ppm	epsilon Nd
Andaman Islands										
AN05-31	Namunagarh Quarry	Namunagarh Grit	Sandstone	4.83	25.3134	0.1909	0.1154	0.512271	16	**-7.2**
AN05 3E	Namunagarh Quarry	Namunagarh Grit	Mudstone	1.99	7.18860	0.2769	0.1674	0.512799	19	**3.1**
AF1A	Corbyns Cove	Andaman Flysch	Mudstone	11.17	50.6900	0.2204	0.1332	0.512068	10	**-11.1**
AF2	Corbyns Cove	Andaman Flysch	Sandstone	5.05	25.7129	0.1966	0.1188	0.512220	12	**-8.2**
Myanmar - Rivers draining Eocene rocks										
MY05 8A	Lemyu River	20°N 49.212, 93°E 18.576	MR Sand	4.02	20.0489	0.2010	0.1215	0.512300	18	**-7.4**
MY05 15A	Kyeintuli River	17°N 057.139, 94°E 33.087	MR Sand	3.33	16.4129	0.2035	0.1250	0.512434	14	**-4.0**
MY05 17B	Thanlwe River	18°N 59.097, 94°E 15.244	MR Mud	3.48	17.6156	0.1977	0.1195	0.512427	18	**-4.1**
MY05 22B	Thandwe river	18°N 27.466, 94°E 23.563	MR Mud	3.60	18.0331	0.1997	0.1207	0.512424	14	**-4.2**
MY05 23B	Irrawaddy River	18°N 48.391, 95°E 12.218	MR Mud	3.67	17.9317	0.2052	0.124	0.512210	18	**-8.3**

*MR = modern river sample

Method:

For this study, sandstone and mudstone samples were collected from type localities from the Andaman Flysch and the Mithakhari Group. Whole rock samples were ignited overnight at 900 °C to remove any organic material. Dissolution and analytical methods follow Ahmad et al. (2000), with the exception that the samples were spiked with a mixed ^{150}Nd-^{149}Sm spike and the ^{143}Nd-^{144}Nd ratios were measured on the spiked fraction. εNd is calculated relative to the present day (i.e., at t = 0) using CHUR $^{143}Nd/^{144}Nd = 0.512638$. Sm and Nd blanks were <10−3 of the sample, and the laboratory Johnson Mathey Nd internal standard gave $^{143}Nd/^{144}Nd = 0.511\ 9 \pm 5$ ($1\sigma = 24$) over the period of the analyses.

Appendix 1 – 6b: Single-grain apatite Sm-Nd data

Sample	Formation/Age	Lithology	147Sm/144Nd	2 sd of NIST610	2 se (internal)	143Nd/144Nd	2se ppm	epsilon Nd (0)
1	Andaman Flysch AF1A Corbyns Cove	Apatite grain	0.123272	0.001140	0.000069	0.512855	134	**4.24**
2	Andaman Flysch AF1A Corbyns Cove	Apatite grain	0.070462	0.000408	0.000065	0.512803	127	**3.21**
3	Andaman Flysch AF1A Corbyns Cove	Apatite grain	0.090724	0.000581	0.000058	0.512237	114	**-7.83**
4	Andaman Flysch AF1A Corbyns Cove	Apatite grain	0.073481	0.000171	0.000054	0.512588	105	**-0.98**
5	Andaman Flysch AF1A Corbyns Cove	Apatite grain	0.082561	0.000180	0.000031	0.512485	61	**-2.98**
6	Andaman Flysch AF1A Corbyns Cove	Apatite grain	0.100785	0.002208	0.000062	0.512404	121	**-4.57**
7	Andaman Flysch AF1A Corbyns Cove	Apatite grain	0.106736	0.000552	0.000046	0.512211	90	**-8.33**
8	Andaman Flysch AF1A Corbyns Cove	Apatite grain	0.093898	0.000488	0.000033	0.511800	65	**-16.35**
9	Andaman Flysch AF1A Corbyns Cove	Apatite grain	0.108342	0.001112	0.000047	0.512545	93	**-1.81**
10	Andaman Flysch AF1A Corbyns Cove	Apatite grain	0.099159	0.000388	0.000033	0.512669	64	**0.61**
11	Andaman Flysch AF1A Corbyns Cove	Apatite grain	0.113837	0.000346	0.000051	0.512794	99	**3.03**
12	Andaman Flysch AF1A Corbyns Cove	Apatite grain	0.120108	0.000750	0.000044	0.512621	86	**-0.33**
13	Andaman Flysch AF1A Corbyns Cove	Apatite grain	0.078972	0.000114	0.000067	0.512291	131	**-6.77**
14	Andaman Flysch AF1A Corbyns Cove	Apatite grain	0.067596	0.000236	0.000075	0.512425	147	**-4.16**
15	Andaman Flysch AF1A Corbyns Cove	Apatite grain	0.114968	0.000317	0.000043	0.511822	83	**-15.92**
16	Andaman Flysch AF1A Corbyns Cove	Apatite grain	0.105069	0.001427	0.000067	0.512792	131	**3.01**
17	Andaman Flysch AF1A Corbyns Cove	Apatite grain	0.117803	0.000238	0.000055	0.512607	108	**-0.60**
18	Andaman Flysch AF1A Corbyns Cove	Apatite grain	0.085210	0.000165	0.000056	0.512321	109	**-6.19**
19	Andaman Flysch AF1A Corbyns Cove	Apatite grain	0.102799	0.000424	0.000051	0.512782	99	**2.80**
20	Andaman Flysch AF1A Corbyns Cove	Apatite grain	0.082935	0.000202	0.000136	0.512486	266	**-2.96**
21	Andaman Flysch AF1A Corbyns Cove	Apatite grain	0.136207	0.000550	0.000118	0.512192	230	**-8.71**
22	Andaman Flysch AF1A Corbyns Cove	Apatite grain	0.131323	0.000741	0.000062	0.512791	122	**2.99**
23	Andaman Flysch AF1A Corbyns Cove	Apatite grain	0.244791	0.003438	0.000076	0.512607	148	**-0.61**
24	Andaman Flysch AF1A Corbyns Cove	Apatite grain	0.172124	0.000850	0.000079	0.512771	154	**2.59**

GPS reference for AF1A Corbyns Cove N11 38.430' E92 45.292'

Method:
A 193 nm homogenized ArF New Wave/Merchantek laser ablation system was linked to a ThermoFinigan Neptune multicollector mass spectrometer at the University of Cambridge (UK). All ablation was carried out in a He environment and mixed with Ar and N after the ablation cell. Laser spot sizes were 65–90 μm. During the analytical period, standards reproduced to better than 0.5 epsilon units, while samples typically gave internal precisions of 1–2 epsilon units. The full methodology of this in situ approach is detailed in Foster and Vance (2006).

Foster, G.L., and Vance, D., 2006, In situ Nd isotopic analysis of geological materials by laser ablation MC-ICP-MS: Journal of Analytical Atomic Spectrometry,21, pp288–296, doi: 10.1039/b513945g

Appendix 2 – 1: Sample List for Burma (Myanmar) samples

Sample no.	Location co-ordinates	Lithology	Location information
MY05-2A	N20 06.834, E092 53.839	sandstone	Sittwe Pt
MY05-3D	N20 50.193, E092 59.186	sandstone	Kyaktaw, besude temple
MY05-4A	N20 39.390, E093 14.563	MR sand	Lemyu R. downstream of tribs. Tidal.
MY05-5A	N20 44.347, E093 16.456	siltstone	Koum Chang (nr Bungalow)
MY05-6B	N20 44.245, E093 16.134	sandstone	as above
MY05-8A	N20 49.212, E093 18.576	MR Sand	Lemyu River upstream of Wek
MY05-10B	N20 50.421, E093 18.391	sandstone	as above
MY05-14E	N18 27.540, E094 17.412	sandstone	Sabagi Point
MY05-15A	N17 57.139, E094 33.087	MR Sand	Kyeintuli River
MY05-16A	N18 10.087, E094 29.429	MR Sand	Pazunbye River
MY05-17B	N18 59.097, E094 15.244	MR Mud	Thanlwe River
MY05-22A	N18 27.466, E094 23.563	MR Sand	Thandwe River
MY05-23A	N18 48.391, E094 12.218	MR Sand	Irrawaddy River
MY05-23B	N18 48.391, E094 12.218	MR Mud	Irrawaddy River

*MR = modern river sand

Appendix 2 – 2: Petrography

location	River name	Sample no.	Q	F	L	Lv	Lc	Lp	Lch	Lm	Lu	total	M.I. Index
Sittwe Pt.		MY05-2A	59	28	13	4	0	0	0	9	0.0	100.0	200
Kyaktaw, Besude temple		MY05 3D	65	10	25	4	0	0	0	21	0.0	100.0	241
Kyauktaw	Kaladan	MY05 3A, B	42	3	55	1	0	32	1	21	0.0	100.0	121
At Bungalow on Lemyu River		MY05-6B	71	11	19	2	0	0	1	16	0.0	100.0	226
lemyu river between Wek and Luee Tribs		MY05-10B	61	14	24	3	0	1	0	20	0.0	100.0	228
Padali		MY05 1A	47	9	44	1	0	14	0	28	0.0	100.0	138
Kyaukphyu island		-	68	11	21	4	0	1	2	14	0.0	100.0	176
Mrauk U	Lemyu	MY05 4A	13	1	86	1	0	38	1	46	0.0	100.0	115
Sabadgi Point		MY05-14E	12	27	61	54	0	1	1	6	0.0	100.0	167
Migyaunglu	Tanlwe	MY05 17A	8	1	91	3	0	52	1	34	0.0	100.0	101
Taunggok	Taunggok	MY05 18A	11	3	86	2	0	36	0	47	0.0	100.0	106
Shwehle	Tahde	MY05 21A	12	2	86	3	0	34	1	49	0.0	100.0	107
Thandwe	Thandwe	MY05 22A	16	2	82	2	0	41	1	38	0.0	100.0	114
Pazunbye	Pazunbye	MY05 16A	19	2	78	3	0	34	0	41	0.0	100.0	107
Kyieintuli	Kalabyin	MY05 15A	10	1	89	6	0	33	0	50	0.0	100.0	105
			Q	F	L	Lv	Lc	Lp	Lch	Lm	Lu	total	M.I.
MY05 8A-Pebble 1Upstream of Wek	Lemu	MY05 8A P1	51	12	37	19	0	0	4	10	4	100.0	181
MY05 8A-Pebble 2Upstream of Wek	Lemu	MY05 8A P2	39	24	37	9	0	0	1	26	0	100.0	202
MY05 8A-Pebble 3Upstream of Wek	Lemu	MY05 8A P3	35	23	43	15	0	0	1	23	4	100.0	218
MY05 8A-Pebble 4Upstream of Wek	Lemu	MY05 8A P4	76	7	16	1	0	0	0	16	0	100.0	246
MY05 8A-Pebble 5Upstream of Wek	Lemu	MY05 8A P5	60	6	34	10	0	0	2	22	0	100.0	188

Q= quartz; KF= K-feldspar; P= plagioclase; Lv= volcanic lithics; Lc= carbonate lithics; Lp= terrigenous (shale/siltstone) lithics; Lch= chert lithics; Lm= metamorphic lithics; MI= Metamorphic Index.

The MI Index ("Metamorphic Index"; Garzanti and Vezzoli 2003) expresses the average rank of metamorphic rock fragments in the studied samples, and varies from 0 in detritus from sedimentary and volcanic cover rocks to 500 in detritus from high-grade basement rocks

Method:
400 points were counted in the selected samples according to the Gazzi-Dickinson method (Dickinson, 1985). A classification scheme of grain types allowed for the collection of fully quantitative information on the sampled sandstones. Transparent dense minerals were counted on grain mounts according to the 'ribbon counting' method, and 200 minerals were counted also to assess the percentage of etched and corroded grains. Dense minerals were concentrated with sodium metatungstate (density 2.9 g/cm^3) using the 63–250 μm fraction treated with hydrogen peroxide, oxalic acid and sodium ditionite to eliminate organic matter, iron oxides and carbonates respectively.

Appendix 2 – 2b: Heavy mineral data

River	Site	Sample	Facies diagenetica	GSZ (micron)	GSZ (phi)	% non-E	HMC%w HM	avg HM density	avg. tHM density	SRD HM	HM% VFS-FS	HM% transp.	% transparent	% opaque	% turbid	Total	Ud%	ZR	ZTR	T&	LgM	Gt	HgM
Sittwe Pt.		MY052A	40	1000	0.0	0.0	0.2	3.78	3.76	2.65	0.2	0.1	64	13	22	100.0	40	36	22	35	9	32	0
Sittwe Pt no. 2		My05 2A 2	SA	1000	0.0	0.0	0.6	3.59	4.01	2.66	0.6	0.2	30	11	59	100.0	62	68	53	15	7	19	1
Kyaktaw, Besude temple		MY3D	40	1000	0.0	0.0	0.5	3.61	3.68	2.66	0.5	0.3	66	6	27	100.0	34	26	25	36	12	26	0
At Bungalow on Lemyu River		MY6B	70	1000	0.0	0.0	0.3	3.49	3.76	2.65	0.3	0.2	58	0	42	100.0	18	34	45	53	1	0	0
lemyu river between Wek and Luee Tri		MY10B	65	1000	0.0	0.0	0.3	3.34	3.93	2.65	0.3	0.08	26	1	73	100.0	26	58	44	54	1	0	0
Sabadgi Point		MY0514E	60	1000	0.0	0.0	0.4	3.72	4.01	2.66	0.4	0.2	52	7	40	100.0	22	56	8	75	0	0	0
Lemyi	Mrauk U	MY05 4A	SA	1000	0.0	0.0	1.1	3.17	4.20	2.67	1.1	0.0	1	3	96	100.0	60	100	60	0	40	0	0

Hb	&A	CPX	OPX	OS	Total	HCl	MMI	% rounded	zircon	davyite	schorlite	rutile	sagenite	titanite	anatase	brookite	Ti aggregates	apatite	xenotime	monazite	barite	others	blue-green hornblende	green hornblende	green-brown hornblende	brown hornblende	oxy-hornblende	glaucophane	sodic amphiboles
0	1	0	0	0.5	100.0	n.d.	0	4%	3	2	4	4	8	1	0	0	13	20	0	0	0	0	0	0	0	0	0	0	0
0	0	0	0	4	100.0	n.d.	8	12%	24	4	12	12	0	2	0	1	9	1	0	0	0	0	0	0	0	0	0	0	0
0	0	0	0	1	100.0	n.d.	0	3%	1	8	10	5	1	1	0	0	17	18	0	0	0	0	0	0	0	0	0	0	0
0	0	0	0	0.5	100.0	n.d.	n.d.	5%	8	12	15	7	2	0	0	2	43	9	0	0	0	0	0	0	0	0	0	0	0
0	0	0	0	0.5	100.0	n.d.	n.d.	5%	14	4	12	12	3	1	0	0	47	6	0	0	0	0	0	0	0	0	0	0	0
0	0	0	0	17	100.0	n.d.	n.d.	0%	4	0	3	0	0	0	0	0	67	8	0	0	0	0	0	0	0	0	0	0	0
0	0	0	0	0	100.0	n.d.	n.d.	20%	60	0	0	0	0	0	0	0	0	0	0	0	0	0	0	0	0	0	0	0	0

Hb	&A	CPX	OPX	OS	tremolite	actinolite	antofillite	other amphiboles	green augite	brown augite	diopside/hedembergite	diallage	other clinopyroxenes	enstatite	hypersthene	olivine	spinel	epidote	clinozoisite	zoisite	other epidotes	prehnite	pumpellyite	chloritoid	lawsonite	carpholite	garnet	staurolite	andalusite	kyanite	sillimanite	Total Transparent
0	1	0	0	0.5	0	1	0	0	0	0	0	0	0	0	0	0	0	3	0	0	0	0	0	5	0	0	32	0	0	0	0	100.0
0	0	0	0	4	0	0	0	0	0	0	0	0	0	0	0	0	4	2	0	0	0	0	0	4	0	0	19	1	0	0	0	100.0
0	0	0	0	1	0	0	0	0	0	0	0	0	0	0	0	0	1	1	0	0	0	0	0	11	0	0	26	0	0	0	0	100.0
0	0	0	0	0.5	0	0	0	0	0	0	0	0	0	0	0	0	0	1	0	0	0	0	0	0	0	0	0	0.5	0	0	0	100.0
0	0	0	0	0.5	0	0	0	0	0	0	0	0	0	0	0	0	0	1	0	0	0	0	0	0	0	0	0	0	0	0	0	100.0
0	0	0	0	17	0	0	0	0	0	0	0	0	0	0	0	0	17	0	0	0	0	0	0	0	0	0	0	0	0	0	0	100.0
0	0	0	0	0	0	0	0	0	0	0	0	0	0	0	0	0	0	20	0	0	0	0	0	20	0	0	0	0	0	0	0	100.0

Appendix 2 – 3: Detrital zircon fission track data

Sample #	No.x tals	Dosimeter ρd	Nd	Spontaneous ρs	Ns	Induced ρi	Ni	Age dispersion $P\chi^2$	$RE_{\%}$	Central age (Ma) ±1σ	Age Components 1st	2nd	3rd	4th	5th
MY05-2A	20	0.418	3140	4.904	1825	6.813	2666	0.0	64.5	**18.1±2.7**	6.3±0.5 (6)	10.1±0.8 (9)	37.6±2.6 (4)		
MY05-3D	20	0.414	2589	6.058	1387	3.132	744	0.0	63.9	**42.6±6.5**	13±4 (1)	21±2 (9)	60±6 (8)	213±33 (2)	
MY05-4A	49	0.422	3140	5.243	4746	5.243	1990	0.0	31.6	**64.8±3.7**	37.8±2.3 (10)	60.1±4.0 (25)	85±10 (13)		
MY05-6B	40	0.414	2589	9.725	7011	3.547	2453	0.0	44.7	**69.3±5.4**	35±6 (5)	55±4 (16)	82±8 (4)	190±22 (5)	
MY05-10B	52	0.413	2589	8.311	7154	3.430	2589	0.0	69.6	**46.6±4.7**	28±1 (27)	47±3 (12)	108±14 (4)	440±39 (7)	
MY05-14E	61	0.413	2589	6.381	8493	2.318	2589	0.0	38.1	**66.1±3.8**	22±8 (1)	45±2 (19)	65±4 (26)	101±6 (13)	1304±534 (1)
MY05-18A	30	0.425	3140	9.710	3332	2.535	1010	0.0	63.8	**86.4±10.7**	36.4±2.4 (8)	83.1±5.1 (16)	288±52 (4)		
MY05-3B	22	5.336	3698	5.260	2031	3.090	1278	0.0	71.1	**48.2±7.6**	18.4±1.3 (9)	56.6±4.2 (9)	152.9±19.7 (4)		
MY05-8A	25	5.336	3698	4.236	1442	3.090	1061	0.0	36.2	**45.0±3.9**	27.8±2.8 (10)	51.6±5.1 (14)			
MY05-15A	11	5.336	3698	6.836	997	3.313	465	0.0	49.0	**74.2±11.8**	28.3±4.5 (1)	70.5±4.7 (8)	113±26 (1)	613±257 (1)	
MY05-16A	39	5.336	3698	8.287	4473	2.842	1589	0.0	55.6	**91.3±8.7**	53.7±2.3 (20)	116.8±11.6 (12)	291.7±4.1(6)		
MY05-22A	25	5.336	3698	5.622	2944	2.336	1207	0.0	42.5	**78.3±7.4**	45.6±2.8 (9)	94.0±4.7 (15)	595±181 (1)		
MY05-23A	96	5.336	3698	4.211	9004	4.329	9004	0.0	62.3	**38.9±2.4**	14.1±0.7 (17)	22.9±0.8 (33)	31.0±1.7 (12)	49.2±2.6 (14)	82.0±4.9 (19)

(i). Track densities are ($x10^6$ tr cm^{-2}) numbers of tracks counted (N) shown in brackets;

(ii). analyses by external detector method using 0.5 for the $4\pi/2\pi$ geometry correction factor;

(iii). ages calculated using dosimeter glass CN-2; (zircon) ζ_{CN2} =127±5
calibrated by multiple analyses of IUGS apatite and zircon age standards (see Hurford 1990);

(iv). $P\chi^2$ is probability for obtaining χ^2 value for v degrees of freedom, where v = no. crystals - 1;

(v). Central age is a modal age, weighted for different precisions of individual crystals (see Galbraith 1993);

(vi) irradiation in thermal facility of Hifar Reactor, Lucas Heights, Australia (cadmium ratio for Au >100). Samples marked * were irradiated using the well thermalised facility of the Forschungsneutronenquelle Heinz Maier Leibnitz (FRMII) research rector at Garching, Germany.

Samples for ZFT analysis were mounted in PTFE Teflon, polished and etched using a binary eutectic of NaOH:KOH at 225°C. Multiple grain mounts were made for each sample and etched for different durations of time to avoid source bias. Samples were then packed with muscovite external detectors and CN2 glass dosimeter and irradiated in the well thermalised (Cd ratio for Au >100) of the Garching facility, Germany. Fission-track densities were measured using an optical microscope at 1250x magnification. Ages (±1s) were calibrated by the zeta method (Hurford and Green, 1983), using a zeta factor for zircon of 127 ± 5, determined by multiple analyses of zircon age standards.

Galbraith, R.F. and Laslett, G.M., 1993. Statistical models for mixed fission track ages. Nucl. Tracks and Radiation Measurement, 21, 459-470, Hurford, A.J., 1990. Standardization of fission track dating calibration: recommendation by the Fission Track Working Group of the IUGS subcommission on geochronology: Chemical Geology, 80, 177-178.

Appendix 2 – 4: Detrital U-Pb data (UCL)

Sample	206/238	err	207/235	err	206/238 age (Ma)	err (Ma)	206/207 age (Ma)	err (Ma)
MY05 2A								
MY2A1	0.00256	0.00004	0.01833	0.0004	**16.5**	**0.3**	275.4	53.63
MY2A2	0.07563	0.00129	0.61313	0.01214	**470**	**7.7**	557.2	46.74
MY2A3	0.14276	0.00269	1.39874	0.03121	**860.3**	**15.2**	957.3	50.18
MY2A4	0.19013	0.00314	2.00883	0.0323	**1122.1**	**17.0**	1110.1	34.83
MY2A5	0.1162	0.00252	1.02591	0.03081	**708.7**	**14.6**	741.5	69.44
MY2A6	0.17695	0.00276	1.86822	0.02529	**1050.3**	**15.1**	1109.4	28.83
MY2A7	0.00929	0.00039	0.07067	0.00556	**59.6**	**2.5**	417.5	184.96
MY2A9	0.11772	0.00208	1.12105	0.02196	**717.4**	**12.0**	901.2	44.08
MY2A10	0.2693	0.00435	3.66742	0.04992	**1537.2**	**22.1**	1601.7	27.29
MY2A11	0.00619	0.00023	0.04486	0.00319	**39.8**	**1.5**	310.4	169.26
MY2A12	0.14892	0.0026	1.43465	0.02683	**894.9**	**14.6**	926	41.65
MY2A14	0.20739	0.00313	2.36294	0.02638	**1214.9**	**16.7**	1262.5	22.09
MY2A15	0.00692	0.00025	0.05214	0.00359	**44.4**	**1.6**	401.7	162.87
MY2A17	0.31573	0.00494	4.92824	0.05772	**1768.9**	**24.2**	1854.4	21.8
MY2A18	0.1269	0.00207	1.15746	0.01796	**770.1**	**11.9**	814.9	34.24
MY2A19	0.00464	0.00017	0.03014	0.00231	**29.8**	**1.1**	60.5	187.97
MY2A20	0.08258	0.00137	0.64657	0.01091	**511.5**	**8.1**	486.9	39.58
MY2A21	0.12041	0.00221	1.18963	0.02409	**732.9**	**12.7**	980.4	44.77
MY2A22	0.15923	0.00264	1.57188	0.02439	**952.5**	**14.7**	978.7	33.33
MY2A23	0.5892	0.01057	21.39754	0.28654	**2986.2**	**42.9**	3270.5	22.58
MY2A24	0.14752	0.00247	1.40615	0.02251	**887**	**13.9**	907.3	34.74
MY2A25	0.43183	0.00787	10.40395	0.15439	**2314**	**35.4**	2607.4	26.89
MY2A27	0.19221	0.00389	2.12318	0.04918	**1133.3**	**21.0**	1204.5	49.86
MY2A28	0.12159	0.0021	1.16894	0.02002	**739.7**	**12.1**	925.3	37.22
MY2A29	0.17141	0.00289	1.68376	0.02641	**1019.9**	**15.9**	969.5	33.33
MY2A30	0.11285	0.00208	0.97522	0.02061	**689.3**	**12.1**	702.5	47.97
MY2A31	0.13024	0.00232	1.19087	0.02233	**789.2**	**13.3**	821.6	41.32

MY2A32	0.31768	0.00536	4.85228	0.06786	**1778.4**	**26.2**	1816.8	25.94
MY2A34	0.17396	0.00361	1.71127	0.04327	**1033.9**	**19.9**	972.4	55.58
MY2A35	0.09196	0.00206	0.70095	0.02294	**567.1**	**12.2**	428.9	77.58
MY2A36	0.0149	0.00095	0.0959	0.0139	**95.3**	**6.0**	39	338.51
MY2A37	0.15684	0.003	1.45437	0.03186	**939.2**	**16.7**	850.6	48.19
MY2A38	0.21145	0.00367	2.48426	0.03919	**1236.5**	**19.6**	1324.7	31.31
MY2A39	0.11636	0.00241	1.03005	0.02705	**709.6**	**13.9**	753.1	59.21
MY2A40	0.08516	0.0026	0.62289	0.03362	**526.9**	**15.4**	335.7	127.93
MY2A42	0.02904	0.00055	0.21063	0.00485	**184.5**	**3.4**	316.6	54.56
MY2A43	0.12947	0.00235	1.18747	0.02234	**784.8**	**13.4**	826.8	40.43
MY2A44	0.60776	0.01005	20.45939	0.26432	**3061**	**40.3**	3150.1	19.02
MY2A45	0.07893	0.00145	0.6162	0.01257	**489.7**	**8.7**	479.9	46.75
MY2A46	0.34489	0.00604	5.23354	0.07939	**1910.2**	**28.9**	1802.6	26.78
MY2A47	0.08375	0.00194	0.64976	0.02199	**518.5**	**11.5**	464.6	80.06
MY2A48	0.55681	0.00969	16.79258	0.24212	**2853.4**	**40.1**	2972.9	21.89
MY2A49	0.00741	0.00018	0.05127	0.00198	**47.6**	**1.1**	205.6	94.31
MY2A50	0.12313	0.00332	1.10322	0.04419	**748.6**	**19.1**	774.9	90.2
MY2A51	0.29386	0.00514	4.19557	0.06388	**1660.8**	**25.6**	1689.4	26.38
MY2A52	0.0302	0.00054	0.49274	0.00772	**191.8**	**3.4**	1931.5	26.96
MY2A53	0.00157	0.00004	0.01066	0.00039	**10.1**	**0.2**	158.6	89.75
MY2A54	0.08154	0.0015	0.62064	0.012	**505.3**	**9.0**	419.8	41.89
MY2A56	0.3185	0.00606	4.70006	0.0863	**1782.4**	**29.6**	1748	33.01
MY2A58	0.30709	0.0056	4.68784	0.07878	**1726.3**	**27.6**	1808.9	28.56
MY2A59	0.18812	0.00352	1.95183	0.03638	**1111.2**	**19.1**	1072.1	35.99
MY2A61	0.20446	0.00403	2.24357	0.04703	**1199.2**	**21.6**	1182.4	40.95
MY2A62	0.01966	0.00124	0.13536	0.02158	**125.5**	**7.8**	185.7	353.7
MY2A63	0.00974	0.00021	0.07023	0.00209	**62.5**	**1.4**	289.8	69.25
MY2A64	0.00837	0.0004	0.06522	0.00588	**53.7**	**2.5**	463.5	207.79
MY2A65	0.09497	0.00282	0.77871	0.03815	**584.8**	**16.6**	574.2	111.33
MY2A66	0.08835	0.00176	0.70582	0.01608	**545.8**	**10.5**	516	48.35
MY2A67	0.19632	0.00377	2.12202	0.0413	**1155.5**	**20.3**	1145.9	34.97
MY2A68	0.14617	0.00379	1.37225	0.05019	**879.4**	**21.3**	858.9	79.08

MY2A69	0.09058	0.00222	0.73268	0.02614	**559**	**13.2**	539.9	80.77
MY2A70	0.10013	0.00268	0.82366	0.03359	**615.2**	**15.7**	576.3	91.81
MY2A71	0.17497	0.00376	1.79523	0.04543	**1039.4**	**20.6**	1037.9	49.82
MY2A72	0.00804	0.00055	0.06044	0.00912	**51.6**	**3.6**	375.2	333.02
MY2A73	0.11477	0.00238	1.01638	0.02455	**700.4**	**13.8**	731.5	48.29
MY2A74	0.00649	0.00035	0.05	0.00592	**41.7**	**2.2**	425.9	263.27
MY2A75	0.14789	0.00328	1.40199	0.03841	**889.2**	**18.4**	871.8	55.24

Sample	206/238	err	207/235	err	206/238 age (Ma)	err (Ma)	206/207 age (Ma)	err (Ma)
MY05 3D								
3DMY1	0.52872	0.00779	6.84366	0.08204	**2736.0**	**32.8**	1502.1	21.0
3DMY2	0.01762	0.00058	0.12133	0.00806	**112.6**	**3.7**	188.4	159.6
3DMY3	0.20707	0.00346	2.05769	0.03020	**1213.2**	**18.5**	985.8	27.1
3DMY7	0.17525	0.00438	1.45602	0.04142	**1041.0**	**24.0**	1044.7	22.0
3DMY8	0.55040	0.01371	7.51478	0.16337	**2826.8**	**57.0**	1144	26.9
3DMY11	0.32582	0.00441	4.91869	0.05418	**1818.1**	**21.4**	1790.7	21.6
3DMY12	0.19715	0.00289	2.10179	0.03182	**1160.0**	**15.6**	1129.3	33.0
3DMY13	0.19654	0.00449	2.09192	0.06850	**1156.7**	**24.2**	1126.2	72.4
3DMY14	0.19728	0.00300	2.12130	0.03494	**1160.7**	**16.2**	1146.4	36.0
3DMY15	0.30794	0.00427	4.38478	0.05229	**1730.6**	**21.0**	1683.7	23.9
3DMY16	0.01849	0.00102	0.12198	0.01782	**118.1**	**6.5**	90	333.1
3DMY18	0.07588	0.00108	0.61285	0.00928	**471.5**	**6.4**	938.2	115.3
3DMY19	0.18392	0.00247	1.89083	0.02195	**1088.3**	**13.4**	551.6	35.5
3DMY20	0.08603	0.00254	0.75730	0.04025	**532.0**	**15.1**	1056.7	25.1
3DMY21	0.16736	0.00223	1.66595	0.01889	**997.5**	**12.3**	736.6	120.3
3DMY22	0.31872	0.00451	4.70856	0.05896	**1783.5**	**22.1**	991.8	24.4
3DMY23	0.01422	0.00052	0.09242	0.00940	**91.0**	**3.3**	1751.8	24.9
3DMY24	0.44758	0.00597	9.86163	0.10039	**2384.5**	**26.6**	56.8	238.1
3DMY26	0.12589	0.00188	1.16992	0.01962	**764.4**	**10.8**	2453.9	18.2
3DMY27	0.06541	0.00126	0.50077	0.01523	**408.4**	**7.6**	4132.5	79.6
3DMY28	0.12754	0.00241	1.16074	0.03158	**773.8**	**13.8**	850.6	37.9

3DMY29	0.40182	0.00558	8.51419	0.09618	**2177.4**	**25.6**	433.8	73.0
3DMY30	0.35946	0.00481	7.82887	0.08168	**1979.6**	**22.8**	807.1	62.1
3DMY31	0.19573	0.00274	2.06688	0.02766	**1152.3**	**14.8**	2387.7	20.9
3DMY33	0.29386	0.00451	4.00055	0.06256	**1660.8**	**22.5**	2434.4	18.7
3DMY35	0.32862	0.00463	5.01370	0.06351	**1831.7**	**22.5**	1111.2	28.7
3DMY36	0.16382	0.00233	1.66514	0.02362	**978.0**	**12.9**	3852.1	192.2
3DMY37	0.19028	0.00302	2.02003	0.03709	**1122.9**	**16.4**	1601.1	32.2
3DMY38	0.23660	0.00403	2.95718	0.05875	**1369.0**	**21.0**	390.1	187.5
3DMY39	0.15585	0.00276	1.58348	0.03643	**933.7**	**15.4**	1810.9	24.8
3DMY40	0.08880	0.00176	0.74971	0.02278	**548.4**	**10.4**	1034.7	30.8
3DMY41	0.18531	0.00248	1.55621	0.02059	**1095.9**	**13.5**	1121.9	40.1
3DMY42	0.23464	0.00370	2.79686	0.04932	**1358.8**	**19.3**	1440	42.1
3DMY43	0.33333	0.00437	5.15679	0.05311	**1854.5**	**21.1**	1033.8	51.1
3DMY44	0.08237	0.00107	0.81405	0.00924	**510.2**	**6.4**	648.3	70.8
3DMY45	0.17565	0.00232	1.90138	0.02206	**1043.2**	**12.7**	1159.6	24.6
3DMY46	0.23565	0.00311	2.85446	0.03155	**1364.0**	**16.2**	1379.1	22.6
3DMY47	0.08991	0.00123	0.73070	0.01048	**555.0**	**7.3**	564.8	33.3
3DMY48	0.18981	0.00306	2.17391	0.04137	**1120.3**	**16.6**	1270.6	41.0
3DMY49	0.11699	0.00202	1.01452	0.02469	**713.2**	**11.6**	704.5	56.2
3DMY50	0.19996	0.00264	2.16596	0.02462	**1175.1**	**14.2**	1160.9	23.9
3DMY51	0.01628	0.00035	0.10577	0.00452	**104.1**	**2.2**	54.9	106.9
3DMY52	0.30237	0.00435	4.46567	0.05880	**1703.0**	**21.5**	1750.8	26.4
3DMY53	0.50198	0.00710	12.34688	0.13768	**2622.3**	**30.5**	2637.8	20.3
3DMY54	0.12056	0.00176	1.36706	0.02051	**733.8**	**10.1**	1251.1	31.9
3DMY55	0.27131	0.00359	3.55072	0.03789	**1547.4**	**18.2**	1526.3	21.1
3DMY56	0.30570	0.00435	4.48613	0.05746	**1719.5**	**21.5**	1739.0	25.5
3DMY57	0.14184	0.00205	1.54212	0.02257	**855.0**	**11.6**	1168.3	31.4
3DMY58	0.13752	0.00203	1.26727	0.02078	**830.6**	**11.5**	832.5	36.8
3DMY59	0.00817	0.00040	0.05471	0.00708	**52.5**	**2.6**	126.0	295.8
3DMY60	0.45735	0.00589	12.07274	0.11145	**2427.8**	**26.1**	2754.5	15.2
3DMY61	0.26293	0.00354	3.50791	0.03895	**1504.8**	**18.1**	1562.4	21.7
3DMY62	0.21999	0.00309	2.57816	0.03353	**1281.8**	**16.3**	1315.2	26.9

3DMY63	0.25091	0.00377	3.46321	0.05133	**1443.2**	**19.4**	1625.8	30.1
3DMY64	0.32671	0.00439	4.79044	0.05202	**1822.4**	**21.3**	1737.4	20.5
3DMY65	0.11482	0.00214	0.99879	0.02708	**700.7**	**12.4**	711.0	62.4
3DMY66	0.40781	0.00534	10.35178	0.10260	**2204.9**	**24.5**	2690.0	16.3
3DMY67	0.19305	0.00304	1.96317	0.03611	**1137.9**	**16.5**	1034.5	40.1
3DMY68	0.12653	0.00203	1.13260	0.02285	**768.0**	**11.6**	771.5	45.7
3DMY69	0.14437	0.00233	1.37850	0.02749	**869.3**	**13.1**	906.0	44.3
3DMY70	0.08966	0.00134	0.72515	0.01266	**553.5**	**8.0**	554.0	40.2
3DMY71	0.27037	0.00386	3.63025	0.04778	**1542.7**	**19.6**	1574.3	25.8
3DMY72	0.51301	0.00787	13.41234	0.18083	**2669.5**	**33.5**	2738.5	24.0
3DMY73	0.34646	0.00479	5.39862	0.06413	**1917.7**	**23.0**	1848.1	21.8
3DMY74	0.20452	0.00422	8.51962	0.15049	**1199.6**	**22.6**	3480.8	34.8
3DMY75	0.18459	0.00258	1.93185	0.02459	**1092.0**	**14.0**	1092.1	25.9
3DMY76	0.08191	0.00121	0.65756	0.01074	**507.5**	**7.2**	537.0	37.9
3DMY77	0.19165	0.00534	2.09538	0.08914	**1130.3**	**28.9**	1179.1	92.3
3DMY78	0.18229	0.00263	1.88686	0.02668	**1079.5**	**14.4**	1070.0	29.3
3DMY79	0.30422	0.00445	4.52937	0.06232	**1712.2**	**22.0**	1765.2	26.0
3DMY80	0.08624	0.00137	0.68973	0.01346	**533.3**	**8.1**	528.9	45.5
3DMY81	0.18120	0.00291	1.81185	0.03390	**1073.5**	**15.9**	999.9	40.1
3DMY82	0.28472	0.00509	3.87758	0.08045	**1615.1**	**25.6**	1600.5	42.1
3DMY83	0.31305	0.00542	4.64652	0.08937	**1755.7**	**26.6**	1759.4	38.0
3DMY84	0.08931	0.00154	0.71866	0.01696	**551.5**	**9.1**	541.9	55.2
3DMY85	0.13547	0.00202	1.18857	0.01868	**819.0**	**11.5**	728.7	33.9
3DMY86	0.18819	0.00363	1.97654	0.05122	**1111.6**	**19.7**	1098.9	56.0
3DMY87	0.22887	0.00340	2.56717	0.03841	**1328.6**	**17.8**	1229.2	29.6
3DMY88	0.15435	0.00227	1.49884	0.02198	**925.3**	**12.7**	940.1	29.9
3DMY89	0.14974	0.00228	1.40771	0.02292	**899.5**	**12.8**	873.3	34.2
3DMY90	0.19391	0.00330	2.07793	0.04274	**1142.5**	**17.8**	1138.9	43.2
3DMY91	0.36033	0.00561	6.06812	0.09690	**1983.7**	**26.6**	1986.9	28.8
3DMY92	0.32778	0.00668	5.04177	0.12307	**1827.6**	**32.4**	1824.0	48.6
3DMY93	0.16360	0.00249	1.55794	0.02502	**976.8**	**13.8**	899.6	32.8
3DMY94	0.13190	0.00205	1.18473	0.02036	**798.7**	**11.7**	777.9	36.2

3DMY95	0.17942	0.00278	1.71376	0.02887	**1063.8**	**15.2**	905.8	34.5
3DMY96	0.17275	0.00280	1.73244	0.03239	**1027.3**	**15.4**	1005.4	38.6
3DMY97	0.13636	0.00235	1.22717	0.02700	**824.1**	**13.3**	781.8	47.9
3DMY98	0.65882	0.01077	22.46210	0.37361	**3262.6**	**41.9**	3166.4	26.5
3DMY99	0.16227	0.00269	1.60508	0.03169	**969.4**	**15.0**	977.2	41.0
3DMY100	0.20809	0.00342	2.32047	0.04389	**1218.6**	**18.3**	1217.2	37.6

Sample	206/238	err	207/235	err	206/238 age (Ma)	err (Ma)	206/207 age (Ma)	err (Ma)
MY05 10B								
MY10B1	0.18033	0.00348	1.86082	0.05101	**1068.8**	**19.0**	1063.2	59.55
MY10B2	0.17257	0.00318	1.74171	0.04558	**1026.2**	**17.5**	1018.2	56.91
MY10B3	0.0348	0.00068	0.26779	0.008	**220.5**	**4.3**	442.7	71.21
MY10B4	0.08624	0.00175	0.68581	0.02145	**533.3**	**10.4**	515.2	73.83
MY10B5	0.37247	0.00709	6.50725	0.17669	**2041.0**	**33.3**	2051	51.33
MY10B6	0.09551	0.00191	0.81777	0.0251	**588.1**	**11.3**	674.9	70.1
MY10B7	0.18179	0.00367	1.87542	0.05719	**1076.8**	**20.0**	1060.9	65.51
MY10B8	0.15349	0.00298	1.49276	0.04417	**920.5**	**16.7**	940.8	64.36
MY10B9	0.41999	0.00859	8.28041	0.25185	**2260.4**	**39.0**	2260.8	55.9
MY10B10	0.00896	0.00059	0.05998	0.01051	**57.5**	**3.8**	121.5	388.58
MY10B11	0.08734	0.00297	0.69966	0.04281	**539.8**	**17.6**	528.4	141.95
MY10B12	0.36775	0.00749	6.56865	0.2105	**2018.8**	**35.3**	2087.6	59.49
MY10B13	0.30189	0.00657	4.47611	0.15316	**1700.7**	**32.5**	1753.3	66.26
MY10B15	0.00953	0.00045	0.06965	0.00677	**61.1**	**2.9**	322	226.15
MY10B17	0.43396	0.00727	9.12068	0.21332	**2323.5**	**32.7**	2375	39.22
MY10B18	0.12501	0.00207	1.13885	0.03154	**759.4**	**11.9**	810.9	57.06
MY10B19	0.17292	0.00306	1.73583	0.05667	**1028.2**	**16.8**	1010.9	65.32
MY10B20	0.1855	0.00313	1.92238	0.05355	**1096.9**	**17.0**	1075.2	54.55
MY10B21	0.1958	0.00359	2.12309	0.07384	**1152.7**	**19.4**	1165.4	67.57
MY10B22	0.21185	0.0037	2.35555	0.07136	**1238.7**	**19.7**	1214.7	57.54
MY10B23	0.17273	0.00319	1.68198	0.0608	**1027.2**	**17.5**	948.1	71.62
MY10B24	0.29915	0.0053	3.9553	0.12317	**1687.1**	**26.3**	1546.7	55.35

MY10B25	0.176	0.00332	1.76648	0.06661	**1045.1**	**18.2**	1008.5	72.85
MY10B28	0.19239	0.00396	1.99074	0.09174	**1134.3**	**21.4**	1063.8	83.99
MY10B29	0.19165	0.00399	2.00826	0.09511	**1130.3**	**21.6**	1087.3	84.69
MY10B30	0.4754	0.01041	11.93781	0.58379	**2507.2**	**45.5**	2664.1	71.4
MY10B31	0.14615	0.00362	1.46262	0.09505	**879.4**	**20.3**	990	120.47
MY10B32	0.10821	0.00265	0.94138	0.06253	**662.3**	**15.4**	695.9	127.09
MY10B33	0.20939	0.00473	2.19951	0.12476	**1225.5**	**25.2**	1082.5	96.13
MY10B34	0.15436	0.00394	1.60567	0.11054	**925.3**	**22.0**	1059.8	120.9
MY10B35	0.1052	0.00281	0.88993	0.06927	**644.8**	**16.4**	626.2	146.86
MY10B37	0.14414	0.00362	1.32968	0.0928	**868.1**	**20.4**	802.1	117.39
MY10B38	0.18988	0.00504	1.99877	0.15135	**1120.7**	**27.3**	1068.6	122.59
MY10B40	0.24713	0.00684	2.98368	0.2425	**1423.7**	**35.4**	1329.5	121.76
MY10B42	0.10163	0.00173	0.89432	0.036	**624.0**	**10.1**	735.5	85.35
MY10B43	0.29412	0.00374	4.14519	0.05666	**1662.1**	**18.6**	1664.5	25.28
MY10B44	0.07767	0.0011	0.60785	0.01634	**482.2**	**6.6**	481.3	59.72
MY10B46	0.30829	0.0042	4.51033	0.07932	**1732.3**	**20.7**	1733.4	32.38
MY10B47	0.2477	0.00443	3.10307	0.10761	**1426.6**	**22.9**	1443.3	66.6
MY10B48	0.15547	0.00236	1.50764	0.04345	**931.6**	**13.2**	937.8	59.52
MY10B49	0.09245	0.00147	0.75119	0.02734	**570.0**	**8.7**	564.3	79.39
MY10B50	0.16672	0.00232	1.98874	0.0412	**994.0**	**12.8**	1349.4	40.47
MY10B51	0.15329	0.00205	1.47508	0.02797	**919.4**	**11.5**	922	39.24
MY10B52	0.08367	0.00179	0.66882	0.04193	**518.0**	**10.7**	528.2	135.77
MY10B53	0.40764	0.00558	8.13233	0.13395	**2204.1**	**25.5**	2283.9	28.45
MY10B55	0.18264	0.00249	1.90723	0.03769	**1081.4**	**13.6**	1087.9	39.92
MY10B56	0.12981	0.00224	1.16495	0.02273	**786.8**	**12.8**	777	43.92
MY10B57	0.23978	0.00423	2.89768	0.05416	**1385.6**	**22.0**	1374.5	38.76
MY10B58	0.16912	0.00275	1.74704	0.02816	**1007.3**	**15.2**	1066.1	34.38
MY10B59	0.08751	0.00145	0.70284	0.01288	**540.8**	**8.6**	538.2	43.18
MY10B60	0.21144	0.00341	2.44833	0.03747	**1236.5**	**18.1**	1291.7	31.51
MY10B61	0.19348	0.00386	1.99135	0.04916	**1140.2**	**20.8**	1058.1	53.9
MY10B62	0.50181	0.00836	11.85179	0.1719	**2621.6**	**35.9**	2570	25.15
MY10B63	0.55181	0.00948	15.45876	0.23364	**2832.7**	**39.4**	2851.6	25.73

MY10B64	0.24504	0.00483	3.08733	0.06961	**1412.8**	**25.0**	1454.1	46.52
MY10B65	0.09569	0.00266	0.80243	0.03758	**589.1**	**15.6**	632.6	107.27
MY10B68	0.15516	0.00372	1.48079	0.0519	**929.8**	**20.8**	905.1	77.58
MY10B69	0.17209	0.00376	1.76801	0.05138	**1023.6**	**20.7**	1055.1	63.27
MY10B70	0.0139	0.00045	0.09348	0.00607	**89.0**	**2.9**	136.5	158.09
MY10B71	0.09291	0.00174	0.75641	0.01783	**572.7**	**10.3**	568.9	53.82
MY10B72	0.191	0.00339	1.98263	0.03879	**1126.8**	**18.3**	1076.2	40.57
MY10B74	0.0951	0.00169	0.75741	0.01544	**585.6**	**10.0**	520.8	46.05
MY10B75	0.17262	0.00394	1.70755	0.0543	**1026.5**	**21.7**	978.9	69.04
MY10B76	0.08991	0.00302	0.7298	0.04429	**555.0**	**17.9**	562.5	138.56
MY10B77	0.19459	0.00361	2.09109	0.04615	**1146.2**	**19.5**	1145.5	44.38
MY10B78	0.1684	0.00374	1.72648	0.05245	**1003.3**	**20.6**	1051.4	64.34
MY10B79	0.15609	0.00303	1.51	0.03702	**935.0**	**16.9**	933.4	51.12
MY10B80	0.16427	0.0043	1.65135	0.06426	**980.5**	**23.8**	1011.6	83.6
MY10B81	0.09072	0.00182	0.73258	0.01963	**559.8**	**10.8**	551.3	59.35
MY10B82	0.32075	0.00642	4.83016	0.12316	**1793.4**	**31.3**	1786.6	46.81
MY10B83	0.30026	0.00606	4.28406	0.11195	**1692.6**	**30.1**	1687.6	48.37
MY10B84	0.34044	0.00707	5.41822	0.1471	**1888.8**	**34.0**	1886.7	49.13
MY10B85	0.21198	0.00492	2.39266	0.07785	**1239.4**	**26.2**	1242.3	65.42
MY10B86	0.30202	0.00673	4.35373	0.13128	**1701.3**	**33.3**	1706.5	56.19
MY10B87	0.22743	0.00479	2.74993	0.07915	**1321.0**	**25.2**	1375.8	54.67
MY10B88	0.10617	0.00237	0.91464	0.02964	**650.5**	**13.8**	690.5	69.23
MY10B89	0.48564	0.0112	11.36984	0.35454	**2551.8**	**48.6**	2555.6	52.16
MY10B90	0.32678	0.00735	4.82697	0.15269	**1822.7**	**35.7**	1751	57.2

Sample	206/238	err	207/235	err	206/238 age (Ma)	err (Ma)	206/207 age (Ma)	err (Ma)
MY05 14E								
14MY1	0.13910	0.00365	1.30517	0.05576	**839.6**	**20.7**	866.9	96.2
14MY2	0.09577	0.00135	0.80102	0.01095	**589.6**	**8.0**	623.9	31.3
14MY3	0.00775	0.00019	0.05201	0.00251	**49.8**	**1.2**	127.1	119.3
14MY4	0.01511	0.00078	-0.05685	0.02194	**96.6**	**5.0**	0.1	0.0

14MY5	0.00736	0.00058	0.08979	0.01408	**47.3**	**3.7**	1390.7	303.4
14MY6	0.00772	0.00039	0.05208	0.00773	**49.5**	**2.5**	142.9	329.6
14MY7	0.31578	0.00443	4.75684	0.05255	**1769.1**	**21.7**	1784.8	21.5
14MY8	0.00872	0.00059	0.05980	0.01485	**56.0**	**3.7**	180.8	509.2
14MY9	0.01533	0.00044	0.10609	0.00672	**98.1**	**2.8**	200.7	151.4
14MY10	0.01675	0.00119	0.13134	0.02264	**107.1**	**7.6**	483.3	365.7
14MY11	0.00786	0.00040	0.05302	0.00823	**50.5**	**2.6**	140.5	342.7
14MY12	0.07885	0.00162	0.61793	0.02106	**489.2**	**9.7**	482.4	81.1
14MY13	0.00759	0.00044	0.06034	0.01019	**48.7**	**2.8**	514.6	350.0
14MY14	0.03457	0.00118	0.24844	0.01865	**219.1**	**7.4**	288.3	175.0
14MY15	0.01137	0.00061	0.08726	0.01183	**72.9**	**3.9**	437.6	294.2
14MY16	0.11952	0.00181	1.12444	0.01808	**727.8**	**10.4**	874.1	35.9
14MY17	0.01543	0.00075	0.10055	0.01141	**98.7**	**4.8**	60.5	269.3
14MY18	0.00882	0.00042	0.13327	0.01046	**56.6**	**2.7**	1790.8	156.9
14MY19	0.00840	0.00049	0.05541	0.00797	**53.9**	**3.2**	87.9	331.7
14MY20	0.00795	0.00027	0.06594	0.00436	**51.0**	**1.7**	609.0	150.4
14MY21	0.00800	0.00040	0.05009	0.00810	**51.3**	**2.6**	0.1	332.0
14MY22	0.08883	0.00179	0.69341	0.02235	**548.6**	**10.6**	474.5	77.1
14MY23	0.09956	0.00189	0.78618	0.02307	**611.8**	**11.1**	500.2	69.6
14MY25	0.01291	0.00145	0.09144	0.04229	**82.7**	**9.2**	256.8	832.5
14MY26	0.09360	0.00174	0.73892	0.02044	**576.8**	**10.3**	499.7	66.0
14MY27	0.01540	0.00074	0.11272	0.01318	**98.5**	**4.7**	331.7	262.3
14MY28	0.19708	0.00313	2.06636	0.03606	**1159.6**	**16.8**	1095.2	37.8
14MY29	0.01262	0.00060	0.11141	0.01161	**80.9**	**3.8**	740.9	223.6
14MY30	0.01491	0.00079	0.10742	0.01306	**95.4**	**5.0**	294.8	275.7
14MY31	0.08316	0.00177	0.63124	0.02237	**515.0**	**10.5**	413.2	84.1
14MY32	0.00749	0.00046	0.06036	0.00998	**48.1**	**3.0**	545.2	344.0
14MY33	0.17676	0.00332	1.74750	0.04426	**1049.3**	**18.2**	976.5	56.2
14MY34	0.10175	0.00157	1.06194	0.01757	**624.7**	**9.2**	1086.1	35.7
14MY35	0.00783	0.00102	0.37468	0.05370	**50.3**	**6.5**	3692.5	266.8
14MY36	0.00821	0.00088	0.05165	0.01645	**52.7**	**5.7**	0.1	637.3
14MY37	0.02220	0.00075	0.14260	0.01069	**141.5**	**4.7**	27.0	183.7

14MY38	0.09721	0.00142	0.85062	0.01224	**598.0**	**8.3**	722.9	31.9
14MY39	0.09152	0.00151	0.76323	0.01590	**564.5**	**8.9**	619.9	48.2
14MY40	0.04576	0.00092	0.32883	0.01085	**288.5**	**5.7**	289.4	80.0
14MY41	0.00785	0.00018	0.04916	0.00234	**50.4**	**1.2**	0.1	84.3
14MY42	0.19227	0.00451	2.06125	0.07062	**1133.7**	**24.4**	1139.7	74.8
14MY43	0.00819	0.00058	0.05795	0.01203	**52.6**	**3.7**	254.8	438.0
14MY44	0.08739	0.00163	0.64782	0.01852	**540.1**	**9.7**	359.9	68.5
14MY45	0.00808	0.00048	0.10383	0.01183	**51.8**	**3.1**	1492.0	224.1
14MY46	0.07948	0.00208	0.61716	0.03162	**493.0**	**12.5**	462.9	119.5
14MY47	0.01427	0.00083	0.10549	0.01479	**91.3**	**5.3**	354.1	309.3
14MY48	0.01531	0.00126	0.10394	0.02776	**98.0**	**8.0**	157.6	548.6
14MY49	0.08790	0.00140	0.76136	0.01428	**543.1**	**8.3**	701.0	42.3
14MY50	0.00823	0.00033	0.05908	0.00572	**52.9**	**2.1**	286.1	221.3
14MY51	0.08285	0.00163	0.64940	0.01979	**513.1**	**9.7**	483.7	72.5
14MY52	0.01397	0.00051	0.09512	0.00816	**89.4**	**3.2**	164.4	202.0
14MY53	0.00875	0.00065	0.08036	0.01241	**56.2**	**4.2**	823.7	320.9
14MY54	0.15160	0.00238	1.52760	0.02667	**910.0**	**13.3**	1014.7	37.3
14MY55	0.01564	0.00050	0.11405	0.00845	**100.1**	**3.2**	322.0	170.5
14MY56	0.00807	0.00094	0.05037	0.01832	**51.8**	**6.0**	0.1	689.7
14MY57	0.10682	0.00168	0.92725	0.01694	**654.3**	**9.8**	705.0	40.8
14MY58	0.00791	0.00028	0.05347	0.00469	**50.8**	**1.8**	146.5	206.0
14MY59	0.01453	0.00106	0.09561	0.02727	**93.0**	**6.7**	82.1	581.2
14MY60	0.00793	0.00061	0.04997	0.01817	**50.9**	**3.9**	0.1	695.8
14MY61	0.09462	0.00183	0.77245	0.02244	**582.8**	**10.8**	572.5	67.3
14MY62	0.01561	0.00078	0.11553	0.01344	**99.9**	**5.0**	354.8	261.6
14MY63	0.00797	0.00051	0.02883	0.01331	**51.2**	**3.3**	0.1	0.0
14MY64	0.00920	0.00096	0.09196	0.02387	**59.0**	**6.2**	997.6	482.9
14MY65	0.01542	0.00127	0.12913	0.03275	**98.6**	**8.0**	627.6	488.8
14MY66	0.01519	0.00117	0.07907	0.03122	**97.2**	**7.5**	0.1	322.3
14MY67	0.32618	0.00611	6.03243	0.12796	**1819.9**	**29.7**	2150.2	40.7
14MY68	0.19815	0.00344	2.15522	0.04644	**1165.4**	**18.5**	1166.2	45.3
14MY69	0.10193	0.00188	0.85658	0.02266	**625.7**	**11.0**	634.0	60.3

14MY70	0.00969	0.00045	0.06593	0.00797	**62.1**	**2.9**	161.4	275.4
14MY71	0.00943	0.00052	0.06375	0.01001	**60.5**	**3.3**	145.6	347.9
14MY72	0.08937	0.00190	0.71856	0.02509	**551.8**	**11.3**	537.1	81.5
14MY73	0.54547	0.00861	17.93589	0.29682	**2806.3**	**35.9**	3107.0	27.0
14MY74	0.00963	0.00023	0.07020	0.00313	**61.8**	**1.5**	319.6	106.2
14MY75	0.00985	0.00068	0.07695	0.01422	**63.2**	**4.3**	472.8	384.9

Sample	206/238	err	207/235	err	206/238 age (Ma)	err (Ma)	206/207 age (Ma)	err (Ma)
MY05 15A								
MY15A2	0.09688	0.00180	0.77467	0.01413	**596.1**	**10.6**	531.8	44.6
MY15A3	0.16431	0.00270	1.66740	0.01878	**980.7**	**15.0**	1033.0	23.5
MY15A4	0.32185	0.00548	4.87722	0.05629	**1798.8**	**26.7**	1800.0	22.7
MY15A5	0.01461	0.00064	0.11553	0.00816	**93.5**	**4.1**	507.3	170.4
MY15A6	0.42909	0.00747	9.34812	0.10595	**2301.6**	**33.7**	2436.4	21.2
MY15A7	0.00246	0.00005	0.01558	0.00031	**15.8**	**0.3**	0.1	47.3
MY15A8	0.25551	0.00432	3.16435	0.03750	**1466.8**	**22.2**	1423.7	24.2
MY15A9	0.35372	0.00621	5.84561	0.07172	**1952.3**	**29.6**	1956.0	24.2
MY15A10	0.32526	0.00553	4.95784	0.05705	**1815.3**	**26.9**	1810.3	22.5
MY15A11	0.09110	0.00163	0.71542	0.01166	**562.0**	**9.6**	491.5	39.4
MY15A12	0.14467	0.00251	1.35976	0.01888	**871.0**	**14.2**	875.6	31.2
MY15A13	0.01299	0.00068	0.08938	0.00799	**83.2**	**4.3**	193.1	221.7
MY15A15	0.09234	0.00181	0.70332	0.01489	**569.3**	**10.7**	423.8	51.7
MY15A16	0.01384	0.00044	0.08978	0.00473	**88.6**	**2.8**	52.7	136.1
MY15A17	0.19607	0.00391	2.05464	0.03908	**1154.2**	**21.1**	1096.5	43.2
MY15A18	0.08601	0.00199	0.67462	0.01937	**531.9**	**11.8**	488.1	71.6
MY15A19	0.03680	0.00081	0.27696	0.00760	**233.0**	**5.1**	396.8	67.7
MY15A20	0.01579	0.00068	0.11254	0.00894	**101.0**	**4.3**	273.6	190.9
MY15A21	0.09873	0.00181	0.78782	0.01358	**606.9**	**10.6**	526.0	41.8
MY15A22	0.05362	0.00119	0.38648	0.01069	**336.7**	**7.3**	298.9	70.0
MY15A23	0.02426	0.00081	0.16203	0.00972	**154.5**	**5.1**	121.8	149.7
MY15A25	0.10543	0.00230	0.97283	0.02282	**646.1**	**13.4**	836.3	55.8

MY15A26	0.09398	0.00169	0.74628	0.01219	**579.1**	**10.0**	514.8	39.5
MY15A27	0.09423	0.00256	0.75250	0.02819	**580.5**	**15.1**	527.0	91.8
MY15A28	0.17289	0.00325	1.70278	0.02902	**1028.0**	**17.9**	970.5	38.7
MY15A29	0.55604	0.00984	14.95780	0.17704	**2850.3**	**40.8**	2786.1	21.1
MY15A30	0.20367	0.00363	2.13386	0.03086	**1195.0**	**19.4**	1095.3	31.6
MY15A31	0.09257	0.00157	0.74909	0.00990	**570.7**	**9.3**	555.8	30.4
MY15A32	0.01385	0.00036	0.09294	0.00358	**88.7**	**2.3**	132.1	99.1
MY15A33	0.01487	0.00068	0.10174	0.00823	**95.1**	**4.3**	178.1	199.8
MY15A35	0.10069	0.00523	0.85284	0.06352	**618.5**	**30.7**	654.2	178.7
MY15A36	0.09260	0.00208	0.73365	0.01990	**570.9**	**12.2**	508.8	66.9
MY15A37	0.01172	0.00023	0.08781	0.00187	**75.1**	**1.5**	384.6	52.8
MY15A38	0.05134	0.00126	0.44652	0.01340	**322.8**	**7.7**	710.4	72.6
MY15A39	0.15021	0.00311	1.33509	0.02933	**902.1**	**17.4**	756.5	51.9
MY15A40	0.09146	0.00162	0.73383	0.01118	**564.1**	**9.6**	536.0	36.5
MY15A41	0.14319	0.00300	1.44637	0.03077	**862.7**	**16.9**	1020.6	48.9
MY15A42	0.18354	0.00345	1.88250	0.03153	**1086.3**	**18.8**	1051.4	37.5
MY15A43	0.01394	0.00030	0.08846	0.00240	**89.3**	**1.9**	0.1	68.3
MY15A44	0.38040	0.00652	6.51791	0.08009	**2078.2**	**30.5**	2017.7	22.9
MY15A45	0.15517	0.00279	1.47089	0.02239	**929.9**	**15.6**	890.4	34.1
MY15A46	0.15182	0.00268	1.44837	0.02089	**911.2**	**15.0**	903.3	31.9
MY15A47	0.00198	0.00004	0.01287	0.00027	**12.8**	**0.3**	48.9	55.1
MY15A49	0.32176	0.00566	4.78770	0.06423	**1798.3**	**27.6**	1763.4	26.2
MY15A50	0.34085	0.00625	5.49892	0.07980	**1890.7**	**30.1**	1909.8	28.7
MY15A51	0.01446	0.00084	0.09966	0.01007	**92.5**	**5.4**	193.3	247.9
MY15A52	0.04098	0.00073	0.28441	0.00456	**258.9**	**4.5**	208.5	39.7
MY15A53	0.14348	0.00264	1.34253	0.02193	**864.3**	**14.9**	862.7	36.9
MY15A54	0.17847	0.00311	1.71886	0.02399	**1058.6**	**17.0**	922.3	30.3
MY15A55	0.10896	0.00217	0.91842	0.01877	**666.7**	**12.6**	642.0	48.8
MY15A56	0.09147	0.00160	0.70832	0.01029	**564.2**	**9.5**	456.4	33.8
MY15A58	0.17215	0.00333	1.72252	0.03113	**1024.0**	**18.3**	999.9	40.7
MY15A59	0.51202	0.00913	11.92046	0.16316	**2665.2**	**38.9**	2544.6	24.5
MY15A60	0.14583	0.00271	1.36840	0.02309	**877.6**	**15.3**	868.0	38.1

MY15A61	0.02082	0.00079	0.13927	0.01109	**132.9**	**5.0**	121.2	192.2
MY15A62	0.01289	0.00046	0.08434	0.00578	**82.6**	**2.9**	68.0	170.7
MY15A63	0.13760	0.00307	1.25889	0.03107	**831.1**	**17.4**	814.7	58.1
MY15A64	0.01585	0.00044	0.10477	0.00441	**101.4**	**2.8**	91.9	109.9
MY15A65	0.34274	0.00619	5.30865	0.07869	**1899.8**	**29.7**	1835.0	28.7
MY15A66	0.03390	0.00061	0.29028	0.00459	**214.9**	**3.8**	674.4	36.1
MY15A67	0.13180	0.00239	1.21779	0.01938	**798.1**	**13.6**	835.1	35.5
MY15A68	0.53419	0.00978	14.09120	0.20856	**2759.1**	**41.1**	2751.0	26.1
MY15A69	0.32071	0.00576	4.67099	0.06966	**1793.2**	**28.1**	1722.5	29.1
MY15A70	0.01553	0.00044	0.10540	0.00461	**99.3**	**2.8**	154.5	111.7
MY15A71	0.22376	0.00347	2.56378	0.04279	**1301.7**	**18.3**	1272.3	35.6
MY15A72	0.01507	0.00054	0.10062	0.00733	**96.4**	**3.4**	121.1	178.3
MY15A73	0.09636	0.00270	0.81203	0.03767	**593.1**	**15.9**	644.1	107.7
MY15A74	0.24687	0.00458	3.19440	0.07020	**1422.3**	**23.7**	1505.8	46.2
MY15A75	0.08459	0.00160	0.68712	0.01827	**523.5**	**9.5**	564.7	63.3
MY15A76	0.01519	0.00052	0.10860	0.00727	**97.2**	**3.3**	279.5	160.5
MY15A79	0.01600	0.00085	0.11352	0.01400	**102.3**	**5.4**	262.5	280.4
MY15A80	0.01102	0.00037	0.07414	0.00509	**70.7**	**2.3**	138.3	167.4
MY15A82	0.01447	0.00036	0.15982	0.00584	**92.6**	**2.3**	1200.5	80.9
MY15A83	0.12128	0.00201	1.07497	0.02287	**738.0**	**11.6**	751.1	48.5
MY15A85	0.02292	0.00038	0.18617	0.00406	**146.1**	**2.4**	564.1	51.1

Sample	206/238	err	207/235	err	206/238 age (Ma)	err (Ma)	206/207 age (Ma)	err (Ma)
MY05 16A								
MY16-1	0.09113	0.80000	0.72482	7.00000	**562.2**	**9.1**	539.6	28.2
MY16-2	0.01491	0.90000	0.11642	2.70000	**97.5**	**1.3**	530.9	58.9
MY16-3	0.13208	0.80000	1.20466	1.30000	**799.7**	**13**	840.9	25.5
MY16-4	0.03921	0.80000	0.27856	1.70000	**247.9**	**4.2**	289.8	37.7
MY16-5	0.19584	0.80000	2.22074	1.60000	**1152.9**	**19.8**	1256.2	25.2
MY16-6	0.01779	0.90000	0.12065	2.40000	**113.7**	**2.2**	183.8	56.2
MY16-7	0.4046	0.80000	7.54704	1.60000	**2190.2**	**40.6**	2138.3	20.3

MY16-8	0.16249	0.80000	1.5987	1.80000	**970.6**	**16.9**	974.6	28.5
MY16-9	0.08954	0.80000	0.71811	1.40000	**552.8**	**9.2**	556	29.4
MY16-10	0.15686	0.80000	1.47614	1.30000	**939.3**	**15.9**	900.8	25.4
MY16-11	0.18439	0.80000	1.88336	1.20000	**1090.9**	**18.7**	1056.9	23.8
MY16-12	0.11297	0.80000	1.00716	1.40000	**690**	**11.6**	752.2	27.3
MY16-13	0.01557	1.10000	0.12397	3.70000	**96.3**	**1.4**	554.9	78.8
MY16-14	0.01417	0.80000	0.09582	2.00000	**90.7**	**1.7**	142.1	48.5
MY16-15	0.15833	0.80000	1.59465	1.20000	**947.5**	**16.2**	978.6	24.4
MY16-16	0.02289	1.00000	0.17246	2.90000	**145.9**	**2.9**	461.5	60.7
MY16-17	0.01593	0.90000	0.11208	2.70000	**101.9**	**2.1**	302.9	60.9
MY16-18	0.10927	0.80000	0.92346	1.40000	**668.5**	**11.5**	637.1	28.3
MY16-19	0.2443	0.80000	4.06154	1.30000	**1395.1**	**10.6**	1983.8	21.5
MY16-20	0.09789	0.80000	0.7941	1.30000	**602**	**10.3**	592	28.3
MY16-21	0.01623	0.90000	0.11839	2.50000	**103.8**	**2.1**	361.8	55.8
MY16-22	0.30984	0.80000	4.52939	1.40000	**1739.9**	**32.7**	1739.5	22.9
MY16-23	0.17637	1.00000	1.75938	3.80000	**1047.1**	**22.8**	1021.2	49.2
MY16-24	0.19548	0.80000	2.22619	1.40000	**1151**	**20.7**	1235.2	25
MY16-25	0.21901	0.80000	2.36486	1.50000	**1276.6**	**23.4**	1211.5	26.4
MY16-26	0.21369	0.80000	2.35108	1.50000	**1248.4**	**22.9**	1241.5	26.1
MY16-27	0.0822	0.90000	0.66128	2.40000	**509.2**	**9.6**	551.1	43.2
MY16-28	0.12481	0.90000	1.13089	1.80000	**758.2**	**13.8**	812.7	32.5
MY16-29	0.52889	0.80000	13.3716	1.90000	**2736.8**	**57.6**	2702	21.9
MY16-30	0.18976	0.90000	2.26709	2.90000	**1120.1**	**22.7**	1303.6	36.3
MY16-31	0.14134	0.90000	1.29947	1.90000	**852.2**	**15.9**	823.1	32.6
MY16-32	0.08157	0.90000	1.13292	2.20000	**501.1**	**5.6**	1695.5	32.8
MY16-33	0.18298	0.90000	1.84937	1.70000	**1083.2**	**20.4**	1051	30.1
MY16-34	0.16771	0.90000	1.71839	2.40000	**999.5**	**19.7**	1073.1	35.5
MY16-35	0.26989	0.90000	3.53993	2.10000	**1540.2**	**30.8**	1580.5	28.9
MY16-36	0.01384	1.20000	0.09507	4.50000	**88.6**	**2.2**	224	100.5
MY16-37	0.15969	0.90000	1.57185	1.70000	**955.1**	**17.9**	954.5	30.6
MY16-38	0.12027	0.90000	1.06706	1.80000	**732.1**	**13.7**	797.2	32.9
MY16-39	0.08655	0.90000	0.68097	2.10000	**535.1**	**10.1**	549.7	39.6

MY16-40	0.10297	0.90000	0.84962	2.00000	**631.8**	**11.9**	652.6	36.4
MY16-41	0.01564	1.00000	0.10847	2.50000	**100**	**2.1**	202.4	54.6
MY16-42	0.17588	0.90000	1.71314	2.40000	**1044.4**	**21**	1018.4	37.4
MY16-43	0.1881	0.90000	3.09068	2.00000	**1128.6**	**9.9**	1986.4	29.3
MY16-44	0.1835	0.90000	1.84944	2.00000	**1086.1**	**21.3**	1074.1	33.7
MY16-45	0.29955	0.90000	4.25878	2.10000	**1689.1**	**35.1**	1730	31
MY16-46	0.10924	0.90000	1.00905	2.20000	**668.3**	**13**	924.2	38.2
MY16-47	0.01388	1.20000	0.09512	4.90000	**88.9**	**2.3**	219.9	109.9
MY16-48	0.2024	0.90000	2.2343	2.30000	**1188.2**	**24.2**	1198.5	36.2
MY16-49	0.38545	0.90000	8.60656	2.00000	**2101.7**	**45.2**	2446.7	29.3
MY16-50	0.01197	1.20000	0.11191	3.50000	**77**	**1.2**	910.4	68
MY16-51	0.33192	0.90000	6.99773	2.20000	**1841.3**	**16**	2363.4	31.2
MY16-52	0.31701	0.90000	4.61236	2.40000	**1775.1**	**38.4**	1772.5	34.7
MY16-53	0.14752	1.10000	1.46106	3.60000	**887**	**20**	987.1	52.8
MY16-54	0.19653	0.90000	2.15509	2.30000	**1156.7**	**23.9**	1174.4	38.5
MY16-55	0.1833	1.00000	1.84176	2.80000	**1085**	**23.1**	1074.1	42.7
MY16-56	0.01475	1.20000	0.09647	3.90000	**94.4**	**2.3**	167.8	85.1
MY16-57	0.20246	1.00000	2.14858	2.70000	**1188.5**	**25.4**	1184.9	41.8
MY16-58	0.01598	1.30000	0.11102	5.40000	**102.2**	**2.8**	234	118.5
MY16-59	0.13188	1.00000	1.22646	2.70000	**798.6**	**16.6**	916.3	44.9
MY16-60	0.01512	1.00000	0.10728	2.90000	**96.7**	**2.1**	261.9	59.3
MY16-61	0.01609	1.10000	0.10621	3.90000	**102.9**	**2.5**	148.3	84.2
MY16-62	0.00637	1.30000	0.03782	4.40000	**40.9**	**1.3**	-114.1	103.2
MY16-63	0.01334	1.20000	0.08968	4.30000	**85.4**	**2.2**	228.1	91.6
MY16-64	0.08734	1.00000	0.71033	2.80000	**539.8**	**11.2**	554.5	50.2
MY16-65	0.20484	1.00000	2.18487	3.10000	**1201.3**	**27**	1194.5	47.9
MY16-66	0.01517	1.10000	0.15636	3.40000	**90.5**	**1.4**	1119.6	59.4
MY16-67	0.15596	1.00000	1.71319	3.00000	**934.3**	**20.5**	1266.2	47.1
MY16-68	0.24464	1.00000	2.83617	3.00000	**1410.8**	**32**	1387.1	46.6
MY16-69	0.03912	1.40000	0.47797	5.10000	**251.9**	**3.8**	1521.5	80.9
MY16-70	0.15848	1.00000	1.48159	3.20000	**948.3**	**21.1**	913.6	52.7
MY16-71	0.13496	1.00000	1.15545	3.10000	**816.1**	**18**	771.4	54.5

MY16-72	0.19537	1.10000	1.97818	3.40000	**1150.4**	**26.8**	1137.9	53.5
MY16-73	0.32137	1.00000	4.62902	3.20000	**1796.4**	**43.2**	1756.6	47.8
MY16-74	0.01702	1.30000	0.12464	4.80000	**108.8**	**2.9**	362.7	98.9
MY16-75	0.01463	1.20000	0.09792	3.80000	**93.6**	**2.3**	194.5	77.7
MY16-76	0.20656	1.10000	2.22427	3.40000	**1210.5**	**28.3**	1200.4	54.4
MY16-77	0.01593	1.30000	0.12025	4.30000	**101**	**1.6**	428.4	86.1
MY16-78	0.1465	1.10000	1.58951	3.40000	**881.3**	**20.2**	1175.1	55.8
MY16-79	0.27608	1.10000	3.93895	3.40000	**1571.6**	**38.1**	1678.5	52.4
MY16-80	0.10223	1.10000	0.85704	3.80000	**627.5**	**14.6**	687.8	65.3

Sample	206/238	err	207/235	err	206/238 age (Ma)	err (Ma)	206/207 age (Ma)	err (Ma)
MY05 22A								
MY22-1	0.04627	1.50000	0.37739	2.50000	**291.6**	**9.1**	547.0	28.0
MY22-2	0.27264	0.10000	3.85013	0.10000	**1554.2**	**2.0**	1661.7	28.3
MY22-3	0.01299	7.80000	0.07943	19.40000	**83.2**	**13.0**	-114.6	46.0
MY22-4	0.08083	0.40000	0.67130	0.70000	**501.1**	**4.2**	560.4	31.9
MY22-5	0.18155	0.80000	1.93661	1.90000	**1075.4**	**19.8**	1107.7	27.7
MY22-6	0.00775	2.10000	0.05748	5.10000	**49.8**	**2.2**	398.8	49.2
MY22-8	0.21750	0.60000	2.94145	1.00000	**1268.7**	**16.9**	1570.9	19.3
MY22-9	0.00829	8.60000	0.17616	5.80000	**53.2**	**9.2**	2357.7	9.0
MY22-10	0.04301	2.90000	0.30707	6.40000	**271.5**	**15.9**	256.1	38.1
MY22-11	0.08652	1.70000	0.70133	3.30000	**534.9**	**18.7**	553.4	32.8
MY22-12	0.08985	1.00000	0.72501	1.90000	**554.6**	**11.6**	560.1	30.8
MY22-13	0.01464	1.20000	0.08302	5.50000	**93.7**	**2.3**	-253.7	129.2
MY22-14	0.01291	0.90000	0.08626	2.30000	**82.7**	**1.7**	97.8	49.8
MY22-15	0.23483	0.50000	2.84207	0.70000	**1359.8**	**16.2**	1385.8	18.8
MY22-16	0.00911	2.40000	0.05334	9.20000	**58.5**	**2.9**	-239.8	93.1
MY22-17	0.08435	0.20000	0.70283	0.40000	**522.0**	**2.1**	571.5	51.5
MY22-18	0.15360	0.60000	1.51389	0.90000	**921.1**	**11.5**	931.3	23.4
MY22-19	0.00678	29.10000	0.04169	127.00000	**43.6**	**25.4**	-96.8	81.6
MY22-20	0.02815	2.80000	0.22386	4.80000	**179.0**	**10.3**	220.4	35.7

MY22-21	0.01439	1.00000	0.10043	3.00000	**92.1**	**2.1**	180.5	62.4
MY22-22	0.01367	18.60000	0.08059	80.90000	**87.5**	**32.7**	-205.1	78.8
MY22-23	0.19713	0.90000	2.13691	3.10000	**1159.9**	**22.8**	1165.1	44.8
MY22-24	0.01407	11.40000	0.09750	31.10000	**90.1**	**20.7**	177.7	48.9
MY22-25	0.19673	0.90000	2.19870	1.70000	**1157.7**	**23.4**	1190.6	26.7
MY22-26	0.14810	1.20000	2.46577	1.40000	**890.3**	**22.9**	1928.6	16.5
MY22-27	0.01405	5.30000	0.09098	17.10000	**89.9**	**9.6**	25.2	59.8
MY22-28	0.15058	0.70000	1.45187	1.40000	**904.2**	**13.8**	945.3	29.9
MY22-29	0.11481	3.90000	1.08186	23.30000	**700.6**	**57.6**	857.2	75.5
MY22-30	0.08917	2.00000	0.73172	8.80000	**550.6**	**22.7**	593.4	57.3
MY22-31	0.20114	0.60000	2.18142	1.10000	**1181.4**	**15.9**	1200.7	25.6
MY22-32	0.01406	5.30000	0.09260	26.90000	**90.0**	**9.7**	152.6	88.3
MY22-33	0.00817	19.30000	0.07278	44.40000	**52.5**	**20.4**	730.4	37.0
MY22-34	0.01087	14.10000	0.09073	45.10000	**69.7**	**19.7**	620.1	47.5
MY22-35	0.18916	1.30000	2.12828	3.50000	**1116.8**	**30.8**	1205.8	37.0
MY22-36	0.08205	0.20000	0.63761	0.70000	**508.3**	**2.2**	434.4	88.2
MY22-37	0.01070	13.00000	0.09378	28.10000	**68.6**	**17.9**	728.7	35.3
MY22-38	0.04474	2.40000	0.34086	5.50000	**282.1**	**13.7**	477.2	40.2
MY22-39	0.31645	0.20000	4.76290	0.30000	**1772.4**	**10.1**	1762.2	18.0
MY22-40	0.01494	6.20000	0.10146	16.40000	**95.6**	**11.9**	166.4	49.2
MY22-41	0.10436	0.10000	0.86266	0.30000	**639.9**	**2.1**	603.2	42.6
MY22-42	0.19812	0.80000	2.28596	1.80000	**1165.2**	**21.0**	1260.0	31.9
MY22-43	0.09544	1.80000	0.82362	7.50000	**587.6**	**21.9**	682.0	69.0
MY22-44	0.11285	1.50000	1.03442	3.50000	**689.3**	**21.3**	773.7	40.8
MY22-45	0.00665	41.10000	0.04489	201.00000	**42.7**	**35.1**	121.3	87.1
MY22-46	0.15924	0.60000	1.58347	1.40000	**952.6**	**13.0**	1042.8	35.4
MY22-47	0.20684	0.10000	2.31299	0.20000	**1212.0**	**2.3**	1249.8	57.2
MY22-48	0.21087	0.90000	2.33112	2.20000	**1233.5**	**24.2**	1230.2	35.5
MY22-49	0.15745	2.20000	1.50819	11.60000	**942.6**	**45.2**	934.5	80.4
MY22-50	0.56589	0.00000	16.64577	0.00000	**2890.9**	**2.0**	2905.4	17.7
MY22-51	0.15087	2.00000	1.45543	10.40000	**905.8**	**39.6**	946.1	80.3
MY22-52	0.01099	27.20000	0.07328	150.00000	**70.5**	**38.4**	138.7	99.1

MY22-53	0.16927	0.90000	1.67770	3.10000	**1008.1**	**20.0**	994.7	52.6
MY22-54	0.02039	9.10000	0.17773	28.40000	**130.1**	**23.9**	746.9	50.7
MY22-55	0.01197	15.00000	0.08673	58.40000	**76.7**	**23.1**	347.9	67.7
MY22-56	0.01414	1.20000	0.09735	3.90000	**90.5**	**2.3**	178.6	84.5
MY22-57	0.42830	0.50000	8.92910	0.60000	**2298.0**	**25.4**	2374.6	18.8
MY22-58	0.01290	1.60000	0.12173	4.90000	**82.6**	**2.8**	888.2	78.6
MY22-59	0.00993	13.00000	0.06214	52.90000	**63.7**	**16.6**	-25.6	80.8
MY22-60	0.19986	0.10000	2.14733	0.10000	**1174.6**	**2.1**	1171.6	33.3
MY22-61	0.01343	1.30000	0.09205	4.50000	**86.0**	**2.5**	278.4	77.7
MY22-62	0.17559	0.00000	1.97132	0.10000	**1042.8**	**1.3**	1237.1	44.2
MY22-63	0.10452	0.20000	2.33568	0.20000	**640.8**	**2.2**	2530.0	20.2
MY22-64	0.17802	0.50000	1.77975	1.10000	**1056.1**	**11.2**	1000.8	37.8
MY22-65	0.01926	10.90000	0.13357	51.20000	**123.0**	**27.0**	203.3	89.7
MY22-66	0.02998	0.60000	1.96892	0.30000	**190.4**	**2.3**	4171.7	7.1
MY22-67	0.15447	1.00000	1.54394	3.30000	**926.0**	**20.5**	998.3	56.1
MY22-68	0.01366	18.20000	0.08403	101.00000	**87.5**	**32.0**	13.8	111.1
MY22-69	0.01119	5.00000	0.09285	26.10000	**71.7**	**7.3**	663.4	141.0
MY22-70	0.01016	16.10000	0.06764	69.60000	**65.2**	**21.1**	192.7	82.9
MY22-71	0.01021	13.70000	0.06631	54.90000	**65.5**	**18.0**	108.6	82.3
MY22-72	0.01394	14.90000	0.09723	69.80000	**89.2**	**26.8**	240.8	94.5
MY22-73	0.44075	0.80000	10.28813	1.50000	**2354.0**	**43.2**	2579.1	27.3
MY22-74	0.01483	1.50000	0.10350	5.80000	**94.9**	**2.9**	231.3	107.3
MY22-75	0.57762	0.00000	22.23074	0.00000	**2939.0**	**2.3**	3359.5	9.4
MY22-76	0.14081	1.60000	1.68676	4.50000	**849.2**	**28.3**	1402.0	47.6
MY22-77	0.00762	2.60000	0.04982	10.50000	**48.9**	**2.7**	53.8	108.4
MY22-78	0.10041	1.60000	0.81937	6.70000	**616.8**	**20.2**	584.0	81.4
MY22-79	0.01596	18.50000	0.11230	120.00000	**102.1**	**38.1**	292.9	127.8
MY22-80	0.42619	0.30000	9.27362	0.30000	**2288.5**	**14.6**	2454.6	20.2

Method:

For U-Pb dating samples were analysed by LA-ICPMS using a New Wave 213 aperture imaged frequency quintupled laser ablation system (213nm) coupled to an Agilent 750 quadrupole-based ICP–MS. Real time data were processed using GLITTER and repeated measurements of external zircon standard PL (Svojtka et al., 2001; TIMS reference age 337.1±0.7 Ma) to correct for instrumental mass bias and downhole fractionation affects. Data were filtered using standard discordance tests with a 10% cutoff. U/Th concentrations were determined relative to of NIST glass 612. Data correction was by the 208 method that assumes concordance of the U–Pb and Th–Pb systems.

The table opposite contains all concordant data (<10% discordance) including ages which were For all samples we use 206/238 ages, as the difference between the 207/235 ages and the 206/238 ages above the standard but arbitrary cut-off of 400 Ma, was negligible.

Appendix 2 – 5: Detrital zircon U-Pb data (NIGL)

Sample	206/238	error %	207/235	error %	206/238 age(Ma)	err (Ma)	207/206 age (Ma)	err (Ma)
MY05 8A								
MY05-8A 1	0.4188	2.0	8.3726	2.0	2255	45	2288	34
MY05-8A 2	0.4437	2.0	9.7887	2.0	2367	47	2456	34
MY05-8A 3	0.3180	2.0	4.8050	2.0	1780	36	1793	36
MY05-8A 4	0.3235	2.0	4.8620	2.0	1807	36	1783	36
MY05-8A 5	0.0103	5.5	0.0724	20.0	66	4	241	922
MY05-8A 6	0.1044	2.0	0.9066	7.8	640	13	708	43
MY05-8A 7	0.0142	3.0	0.0919	14.0	91	3	49	669
MY05-8A 8	0.0721	2.0	0.5072	9.0	449	9	241	46
MY05-8A 9	0.2050	2.0	2.2608	5.0	1202	24	1197	39
MY05-8A 10	0.1554	2.0	1.4788	2.0	931	19	899	41
MY05-8A 11	0.0353	2.0	0.2485	3.0	224	4	241	46
MY05-8A 12	0.0377	2.0	0.2545	4.7	238	5	148	47
MY05-8A 13	0.0940	2.0	0.7643	2.0	579	12	567	44
MY05-8A 14	0.0835	2.0	0.6445	2.0	517	10	452	44
MY05-8A 15	0.1873	2.0	2.0140	2.0	1107	22	1147	40
MY05-8A 16	0.0094	2.7	0.0559	20.0	60	2	-168	996
MY05-8A 17	0.0862	2.0	0.6891	2.0	533	11	530	44
MY05-8A 18	0.4531	2.0	10.0590	2.0	2409	48	2466	34
MY05-8A 19	0.1345	2.0	1.2907	2.0	813	16	917	41
MY05-8A 20	0.4725	2.0	10.3909	2.0	2494	50	2450	34
MY05-8A 21	0.0873	2.0	0.7158	25.0	539	11	585	43
MY05-8A 22	0.1481	2.0	1.2458	18.0	890	18	639	43
MY05-8A 23	0.2422	2.0	3.1056	2.0	1398	28	1488	38
MY05-8A 24	0.1394	2.0	1.2490	2.0	841	17	774	42
MY05-8A 25	0.0802	2.0	0.5863	4.0	497	10	329	45
MY05-8A 26	0.1158	2.0	0.9260	10.0	706	14	530	44
MY05-8A 27	0.3238	2.0	4.8711	2.0	1808	36	1784	36
MY05-8A 28	0.6743	2.0	28.6468	2.0	3323	66	3511	31
MY05-8A 29	0.0151	2.0	0.0897	31.0	97	2	-168	50
MY05-8A 30	0.0082	2.0	0.0453	28.0	53	1	-351	52

Method

Zircons were analysed in this study during January 2006 using zircons that were subjected to a thermal annealing procedure followed by a chemical partial dissolution step, using the method of Mattinson (2005) to improve concordance of residual analysed zircon. This procedure reduces the proportion of analyses that are discordant in the U-Pb systematics sense, providing a higher proportion of useful data. Overall in this study the proportion of concordant analyses is >90%, generally much higher than many other zircon ICP-MS studies published in the literature. There is no evidence we are aware of that this procedure introduces any age bias in the provenance signatures, though undoubtedly in some cases it does bias the samples towards lower uranium concentrations. Following the annealing and partial dissolution procedure, samples of zircon were mounted in epoxy resin, ground and polished to expose a portion of the internal surface and then analysed.

The laser used was the New Wave 193nm solid state laser. It was operated in either a 50μm spot, usually 5Hz and approximately 5-6J/cm^2 power. The mass spectrometer used for sample MY05 was the Thermo-Elemental Axiom multicollector instrument was used in the first half of the project in multicollection mode using a single ion counting detector and an array of faraday detectors with several magnet peak hops to align appropriate ion beams into detectors using the method of Horstwood et al. (2003). As in all cases of in situ U-Pb dating, measurements on unknowns must be referenced back to measurements of standards of known age for calibration to ensure accuracy and properly estimate uncertainty. In this work data produced on the Axiom used the Manangotry 554Ma monazite standard supplemented by the 54 Ma FC-1 xenotime standard. We are satisfied that the factors affecting elemental fractionation were properly controlled during the procedures to ensure that the Pb/U uncertainties are correct. The reproducibility of the standards was approximately 1-2% on the Axiom during the session in which sample MY05 was analysed. A correction for common Pb was made using the excess ^{204}Pb signal after subtraction for ^{204}Hg, according to the method of Horstwood et al. (2003).

Horstwood, MSA, Parrish, RR, Nowell, GM, and Noble, SR, 2003,Accessory mineral U-Th-Pb geochronology by laser-ablation plasma-ionisation multi-collector mass spectrometry (LA-PIMMS), J. Anal. At. Spectrom., 2003, 18, 837 - 846.

Mattinson, JM, 2005, Zircon U–Pb chemical abrasion (bCA-TIMSQ) method: Combined annealing and multi-step partial dissolution analysis for improved precision and accuracy of zircon ages, Chemical Geology,220, 47-66.

Appendix 2 – 6: Detrital white mica ^{40}Ar-^{39}Ar data

Sample Ref.	40Ar	1σ	39Ar	1σ	38Ar	1σ	37Ar	1σ	36Ar	1σ	40Ar (ATM)%	40Ar*/39Ark	σF	Age (Ma)	1σ
MY05 2A															
4283	0.10112	0.00195	0.02875	0.00002	0.00041	0.00001	0.00054	0.00001	0.000090	0.00001	26.5	2.579	0.005	14.7	0.2
4294	0.06121	0.00194	0.01789	0.00002	0.00020	0.00001	0.00030	0.00001	0.000040	0.00001	19.3	2.755	0.012	15.7	0.2
4286	0.11188	0.00195	0.03074	0.00003	0.00041	0.00001	0.00005	0.00001	0.000078	0.00001	20.8	2.875	0.004	16.4	0.2
4285	0.10037	0.00194	0.02296	0.00003	0.00032	0.00001	0.00001	0.00001	0.000101	0.00001	30.0	3.049	0.007	17.4	0.2
4296	0.08251	0.00194	0.01911	0.00002	0.00024	0.00001	0.00035	0.00001	0.000055	0.00001	19.9	3.448	0.010	19.7	0.2
4300	0.14994	0.00194	0.02850	0.00003	0.00037	0.00001	0.00001	0.00001	0.000064	0.00001	12.7	4.579	0.005	26.1	0.3
4311	0.05940	0.00193	0.00893	0.00002	0.00016	0.00001	0.00092	0.00001	0.000038	0.00001	19.2	5.368	0.047	30.6	0.5
4308	0.38150	0.00193	0.04175	0.00002	0.00052	0.00001	0.00100	0.00001	0.000074	0.00001	5.8	8.586	0.002	48.6	0.5
MY05 10B															
4355	0.08398	0.00191	0.01218	0.00001	0.00016	0.00001	0.00109	0.00001	0.000095	0.00001	33.8	4.558	0.025	26.0	0.3
4327	0.07126	0.00192	0.00930	0.00001	0.00010	0.00001	0.00096	0.00001	0.000075	0.00001	31.4	5.252	0.043	29.9	0.5
4339	0.10242	0.00192	0.01112	0.00001	0.00012	0.00001	0.00025	0.00001	0.000060	0.00001	17.3	7.594	0.030	43.1	0.5
4319	0.05783	0.00193	0.00406	0.00001	0.00007	0.00001	0.00037	0.00001	0.000044	0.00001	22.8	10.988	0.227	62.0	1.7
4337	0.08047	0.00192	0.00630	0.00001	0.00005	0.00001	0.00035	0.00001	0.000002	0.00001	0.9	12.640	0.094	71.1	1.0
4354	0.21021	0.00191	0.00435	0.00001	0.00005	0.00001	0.00084	0.00001	0.000091	0.00001	12.9	42.004	0.211	226.3	2.7
4333	0.75542	0.00193	0.00683	0.00001	0.00004	0.00001	0.00003	0.00001	0.000010	0.00001	0.4	109.924	0.141	541.1	5.3

Sample Ref.	40Ar	1σ	39Ar	1σ	38Ar	1σ	37Ar	1σ	36Ar	1σ	40Ar (ATM)%	40Ar*/39Ark	σF	Age (Ma)	1σ
23A Irrawaddy															
4280	0.07988	0.00195	0.03072	0.00003	0.00041	0.00001	0.00111	0.00001	0.00008	0.00001	30.7	1.800	0.004	10.3	0.1
4279	0.11810	0.00195	0.03661	0.00003	0.00045	0.00001	0.00091	0.00001	0.00005	0.00001	13.7	2.778	0.003	15.9	0.2
4231	0.07369	0.00197	0.01631	0.00002	0.00021	0.00001	0.00031	0.00001	0.00005	0.00001	18.7	3.663	0.015	20.9	0.3
4249	0.07531	0.00196	0.01791	0.00003	0.00024	0.00001	0.00029	0.00001	0.00003	0.00001	11.6	3.707	0.012	21.2	0.3
4265	0.08919	0.00195	0.01819	0.00002	0.00022	0.00001	0.00031	0.00001	0.00007	0.00001	23.5	3.739	0.012	21.3	0.3
4225	0.11644	0.00198	0.02572	0.00003	0.00033	0.00001	0.00046	0.00001	0.00007	0.00001	17.2	3.740	0.006	21.3	0.2
4213	0.07806	0.00198	0.01777	0.00003	0.00022	0.00001	0.00015	0.00001	0.00004	0.00001	14.2	3.757	0.013	21.4	0.3
4217	0.14102	0.00198	0.02342	0.00003	0.00030	0.00001	0.00043	0.00001	0.00010	0.00001	20.7	4.761	0.007	27.1	0.3
4211	0.27964	0.00199	0.05055	0.00005	0.00058	0.00001	0.00113	0.00001	0.00007	0.00001	7.4	5.110	0.002	29.1	0.3
4251	0.10753	0.00196	0.01931	0.00003	0.00024	0.00001	0.00053	0.00001	0.00002	0.00001	5.1	5.272	0.010	30.0	0.3
4229	0.14321	0.00198	0.02504	0.00003	0.00033	0.00001	0.00135	0.00001	0.00002	0.00001	3.5	5.510	0.006	31.4	0.4
4219	0.24809	0.00198	0.03395	0.00003	0.00043	0.00001	0.00018	0.00001	0.00013	0.00001	15.1	6.189	0.004	35.2	0.4
4227	0.17011	0.00198	0.02285	0.00003	0.00025	0.00001	0.00040	0.00001	0.00004	0.00001	6.9	6.911	0.008	39.2	0.4
4209	0.24781	0.00200	0.03193	0.00004	0.00039	0.00001	0.00013	0.00001	0.00000	0.00001	0.0	7.754	0.004	44.0	0.5
4257	0.38012	0.00196	0.03370	0.00002	0.00045	0.00001	0.00008	0.00001	0.00028	0.00001	22.1	8.769	0.004	49.6	0.6
4277	0.39282	0.00195	0.03986	0.00002	0.00047	0.00001	0.00058	0.00001	0.00012	0.00001	9.5	8.901	0.003	50.4	0.6
4223	0.41313	0.00198	0.04373	0.00002	0.00050	0.00001	0.00074	0.00001	0.00005	0.00001	3.3	9.112	0.002	51.6	0.6
4259	0.32643	0.00197	0.02348	0.00003	0.00032	0.00001	0.00031	0.00001	0.00010	0.00001	9.6	12.541	0.008	70.6	0.8
4247	0.57900	0.00197	0.02704	0.00002	0.00037	0.00001	0.00058	0.00001	0.00007	0.00001	3.4	20.631	0.006	114.7	1.3
3000	10.52935	0.05885	0.10377	0.00005	0.00108	0.00004	0.00010	0.00002	0.00086	0.00021	2.4	98.775	0.346	493.1	5.2

*Blank, decay and Cl-corrected peaks are expressed in volts

Appendix 2 – 6 continued.

Method:

Laser 40Ar/39Ar single fusion experiments were carried out in the NERC Argon Isotope Laboratory, East Kilbride, Scotland. For each sample ca 50 grains varying in grain size from larger than 1 mm to ca. 100 micrometer diameter were packed in approximately 1 cm square Al-foil packages, stacked and interspersed with packages containing a mineral standard into a 25 mm OD Al irradiation tube. The monitor mineral standard is Taylor Creek Rhyolite sanidine (TCR2a) with a 40Ar/39Ar age of 28.34 Ma (Renne et al. 1998). Samples and monitors were irradiated for 10 hrs in a Cd-lined facility (RODEO) at the Petten HFR, Netherlands.

Following irradiation samples were loaded onto a 52 mm diameter Cu-sample tray that contained circular machined depressions (2 mm deep, 2 mm diameter), and placed in a UHV laser cell. The laser cell is fitted with a zinc-selenide UHV-window for transmission of IR laser light. Because the ZnSe window was attached to the stainless steel housing of the with a braised seal, the laser cell was limited to a bake-out temperature of <100°C. A 25W CO2 laser was used to fuse samples. At these settings 15% laser power setting was sufficient to fuse the samples. System blanks were measured every 2-5 grains. and found to be stable through the course of analysis. Data were collected on a GVi instruments Argus multi-collector mass spectrometer using a variable sensitivity faraday collector array in static (non-peak hopping) mode.

For off-line data reduction, we used an in-house Excel-based method of age calculation. The ages are reported with uncertainties at 1-sigma level. Younger and smaller grains were more difficult to measure, and it was found empirically that when sample to blank ratios of 39Ar (and then filtered a second time by looking at sample-blank ratio of 40Ar were lower than ca 8-10, uncertainties in the calculated age were very high, preventing the use of these grains for interpretation. Accepted analyses all yielded ages that are realistic for the sample, e.g., greater than the stratigraphic age, and fall into age ranges for known events or rock sequences in the hinterland.

Koppers, A. 2002. ArArCalc – software for Ar-40/Ar-39 age calculations. Computers and Geosciences 28 : 605-619.

Appendix 2 – 7: Bulk rock Sm-Nd data

Sample	Location	GPS/ formation	Lithology	Sm	Nd	Sm/Nd	147Sm/144Nd	143Nd/144Nd	1s ppm	epsilon Nd
Myanmar - Bedrock and Rivers draining Neogene rocks										
MY05 2A	Sittwe Point	N20 06.834, E092 53.839	Sandstone	4.70	22.6356	0.2074	0.1254	0.512090	21	**-10.7**
MY05 5A	Koum Chaung	N20 44.347, E093 16.456	Siltstone	4.52	23.2518	0.1944	0.1175	0.512015	10	**-12.2**
Myanmar - Rivers draining Palaeogene rocks										
MY05 8A	Lemyu River	N20 49.212, E093 18.576	MR Sand	4.02	20.0489	0.2010	0.1215	0.512300	18	**-7.4**
MY05 15A	Kyeintuli River	N17 057.139, E094 33.087	MR Sand	3.33	16.4129	0.2035	0.1250	0.512434	14	**-4.0**
MY05 17B	Thanlwe River	N18 59.097, E094 15.244	MR Mud	3.48	17.6156	0.1977	0.1195	0.512427	18	**-4.1**
MY05 22B	Thandwe river	N18 27.466, E094 23.563	MR Mud	3.60	18.0331	0.1997	0.1207	0.512424	14	**-4.2**
MY05 23B	Irrawaddy River	N18 48.391,E094 12.218	MR Mud	3.67	17.9317	0.2052	0.1240	0.512210	18	**-8.3**

Method:

Whole rock Sm and Nd isotope data in sedimentary rocks are widely used to fingerprint sediment source. $^{143}Nd/^{144}Nd$ ratios are generally normalised and expressed in epsilon units as deviation from a chondritic uniform reservoir, where CHUR $\varepsilon Nd = 0$. A single epsilon unit is equivalent to a difference in $^{143}Nd/^{144}Nd$ ratio at the 4th digit. For clastic sedimentary rocks εNd will in part represent the weighted average of when the sediment sources were extracted from the mantle. When melt is extracted from the mantle it has a lower Sm/Nd ratio than its parent and therefore evolves over time to have a lower εNd than CHUR, the residual has a higher Sm/Nd than CHUR evolving to higher εNd over time.

For this study sandstone, mudstone and modern river samples were collected from type locations from the Palaeogene and Neogene Indo-Burman Ranges. Whole rock samples were ignited overnight at 900°C to remove any organic material. Dissolution and analytical methods follow Ahmad et al. (2000) with the exception that the samples were spiked with a mixed ^{150}Nd-^{149}Sm spike and ^{143}Nd-^{144}Nd ratios measured on the spiked fraction. εNd is calculated relative to the present-day (i.e. at t = 0) using CHUR $^{143}Nd/^{144}Nd = 0.512638$. Sm and Nd blanks were less than 10^{-3} of sample and the laboratory Johnson Mathey Nd internal standard gave $^{143}Nd/^{144}Nd = 0.511119 \pm 5$ (1 sigma=24) over the period of the analyses.

* MR = modern river sample

Sample	GPS ref	Location	Formation (lithostrat)	Megasequence (before remapping)	Megasequence After Remapping
BGL05 1A	22°N 09.518, 92°E 04.372	Sangu River,Chitt.Division	Modern river sand	modern	modern
BGL05 5A	21°N 20.972, 92°E 08.525	Ulataung Anticline	Lower/Mid Tipam	MS2	MS2
BGL05 6A	21°N 20.875, 92°E 08.290	Ulataung Anticline	Tipam	MS2	MS2
BGL05 9A	21°N 07.383, 92°E 11.953	Dakhin Nila	Dupi Tila (lower?)	MS3	MS3
BGL05 11A	21°N 00.633, 92°E 15.168	Dakhin Nila	Dupi Tila (upper?)	MS3	MS3
BGL05 12A	20°N 53.389, 92°E 17.976	Dakhin Nila	Upper Boka Bil	MS1	MS2
BGL05 13A	21°N 05.035, 92°E 13.197	Dakhin Nila	Lower Tipam	MS2	MS2
BGL05 14A	20°N 52.735, 92°E 18.003	Dakhin Nila	Upper Boka Bil	MS1	MS2
BGL05 15B	20°N 57.756, 92°E 12.900	Dakhin Nila	Lower/Mid Bhuban	MS1	MS2
BGL05 16A	20°N 57.714, 92°E 12.840	Dakhin Nila	Upper Bhuban	MS1	MS2
BA05 21A	22°N 37.869, 92°E 06.995	Sitapahar Anticline	Bhuban	MS1	MS2
BA05 22A	22°N 38.634, 92°E 07.924	Sitapahar Anticline	Boka Bil	MS1	MS2
BA05 23A	22°N 38.894, 92°E 08.523	Sitapahar Anticline	Boka Bil	MS1	MS2
BA05 24A	22°N 37.784, 92°E 11.437	Sitapahar Anticline	Dupi Tila (?)	MS3	MS3
BA05 25A	22°N 38.612, 92°E 11.716	Sitapahar Anticline	Dupi Tila (?)	MS3	MS3
BA05 27A	22°N 37.772, 92°E 06.841	Sitapahar Anticline	Bhuban	MS1	MS2
BA05 28A	22°N 36.263, 92°E 05.720	Sitapahar Anticline	Tipam	MS2	MS2
BNG5 26A	23°N 16.733, 92°E 09.132	Kasalong East Flank	Tipam	MS2	MS2
BNG5 26B	23°N 16.733, 92°E 09.132	Kasalong East Flank	Tipam	MS2	MS2
BNG5 32	23°N 12.893, 92°E 08.610	Kasalong Crestal Part	Bhuban	MS1	MS2
BNG5 33	23°N 13.174, 92°E 08.888	Kasalong Crestal Part	Bhuban	MS1	MS2
BNG5 40	23°N 15.317, 92°E 07.728	Kasalong West Flank	Bokabil	MS1	MS2
BNG5 46	23°N 14.094, 92°E 03.379	Gobamura North E. Flank	Dupitila?	MS3	MS3
BNG5 76	22°N 43.566, 92°E 23.055	Barkal East Flank	M. Bhuban	MS1	MS2
BNG5 78	22°N 43.420, 92°E 22.858	Barkal West Flank	M. Bhuban	MS1	MS2
BNG5 83	22°N 43.486, 92°E 22.390	Barkal West Flank	M Bhuban	MS1	MS2

BNG5 95	22°N 45.775, 92°E 18.716	Barkal West Flank	Tipam	MS2	MS2
BNG5 96	22°N 45.554, 92°E 18.338	Barkal West Flank	Tipam	MS2	MS2
BNG5 123	22°N 04.343, 92°E 15.880	Bandarban Crest	U. Bhuban	MS1	MS2
BNG5 125B	22°N 05.224, 92°E 15.280	Bandarban Crest	U. Bhuban	MS1	MS2
SHABAZPUR	SBZ core 1004-1005	SW Hatia trough	Tipam	MS2	MS2
SHABAZPUR	SBZ core 1799-1800	SW Hatia trough	Tipam	MS2	MS2
SHABAZPUR	SBZ core 2010-2011	SW Hatia trough	Tipam	MS2	MS2
SHABAZPUR	SBZ core 3014-3015	SW Hatia trough	Surma Group	MS1	MS1
SHABAZPUR	SBZ core 3016-3022	SW Hatia trough	Surma Group	MS1	MS1
SHABAZPUR	SBZ core 3022-3023	SW Hatia trough	Surma Group	MS1	MS1
SHABAZPUR	SBZ core 3401-3402	SW Hatia trough	Surma Group	MS1	MS1
SANGU1	Sangu 1 cut 150-160	SE Hatia Trough Offshore	Dupi Tila	MS3	MS3
SANGU1	Sangu 1 cut 170-180	SE Hatia Trough Offshore	Dupi Tila	MS3	MS3
SANGU1	Sangu 1 cut 180-190	SE Hatia Trough Offshore	Dupi Tila	MS3	MS3
SANGU1	Sangu 1 cut 360-370	SE Hatia Trough Offshore	Dupi Tila	MS3	MS3
SANGU1	Sangu 1 cut 280-290	SE Hatia Trough Offshore	Dupi Tila	MS3	MS3
SANGU1	Sangu 1 cut 1070-1080	SE Hatia Trough Offshore	Tipam	MS2	MS2
SANGU1	Sangu 1 cut 980-990	SE Hatia Trough Offshore	Tipam	MS2	MS2
SANGU1	Sangu 1 cut 990-1000	SE Hatia Trough Offshore	Tipam	MS2	MS2
SANGU1	Sangu 1 cut 1000-1010	SE Hatia Trough Offshore	Tipam	MS2	MS2
SITAKUND1	SIT 1 core 2648-2654	SE Hatia Trough Onshore	Barail	MS1	MS1
SITAKUND1	SIT 1 core 2793-2799	SE Hatia Trough Onshore	Barail	MS1	MS1
SITAKUND1	SIT 1 cut 3800-3850	SE Hatia Trough Onshore	Barail	MS1	MS1
SANGU3	Sangu 3 core 3840-3864	SE Hatia Trough Offshore	Barail	MS1	MS1
SANGU3	Sangu 3 core 3849-3850	SE Hatia Trough Offshore	Barail	MS1	MS1
SONADIA1	Sonadia 1 3237	SE Hatia Trough Offshore	Tipam	MS2	MS2

Appendix 3 – 1: Bangladesh sample list

Appendix 3 – 2: XRD Illite Crystallinity Data and Procedural Method

			Illite (001) Half height peak width (mm)				Error on Hbrel precision ± 20%	Paleotemp. (Hbrel)		Paleotemp.(clay mineralogy)
Sample	**Lithology**	**Depth**	**1**	**2**	**3**	**AV**	**Hbrel**		**XRD Clays**	
SBZ - core	Grey siltstone	997	0.25	0.26	0.26	0.26	145.8	Epizone	K I Ch/Sm	Diagenetic zone
	rich in musc	998	0.25	0.24	0.25	0.25	140.2	Epizone	K I Ch/Sm	Diagenetic zone
	and biotite	1001	0.28	0.28	0.28	0.28	159.1	U. anchizone	K I Ch/Sm	Diagenetic zone
	"	1003	0.33	0.33	0.33	0.33	187.5	U. anchizone	K I Ch/Sm	Diagenetic zone
	"	1794	0.32	0.32	0.32	0.32	181.8	U. anchizone	K I Ch/Sm	Diagenetic zone
	"	2295	0.30	0.30	0.30	0.30	170.5	U. anchizone	K I Ch/Sm	Diagenetic zone
Sangu 3 - core	Grey siltstones	3840	0.31	0.31	0.31	0.31	176.1	U. anchizone	K I Ch	Diagenetic zone
	rich in musc	3850	0.36	0.37	0.36	0.36	206.4	L. anchizone	K I Ch	Diagenetic zone
	and biotite	3851	0.31	0.31	0.31	0.31	176.1	L. anchizone	K I Ch	Diagenetic zone
Sitakund 1 core	Grey mudst	1689	0.30	0.30	0.30	0.30	170.5	M. anchizone	K_{vs} I Ch	Diagenetic zone
	Grey siltst, b+m	1936	0.32	0.31	0.32	0.32	179.9	M. anchizone	K_{vs} I Bar	Diagenetic zone
SBZ-Cut		3000	0.33	0.32	0.32	0.32	183.7	U. anchizone	K I Ch	Diagenetic zone
		3010	0.35	0.35	0.35	0.35	198.9	U. anchizone		
	Lt grey siltst, b+m	3014	0.31	0.30	0.30	0.30	172.3	U. anchizone		
		3016	0.33	0.34	0.35	0.34	193.2	U. anchizone		
		3050	0.36	0.36	0.37	0.36	206.4	U. anchizone	K I Ch	Diagenetic zone
		3060	0.35	0.35	0.35	0.35	198.9	U. anchizone		
		3120	0.32	0.31	0.32	0.32	179.9	U. anchizone		
	Lt grey siltst, b+m	3140	0.32	0.32	0.32	0.32	181.8	U. anchizone		
		3220	0.31	0.30	0.30	0.30	172.3	U. anchizone		

		3230	0.35	0.36	0.35	0.35	200.8	U. anchizone	K I Ch	Diagenetic zone
		3270	0.31	0.31	0.30	0.31	174.2	U. anchizone		
		3280	0.30	0.30	0.31	0.30	172.3	U. anchizone		
	Grey shale	3290	0.54	0.53	0.53	0.53	303.0	diagenetic zone		
		3300	0.38	0.37	0.37	0.37	212.1	U. anchizone	K I Ch Ch/Sm	Diagenetic zone
		3310	0.29	0.29	0.29	0.29	164.8	U. anchizone		
		3320	0.34	0.35	0.34	0.34	195.1	U. anchizone		
	Lt grey siltst, b+m	3330	0.30	0.31	0.31	0.31	174.2	U. anchizone		
		3340	0.35	0.34	0.35	0.35	197.0	U. anchizone	K I Ch Ch/Sm	Diagenetic zone
Sangu 1 -Cut	Dk grey siltst, b+m	590	0.32	0.33	0.35	0.33	189.4	sp, U. anchizone	Cal, Small I & K	Diagenetic zone
		600	0.29	0.33	0.33	0.32	179.9	sp, U. anchizone		
		610	0.29	0.31	0.30	0.30	170.5	sp, U. anchizone		
	Dk grey siltst, b+m	620	0.32	0.32	0.33	0.32	183.7	sp, U. anchizone	Cal, Small I K Chl	Diagenetic zone
	Dk grey siltst, b+m	2370	0.33	0.33	0.33	0.33	187.5	U. anchizone	K I Ch	Diagenetic zone
	Dk grey siltst, b+m	2380	0.32	0.33	0.32	0.32	183.7	U. anchizone	K I Ch	Diagenetic zone
		2390	0.35	0.35	0.35	0.35	198.9	U. anchizone		
		2410	0.35	0.35	0.35	0.35	198.9	U. anchizone		
		2420	0.38	0.37	0.38	0.38	214.0	L. anchizone		
	Dk grey siltst, b+m	2450	0.38	0.38	0.38	0.38	215.9	L. anchizone	K I Ch	Diagenetic zone
		2460	0.37	0.37	0.37	0.37	210.2	L. anchizone		
		2480	0.38	0.38	0.37	0.38	214.0	L. anchizone		
		2490	0.36	0.36	0.36	0.36	204.5	L. anchizone		
	Dk grey siltst, b+m	2500	0.46	0.47	0.46	0.46	263.3	L. anchizone	K I Ch	Diagenetic zone
		2520	0.42	0.42	0.42	0.42	238.6	L. anchizone		
		2530	0.41	0.41	0.41	0.41	233.0	L. anchizone		
	Dk grey siltst, b+m	2540	0.40	0.40	0.40	0.40	227.3	L. anchizone	K I Ch	Diagenetic zone
Sitakund 1 cut	Grey mudst, b	2900	0.27	0.26	0.25	0.26	147.7	Epizone	K I Bar	Drill mud?
Sitakund 1 cut	Grey siltst, b+m	3100	0.34	0.32	0.32	0.33	185.6	sp, M. anchizone	K I Bar	Drill mud?

Key:

Quartz (100) Half height peak
width = 0.176 mm SP = small peak vs = very small peak
Hbrel = Illite (001) half height peak width/ Quartz (100) half height peak width x 100
Hbrel >278 = diagenetic zone (<~200oC)
278-200 = lower anchizone
199-147 = upper anchizone Depth in m
<147 = epizone (>~375oC) b + m = abundant detrital biotite and muscovite

K = kaolinite, I = illite, Ch = chlorite Bar = barites (from drilling mud?)
Sm = smectite, I/S = mixed layer illite/smectite, Ch/S = mixed layer chlorite/smectite

Method:

Sample Preparation for Bulk Mineralogy
The sample is first crushed to <10μm using an agate ball mill. This is then back-packed into standard Philips sample holders to produce maximum random orientation. Typical detection limits are 0.5 - 2% depending on the bulk matrix.

Sample Preparation for Clay Mineralogy
The 2μm fractions were separated and analysed in an attempt to measure the diagenetic rather than detrital component, and thus obtain an indication of the temperatures to which the rock has been subjected after deposition.
Clays are released by dissaggregation in an ultrasonic bath: the sample is mixed with de-ionised water and placed in the bath for 30mins. The sample is then centrifuged to remove the >2 micron size fraction. The <2 micron (clay) fraction is then mixed with a 50% H2O2 solution to remove organics. The sample is left for 1-2 days then washed and centrifuged to remove the unreacted H2O2. The sample slurry is then sedimented onto a frosted glass slide, left to slowly dry, ready for XRD analysis. The sample is then placed into a sample holder ensuring it is perfectly flat and level with the top of the sample holder.

Instrumental Parameters
Instrument: Philips PW1050 / Hilton brooks DG2
Anode: Cobalt

kV: 40
mA: 40
Divergence Slit: 1 deg
Receiving Slit : 0.2mm + graphite Monochromator
Scan: 5o to 70o 2? - Bulk / 5o to 40o 2? - Clay
Scan speed: 0.02o 2 ? /sec
Count Time: 3 seconds

Software
Control: WinXRD ver2
Identification: Diffrac-AT ver3.0, using ICDD PDF Mineral Subfile
Quantification: SiroQuant ver3.0 http://www.sietronics.com.au/siroqnt/siroqnt.htm

Illite Crystallinity Measurement
The thickness of illite crystals is dependant on metamorphic grade. Deeper burial and higher grade metamorphism forms thicker crystals. Kubler (1967) and Weber (1972a) have shown that the width at half height of the 10-Å illite peak on X-ray diffraction patterns decreases with an increase in metamorphic grade as Fe2+, Mg2+, H2O and OH- are expelled from the crystal lattice and K+ is absorbed. The half peak width is known as Hb. To enable better correlation between labs and their machines the Weber Index (Weber, 1972) is used where quartz is used as a standard. The quartz standard allows for inter-lab comparison and machine drift. Hbrel value (= Halbwertsbreite or relative full width at half maximum height) is an indirect measure of the illite crystal thickness and represents Hb value relative to the quartz standard. Kubler (1967) used the Hb value to define diagenetic zone (<200°C), the anchizone (200-370°C) and the epizone (>370°C). It was then established that the Hbrel upper and lower limits of the anchizone were 278 and 149 respectively (Blenkinsop, 1988). With values of <147 indicative of the epizone, and values of >278 indicative of the diagenetic zone. Standard procedure is to analyse the <2 μm clay fraction from mudstones, thus eliminating coarser detrital mica that would interfere with the 10Å illite (001) peak. Experience show that several different samples from the same location commonly give a Hbrel precision of +/-20%. Bulk mineral XRD-analysis (see above) will often identify kaolin and/or mixed layered clays in the diagenetic zone but not at higher grades.

River	Site		Sample	Q	F	Li	Lv	Lc	Lp	Lch	Lm	Lu	total	Qp/Q	P/F	Vm/V	Cd/C	Mb/M	Sc/S	Q	KF	P	Lvf	Lvm	Lcc	Lcd	Lp	Lch	Lms
Dakhin Nila	Dupi Tila	MS3	BGL05 9A	79	7	0.0	5	0	2	2	5	0	100.0	23	0	0	n.d.	0	n.d.	78	7	0	5	0	0	0	2	2	2
Gobamura	Dupi Tila	MS3	BNG5 46	83	10	0.0	3	0	1	0	4	0	100.0	18	26	0	n.d.	0	n.d.	80	7	2	2	0	0	0	1	0	2
Dakhin Nila	Tipam	MS2	BGL05 13A	94	4	0.0	0	0	0	2	0	0	100.0	17	0	n.d.	n.d.	0	n.d.	93	4	0	0	0	0	0	0	2	0
Barkal	Tipam	MS2	BNG5 96	83	3	0.0	4	0	1	1	7	0	100.0	11	0	9	n.d.	2	n.d.	78	3	0	4	0	0	0	1	1	4
Kasalong Tiang	Tipam	MS2	BNG5 26A	75	3	0.0	1	0	5	0	15	0	100.0	15	14	0	n.d.	0	n.d.	62	2	0	1	0	0	0	4	0	9
Dakhin Nila	Boka Bil	MS2	BGL05 14A	71	16	0.0	2	0	2	0	9	0	100.0	22	38	20	n.d.	3	n.d.	63	9	5	1	0	0	0	2	0	4
Kasalong Tiang	Boka Bil	MS2	BNG5 40	68	14	0.0	6	0	3	2	8	0	100.0	27	44	38	n.d.	4	n.d.	64	7	6	3	2	0	0	3	1	3
Dakhin Nila	Bhuban	MS2	BGL05 16A	73	18	0.0	0	0	2	0	6	0	100.0	12	38	0	n.d.	16	n.d.	62	10	6	0	0	0	0	2	0	2
Barkal	Bhuban	MS2	BNG5 78	73	17	0.0	2	0	3	0	5	0	100.0	31	42	40	n.d.	0	n.d.	71	10	7	1	1	0	0	3	0	1
Barkal	Bhuban	MS2	BNG5 83	76	18	0.0	0	0	0	0	7	0	100.0	46	32	n.d.	n.d.	0	n.d.	60	10	4	0	0	0	0	0	0	3
Kasalong Tiang	Bhuban	MS2	BNG5 33	78	10	0.0	2	0	1	0	9	0	100.0	23	29	50	n.d.	5	n.d.	66	6	3	1	1	0	0	1	0	4
Kasalong Tiang	Bhuban	MS2	BNG5 34	77	12	0.0	3	0	2	1	5	0	100.0	21	41	0	n.d.	0	n.d.	61	5	4	3	0	0	0	2	0	3
Bandarban	Bhuban	MS2	BNG5 123	78	11	0.0	3	0	2	1	5	0	100.0	20	24	40	n.d.	0	n.d.	73	8	2	2	1	0	0	2	1	0

Lmv	Lmf	Lmb	Lu	Mu	Bi	pyriboles	& dense minerals	total	avg. L density	Qr/Q	Qv/Q	Q/F	Q+F+Lm	Mic/F	bt/miche	**M.I. completo**
0	2	0	0	0.3	0.3	0.0	2	100.0	2.64	6	3	11.8	91	24	n.d.	93
1	1	0	0	1.4	1.7	0.0	1.0	100.0	2.65	2	0	8.5	96	8	56	100
0	0	0	0	0.0	0.0	0.3	0.3	100.0	2.65	14	3	23.7	98	0	n.d.	156
1	1	0	0	0.7	0.3	0.0	4	100.0	2.64	8	0	25.3	93	22	n.d.	189
0	4	0	0	5	13	0.0	0	100.0	2.70	0	0	22.0	94	17	73	223
1	3	0	0	1.1	7	1.4	1.4	100.0	2.67	0	0	4.5	96	21	87	156
1	3	0	0	0.7	4.0	0.0	0.7	100.0	2.65	1	0	4.9	89	9	85	115
2	1	0	0	3	9	1.7	0.8	100.0	2.68	0	0	4.0	97	6	72	146
0	3	0	0	1.5	1.1	0.0	0.7	100.0	2.65	2	0	4.3	95	7	43	152
0	2	0	0	8	13	0.0	0.3	100.0	2.71	0	0	4.2	100	8	63	n.d.
1	3	0	0	4	10	0.0	0.4	100.0	2.69	6	0	7.4	97	9	69	174
0	1	0	0	12	9	0.0	0.4	100.0	2.69	1	0	6.6	94	5	39	100
0	4	0	0	2	5	0.0	0.3	100.0	2.66	7	0	7.2	94	23	72	165

Appendix 3 – 3:

Petrographic data (Surface Samples) ***This page***

Heavy Mineral Data (Surface samples) ***Below***

River	Site	Sample	GSZ (micron)	GSZ (phi)	% non-E	HMC%w HM	HM density	tHM density	SRD HM	HM% VFS-FS	HM% transp.	% transparent	% opaque	% turbid	Total	Ud%	ZR	ZTR	T&	LgM	Gt	HgM	Hb	&A	CPX	OPX
Dakhin Nila	Dupi Tila	BGL05 9A	1000	0.0	0.0	2.7	3.68	3.58	2.68	2.7	2.1	76	11	13	100.0	4	26	15	7	27	0	49	0	2	0.0	0.0
Gobamura	Dupi Tila	BNG5 46	1000	0.0	0.0	1.1	3.94	3.70	2.66	1.1	0.7	61	25	14	100.0	17	72	22	14	37	1	21	0	5	0.0	0.0
Dakhin Nila	Tipam	BGL05 13A	1000	0.0	0.0	1.6	4.07	3.74	2.67	1.6	0.9	56	32	12	100.0	14	72	18	16	12	0	54	0	1	0.0	0.0
Barkal	Tipam	BNG5 96	1000	0.0	0.0	0.6	3.43	3.57	2.66	0.6	0.3	43	7	50	100.0	5	53	10	3	45	0	34	4	7	0.0	0.0
Kasalong Tiang	Tipam	BNG5 26A	1000	0.0	0.0	0.9	3.41	3.41	2.66	0.9	0.6	68	5	27	100.0	4	28	9	5	47	1	3	27	8	0	0
Dakhin Nila	Boka Bil	BGL05 14A	1000	0.0	0.0	3.2	3.42	3.38	2.68	3.2	2.5	80	5	15	100.0	11	0	2	5	25	11	2	53	2	0	0
Kasalong Tiang	Boka Bil	BNG5 40	1000	0.0	0.0	0.8	3.89	3.73	2.66	0.8	0.5	67	19	14	100.0	46	36	20	26	9	38	6	0	0	0	0
Dakhin Nila	Bhuban	BGL05 16A	1000	0.0	0.0	1.0	3.63	3.54	2.66	1.0	0.7	72	11	17	100.0	27	40	7	11	30	24	5	22	1	0	0
Barkal	Bhuban	BNG5 78	1000	0.0	0.0	0.3	3.51	3.78	2.65	0.3	0.2	60	0	40	100.0	56	36	16	23	6	50	2	2	0	0	0
Barkal	Bhuban	BNG5 83	1000	0.0	0.0	0.1	3.83	3.86	2.65	0.1	0.1	89	3	8	100.0	51	55	16	33	10	40	0	0	0	0	0
Kasalong Tiang	Bhuban	BNG5 33	1000	0.0	0.0	0.3	3.81	3.74	2.65	0.3	0.1	47	22	31	100.0	25	41	48	24	22	4	2	0	0	0	0
Kasalong Tiang	Bhuban	BNG5 34	1000	0.0	0.4	0.2	3.60	3.62	2.65	0.2	0.2	83	4	14	100.0	31	22	29	30	17	24	0	0	0	0	0
Bandarban	Bhuban	BNG5 123	1000	0.0	0.0	0.3	3.61	3.85	2.65	0.3	0.2	61	3	36	100.0	23	43	38	36	11	4	9	0	0	0	0

OS	tofillite Total	ner amph. HCl	een augite MMI	own augite % rounded	opside zircon	allage	ner clinopx.	stattite	persthene	vine	inel	idote	nozoisite	isite	ner epidotes	ehnite	mpellyite	lorthoid	wsonite	rphollite	rnet	aurolite	dalusite	ante	limanite	sodic amphi.	tremolite	tal Transp.
0.0	100.0	n.d.	48	2%	1	2	9	3	0	0	0	0	6	0	0	0	0	0	0	0	0	0	0	0	0	0	0	0
0.0	100.0	n.d.	48	2%	8	2	4	8	0	0	0	0	13	0	0	0	0	0	0	0	0	0	0	0	0	0	0	0
0.0	100.0	n.d.	58	1%	7	1	5	7	0	0	0	0	15	0	0	0	0	0	0	0	0	0	0	0	0	0	0	0
0.0	100.0	n.d.	42	2%	1	1	1	4	4	0	0	0	2	1	0	0	0	0	0	0	0	0	0	0	0	0	0	0
0.0	100.0	4	14	0%	0	2	3	2	1	3	0	0	2	0	0	0	0	0	0	0	0	0	0	0	0	0	0	0
0.0	100.0	3	26	1%	0	1	0	0	0	3	0	0	0	1	0	0	0	0	49	2	1	0	0	0	0	0	0	0
1.0	100.0	n.d.	18	3%	4	3	10	3	0	7	0	0	5	14	0	0	0	0	0	0	0	0	0	0	0	0	0	0
0.0	100.0	4	33	1%	1	3	1	2	0	5	0	0	1	6	0	0	0	0	20	1	0	0	0	0	0	0	0	0
0.0	100.0	n.d.	10	1%	0	2	8	5	0	0	0	0	10	12	0	0	0	0	2	0	0	0	0	0	0	0	0	0
1.5	100.0	n.d.	0	0%	3	1	5	6	1	0	0	0	21	11	0	0	0	0	0	0	0	0	0	0	0	0	0	0
0.5	100.0	n.d.	4	3%	8	8	19	12	0	0	0	0	20	3	0	0	0	0	0	0	0	0	0	0	0	0	0	0
0.5	100.0	n.d.	0	1%	2	3	20	4	0	0	0	0	11	19	0	0	0	0	0	0	0	0	0	0	0	0	0	0
1.5	100.0	n.d.	15	3%	10	3	18	6	0	0	0	0	35	0	0	0	0	0	0	0	0	0	0	0	0	0	0	0

actinolite	antofillite	other amph.	green augite	brown augite	diopside	diallage	other clinoprx.	enstatite	hypersthene	olivine	spinel	epidote	clinozoisite	zoisite	other epidotes	prehnite	pumpellyite	chloritoid	lawsonite	carpholite	garnet	staurolite	andalusite	kyanite	sillimanite	Total Transp.
2	0	0	0	0	0	0	0	0	0	0	0	24	0	0	1	0	0	2	0	0	0	26	1	19	3	100.0
5	0	0	0	0	0	0	0	0	0	0	0	32	0	0	1	0	0	3	0	0	1	11	0	7	3	100.0
1	0	0	0	0	0	0	0	0	0	0	0	11	0	0	0	0	0	1	0	0	0	18	1	29	7	100.0
7	0	0	0	0	0	0	0	0	0	0	0	38	0	1	2	0	0	4	0	0	0	19	2	14	0	100.0
8	0	0	0	0	0	0	0	0	0	0	0	36	0	1	2	0	0	7	0	0	1	2	0	1	0	100.0
2	0	0	0	0	0	0	0	0	0	0	0	20	1	1	0	0	0	2	0	0	11	1	0	1	0	100.0
0	0	0	0	0	0	0	0	0	0	0	1	1	0	0	1	0	0	6	0	0	38	6	0	0	0	100.0
1	0	0	0	0	0	0	0	0	0	0	0	26	0	0	1	0	0	2	0	0	24	2	0	2	0	100.0
0	0	0	0	0	0	0	0	0	0	0	0	1	0	0	0	0	0	5	0	0	50	2	0	0	0	100.0
0	0	0	0	0	0	0	0	0	0	0	1	0	0	0	0	0	0	9	0	0	40	0	0	0	0	100.0
0	0	0	0	0	0	0	0	0	0	0	0	1	0	0	2	0	0	18	0	0	4	2	0	0	0	100.0
0	0	0	0	0	0	0	0	0	0	0	0	0	0	0	0	0	0	16	0	0	24	0	0	0	0	100.0
0	0	0	0	0	0	0	0	0	0	0	1	0	0	0	0	0	0	11	0	0	4	9	0	0	0	100.0

Location & Sample no.	Formation	Q	F	Lv	Lc	Lp	Lch	Lm	Lu	total	P/F	Cd/C	Mb/M	micas	Bt/ micas	Qr/Q	M.I.	Qt	F	L-c	Qm	F	Lt-c	Qm
SW Hatia Trough																								
SBZ core 1799-1800	MS2	84	5	0	0	0	0	11	0	100	n.d.	n.d.	n.d.	27%	71	0	n.d.	84	5	11	84	5	11	94
SBZ core 2010-2011	MS2	75	2	0	10	0	0	14	0	100	n.d.	40	0	28%	67	0	186	83	2	15	83	2	15	97
SBZ core 3014-3015	MS1	82	10	2	1	0	0	6	0	100	69	n.d.	0	11%	65	4	275	83	10	8	82	10	8	89
SBZ core 3401-3402	MS1	79	13	1	2	0	0	5	0	100	58	n.d.	0	18%	73	1	186	80	14	6	80	14	6	85
SE Hatia Trough																								
Sangu 1 cut 150-160	MS3	83	12	1	0	1	0	3	0	100	11	n.d	5	0%	n.d	2	258	83	12	5	83	12	5	88
Sangu 1 cut 360-370	MS3	79	12	2	0	1	1	6	0	100	16	n.d.	0	1%	n.d	1	245	80	12	8	79	12	10	87
Sangu 1 cut 1070-1080	Upper MS2	72	20	3	0	0	0	5	0	100	40	n.d	5	1%	n.d	1	239	72	20	8	71	20	9	78
SIT 1 core 2648-2654	Barail / MS1	84	6	1	0	1	0	7	0	100	25	n.d.	0	10%	75	0	200	84	6	10	84	6	10	93
SIT 1 core 2793-2799	Barail / MS1	80	11	1	1	1	0	6	0	100	53	n.d.	0	8%	79	0	200	80	11	9	80	11	9	88

P	K	Qp	Lvm	Lsm	Lm	Lv	Ls	Ls	Lm1	Lm2+	Lm1	Lm2	Lm3+
0	6	n.d.	n.d.	n.d.	n.d.	n.d.	n.d.	n.d.	n.d.	n.d.	n.d.	n.d.	n.d.
3	0	n.d.	n.d.	n.d.	n.d.	n.d.	n.d.	42	17	42	29	57	14
7	3	9	18	73	80	20	0	11	11	78	13	13	75
8	6	n.d.	n.d.	n.d.	n.d.	n.d.	n.d.	30	30	40	43	29	29
1	11	6	41	53	56	19	25	31	7	62	11	42	47
2	11	13	30	57	63	17	20	24	10	66	14	41	45
9	13	11	52	37	64	32	4	6	27	67	29	25	46
2	5	n.d.	n.d.	n.d.	n.d.	n.d.	n.d.	17	17	67	20	60	20
6	6	0	21	79	71	14	14	23	31	46	40	20	40

Petrographic data (core samples)

Location & sample no.	Formation	HMC	Zircon	tourmaline	rutile	sphene	anatase/brookite	apatite	amphiboles	pyroxenes	spinel	epidote-gp	chloritoid	garnet	staurolite	kyanite	others	
SW Hatia Trough																		
SBZ core 1799-1800	MS2	0.1	3	9	13	6	2	0	0	0	0	34	10	20	1	1	0	100
SBZ core 2010-2011	MS2	0.01	3	17	16	8	0	7	0	0	0	2	15	26	3	1	1	100
SBZ core 3014-3015	MS1	0.6	4	11	11	0	0	6	0	0	0	1	9	58	0	0	0	100
SBZ core 3401-3402	MS1	0.1	4	19	14	1	1	3	0	0	0	1	14	43	0	0	0	100
SE Hatia Trough																		
Sangu 1 cut 150-160	MS3	1	0	4	2	1	0	0	38	0	0	22	1	4	9	7	9	100
Sangu 1 cut 360-370	MS3	1.3	0	2	2	0	0	0	52	0	0	25	1	3	3	2	7	100
Sangu 1 cut 1070-1080	Upper MS2	3.6	0	2	0	1	0	0	52	0	0	21	1	19	1	2	0	100
SIT 1 core 2648-2654	Barail / MS1	0.2	5	11	8	0	0	11	0	0	0	0	7	55	0	0	2	100
SIT 1 core 2793-2799	Barail / MS1	0.1	5	23	12	0	0	10	0	0	2	0	13	33	0	0	1	100

Heavy mineral data (core samples)

Key:

Q=quartz (Qp= polycrystalline; Qr= rounded outlines; Qm = monocrystalline; Qt = total); F=feldspars; (P=plagioclase, K = Kspar); L=lithic fragments (Lv=volcanic; Lc=carbonatic; Lp=terrigenous; Lch=chert; Lm=metamorphic; Lu=ultramafic; Ls = sedimentary). Cd/C= dolostone rock fragments/total carbonate rock fragments; Mb/M= metabasite rock fragments/total metamorphic rock fragments; bt= biotite. Key indices and P/F ratio calculated by the Gazzi-Dickinson point-counting method, other ratios by the traditional QFR method. Percent micas and dense minerals calculated on total framework grains. MI=metamorphic index (average rank of metamorphic lithics[52]. Lm1(very-low rank metamorphic); Lm2+(low to higher rank metamorphic); Lm1(very low rank); Lm2 (low rank); Lm3+ (medium and high rank metamorphic). N.d. = not determined.

The MI Index ("Metamorphic Index"; Garzanti and Vezzoli 2003) expresses the average rank of metamorphic rock fragments in the studied samples, and varies from 0 in detritus from sedimentary and volcanic cover rocks to 500 in detritus from high-grade basement rocks

Method:

400 points were counted in the selected samples according to the Gazzi-Dickinson method (Dickinson, 1985). A classification scheme of grain types allowed for the collection of fully quantitative information on the sampled sandstones. Transparent dense minerals were counted on grain mounts according to the 'ribbon counting' method, and 200 minerals were counted also to assess the percentage of etched and corroded grains. Dense minerals were concentrated with sodium metatungstate (density 2.9 g/cm3) using the 63–250 μm fraction treated with hydrogen peroxide, oxalic acid and sodium ditionite to eliminate organic matter, iron oxides and carbonates respectively

Appendix 3 – 4: Bulk rock Sm-Nd data and procedural method

Sample	Location	GPS ref	Lithology	87Sr/86Sr*	Sm	Nd	Sm/Nd	147Sm/144Nd	143Nd/144Nd	1s ppm	ε_{Nd} (0 Ma)
BGL05 15B	Dakhin Nila anticline	20°N 57.756, 92°E 12.900	Mudstone	0.726519	4.672	22.0735	0.2117	0.1279	0.511998	8	**-12.5**
BNG5 26B	Kasalong Tiang anticline	23°N 16.733, 92°E 09.132	Mudstone	0.724853	4.5187	24.6805	0.1831	0.1107	0.512067	7	**-11.1**
BNG5 32	Kasalong Tiang anticline	23°N 12.893, 92°E 08.610	Mudstone	0.737638	6.7403	35.5878	0.1894	0.1145	0.511989	9	**-12.7**
BNG5 76	Barkal anticline	22°N 43.566, 92°E 23.055	Mudstone	0.727609	4.9152	25.0219	0.1964	0.1187	0.511994	9	**-12.6**
BNG5 95	Barkal anticline	22°N 45.775, 92°E 18.716	Mudstone	0.729432	5.1831	25.2334	0.2054	0.1242	0.511975	7	**-12.9**
BNG5 125B	Bandarban anticline	22°N 05.224, 92°E 15.280	Mudstone	0.725400	4.5278	23.7432	0.1907	0.1153	0.512021	7	**-12.0**
Sangu 1 980-990	Hatia Trough MS2	Sangu 1 cut 980-990	Siltstone	0.721144	4.827	25.67	0.18804	0.11366	0.511976	6	**-12.9**
Sangu 1 990-1000	Hatia Trough MS2	Sangu 1 cut 990-1000	Siltstone	0.719748	4.58	21.591	0.21211	0.12821	0.511991	16	**-12.6**
Sangu 1 1000-1010	Hatia Trough MS2	Sangu 1 cut 1000-1010	Siltstone	0.723231	4.971	28.844	0.17235	0.10418	0.511964	12	**-13.1**
Sangu 3 3849-3850	Hatia Trough MS1	Sangu 3 core 3849-3850	Siltstone	0.724297	6.832	31.137	0.21942	0.13263	0.511918	8	**-14**
Sit 1 3800-3850	Hatia Trough Barail/MS1	Sit 1 cut 3800-3850	Siltstone	0.71489	5.583	26.724	0.20892	0.12628	0.511931	7	**-13.8**
Sangu 1 170-180	Hatia Trough MS3	Sangu 1 cut 170-180	Siltstone	0.727824	1.022	5.219	0.19581	0.11836	0.511953	11	**-13.4**
Sangu 1 180-190	Hatia Trough MS3	Sangu 1 cut 180-190	Siltstone	0.726033	1.659	9.477	0.17503	0.1058	0.511949	8	**-13.4**
Sit 1 2648-2654	Hatia Trough Barail/MS1	Sit 1 core 2648-2654	Siltstone	0.728947	4.417	21.22	0.20816	0.12582	0.511939	9	**-13.6**
SBZ 1004-1005	Hatia Trough MS2	SBZ core 1004-1005	Siltstone	0.728042	4.442	21.248	0.20904	0.12636	0.511952	9	**-13.4**
SBZ 3022-3023	Hatia Trough MS1	SBZ core 3022-3023	Siltstone	0.732386	6.147	31.713	0.19385	0.11717	0.51186	9	**-15.2**
Padma MO1	Padma/Ganges		MRS	0.752501	19.6056	101.9959	0.1922	0.1162	0.511727	5	**-17.8**

* not leached

MRS = modern river sand

Total # Samples = 17

Method:

Whole rock Sm and Nd isotope data in sedimentary rocks are widely used to fingerprint sediment source. 143Nd/144Nd ratios are generally normalised and expressed in epsilon units as deviation from a chondritic uniform reservoir, where CHUR eNd = 0. A single epsilon unit is equivalent to a difference in 143Nd/144Nd ratio at the 4th digit. For clastic sedimentary rocks eNd will in part represent the weighted average of when the sediment sources were extracted from the mantle. When melt is extracted from the mantle it has a lower Sm/Nd ratio than its parent and therefore evolves over time to have a lower eNd than CHUR, the residual has a higher Sm/Nd than CHUR evolving to higher eNd over time. The εNd value reflects the age and composition of the rock ranging from very negative values in crustal rocks, to very positive values in young mafic rocks.

For this study mudstones were collected from the Neogene Chittagong Hill Tracts (SE Bangladesh). Whole rock samples were ignited overnight at 900°C to remove any organic material. Dissolution and analytical methods follow Ahmad et al. (2000) with the exception that the samples were spiked with a mixed 150Nd-149Sm spike and 143Nd-144Nd ratios measured on the spiked fraction. eNd is calculated relative to the present-day (i.e. at t = 0) using CHUR 143Nd/144Nd = 0.512638. Sm and Nd blanks were less than 10-3 of sample and the laboratory Johnson Mathey Nd internal standard gave 143Nd/144Nd = 0.511119 ± 5 (1 sigma=24) over the period of the analyses. Isotope ratios were analysed on a T40 Sector 54 VG mass spectrometer using a triple filament assembly.

Appendix 3 – 5: Detrital white mica data ^{40}Ar-^{39}Ar core and surface data with procedural method

Incremental Heating			36Ar(a)	37Ar(ca)	38Ar(cl)	39Ar(k)	40Ar(r)	Age ± 2σ (Ma)	40Ar(r) (%)	39Ar(k) (%)	K/Ca ± 2σ
05M0076A	1.00 W		0.00001	0.00000	0.00000	0.11669	0.46697	**15.29 ± 1.84**	99.26	22.96	0.000 ± 0.000
05M0076B	1.00 W		0.00017	0.00051	0.00000	0.02783	0.07543	**10.37 ± 8.01**	59.82	5.48	23.263 ± 74.551
05M0076C	1.00 W		0.00006	0.00134	0.00000	0.01788	0.06425	**13.74 ± 12.53**	78.95	3.52	5.728 ± 12.166
05M0076D	1.00 W		0.00007	0.00032	0.00000	0.01235	0.73972	**216.30 ± 17.41**	97.36	2.43	16.639 ######
05M0076E	1.00 W		0.00003	0.00025	0.00000	0.04603	0.20692	**17.17 ± 5.02**	96.24	9.06	79.311 ######
05M0076G	1.00 W		0.00009	0.00088	0.00000	0.02077	0.21436	**39.18 ± 7.77**	89.34	4.09	10.102 ± 17.767
05M0076H	1.00 W		0.00011	0.00000	0.00000	0.00842	0.04534	**20.54 ± 36.27**	58.14	1.66	0.000 ± 0.000
05M0076I	1.00 W		0.00025	0.00000	0.00000	0.01900	0.09845	**19.77 ± 11.32**	57.03	3.74	0.000 ± 0.000
05M0076J	1.00 W		0.00001	0.00000	0.00000	0.00935	0.04114	**16.80 ± 13.65**	95.48	1.84	0.000 ± 0.000
05M0076M	1.00 W		0.00081	0.00183	0.00000	0.01810	0.08656	**18.26 ± 6.83**	26.46	3.56	4.255 ± 2.343
05M0076N	1.00 W		0.00002	0.00139	0.00000	0.01079	0.03521	**12.48 ± 21.85**	85.53	2.12	3.333 ± 3.339
05M0076O	1.00 W		0.00001	0.00114	0.00000	0.01394	0.05212	**14.29 ± 19.33**	92.68	2.74	5.267 ± 5.715
05M0076P	1.00 W		0.00039	0.00145	0.00000	0.04138	0.19774	**18.24 ± 3.80**	62.91	8.14	12.264 ± 9.335
05M0076Q	1.00 W		0.00006	0.00223	0.00000	0.00565	0.02776	**18.76 ± 28.00**	61.26	1.11	1.089 ± 0.871
05M0076S	1.00 W		0.00017	0.00000	0.00000	0.01227	0.10127	**31.41 ± 18.67**	66.23	2.41	0.000 ± 0.000
05M0076T	1.00 W		0.00004	0.00000	0.00000	0.00815	0.08770	**40.82 ± 27.43**	87.81	1.60	0.000 ± 0.000
05M0076W	1.00 W		0.00001	0.00000	0.00000	0.03637	0.14504	**15.24 ± 5.68**	98.92	7.16	0.000 ± 0.000
05M0076Y	1.00 W		0.00013	0.00105	0.00000	0.00971	0.10679	**41.71 ± 17.64**	73.00	1.91	3.978 ± 7.151
05M0076Z	1.00 W		0.00005	0.00000	0.00000	0.01331	0.10523	**30.09 ± 14.14**	88.46	2.62	0.000 ± 0.000
05M0077A	1.00 W		0.00009	0.00069	0.00000	0.00963	0.04810	**19.07 ± 19.22**	64.46	1.89	5.971 ± 19.499
05M0077B	1.00 W		0.00018	0.00078	0.00000	0.01414	0.04163	**11.26 ± 10.68**	44.16	2.78	7.758 ± 17.072
05M0077C	1.00 W		0.00006	0.00074	0.00000	0.01395	0.04190	**11.48 ± 14.48**	71.58	2.75	8.116 ± 18.957
05M0077E	1.00 W		0.00003	0.00000	0.00002	0.00742	0.02557	**13.17 ± 38.33**	73.04	1.46	0.000 ± 0.000
05M0077F	1.00 W		0.00011	0.00039	0.00008	0.01511	0.03021	**7.66 ± 19.17**	48.58	2.97	16.559 ± 60.094

Ar-Ar ages of 24 detrital white mica grains from sample Sitakund 1 2648, Barail or MS1 Formation, SE Hatia Trough / CHT. This sample had low 40Ar, and uncertainties of individual analyses of many grains were too large to reliably use. In this sample however, apart from two outliers, we at least were able to show that all young grains statistically formed one single population of ca 19 Ma. The weighted mean of all analyses including and excluding the single large grain of 15.3 Ma (that on its own accounts for 22% of the total gas released from all grains analysed for this sample) are indistinguishable, clearly indicating that we are dealing with one homogeneous population of ca 19 Ma. The two older grains excluded from this calculation yielded ages of 216 +/- 17 Ma and 39 +/- 8 Ma respectively.

Incremental Heating		36Ar(a)	37Ar(ca)	38Ar(cl)	39Ar(k)	40Ar(r)	Age ± 2σ (Ma)	40Ar(r) (%)	39Ar(k) (%)	K/Ca ± 2σ
05M0078A	1.00 W	0.00031	0.00000	0.00000	0.39812	1.68858	**16.20 ± 0.90**	94.75	4.73	0.000 ± 0.000
05M0078B	2.00 W	0.00023	0.00000	0.00000	0.31316	1.63413	**19.91 ± 1.04**	95.92	3.72	0.000 ± 0.000
05M0078D	3.00 W	0.00006	0.00000	0.00000	0.08262	0.32391	**14.98 ± 2.30**	95.09	0.98	0.000 ± 0.000
05M0078E	4.00 W	0.00031	0.00067	0.00000	0.44919	1.72781	**14.70 ± 0.37**	94.90	5.34	287.527 ######
05M0078F	5.00 W	0.00001	0.00000	0.00000	0.07448	0.37371	**19.15 ± 2.86**	99.50	0.89	0.000 ± 0.000
05M0078G	6.00 W	0.00028	0.00134	0.00000	0.45887	1.98248	**16.50 ± 0.59**	95.94	5.46	146.838 ######
05M0078H	7.00 W	0.00081	0.00000	0.00000	0.15058	0.65673	**16.66 ± 1.33**	73.31	1.79	0.000 ± 0.000
05M0078J	8.00 W	0.00023	0.00058	0.00000	0.22225	1.36812	**23.47 ± 1.11**	95.17	2.64	164.721 ######
05M0078K	9.00 W	0.00009	0.00285	0.00000	0.18129	0.70900	**14.94 ± 1.15**	96.46	2.16	27.368 ± 13.411
05M0078L	10.00 W	0.00042	0.00559	0.00000	0.30064	1.44239	**18.32 ± 0.70**	92.00	3.58	23.112 ± 6.007
05M0078M	11.00 W	0.00097	0.00771	0.00000	0.73973	3.64870	**18.83 ± 0.32**	92.66	8.80	41.254 ± 8.129
05M0078N	12.00 W	0.00008	0.00101	0.00000	0.07541	0.74084	**37.31 ± 2.63**	96.73	0.90	32.066 ± 68.497
05M0078P	13.00 W	0.00023	0.00054	0.00000	0.68834	3.09704	**17.18 ± 0.43**	97.79	8.19	551.505 ######
05M0078Q	14.00 W	0.00015	0.00010	0.00000	0.36951	2.12417	**21.92 ± 0.62**	97.97	4.39	###### ######
05M0078R	15.00 W	0.00011	0.00224	0.00000	0.08838	0.59945	**25.84 ± 2.60**	94.85	1.05	16.933 ± 18.614
05M0078S	16.00 W	0.00098	0.00019	0.00000	0.64450	3.18183	**18.85 ± 0.34**	91.61	7.66	###### ######
05M0078T	17.00 W	0.00072	0.00000	0.00000	0.69991	3.25836	**17.78 ± 0.32**	93.86	8.32	0.001 ± 0.000
05M0078V	18.00 W	0.00004	0.00055	0.00000	0.24487	2.47435	**38.36 ± 1.05**	99.52	2.91	191.918 ######
05M0078W	19.00 W	0.00003	0.00000	0.00000	0.15258	0.59096	**14.80 ± 1.27**	98.69	1.81	0.001 ± 0.000
05M0078X	20.00 W	0.00094	0.00000	0.00000	0.78846	3.23573	**15.68 ± 0.22**	92.05	9.38	0.001 ± 0.000
05M0078Y	21.00 W	0.00012	0.00000	0.00000	0.32652	2.95124	**34.35 ± 0.63**	98.74	3.88	0.001 ± 0.000
05M0078Z	22.00 W	0.00002	0.00000	0.00000	0.59859	2.72712	**17.40 ± 0.36**	99.72	7.12	0.001 ± 0.000
05M0079B	23.00 W	0.00002	0.00000	0.00000	0.15775	0.73152	**17.71 ± 1.47**	99.19	1.88	0.001 ± 0.000
05M0079C	24.00 W	0.00004	0.00209	0.00000	0.08506	0.40916	**18.36 ± 3.50**	96.88	1.01	17.491 ± 13.902
05M0079D	25.00 W	0.00004	0.00052	0.00000	0.11852	0.51425	**16.57 ± 2.18**	97.53	1.41	97.136 ######

Ar-Ar ages of 25 detrital white mica grains from sample Sonadia 1 3237, MS2, SE Hatia Trough

Incremental Heating			36Ar(a)	37Ar(ca)	38Ar(cl)	39Ar(k)	40Ar(r)	Age ± 2σ (Ma)	40Ar(r) (%)	39Ar(k) (%)	K/Ca ± 2σ
05M0073A	1.00 W		0.00009	0.00043	0.00000	0.68245	1.89020	**10.60 ± 0.42**	98.59	9.83	676.942 ######
05M0073B	2.00 W		0.00099	0.00099	0.00000	0.52801	1.66072	**12.03 ± 0.49**	84.94	7.60	230.054 ######
05M0073C	3.00 W		0.00016	0.00100	0.00000	0.26474	0.71752	**10.37 ± 0.89**	93.87	3.81	114.055 ######
05M0073D	4.00 W		0.00006	0.00000	0.00000	0.50232	0.18365	**1.40 ± 0.56**	90.27	7.23	0.000 ± 0.000
05M0073E	5.00 W		0.00048	0.00000	0.00000	0.36296	2.83928	**29.77 ± 0.75**	95.22	5.23	0.000 ± 0.000
05M0073G	6.00 W		0.00038	0.00137	0.00000	0.19202	0.79509	**15.82 ± 0.89**	87.67	2.76	60.154 ± 86.399
05M0073H	7.00 W		0.00010	0.00000	0.00000	0.13102	0.43165	**12.60 ± 1.32**	93.32	1.89	0.000 ± 0.000
05M0073I	8.00 W		0.00014	0.00117	0.00000	0.24336	1.02784	**16.13 ± 0.81**	96.16	3.50	89.111 ######
05M0073J	9.00 W		0.00035	0.00181	0.00000	0.18173	0.96350	**20.23 ± 0.71**	90.25	2.62	43.168 ± 42.080
05M0073K	10.00 W		0.00018	0.00184	0.00000	0.30264	0.71311	**9.02 ± 0.72**	93.11	4.36	70.582 ± 60.665
05M0073M	11.00 W		0.00035	0.00000	0.00000	0.29672	1.09197	**14.07 ± 0.65**	91.20	4.27	0.000 ± 0.000
05M0073N	12.00 W		0.00003	0.00000	0.00000	0.08991	0.41295	**17.54 ± 2.47**	97.86	1.29	0.000 ± 0.000
05M0073O	13.00 W		0.00057	0.00000	0.00000	0.40009	1.71660	**16.39 ± 0.63**	91.02	5.76	0.000 ± 0.000
05M0073P	14.00 W		0.00011	0.00046	0.00000	0.30011	0.73554	**9.38 ± 0.71**	95.67	4.32	281.434 ######
05M0073Q	15.00 W		0.00002	0.00000	0.00000	0.48168	1.71202	**13.59 ± 0.49**	99.66	6.94	0.005 ± 0.000
05M0073S	16.00 W		0.00028	0.00000	0.00000	0.14744	0.47963	**12.44 ± 1.28**	85.44	2.12	0.005 ± 0.000
05M0073T	17.00 W		0.00009	0.00000	0.00000	0.22388	0.87285	**14.90 ± 0.76**	96.86	3.22	0.005 ± 0.000
05M0073U	18.00 W		0.00020	0.00000	0.00000	0.33782	1.38059	**15.61 ± 0.62**	95.88	4.86	0.005 ± 0.000
05M0073V	19.00 W		0.00019	0.00000	0.00000	0.69701	2.72826	**14.96 ± 0.29**	97.98	10.04	0.005 ± 0.000
05M0073W	20.00 W		0.00024	0.00000	0.00000	0.57898	2.14496	**14.16 ± 0.30**	96.79	8.34	0.005 ± 0.000

Ar-Ar ages of 20 detrital white mica grains from sample Sangu 1 280, MS3, SE Hatia Trough

Sample Ref.	40Ar	1σ	39Ar	1σ	38Ar	1σ	37Ar	1σ	36Ar	1σ	40Ar(ATM)%	40Ar*/39Ark	σF	Age(Ma)	1σ
BGL05 9A															
5310	0.0821	0.0003	0.0458	0.0000	0.0005	0.0000	0.0000	0.0000	0.0000	0.0000	1.7384	1.7567	0.0000	**9.5**	0.05
5312	0.0885	0.0003	0.0214	0.0000	0.0002	0.0000	0.0000	0.0000	0.0000	0.0000	-16.3769	4.7874	0.0002	**25.7**	0.13
5287	0.0903	0.0003	0.0609	0.0000	0.0007	0.0000	0.0000	0.0000	0.0000	0.0000	10.0656	1.3261	0.0001	**7.2**	0.04
5266	0.0930	0.0003	0.0441	0.0000	0.0005	0.0000	0.0000	0.0000	0.0001	0.0000	16.5200	1.7536	0.0001	**9.5**	0.05
5313	0.1049	0.0003	0.0445	0.0000	0.0005	0.0000	0.0000	0.0000	0.0000	0.0000	-1.9743	2.3940	0.0001	**12.9**	0.06
5290	0.1151	0.0003	0.0567	0.0000	0.0006	0.0000	0.0000	0.0000	0.0000	0.0000	3.0230	1.9592	0.0000	**10.6**	0.05
5316	0.1178	0.0003	0.0280	0.0000	0.0003	0.0000	-0.0001	0.0000	0.0000	0.0000	3.0619	4.0644	0.0002	**21.9**	0.11
5278	0.1294	0.0003	0.0726	0.0000	0.0008	0.0000	0.0000	0.0000	0.0000	0.0000	8.9652	1.6173	0.0000	**8.7**	0.04
5273	0.1374	0.0003	0.0427	0.0000	0.0005	0.0000	0.0001	0.0000	0.0000	0.0000	8.6185	2.9336	0.0001	**15.8**	0.08
5276	0.1512	0.0003	0.0624	0.0000	0.0007	0.0000	0.0001	0.0000	0.0000	0.0000	8.0583	2.2245	0.0000	**12.0**	0.06
5267	0.1519	0.0003	0.0452	0.0000	0.0005	0.0000	0.0000	0.0000	0.0001	0.0000	11.9701	2.9461	0.0001	**15.9**	0.08
5279	0.1520	0.0003	0.0379	0.0000	0.0005	0.0000	0.0000	0.0000	0.0001	0.0000	19.5146	3.2176	0.0001	**17.3**	0.09
5261	0.1559	0.0003	0.0583	0.0000	0.0007	0.0000	0.0001	0.0000	0.0000	0.0000	2.6285	2.5983	0.0000	**14.0**	0.07
5289	0.1546	0.0003	0.0624	0.0000	0.0007	0.0000	0.0000	0.0000	0.0000	0.0000	5.6419	2.3299	0.0000	**12.6**	0.06
5269	0.1807	0.0003	0.0598	0.0000	0.0007	0.0000	0.0000	0.0000	0.0001	0.0000	22.1122	2.3418	0.0000	**12.6**	0.06
5263	0.2048	0.0003	0.0505	0.0000	0.0006	0.0000	0.0000	0.0000	0.0000	0.0000	0.7268	4.0112	0.0001	**21.6**	0.11
5296	0.2054	0.0003	0.0547	0.0000	0.0006	0.0000	0.0000	0.0000	0.0001	0.0000	10.6069	3.3477	0.0001	**18.0**	0.09
5315	0.2118	0.0003	0.0506	0.0000	0.0006	0.0000	0.0000	0.0000	0.0000	0.0000	1.9100	4.0889	0.0001	**22.0**	0.11
5286	0.2159	0.0003	0.0828	0.0000	0.0010	0.0000	-0.0000	0.0000	-0.0000	0.0000	1.9964	2.5463	0.0000	**13.7**	0.07
5309	0.2505	0.0003	0.0668	0.0000	0.0007	0.0000	0.0001	0.0000	0.0001	0.0000	-6.1389	3.9620	0.0001	**21.3**	0.11
5264	0.2727	0.0003	0.0752	0.0000	0.0009	0.0000	0.0000	0.0000	0.0001	0.0000	12.5254	3.1604	0.0001	**17.0**	0.08
5292	0.2861	0.0003	0.0651	0.0000	0.0007	0.0000	0.0000	0.0000	0.0000	0.0000	3.9178	4.2088	0.0001	**22.6**	0.11
5270	0.3186	0.0003	0.0942	0.0000	0.0011	0.0000	0.0000	0.0000	0.0003	0.0000	23.4358	2.5815	0.0000	**13.9**	0.07
5275	0.5329	0.0003	0.1410	0.0000	0.0016	0.0000	0.0000	0.0000	0.0001	0.0000	5.7862	3.5468	0.0000	**19.1**	0.09
BGL05 13A															
5208	0.0938	0.0003	0.0182	0.0000	0.0002	0.0000	0.0000	0.0000	0.0000	0.0000	-3.1985	5.2910	0.0004	**28.41**	0.14
5243	0.1008	0.0003	0.0240	0.0000	0.0002	0.0000	0.0000	0.0000	0.0000	0.0000	5.5018	3.9441	0.0002	**21.22**	0.11
5241	0.1105	0.0003	0.0252	0.0000	0.0003	0.0000	0.0000	0.0000	0.0001	0.0000	23.9151	3.3352	0.0002	**17.96**	0.09

5250	0.1179	0.0003	0.0086	0.0000	0.0001	0.0000	0.0000	0.0000	0.0000	0.0000	4.0983	13.0572	0.0019	**69.32**	0.34
5229	0.1222	0.0003	0.0335	0.0000	0.0003	0.0000	0.0000	0.0000	0.0000	0.0000	-1.2559	3.6801	0.0001	**19.81**	0.10
5231	0.1433	0.0003	0.0366	0.0000	0.0004	0.0000	0.0000	0.0000	0.0001	0.0000	13.9402	3.3594	0.0001	**18.09**	0.09
5203	0.1517	0.0003	0.0377	0.0000	0.0005	0.0000	0.0000	0.0000	-0.0001	0.0000	-9.8860	4.4151	0.0001	**23.74**	0.12
5185	0.1620	0.0003	0.0813	0.0001	0.0009	0.0000	0.0000	0.0000	0.0000	0.0000	-2.1185	2.0244	0.0000	**10.92**	0.05
5226	0.1960	0.0003	0.0531	0.0000	0.0006	0.0000	0.0000	0.0000	0.0000	0.0000	3.9148	3.5329	0.0001	**19.02**	0.09
5200	0.2001	0.0003	0.0492	0.0000	0.0006	0.0000	0.0000	0.0000	0.0000	0.0000	-4.3789	4.2291	0.0001	**22.74**	0.11
5206	0.2110	0.0003	0.0683	0.0000	0.0008	0.0000	0.0001	0.0000	0.0001	0.0000	13.0193	2.6827	0.0000	**14.46**	0.07
5244	0.2256	0.0003	0.0544	0.0000	0.0006	0.0000	0.0000	0.0000	0.0001	0.0000	13.1599	3.5925	0.0001	**19.34**	0.10
5183	0.2457	0.0003	0.1094	0.0001	0.0013	0.0000	0.0000	0.0000	0.0000	0.0000	4.3181	2.1405	0.0000	**11.55**	0.06
5225	0.2487	0.0003	0.0514	0.0000	0.0006	0.0000	0.0000	0.0000	0.0000	0.0000	1.4889	4.7523	0.0001	**25.54**	0.13
5209	0.2553	0.0003	0.0668	0.0000	0.0008	0.0000	0.0001	0.0000	0.0000	0.0000	3.4328	3.6783	0.0001	**19.80**	0.10
5202	0.3196	0.0003	0.0881	0.0000	0.0011	0.0000	0.0001	0.0000	0.0001	0.0000	9.6632	3.2685	0.0000	**17.60**	0.09
5237	0.5775	0.0003	0.0300	0.0000	0.0003	0.0000	0.0000	0.0000	0.0000	0.0000	0.0471	19.1918	0.0010	**100.99**	0.49
5235	0.6050	0.0003	0.0291	0.0000	0.0003	0.0000	0.0000	0.0000	0.0000	0.0000	-0.7059	20.8884	0.0012	**109.65**	0.53
BGL05 14A															
4857	0.0911	0.0003	0.0139	0.0000	0.0002	0.0000	0.0000	0.0000	0.0001	0.0000	34.9502	4.2410	0.0007	**22.81**	0.11
4868	0.0946	0.0003	0.0232	0.0000	0.0003	0.0000	0.0000	0.0000	0.0001	0.0000	28.0379	2.9277	0.0003	**15.78**	0.08
5128	0.3339	0.0004	0.0315	0.0000	0.0004	0.0000	0.0000	0.0000	0.0000	0.0000	2.2827	10.3390	0.0005	**55.11**	0.27
5118	0.3777	0.0003	0.0321	0.0000	0.0004	0.0000	0.0000	0.0000	0.0000	0.0000	0.3790	11.6784	0.0005	**62.12**	0.31
5116	0.1972	0.0003	0.0335	0.0000	0.0004	0.0000	0.0001	0.0000	0.0000	0.0000	5.4357	5.5473	0.0002	**29.78**	0.15
4875	0.1711	0.0003	0.0368	0.0000	0.0004	0.0000	-0.0001	0.0000	0.0000	0.0000	1.2729	4.5728	0.0001	**24.58**	0.12
5127	0.1284	0.0003	0.0375	0.0000	0.0005	0.0000	0.0000	0.0000	0.0000	0.0000	0.0631	3.4113	0.0001	**18.37**	0.09
5134	0.2695	0.0003	0.0416	0.0000	0.0004	0.0000	0.0000	0.0000	0.0000	0.0000	1.9586	6.3291	0.0002	**33.93**	0.17
4861	0.1225	0.0003	0.0430	0.0000	0.0004	0.0000	0.0000	0.0000	0.0001	0.0000	13.0052	2.4712	0.0001	**13.33**	0.07
5125	0.1890	0.0003	0.0470	0.0000	0.0005	0.0000	0.0000	0.0000	0.0000	0.0000	5.6439	3.7795	0.0001	**20.34**	0.10
BNG5 26															
4778	0.1034	0.0003	0.0111	0.0000	0.0002	0.0000	0.0000	0.0000	0.0001	0.0000	24.8435	7.0082	0.0014	**37.54**	0.19
4816	0.1052	0.0003	0.0418	0.0000	0.0006	0.0000	0.0001	0.0000	0.0001	0.0000	17.4757	2.0717	0.0001	**11.18**	0.06
4804	0.1233	0.0003	0.0375	0.0000	0.0005	0.0000	0.0000	0.0000	0.0001	0.0000	17.7664	2.6964	0.0001	**14.53**	0.07

4776	0.1574	0.0003	0.0147	0.0000	0.0002	0.0000	0.0001	0.0000	0.0001	0.0000	15.5079	9.0559	0.0009	**48.36**	0.24
4803	0.1671	0.0003	0.0589	0.0000	0.0007	0.0000	0.0000	0.0000	0.0001	0.0000	20.9256	2.2375	0.0001	**12.07**	0.06
4785	0.1803	0.0004	0.0577	0.0000	0.0007	0.0000	0.0000	0.0000	0.0001	0.0000	9.1037	2.8329	0.0001	**15.27**	0.08
4815	0.1856	0.0003	0.0587	0.0000	0.0007	0.0000	0.0001	0.0000	0.0001	0.0000	17.1669	2.6141	0.0001	**14.09**	0.07
4787	0.2057	0.0003	0.0331	0.0000	0.0004	0.0000	0.0000	0.0000	0.0001	0.0000	8.6312	5.6644	0.0002	**30.40**	0.15
4802	0.7151	0.0003	0.2498	0.0000	0.0029	0.0000	0.0000	0.0000	0.0003	0.0000	11.0523	2.5375	0.0000	**13.68**	0.07
4769	0.8213	0.0003	0.2201	0.0000	0.0025	0.0000	0.0000	0.0000	0.0002	0.0000	8.9073	3.3881	0.0000	**18.24**	0.09
4832	0.8091	0.0005	0.1755	0.0001	0.0021	0.0000	0.0001	0.0000	0.0003	0.0000	11.8607	4.0502	0.0001	**21.79**	0.11
4831	1.0133	0.0008	0.4669	0.0003	0.0054	0.0000	0.0001	0.0000	0.0006	0.0000	18.1828	1.7688	0.0000	**9.55**	0.05
BNG5 33															
5091	0.0807	0.0003	0.0090	0.0000	0.0001	0.0000	0.0000	0.0000	0.0002	0.0000	64.7358	3.1424	0.0019	**16.93**	0.08
4982	0.1232	0.0003	0.0382	0.0000	0.0005	0.0000	0.0001	0.0000	0.0002	0.0000	42.7036	1.8502	0.0001	**9.99**	0.05
4963	0.1263	0.0003	0.0274	0.0000	0.0003	0.0000	0.0000	0.0000	0.0001	0.0000	31.2074	3.1609	0.0002	**17.03**	0.08
4989	0.1303	0.0003	0.0369	0.0000	0.0005	0.0000	0.0002	0.0000	0.0002	0.0000	36.2777	2.2555	0.0001	**12.17**	0.06
4985	0.1362	0.0003	0.0351	0.0000	0.0005	0.0000	0.0001	0.0000	0.0001	0.0000	25.4785	2.8899	0.0001	**15.57**	0.08
5097	0.1473	0.0003	0.0443	0.0000	0.0006	0.0000	0.0000	0.0000	0.0000	0.0000	-5.2825	3.4896	0.0001	**18.79**	0.09
							-								
5093	0.1518	0.0003	0.0393	0.0000	0.0004	0.0000	0.0001	0.0000	0.0001	0.0000	15.1399	3.2577	0.0002	**17.55**	0.09
4983	0.1916	0.0003	0.0396	0.0000	0.0005	0.0000	0.0001	0.0000	0.0002	0.0000	29.1179	3.4227	0.0001	**18.43**	0.09
4986	0.2103	0.0003	0.0800	0.0000	0.0009	0.0000	0.0000	0.0000	0.0002	0.0000	27.6991	1.8948	0.0000	**10.23**	0.05
5001	0.2311	0.0003	0.0876	0.0000	0.0011	0.0000	0.0002	0.0000	0.0001	0.0000	17.0713	2.1851	0.0000	**11.79**	0.06
4966	0.3145	0.0003	0.1095	0.0000	0.0013	0.0000	0.0000	0.0000	0.0003	0.0000	30.4068	1.9924	0.0000	**10.75**	0.05
5094	0.3175	0.0003	0.0927	0.0001	0.0011	0.0000	0.0000	0.0000	0.0001	0.0000	5.1521	3.2375	0.0000	**17.44**	0.09
							-								
5387	0.3059	0.0003	0.0561	0.0000	0.0006	0.0000	0.0001	0.0000	0.0002	0.0000	19.1328	4.3899	0.0001	**23.60**	0.12
5388	0.3189	0.0003	0.1023	0.0000	0.0012	0.0000	0.0000	0.0000	0.0002	0.0000	19.5678	2.5004	0.0000	**13.48**	0.07
4967	0.5506	0.0004	0.1737	0.0001	0.0021	0.0000	0.0001	0.0000	0.0004	0.0000	19.8767	2.5321	0.0000	**13.65**	0.07
4969	1.5433	0.0017	0.3345	0.0004	0.0040	0.0000	0.0002	0.0000	0.0008	0.0000	16.2461	3.8525	0.0001	**20.73**	0.10
4970	2.2970	0.0030	0.5049	0.0006	0.0061	0.0000	0.0002	0.0000	0.0009	0.0000	11.4604	4.0155	0.0001	**21.60**	0.11
BNG5 40															
4938	0.0921	0.0003	0.0346	0.0000	0.0004	0.0000	0.0000	0.0000	0.0001	0.0000	28.9861	1.8846	0.0001	**10.17**	0.05
4958	0.0926	0.0003	0.0297	0.0000	0.0004	0.0000	0.0001	0.0000	0.0002	0.0000	53.1537	1.4625	0.0002	**7.90**	0.04

4930	0.1389	0.0003	0.0332	0.0000	0.0005	0.0000	0.0001	0.0000	0.0002	0.0000	38.0630	2.5900	0.0002	**13.96**	0.07
4954	0.1434	0.0003	0.0332	0.0000	0.0004	0.0000	0.0000	0.0000	0.0001	0.0000	30.2518	3.0099	0.0002	**16.22**	0.08
4937	0.1912	0.0003	0.0450	0.0000	0.0006	0.0000	0.0001	0.0000	0.0001	0.0000	15.8245	3.5648	0.0001	**19.19**	0.10
4941	0.3889	0.0003	0.0348	0.0000	0.0005	0.0000	0.0000	0.0000	0.0000	0.0000	3.7941	10.7312	0.0004	**57.16**	0.28
4957	0.4215	0.0003	0.1062	0.0000	0.0013	0.0000	0.0000	0.0000	0.0003	0.0000	21.9264	3.0904	0.0000	**16.65**	0.08
4929	1.2253	0.0017	0.4382	0.0006	0.0053	0.0000	0.0002	0.0000	0.0011	0.0000	25.6888	2.0714	0.0000	**11.18**	0.06
4948	3.6457	0.0009	0.0095	0.0000	0.0024	0.0000	0.0000	0.0000	0.0122	0.0000	99.8175	0.6991	0.4774	**3.78**	2.58
BNG5 78															
4389	0.0529	0.0019	0.0164	0.0000	0.0002	0.0000	0.0000	0.0000	0.0001	0.0000	35.6041	2.0773	0.0133	**11.21**	0.09
4360	0.0543	0.0019	0.0148	0.0000	0.0002	0.0000	0.0000	0.0000	0.0000	0.0000	16.9408	3.0246	0.0165	**16.30**	0.12
4364	0.0570	0.0019	0.0115	0.0000	0.0002	0.0000	0.0000	0.0000	0.0001	0.0000	26.4771	3.6357	0.0274	**19.57**	0.18
4439	0.0573	0.0019	0.0171	0.0000	0.0002	0.0000	0.0000	0.0000	0.0000	0.0000	7.2529	3.0907	0.0119	**16.65**	0.10
4388	0.0585	0.0019	0.0102	0.0000	0.0001	0.0000	0.0000	0.0000	0.0000	0.0000	24.0109	4.3302	0.0343	**23.29**	0.22
4441	0.0587	0.0019	0.0126	0.0000	0.0002	0.0000	0.0000	0.0000	0.0000	0.0000	11.1568	4.1156	0.0219	**22.14**	0.16
4420	0.0596	0.0019	0.0123	0.0000	0.0002	0.0000	0.0000	0.0000	0.0000	0.0000	3.9946	4.6203	0.0232	**24.83**	0.17
4419	0.0612	0.0019	0.0098	0.0000	0.0001	0.0000	0.0000	0.0000	0.0000	0.0000	7.5588	5.7286	0.0365	**30.74**	0.25
4370	0.0678	0.0019	0.0221	0.0000	0.0003	0.0000	0.0001	0.0000	0.0001	0.0000	23.2502	2.3477	0.0074	**12.66**	0.07
4376	0.0689	0.0019	0.0235	0.0000	0.0003	0.0000	0.0000	0.0000	0.0000	0.0000	13.6252	2.5219	0.0066	**13.60**	0.08
4383	0.0710	0.0019	0.0186	0.0000	0.0002	0.0000	0.0000	0.0000	0.0001	0.0000	25.3471	2.8266	0.0104	**15.23**	0.09
4435	0.0785	0.0019	0.0136	0.0000	0.0002	0.0000	0.0000	0.0000	0.0000	0.0000	4.5910	5.4834	0.0189	**29.44**	0.18
4363	0.0934	0.0019	0.0268	0.0000	0.0004	0.0000	0.0001	0.0000	0.0001	0.0000	20.3059	2.7754	0.0051	**14.96**	0.08
4392	0.0974	0.0019	0.0258	0.0000	0.0004	0.0000	0.0000	0.0000	0.0001	0.0000	23.8075	2.8724	0.0054	**15.48**	0.08
4410	0.1077	0.0019	0.0298	0.0000	0.0003	0.0000	0.0000	0.0000	0.0000	0.0000	1.0758	3.5645	0.0040	**19.19**	0.10
4361	0.1093	0.0019	0.0304	0.0000	0.0004	0.0000	0.0000	0.0000	0.0001	0.0000	17.8550	2.9463	0.0040	**15.88**	0.08
4377	0.1274	0.0019	0.0282	0.0000	0.0003	0.0000	0.0000	0.0000	0.0000	0.0000	6.2050	4.2197	0.0046	**22.69**	0.12
4386	0.1274	0.0019	0.0270	0.0000	0.0004	0.0000	0.0000	0.0000	0.0001	0.0000	12.9297	4.0971	0.0050	**22.04**	0.11
4404	0.1368	0.0019	0.0420	0.0000	0.0005	0.0000	0.0001	0.0000	0.0000	0.0000	9.5007	2.9412	0.0021	**15.85**	0.08
4201	0.1793	0.0020	0.0460	0.0001	0.0006	0.0000	0.0001	0.0000	0.0001	0.0000	18.4301	3.1696	0.0019	**17.07**	0.09
4385	0.1957	0.0019	0.0269	0.0000	0.0003	0.0000	0.0000	0.0000	0.0000	0.0000	4.8059	6.9010	0.0052	**36.97**	0.19
4369	0.7293	0.0019	0.0626	0.0000	0.0007	0.0000	0.0000	0.0000	0.0001	0.0000	5.9668	10.9186	0.0013	**58.15**	0.29
BNG5 96															
4922	0.0917	0.0003	0.0183	0.0000	0.0003	0.0000	0.0001	0.0000	0.0002	0.0000	52.0421	2.4095	0.0004	**12.99**	0.06

4925	0.1921	0.0003	0.0221	0.0000	0.0003	0.0000	0.0001	0.0000	0.0000	0.0000	6.6465	8.1002	0.0004	**43.32**	0.21
4897	0.2893	0.0003	0.0863	0.0000	0.0010	0.0000	0.0000	0.0000	0.0002	0.0000	23.7857	2.5458	0.0000	**13.73**	0.07
4898	0.3961	0.0003	0.0478	0.0000	0.0006	0.0000	0.0001	0.0000	0.0001	0.0000	7.6110	7.6390	0.0002	**40.88**	0.20
4912	0.9214	0.0005	0.2841	0.0001	0.0034	0.0000	0.0000	0.0000	0.0004	0.0000	12.7355	2.8203	0.0000	**15.20**	0.08
4913	1.0597	0.0006	0.2267	0.0001	0.0027	0.0000	0.0001	0.0000	0.0005	0.0000	14.1288	4.0019	0.0001	**21.53**	0.11
Sangu 1															
5060	0.0869	0.0003	0.0352	0.0000	0.0004	0.0000	0.0000	0.0000	0.0001	0.0000	17.8973	2.0203	0.0001	**10.90**	0.05
5158	0.0960	0.0003	0.0328	0.0000	0.0004	0.0000	0.0001	0.0000	0.0001	0.0000	22.6468	2.2613	0.0001	**12.20**	0.06
5062	0.1056	0.0003	0.0528	0.0001	0.0006	0.0000	0.0001	0.0000	0.0001	0.0000	14.9741	1.6980	0.0001	**9.17**	0.05
5053	0.1304	0.0004	0.0452	0.0000	0.0005	0.0000	0.0000	0.0000	0.0001	0.0000	13.8322	2.4781	0.0001	**13.36**	0.07
5057	0.1226	0.0003	0.0521	0.0001	0.0006	0.0000	0.0001	0.0000	0.0000	0.0000	11.3514	2.0796	0.0001	**11.22**	0.06
5043	0.1559	0.0004	0.0357	0.0000	0.0004	0.0000	0.0000	0.0000	0.0000	0.0000	-1.9454	4.4354	0.0002	**23.85**	0.12
5367	0.1037	0.0003	0.0338	0.0000	0.0004	0.0000	0.0000	0.0000	0.0000	0.0000	-3.1423	3.1502	0.0001	**16.97**	0.08
5065	0.1280	0.0003	0.0467	0.0000	0.0006	0.0000	0.0000	0.0000	0.0000	0.0000	10.3329	2.4510	0.0001	**13.22**	0.07
5156	0.1351	0.0003	0.0302	0.0000	0.0004	0.0000	0.0001	0.0000	0.0000	0.0000	10.5258	3.9908	0.0002	**21.47**	0.11
5143	0.1433	0.0003	0.0490	0.0000	0.0006	0.0000	0.0000	0.0000	0.0000	0.0000	-4.8745	3.0574	0.0001	**16.47**	0.08
5080	0.1057	0.0002	0.0422	0.0000	0.0005	0.0000	0.0001	0.0000	0.0000	0.0000	-0.9883	2.5217	0.0001	**13.60**	0.07
5054	0.1902	0.0004	0.0418	0.0000	0.0005	0.0000	0.0000	0.0000	0.0000	0.0000	5.8349	4.2732	0.0001	**22.98**	0.11
5063	0.1679	0.0003	0.0532	0.0000	0.0006	0.0000	0.0000	0.0000	0.0001	0.0000	13.6936	2.7147	0.0001	**14.63**	0.07
5366	0.1587	0.0003	0.0206	0.0000	0.0003	0.0000	0.0000	0.0000	0.0003	0.0000	65.1343	2.6811	0.0004	**14.45**	0.07
5068	0.1783	0.0003	0.0441	0.0000	0.0005	0.0000	0.0000	0.0000	0.0000	0.0000	5.9565	3.7899	0.0001	**20.40**	0.10
5045	0.2821	0.0004	0.0647	0.0001	0.0008	0.0000	0.0001	0.0000	0.0000	0.0000	3.3317	4.1998	0.0001	**22.59**	0.11

Method:

White mica has a closure temperature of ~350 -400°C in the Ar-Ar system (McDougall and Harris, 1999) and as such records post-metamorphic cooling in the source region, making 40Ar-39Ar dating ideally suited provenance determination of clastic sequences such as this, which have not undergone post depositional resetting

Laser 40Ar/39Ar single fusion experiments were carried out in the NERC Argon Isotope Laboratory, East Kilbride, Scotland and Vrije Universitaat, Amsterdam. For each sample ca 50 grains varying in grain size from larger than 1 mm to ca. 100 micrometer diameter were packed in approximately 1 cm square Al-foil packages, stacked and interspersed with packages containing a mineral standard into a 25 mm OD Al irradiation tube. The monitor mineral standard is Taylor Creek Rhyolite sanidine (TCR2a) with a 40Ar/39Ar age of 28.34 Ma (Renne et al. 1998). Samples and monitors were irradiated for 10 hrs in a Cd-lined facility (RODEO) at the Petten HFR, Netherlands.
Following irradiation samples were loaded onto a 52 mm diameter Cu-sample tray that contained circular machined depressions (2 mm deep, 2 mm diameter), and placed in a UHV laser cell. The laser cell is fitted with a zinc-selenide UHV-window for transmission of IR laser light. Because the ZnSe window was attached to the stainless steel housing of the with a braised seal, the laser cell was limited to a bake-out temperature of <100°C. A 25W CO2 laser was used to fuse samples. At these settings 15% laser power setting was sufficient to fuse the samples. System blanks were measured every 2-5 grains. and found to be stable through the course of analysis. Data were collected on a GVi instruments Argus multi-collector mass spectrometer using a variable sensitivity faraday collector array in static (non-peak hopping) mode.
For off-line data reduction, we used an in-house Excel-based method of age calculation and ArArCALC. The ages are reported with uncertainties at 1-sigma level. Younger and smaller grains were more difficult to measure, and it was found empirically that when sample to blank ratios of 39Ar (and then filtered a second time by looking at sample-blank ratio of 40Ar were lower than ca 8-10, uncertainties in the calculated age were very high, preventing the use of these grains for interpretation. Accepted analyses all yielded ages that are realistic for the sample, e.g., greater than the stratigraphic age, and fall into age ranges for known events or rock sequences in the hinterland.

Koppers, A. 2002. ArArCalc – software for Ar-40/Ar-39 age calculations. Computers and Geosciences 28 : 605-619.

Sample #	No.x tals	Dosimeter ρd	Nd	Spontaneous ρs	Ns	Induced ρi	Ni	Age dispersion $P\chi^2$	RE_{∞}	Central age (Ma) ±1σ	Age Components 1st	2nd	3rd	4th	5th
SB 3016	*63*	*0.606*	*6715*	*4.056*	*4604*	*6.634*	*7531*	*<1*	54.1	**23.6±1.7**	13±1 (13)	18±1 (40)	31±2 (12)	99±18 (2)	190±21 (2)
Sangu 3840	*43*	*0.606*	*6715*	*6.583*	*5146*	*7.536*	*5891*	*<1*	62.7	**30.9±3.1**	13±1 (7)	23±1 (17)	36±2 (17)	210±38 (2)	
BGL05-1A	48	0.478	3140	6.421	5785	5.537	6236	0.0	81.1	**29.1±3.5**	10.2±0.4 (14)	26.3±0.9 (26)	121.5±13.7 (3)	420.8±54.6 (4)	
BGL05-5A	26	0.483	3140	6.430	3219	6.037	3797	0.0	83.5	**31.1±5.2**	14.8±0.5 (10)	26.9±1.1 (8)	64.7±5.5 (3)	205.9±28.4 (3)	
BGL05-6A	28	0.448	3120	7.418	4092	8.217	4929	0.0	67.9	**27.0±3.6**	9.0±0.5 (4)	18.7±1.1 (10)	31.2±1.3 (8)	67.9±7.7 (5)	388±101 (1)
BGL05-11A	8	0.490	3140	5.429	734	4.757	638	0.0	60.0	**39.7±8.8**	21.3±1.7 (3)	42.9±4.0 (3)	181±46 (1)		
BGL05-12A	9	0.548	3093	4.563	511	6.249	859	0.0	86.9	**22.9±6.8**	6.1±0.8 (3)	29.6±2.0 (5)	225±119 (1)		
BGL05-14A	33	0.548	3016	5.767	4284	7.085	4284	0.0	80.7	**27.5±4.0**	12.5±0.5 (13)	24.6±1.3 (16)	64.0±7.3 (1)	423.7±90.5 (2)	
BA05-21A	46	0.454	3140	8.245	6629	6.692	5578	0.0	77.0	**35.0±4.1**	12.8±0.8 (9)	23.4±0.8 (18)	41.0±1.7 (13)	355.7±39.5 (4)	
BA05-22A	23	0.461	3140	7.065	2591	7.457	2920	0.0	56.4	**26.3±3.4**	15.2±0.8 (8)	25.9±1.2 (8)	45.1±4.0 (2)	125±14 (2)	
BA05-23A	51	0.534	3698	3.923	4743	7.836	10261	0.0	65.5	**17.2±1.6**	7.0±0.5 (3)	10.5±0.9 (14)	14.6±0.9 (13)	25.6±0.9 (13)	133.5±14 (5)
BA05-24A	20	0.534	3698	9.174	2806	7.217	2622	0.0	84.4	**26.3±5.0**	9.5±0.6 (8)	28.8±1.6 (9)	264.9±27.3 (2)		
BA05-25A	53	0.469	3140	4.690	6092	6.505	9582	0.0	71.0	**21.4±2.2**	5.3±0.4 (7)	13.8±0.7 (14)	21.8±0.8 (16)	32.8±1.2 (12)	85.4±13.2(2) 228±28 (2)
BA05-27A	31	0.534	3698	4.797	2027	5.665	2542	0.0	46.1	**29.0±2.6**	9.9±1.5 (3)	19.2±1.7 (7)	30.7±1.9 (13)	51.2±5.0 (6)	
BA05-28A	24	0.473	3140	5.028	3066	6.033	4115	0.0	54.8	**24.1±2.8**	14.5±1.3 (8)	23.7±0.9 (15)	531±173 (1)		
BNG5 33	63	5.232	3626	6.385	5593	7.992	7141	0.0	49.3	**25.5±1.7**	16.6±0.5 (30)	28.7±0.9 (24)	48.1±4.0 (6)	110±15 (3)	
BNG5 40	79	5.232	3626	6.525	7107	6.725	7588	0.0	62.9	**31.5±2.4**	15.0±0.3 (24)	28.5±1.1 (30)	42.6±2.6 (21)	146±23 (3)	
BNG5 46	61	5.232	3626	6.316	6443	9.332	9606	0.0	40.3	**23.1±1.3**	9.3±0.9 (2)	14.7±0.5 (16)	23.0±0.7 (30)	39.3±3.1 (12)	
BNG5 123	50	5.232	3626	6.555	7062	8.511	9239	0.0	43.6	**25.1±1.7**	16.5±0.8 (15)	23.2±0.8 (24)	42.1±2.8 (9)	242±39 (1)	

Appendix 3 - 6: Detrital Zircon Fission track analytical data

Zircon track annealing takes place between ~200°C-310°C. Above this, fission tracks will fully anneal. The relatively higher closure temperature compared to apatite (~120°C) makes this technique suitable for provenance work, as the zircon fission track grain ages are not as susceptible to resetting by burial related heating.

(i). Track densities are ($x10^6$ tr cm^{-2}) numbers of tracks counted (N) shown in brackets;
(ii). analyses by external detector method using 0.5 for the $4\pi/2\ \pi$ geometry correction factor;
(iii). ages calculated using dosimeter glass CN-2; (zircon) ξ_{CN2} =127±5
calibrated by multiple analyses of IUGS apatite and zircon age standards (see Hurford 1990);
(iv). $P\chi^2$ is probability for obtaining χ^2 value for v degrees of freedom, where v = no. crystals - 1;
(v). Central age is a modal age, weighted for different precisions of individual crystals (see Galbraith 1992)

Samples for ZFT analysis were mounted in PTFE Teflon, polished and etched using a binary eutectic of NaOH:KOH at 225°C. Multiple grain mounts were made for each sample and etched for different durations of time to avoid source bias. Samples were then packed with muscovite external detectors and CN2 glass dosimeter and irradiated in the well thermalised (Cd ratio for Au >100) of the Garching facility, Germany. Fission-track densities were measured using an optical microscope at 1250x magnification. Ages (±1s) were calibrated by the zeta method (Hurford and Green, 1983), using a zeta factor for zircon of 127 ± 5, determined by multiple analyses of zircon age standards.

Galbraith, R.F. and Laslett, G.M., 1993. Statistical models for mixed fission track ages. Nucl. Tracks and Radiation Measurement, 21, 459-470.
Hurford, A.J., 1990. Standardization of fission track dating calibration: recommendation by the Fission Track Working Group of the IUGS subcommission on geochronology: Chemical Geology, 80, 177-178.

Appendix 3 – 7: Detrital zircon U-Pb data and procedural method

Sample BNG5 96	206/238	err	207/235	err	206/238 age (Ma)	err (Ma)	206/207 age (Ma)	err (Ma)
BNG96 1	0.12591	0.8	1.17632	1.2	**764.5**	**13.4**	775.6	25.3
BNG96-2	0.08661	0.8	0.6423	1.4	**535.5**	**9.4**	480.3	30.1
BNG96-3	0.20743	1.2	1.8866	5.2	**1215.1**	**31.2**	1087.9	61.7
BNG96-4	0.49331	0.8	11.73395	1.4	**2585**	**52.3**	2665.8	19.3
BNG96-5	0.21695	1.1	2.05999	4.8	**1265.7**	**30.7**	1126.6	55
BNG96-6	0.18117	0.9	1.7469	2.2	**1073.4**	**20.5**	1026.4	32.5
BNG96-7	0.08638	0.8	0.65425	1.5	**534.1**	**9.6**	544.8	30.7
BNG96-8	0.01679	1.4	0.10591	6	**107.3**	**3.5**	72.4	137.8
BNG96-9	0.09031	0.9	0.69029	2.3	**557.4**	**10.7**	531.6	42.7
BNG96-10	0.2122	0.8	2.16004	1.6	**1240.5**	**23**	1103.5	26.5
BNG96-11	0.07612	0.8	0.63825	1.3	**472.9**	**8.4**	499.3	28.9
BNG96-12	0.27716	0.8	4.32817	1.3	**1577**	**29.6**	1737.4	22.7
BNG96-13	0.22165	1.2	2.35562	5.6	**1290.6**	**34**	1235.2	60.9
BNG96-14	0.19651	0.8	1.96468	1.6	**1156.5**	**21.6**	1070.9	27.9
BNG96-15	0.05665	0.8	0.47573	1.5	**348.7**	**3.5**	340.3	24
BNG96-16	0.14959	0.9	1.35307	1.7	**898.7**	**16.6**	834.7	30.9
BNG96-17	0.10722	0.9	0.86433	2.3	**656.6**	**12.6**	563	41.5
BNG96-18	0.4675	0.9	10.30908	1.9	**2472.6**	**51.4**	2480.5	22.7
BNG96-19	0.09049	1	0.67686	3	**558.4**	**11.5**	492.3	53.4
BNG96-20	0.14617	0.9	1.29906	2	**879.5**	**16.7**	802.6	34.4
BNG96-22	0.2527	0.9	2.96819	3	**1452.4**	**30.5**	1322.4	36.2
BNG96-23	0.20781	0.9	2.25305	2.3	**1217.1**	**24**	1145.6	33.4
BNG96-24	0.07564	0.9	0.63668	2.1	**470**	**8.9**	463	39.8
BNG96-25	0.11994	0.9	1.15543	1.7	**730.2**	**13.5**	777.6	33
BNG96-26	0.20486	0.9	2.23374	2.5	**1201.4**	**24.3**	1170.1	36.4
BNG96-27	0.01353	1.3	0.09298	5	**86.6**	**2.8**	228.1	112.1

BNG96-28	0.21036	0.9	2.50612	1.8	**1230.7**	**23.7**	1255.5	31.1
BNG96-32	0.1805	0.9	1.89302	2.2	**1069.7**	**21.1**	1088.7	36.3
BNG96-33	0.1121	0.9	1.01791	2.1	**684.9**	**13.3**	802.6	38.8
BNG96-34	0.0744	0.9	0.65295	2	**462.6**	**8.8**	502.7	40
BNG96-35	0.04448	0.9	0.32627	2.5	**280.5**	**5.7**	324.1	49.4
BNG96-36	0.01099	1.6	0.08401	7	**71.1**	**2.2**	72	54.2
BNG96-37	0.43802	0.9	10.06509	2.4	**2341.8**	**51.5**	2539.7	31.4
BNG96-38	0.07546	0.9	0.67705	2.2	**467**	**4.6**	454.2	40
BNG96-39	0.15662	0.9	1.87855	2.4	**879.9**	**8.8**	831.3	61.9
BNG96-40	0.07999	1	0.64928	2.6	**496.1**	**10**	539.2	48.5
BNG96-41	0.07775	1	0.64384	2.6	**482.7**	**9.7**	522.9	49
BNG96-42	0.00518	1	0.0368	3	**33.3**	**1.9**	16.4	66.4
BNG96-43	0.17064	0.9	2.20272	2.6	**986.1**	**9.6**	983	122.9
BNG96-44	0.26019	1	3.54815	3.4	**1490.8**	**33.7**	1538.5	45.3
BNG96-46	0.01355	1.3	0.11638	4.6	**86.8**	**2.8**	637.5	92.9
BNG96-47	0.07549	1	0.6224	3.1	**469.1**	**10**	550.4	56.3
BNG96-49	0.01328	1.7	0.08896	8	**85**	**3.5**	116.4	181.5
BNG96-50	0.18883	1	2.01249	3.1	**1115**	**24.4**	1120.9	50.3
BNG96-51	0.08613	1	0.82889	3.1	**513.9**	**5.6**	535.4	93.5
BNG96-52	0.01391	1.9	0.09792	8.4	**89.1**	**3.8**	202.4	186
BNG96-53	0.08389	1	0.66423	3.3	**519.3**	**11.2**	486.9	60.6
BNG96-55	0.2026	1.1	2.37547	3.6	**1189.3**	**27.6**	1281.9	54.8
BNG96-57	0.13917	1.1	1.31919	3.9	**840**	**19.6**	889.1	63.2
BNG96-58	0.14327	1.1	1.32749	3.6	**863.1**	**19.6**	837.8	60.6
BNG96-59	0.24105	1.1	3.06661	3.6	**1392.2**	**32.8**	1449.7	55.2
BNG96-60	0.0185	1.6	0.13235	7	**118.2**	**4.1**	191.7	150
BNG96-61	0.17743	1.1	1.88186	3.9	**1052.9**	**25**	1109.8	62.4
BNG96-63	0.15303	1.1	1.52623	4	**917.9**	**22**	963.2	66
BNG96-64	0.05734	1.2	0.44543	4.3	**359.4**	**8.7**	463	78
BNG96-65	0.2118	1.1	2.49373	4.3	**1238.4**	**31**	1248.6	65.8
BNG96-67	0.00713	2.2	0.05244	10.7	**44.5**	**2.1**	39.2	11
BNG96-68	0.00953	2.1	0.07986	9.2	**60.3**	**2.3**	56.9	7.1

BNG96-70	0.01038	1.6	0.0705	7.2	**66.6**	**2.8**	171.6	157.1
BNG96-71	0.17015	1.2	1.79819	4.5	**1012.9**	**25.8**	1065.6	72.8
BNG96-72	0.1612	1.2	1.61491	4.5	**963.4**	**24.6**	971.5	75.3
BNG96-73	0.02411	1.2	0.19132	4.6	**153**	**2.6**	151	29.2
BNG96-76	0.13938	1.3	1.30113	5.1	**841.2**	**22.6**	830.6	85
BNG96-77	0.07574	1.2	0.64574	4.9	**470.6**	**12.1**	532.8	87.9
BNG96-78	0.26032	1.2	4.02875	4.9	**1491.5**	**41.3**	1650.1	74.1
BNG96-80	0.18466	1.3	2.06601	5.4	**1092.4**	**30.8**	1144.6	84.5
BNG96-81	0.20427	1.3	2.28823	5.4	**1198.2**	**34.1**	1191.3	84.9
BNG96-82	0.08853	1.3	0.7726	5.2	**546.8**	**14.8**	590.5	93.5
BNG96-83	0.06896	1.3	0.61642	5.3	**427.5**	**5.7**	428.1	52.2
BNG96-85	0.13927	1.3	1.37503	5.5	**840.5**	**23.9**	974.6	91.7
BNG5 40								
BNG40-1	0.07933	0.9	0.63657	1.2	**492.8**	**5.3**	569.7	7.6
BNG40-2	0.05678	0.9	0.54032	1.2	**338.6**	**3.2**	899.9	7.5
BNG40-5	0.07923	1	0.68556	2.1	**501.2**	**5.1**	712.9	9.2
BNG40-6	0.19018	1	2.68494	1.8	**1032.3**	**12.6**	1727	7.5
BNG40-11	0.0728	1	0.6522	1.6	**434.7**	**4.4**	798.4	8.3
BNG40-15	0.13339	1	1.49813	1.6	**769.8**	**7.8**	1213.2	8
BNG40-16	0.21686	1	2.80585	1.7	1265.3	27	**1239.6**	**21**
BNG40-18	0.19259	1	2.80971	1.7	1135.4	24.1	**1169.3**	**11.2**
BNG40-20	0.08755	1	1.12779	1.8	**462.8**	**5.5**	1470.1	8.4
BNG40-21	0.00182	1.1	0.01827	2.7	**10.3**	**0.1**	1014.5	10.7
BNG40-23	0.17103	1	2.13188	2	**965.7**	**9.9**	1435.3	8.7
BNG40-26	0.1846	1	2.04512	2.2	**1092.1**	**24**	1192.8	9.1
BNG40-27	0.08738	1	0.81535	2.5	**524.9**	**5.5**	858.5	9.8
BNG40-28	0.25197	1	3.19057	2.8	**1448.6**	**34.1**	1508.9	9.5
BNG40-33	0.15032	1.1	1.55286	2.9	**864.3**	**9.7**	1133.3	10.3
BNG40-34	0.07765	1.1	0.6497	2.8	**482.1**	**11**	633.6	10.7
BNG40-35	0.17968	1.1	1.98823	2.9	1065.2	25.1	**1101.1**	**10.2**
BNG40-37	0.13653	1.1	1.30508	3.2	**810.3**	**9.1**	914.2	10.9
BNG40-40	0.51127	1.1	14.6682	3.3	2662	74	**2691.3**	**12.4**

BNG40-42	0.06682	1.2	0.60588	3.5	**399.8**	**4.7**	803.8	11.6
BNG40-46	0.1432	1.2	1.41012	3.9	**852.7**	**10**	975.7	12
BNG40-49	0.07794	1.2	0.96257	4.2	**417.2**	**6.3**	1409.7	12.1
BNG40-56	0.00602	1.3	0.08004	5.1	**29.5**	**0.6**	1543.3	13
BNG40-57	0.0096	1.6	0.11398	5.8	**50.5**	**1.1**	1360.5	14.2
BNG40-59	0.10213	1.5	0.8233	5.6	**626.9**	**19.4**	697.4	14.4
BNG40-62	0.0878	1.5	0.73822	5.9	**542.5**	**17.5**	639.2	14.8
BNG40-64	0.08556	1.6	0.90433	6.4	**529.2**	**18**	1083.7	14.9
BNG40-68	0.21938	1.7	2.60582	6.8	**1278.6**	**47.5**	1042.1	16.9
BNG40-69	0.01668	1.9	0.16651	7.8	**93.6**	**2.3**	1027.2	16.7
BNG40-70	0.00803	1.7	0.05361	7.4	**51.6**	**3.2**	195.5	17.3
BNG40-71	0.18742	1.8	1.95505	7.2	**1104.9**	**19**	1110.5	15.6
BNG40-72	0.00817	1.8	0.05402	7.5	**52.5**	**3.3**	85.4	17.4
BNG40-73	0.13512	1.8	1.22357	7.5	**817**	**31.6**	806.7	16.3
BNG40-75	0.08228	1.9	0.64133	7.8	**509.7**	**20**	466.6	17
BNG40-76	0.01563	2	0.10877	8.2	**100**	**4.8**	209.8	18
BNG40-79	0.07274	2	0.57001	8.5	**452.6**	**19.1**	509.6	17.6
BNG40-80	0.01000	2.1	0.08779	8.7	**59.8**	**1.4**	736	17.6
BNG5 46								
BNG46-1	0.07582	0.7	0.64138	1.4	**471.1**	**6.6**	503.2	18.7
BNG46-4	0.12113	0.7	1.15813	1.7	**737.1**	**10.7**	781.1	39.4
BNG46-5	0.08751	0.9	0.71060	4	**540.8**	**10.5**	545.1	55.6
BNG46-6	0.31356	0.7	4.35641	2.4	**1758.2**	**28.6**	1704.1	193.3
BNG46-7	0.08880	0.7	0.76398	2.4	**548.4**	**8.6**	576.3	36.9
BNG46-10	0.09186	0.8	0.74347	3.2	**566.5**	**9.9**	564.4	47.5
BNG46-11	0.07842	1	0.67665	4.1	**486.7**	**9.8**	524.7	54.7
BNG46-12	0.01728	1.7	0.11450	8.6	**110.4**	**4**	110.1	19.9
BNG46-15	0.07944	0.8	0.68528	3	**492.8**	**8.5**	530	40.6
BNG46-16	0.07708	0.8	0.66280	2.5	**478.7**	**7.7**	516.3	33.7
BNG46-17	0.20226	0.7	2.26245	2.2	**1187.4**	**19**	1200.7	96.4
BNG46-18	0.11470	0.7	1.13962	2.4	**700**	**11.2**	772.3	54.7
BNG46-19	0.17287	0.8	1.95888	2.6	**1027.9**	**17.2**	1101.5	98.6

BNG46-20	0.21159	0.8	2.54798	2.9	**1237.3**	**21.5**	1285.9	138.9
BNG46-21	0.11644	0.8	1.02046	3	**710**	**12.5**	714.1	60.9
BNG46-22	0.08644	0.8	0.73259	2.9	**534.4**	**9.1**	558.1	42.6
BNG46-26	0.08076	0.9	0.67223	3.3	**500.7**	**9.1**	522.1	44.3
BNG46-27	0.07998	0.9	0.66312	3.4	**496**	**9.1**	516.5	44.5
BNG46-28	0.13195	0.9	1.20448	4	**799**	**16.2**	802.7	94.2
BNG46-29	0.09900	0.9	0.86063	3.6	**608.5**	**11.6**	630.5	60.3
BNG46-30	0.08172	0.9	0.66662	3.7	**506.4**	**9.9**	518.7	49.3
BNG46-31	0.18536	0.9	2.14996	3.9	**1096.2**	**22.6**	1165	157.8
BNG46-32	0.19250	1	2.08672	4.2	**1134.9**	**24.2**	1144.4	163.4
BNG46-33	0.10026	1	0.85850	4.2	**615.9**	**13**	629.3	71.1
BNG46-34	0.07433	1	0.64899	4.1	**462.2**	**9.5**	507.9	52.6
BNG46-35	0.13339	1	1.30729	4.5	**807.2**	**17.8**	848.9	112.3
BNG46-36	0.16967	1.1	2.09877	5	**1010.3**	**24.1**	1148.4	194.3
BNG46-37	0.13928	1.1	1.29693	4.6	**840.6**	**19**	844.4	114.7
BNG46-39	0.03318	1.2	0.30079	5.6	**210.4**	**5.5**	267	33.5
BNG46-40	0.08113	1.1	0.67784	5	**502.9**	**11.9**	525.5	67
BNG46-41	0.07475	1.2	0.62669	5.2	**464.7**	**11.2**	494	64
BNG46-44	0.09310	1.3	0.80231	5.8	**573.8**	**15.3**	598.1	90.9
BNG46-45	0.19343	1.3	1.99250	6.1	**1139.9**	**32.3**	1113	220.1
BNG46-46	0.17178	1.4	1.91469	6.5	**1021.9**	**30.1**	1086.2	225.7
BNG46-47	0.16335	1.4	1.92365	6.5	**975.4**	**28.9**	1089.3	227
BNG46-48	0.18834	1.4	2.18910	6.6	**1112.4**	**33.6**	1177.6	257.1
BNG46-49	0.21380	1.4	2.49869	6.8	**1249**	**39.4**	1271.7	298.9
BNG46-50	0.08979	1.5	0.88594	7.1	**554.3**	**17.2**	644.2	119.8
BNG46-51	0.17194	1.6	1.79357	7.6	**1022.8**	**34.4**	1043.1	246
BNG46-52	0.09396	1.5	0.76273	7.4	**578.9**	**18.6**	575.6	108.2
BNG46-56	0.08452	1.7	0.72908	8.1	**523**	**18.2**	556	113.8
BNG46-58	0.23468	1.8	2.71135	8.6	**1359**	**52.8**	1331.6	389
BNG46-59	0.15711	1.8	1.65888	8.8	**940.7**	**36.3**	992.9	261
BNG46-60	0.08321	1.8	0.75830	9	**515.3**	**19.8**	573	130.3
BNG46-62	0.08828	2.1	0.76372	10.5	**545.4**	**24.2**	576.2	151.6

BNG46-63	0.07944	2.2	0.69873	10.8	**492.8**	**22.2**	538	142.3
BNG46-65	0.28313	2.3	3.93583	11.5	**1607.1**	**83**	1621.1	652.6
BNG46-67	0.30637	2.4	4.38124	11.9	**1722.8**	**94**	1708.8	727.3
BNG46-68	0.10466	2.4	0.90319	12.2	**641.7**	**33**	653.4	201.8
BNG46-69	0.11508	2.5	0.99531	12.5	**702.2**	**37.2**	701.4	225.3
BNG46-70	0.20964	2.6	2.12869	12.8	**1226.9**	**69.3**	1158.2	442.6
BNG46-71	0.21173	2.6	2.21436	13.1	**1238**	**71.6**	1185.6	465.2
BNG46-73	0.20098	2.8	2.17395	13.9	**1180.6**	**71.7**	1172.7	479
BNG46-75	0.12560	2.9	1.06701	14.5	**762.7**	**47.2**	737.3	273.9
BNG46-76	0.32211	3	4.14852	15.2	**1800**	**124.3**	1663.9	826.7

Method:

The U-Pb system has a much higher closure temperature for zircon and is stable to ~750°C, beyond which uranium is lost. Zircon U-Pb ages from detrital grains in a sedimentary rock are therefore either considered to be primary crystallization ages representing the range of crustal ages within the contributing source region or they represent high temperature metamorphic ages.

For U-Pb dating, samples were analysed by LA-ICPMS using a New Wave 213 aperture imaged frequency quintupled laser ablation system (213nm) coupled to an Agilent 750 quadrupole-based ICP–MS. Real time data were processed using GLITTER and repeated measurements of external zircon standard PL (Svojtka et al., 2001; TIMS reference age 337.1±0.7 Ma) to correct for instrumental mass bias and downhole fractionation affects. Data were filtered using standard discordance tests with a 10% cutoff. U/Th concentrations were determined relative to of NIST glass 612. Data correction was by the 208 method that assumes concordance of the U–Pb and Th–Pb systems.

In the first instance a concordancy test is applied to uncorrected age data. The data which is >10% discordant can then be looked at to see if their common Pb corrected ages make sense with the concordant data. Concordant data as well as any Pb corrected previously discordant data is then used and presented. The table opposite contains all concordant data including ages which were corrected for common Pb.

Appendix 4 – 1: Seismic data and composite satellite sample maps (CD)

Contents of CD

1. Seismic basemaps for all interpreted seismic lines
2. Interpreted seismic lines
3. Palaeoshelf maps
4. Composite satellite sample maps
5. Appendix 4 – 2: Biostratigraphic correlation of wells across Bangladesh

2D seismic refelction data was interpreted between 2004-2007 at Cairn Energy Plc, Edinburgh (Scotland).

Appendix 5 – 1: Published conference abstracts

1. Journal of Asian Earth Sciences, v. 26, No. 2, p123 (2006)

Evidence of early Himalayan erosion? Are the sediments of the subduction zone from Bangladesh to the Andaman Islands, the early accreted Bengal fan?

ALLEN, R[1]., NAJMAN, Y.[1], CARTER, A.[2], WILLETT, E.[3], GARZANTI, E.[4], WIJBRANS, J.[5], BICKLE, M. J.[6], OLIVER, G.[7], UDDIN, M. J.[3]

[1]Dept of Env Science, Lancaster University, LA1 4YQ, UK.
Email First author: R.Allen1@lancs.ac.uk
[2]Dept of Earth Sciences, Birkbeck-UCL, UK
[3]Cairn Energy Plc, Edinburgh, UK.
[4]Dip. Di Geologiche, Universita Milano-Bicocca, Italy.
[5]Faculty of Earth Sciences, Vrije Universiteit, Netherlands.
[6]Dept Earth Sciences, Cambridge University, UK
[7]School of Geosciences, St-Andrews University, UK.

The sediment record of material eroded from the Himalaya provides a chronicle of early development of the orogen. The earliest erosive sediments of the Himalaya, seemingly missing from the foreland basins, and inaccessible in the Bengal Fan, may be preserved as accretionary prism sediments along the subduction zone that runs from Bangladesh and Myanmar, to the Andaman Islands and further south[1-3]. However, Burman and Sumatran provenances have also been proposed for these rocks[4,5]. We present initial results of a study to determine the age, stratigraphy and provenance of the accretionary prism sediments of the Arakan-Yoma of the Indo-Burman ranges, Myanmar, the Chittagong Hill Tracts (CHT), Bangladesh, and the Tertiary sedimentary rocks of the Andaman Islands.

In Bangladesh, the stratigraphy of the CHT) (Mio-Plioc. Surma, Tipam & Dupi Tila Formations) has previously been based on lithostratigraphic correlation with rocks in Assam, poorly constrained by biostratigraphy. Recent work has improved the biostratigraphy and reassigned the Tertiary rocks of Bangladesh, including those of the CHT, into 3 seismically-defined Megasequences[6]. Our seismic correlation of the offshore sequence stratigraphy and biostratigraphy with the onshore geology of the CHT has shown that the rocks of the CHT are younger than previously believed. Petrographic, heavy mineral, ^{40}Ar-^{39}Ar, Sm-Nd and fission track analyses, undertaken on rocks from both the Arakan-Yoma and the CHT, indicate a Himalayan rather than Indo-Burman source for the rocks of the CHT.

In the Andaman Islands, the age of the Andaman Flysch is poorly constrained at L. Eocene - Olig[7]. Provenance data will be discussed in terms of Himalayan and other sources.

[1]Curray, J. et al. AAPG Mem., 1979; [2]Curray, J. et al. Marine & Petr Geology, 2003; [3]Gani. M. & Alam, Sediment Geol, 1999; [4]Mitchell, A., J. Geol Soc, Lond, 1993; [5]Pal, T. et al, Geol. Mag. 2003; [6]Partington, M., et al, Cairn Energy Int Rep, 2005, [7] Bandopadhyay, P. & Ghosh, J. Geol. Soc. Ind., 1998.

2. Eos. Trans. AGU 87 (52), Fall Meet Supple Abstract, T41C-1587 (2006)

Bangladesh-Burma Accretionary Prism: Evolution and Provenance

R. ALLEN[1], Y. NAJMAN[1], A. CARTER[2], E. WILLETT[3], E. GARZANTI[4], J. WIJBRANS[5], M. J. BICKLE[6], G. VEZZOLI[4], S. ANDÒ[4], P. ALEXANDRE[7], AND M. J. UDDIN[3].

[1]Dept of Env Science, Lancaster University, LA1 4YQ, UK (r.allen1@lancaster.ac.uk)
[2]Dept of Earth Sciences, Birkbeck-UCL, UK
[3]Cairn Energy Plc., Edinburgh, UK
[4]Dip. Di Geologiche, Universita Milano-Bicocca, Italy
[5]Faculty of Earth Sciences, Vrije Universiteit, Netherlands
[6]Dept of Earth Sciences, Cambridge University, UK
[7]Argon Lab, SUERC, Glasgow, UK

The Chittagong Hill Tracts of Bangladesh and the Indo-Burman Ranges (Arakan Yoma) of Myanmar constitute an accretionary prism which runs along the India-Asian subduction zone. It consists of Palaeogene as well as Neogene sedimentary rocks that may preserve a record of early Himalayan erosion, which is as yet inaccessible in the deeper parts of the Bengal Fan, or missing in other sediment repositories of the region (Curray et al. 1979, 2003 and Gani et al. 1999). However, a Burman provenance has also been suggested for these rocks (Mitchell, 1993; Pal et al. 2003). In order to characterise the provenance signature of the accretionary prism rocks and determine Himalayan or Burman source, we have used petrographic, heavy mineral, U-Pb, fission track, Sm-Nd and Ar-Ar analyses. We present results of the initial study, including new seismic data (obtained by Cairn Energy plc.) which provides a seismic stratigraphy of the Chittagong Hill Tracts calibrated to offshore well seismic data, as well as comprehensive palaeoshelf mapping of the Bengal Basin region during the Eocene to Pliocene, which documents source input direction.

Appendix 5 – 2: Co-authored publications

1. Earth and Planetary Science Letters (*Accepted for Publication*)

The "missing" record of Himalayan erosion, Bengal Basin, Bangladesh

Y. Najman, M. Bickle, M. BouDagher-Fadel, A. Carter, E. Garzanti, M. Paul, J. Wijbrans, E. Willett, G. Oliver, R. Parrish, H. Akhter, **R. Allen**, S. Ando, E. Christy, L. Reisberg, G. Vezzoli

Abstract:

Dating onset of Himalayan erosion is critical to understanding crustal deformation, and the proposed link with global climate and ocean geochemistry. The most commonly quoted age of India-Asia collision is ~50 Ma, yet the record of Palaeogene Himalayan erosion is scant - either absent or of low age resolution. We identify sediments shed from the rapidly exhuming southern flanks of the eastern-central Himalaya at 38 Ma, in the >1 km thick deltaic Barail Formation of the Bengal Basin, Bangladesh. This formation was previously of disputed provenance and poorly dated. Our new provenance data from the Barail Formation, encompassing petrographic, isotopic and seismic techniques, is consistent with Himalayan derivation, and inconsistent with Indian cratonic or Burman sources. Our biostratigraphic and isotopic mineral ages date the formation as spanning Late Eocene to Early Miocene. We consider the Barail Formation to represent onset of significant accelerated erosion from the southern flanks of the central eastern Himalaya at a regionally applicable scale given that 1) earlier input of significant clastic material to the Bengal Basin would be inconsistent with the prevailing (pre Barail) carbonate shelf depositional environment 2) the Bengal Basin is the only obvious exit point for such detritus, 3) our interpretations from Northeast Bengal Basin can be correlated over a large area of the delta in which major Himalayan-derived input initiated sometime around 40 Ma and 4) our data is consistent with the regional picture of transition from slow to exponentially increasing accumulation rates at the start of the Oligocene in basins surrounding the collision zone. Our lag time data shows that exhumation of the orogen was rapid by 38 Ma, and indicates that thrusting and crustal thickening had generated sufficient relief by 38 Ma to generate efficient erosion. Our study 1) supports orogenic models that require or result in delayed erosion, although implies rapid exhumation earlier than is consistent with development of "channel flow" as currently modelled 2) supports the contention that Himalayan erosion resulted in increase of the marine 87Sr/86Sr ratio at ~40 Ma and 3) brings into question the proposed link between Himalayan erosion and onset of Cenozoic global cooling.

2. Journal TBC (*In Preparation*)

Evolution, Palaeogeography and Sediment Provenance of the bay of Bengal Region

J. Curray and R. Allen

Introduction:

The Bay of Bengal (Fig. 1) is an obvious result of the India-Asia collision, but the details are elusive and controversial. Factors to be considered are: 1. The location of Eurasia and other tectonic units in the Tethys complex south of Eurasia, 2. The extent and size of "Greater India", 3. The motion of India relative to Eurasia and the other tectonic elements in the Tethys complex, and 4. The alignment and hence the location of the subduction margin at the southern margin of the Eurasia complex.

One of the principal problems is the timing of the events in a very complex collision history and determination of what tectonic elements collided with what other tectonic elements. The India-Asia collision occurred between the northward moving Indian subcontinent's passive continental margin and the subduction margin bordering the southern margin of the Lhasa block lying at the southern margin of the Asian continent. There appears to be a wide range of thought on the timing of the India-Asia collision, i.e., between India and the Lhasa block, from as early as 70 Ma to around the Eocene/Oligocene boundary at about 34 Ma. Many authors believe that initial contact may have occurred during the Paleocene, the so-called "soft collision", and the main collision event, the "hard collision", was from about 55 to 45 Ma in early Eocene.

Another major problem is interpretation of the history of the eastern margin of the Bay of Bengal, namely the western Sunda Arc. Some investigators have assumed that the arc, from Myanmar, the Andaman-Nicobar Ridge, Sumatra and Java were rotated counterclockwise, while others interpret the rotation as having been clockwise. Part of the latter argument is that the Indian subcontinent lies in an obvious indentation in the southern margin of Asia (Fig. 1) and that the indentation was created by India pushing its way into Asia. This implies extrusion and clockwise rotation of parts of Asia lying to the east and south of the eastern Himalayan Syntaxis.

What brought about this paper is that for many years Curray (refs) had speculated that the Eocene and Oligocene sandstones in the Indo-Burman Ranges and the Andaman and Nicobar Islands were Bengal Fan sediments with a Himalayan provenance. Seismic reflection profiles show Bengal Fan sediments at the foot of the slope above the Sunda trench being folded and uplifted into these accretionary prisms. Allen, however, (refs) demonstrated that these deposits, where sampled in outcrops at the crest of the ridge, had not been sourced in the Himalayas, but instead had come from an arc source. So we teamed up to resolve the contradiction.

What we propose to do in this paper is to review various problems of the India/Asia collision scenario, select our preferred model and then test our model with provenance studies of the sedimentary deposits.

The sedimentary deposits of concern here are the Bengal submarine fan and the rocks in the accretionary prisms in the Indo-Burman Ranges, the Andaman-Nicobar Ridge and the outer arc ridge off Sumatra and Java. Provenance studies to date have shown a Himalayan source for the Bengal Fan, sampled thus far only to early Miocene, arc sources for the accretionary prism rocks of Paleogene age and a Himalayan source for the Miocene rocks. This change can give insight to the history of the collision and uplift of the possible source areas.